Conception by surface organometallic chemistry of molecular solid activators for olefin polymerization

Vittoria Chiari

N°d'ordre NNT : 2020LYSE1109

THESE de DOCTORAT DE L'UNIVERSITE DE LYON

opérée au sein de

l'Université Claude Bernard Lyon 1

Ecole Doctorale de Chimie de Lyon

N° ED 206 Chimie, Procédés, Environnement

Spécialité de doctorat : **Chimie**

Discipline : Catalyse de polymérisation

Soutenue publiquement le 06/07/2020, par :

Vittoria CHIARI

Conception by surface organometallic chemistry of molecular solid activators for olefin polymerization.

Directeur de thèse :

Dr. BOISSON Christophe

Co-directeur de thèse :

Dr. TAOUFIK Mostafa

Devant le jury composé de :

Prof. AMGOUNE Abderrahmane	Université Lyon 1	Président du jury
Prof. CIPULLO Roberta	Università di Napoli « Federico II »	Rapporteure
Dr. GIULLAUME Sophie	Université de Rennes	Rapporteure
Dr. GAUVIN Régis	Chimie ParisTech	Examinateur
Dr. BETTONVILLE Serge	INEOS	Invité
Dr. BOISSON Christophe	CNRS	Directeur de thèse

Université Claude Bernard – LYON 1

Président de l'Université	M. Frédéric FLEURY
Président du Conseil Académique	M. Hamda BEN HADID
Vice-Président du Conseil d'Administration	M. Didier REVEL
Vice-Président du Conseil des Etudes et de la Vie Universitaire	M. Philippe CHEVALLIER
Vice-Président de la Commission de Recherche	M. Jean-François MORNEX
Directeur Général des Services	M. Damien VERHAEGHE

Composantes Santé

Faculté de Médecine Lyon-Est – Claude Bernard	Doyen : M. Gilles RODE
Faculté de Médecine et Maïeutique Lyon Sud Charles. Mérieux	Doyenne : Mme Carole BURILLON
UFR d'Odontologie	Doyenne : Mme Dominique SEUX
Institut des Sciences Pharmaceutiques et Biologiques	Directrice : Mme Christine VINCIGUERRA
Institut des Sciences et Techniques de la Réadaptation	Directeur : M. Xavier PERROT
Département de Formation et Centre de Recherche en Biologie Humaine	Directrice : Mme Anne-Marie SCHOTT

Composantes et Départements de Science et Technologie

UFR Biosciences	Directrice : Mme Kathrin GIESELER
Département Génie Electrique et des Procédés (GEP)	Directrice : Mme Rosaria FERRIGNO
Département Informatique	Directeur : M. Behzad SHARIAT
Département Mécanique	Directeur M. Marc BUFFAT
UFR - Faculté des Sciences	Administrateur provisoire : M. Bruno ANDRIOLETTI
UFR (STAPS)	Directeur : M. Yannick VANPOULLE
Observatoire de Lyon	Directrice : Mme Isabelle DANIEL
Ecole Polytechnique Universitaire Lyon 1	Directeur : Emmanuel PERRIN
Ecole Supérieure de Chimie, Physique, Electronique (CPE Lyon)	Directeur : Gérard PIGNAULT
Institut Universitaire de Technologie de Lyon 1	Directeur : M. Christophe VITON
Institut de Science Financière et d'Assurances	Directeur : M. Nicolas LEBOISNE
ESPE	Administrateur Provisoire : M. Pierre CHAREYRO

Abstract

In this manuscript is presented the synthesis and application of Al- and Y-based activating support for metallocene catalysts for olefin polymerization. The approach used for the synthesis of the supported species is the Surface Organometallic Chemistry which allows a certain control on the structure of the grafted species.

The activators synthesized were then tested, in presence of *rac*-$EtInd_2ZrCl_2$, in ethylene/1-hexene slurry copolymerization. Of all the species produced (differing either in the nature of the metal core, the nature of the functionalizing ligand or the acidity of the organometallic precursor) only one demonstrated a productivity sufficient to justify further studies: $[(\equiv SiO)_2Al(OC_6F_5)_2]^-[HNEtMe_2]^+$, AS1. The system AS1/*rac*-$EtInd_2ZrCl_2$ shows activities around 1100 $g_{PE}\ g_{cat}^{-1}\ h^{-1}$ at lab-scale and around 4000 $g_{PE}\ g_{cat}^{-1}\ h^{-1}$ at pre-industrial scale. AS1 was also used for the isolation of formulated 'dry' catalysts, by reaction with $EtInd_2ZrMe_2$. The catalysts thus obtained showed high initial activities followed by a rapid decomposition of the active species at room temperature.

In this thesis work, was also developed an innovative catalyst based on a silica-supported Y organometallic complex, which produces UHMWPE with activities up to 7500 $g_{PE}\ g_{cat}^{-1}\ h^{-1}$.

Résumé

Ce manuscrit décrit la synthèse et l'application de supports activateurs, basés sur Al et Y, pour des catalyseurs métallocènes pour la polymérisation des oléfines. La méthode utilisée pour la synthèse des espèces supportées est la Chimie Organométallique de surface, qui permet un contrôle certain sur la structure des produits greffés.

Les activateurs synthétisés ont été testés, en présence de *rac*-$EtInd_2ZrCl_2$, en copolymérization slurry éthylène/1-héxène. Entre toutes les espèces testées (qui différaient pour soit par la nature du centre métallique, soit par la nature du ligand fonctionnel, soit par l'acidité du précurseur organométallique), seulement un a été considéré suffisamment actif pour justifier des études ultérieures : $[(\equiv SiO)_2Al(OC_6F_5)_2]^-[HNEtMe_2]^+$, AS1. Le système AS1/*rac*-$EtInd_2ZrCl_2$ démontra des activités aux alentours de 1100 $g_{PE}\ g_{cat}^{-1}\ h^{-1}$ à échelle laboratoire et de 4000 $g_{PE}\ g_{cat}^{-1}\ h^{-1}$ à échelle préindustrielle. AS1 a aussi été utilisé pour la formulation des catalyseurs dits 'secs', par réaction avec $EtInd_2ZrMe_2$. Ces catalyseurs ont montré des activités initiales élevées, suivies d'une rapide décomposition des espèces actives à température ambiante.

Dans ce travail de thèse, on a aussi développé un catalyseur novateur basé sur un complexe organométallique d'yttrium greffé sur silice, qui produit l'UHMWPE avec des activités supérieures à 7000 $g_{PE}\ g_{cat}^{-1}\ h^{-1}$.

Key words : Polyolefin; Polyethylene; Slurry Polymerization; Activating Support; Silica; SOMC; metallocene; zirconocene; Aluminium; Yttrium.

Alle partenze,

ma anche agli arrivi

Acknowledgments

The work present in this manuscript would have never been possible without the presence, physical and not, of a great number of people, both close and far away.

Foremost, I would like to thank Timothy McKenna, director of the lab Chimie, Catalyse, Polymères et Procédés (C2P2), for welcoming me in the lab. I would also like to kindly thank the members of my Jury, Prof. Roberta Cipullo, professor of the Università degli Studi di Napoli 'Federico II', Dr. Sophie Guillaume, HDR at the Université de Rennes, Prof. Abderrahmane Amgoune, professor of the Université Lyon 1, and Dr. Règis Gauvin, HDR at the ParisTech, for having accepted to evaluate my thesis work.

I have to deeply thank, than, my two supervisors for giving me this amazing opportunity to grow from both a scientific and a personal point of view. I am so profoundly grateful to Dr. Christophe Boisson for all the discussions concerning olefin polymerization and catalysts, the exchange of ideas, the explanations an all the patience in the course of these three years. I value incredibly all the advices received from you. In all the same ways I have to thank Dr. Mostafa Taoufik for bearing with me as I first approached myself to Surface Organometallic Chemistry, for managing to always find time to shed light on my doubts, even if it was only a five minutes discussion while walking in the lab hallways, I have treasured all of your scientific advices. But, beyond the science I truly have to thank you for the amazing welcome you have given me in France and in Lyon particularly, I couldn't have hoped for better in moving out of Italy.

Of course when talking about the opportunity that was given to me with this thesis, it is impossible to forget my supervisors within INEOS. I am forever grateful to Dr. Serge Bettonville, Dr. Gaêlle Pannier and Dr. Layane Deghedi for all their support and the enriching discussions throughout these three years. A huge thanks goes to the people at NOH who have welcomed and helped me in the occasion of my brief internship at INEOS facilities in NOH, particularly to Stéphane Paye who's helped me with the experiments.

A warm and felt thank you goes, then, to all the people in the C2P2 lab that have supported and helped me in this scientific journey: Dr. Aimery De Mallmann who has helped me with the EXAFS characterizations presented in this thesis, Dr. Kai Szeto who's been indispensable in my learning

all the SOMC synthesis and characterization techniques, Dr. Sébastien Norsic for helping me become comfortable with the polymerization apparatus that's been my companion for three years. I need then to thank from the bottom of my heart my desk neighbor, Pascal who, since my arrival, has always been a reference point in the lab, always there to answer all of my questions, even the most trivial ones, always with great patience and knowledge.

I was so lucky as to share this PhD journey within C2P2 and INEOS with an amazing lab mate, Yashmin. Having a companion made this three years of work so much more fun, I believe we made a great supporting team for each other. We'll never forget the SEM sessions loving each and every one of our samples.

Beyond the scientific achievements, these three years allowed me to understand how it is actually possible to have a second family away from your blood one. Being so very attached and fond of my birth place, Napoli, I was able to fully enjoy this experience thanks to the amazing friends I was so incredibly lucky to meet in Lyon. Pooja, Marc, Clément, Iurii, Tapish, Valeriia, Matthieu you have been so much more than just lab mates. I have been so blessed to meet you all. I will never forget all the adventures, the skiing trips, the trips thought and organized in the span of a couple of days (sometimes hours, Pooja), all the crazy evenings playing, eating, drinking (fighting over Hawaii pizza), laughing our hearts out. You truly are my family away from home.

E infine, un passaggio all'italiano si rivela necessario per ringraziare chi c'è sempre stato, gli amici che nonostante la distanza sono sempre al tuo fianco, e che oramai ci saranno sempre. Giulia, Max, grazie, per esserci.

E la mia famiglia, quella vera, piena di un amore profondo che è difficile esprimere e che proprio per questo, spesso e volentieri, fuoriesce sotto forma di litigi passionali e ad alta voce. Mia sorella che spesso è l'unica che mi capisce davvero, grazie a (o forse a causa di) ventisei anni di presenza costante l'una a fianco dell'altra. Mamma e papà, che mi hanno sempre lasciato la possibilità e la libertà di scegliere il mio percorso sempre stando alle mie spalle nel caso mi voltassi per aiuto, mostrando sempre interesse per quello di cui fossi appassionata (anche nel caso in cui non ci capissero un granché). Grazie.

Table of contents

Table of contraptions

AS	Activating Support
AzuZrCl2	rac-dimethylsilylenebis[1,1-{2-methyl-4-(4-chlorophenyl)-4-hydroazulenyl}]zirconium dichloride
BARF	tetrakis(pentafluorophenyl)borate,
Bu	Butyl
CCP	Composite Central Plane
CGC	Constrained Geomery Catalyst
Cp	Cyclopentadienyl
Cp*	Pentamethycyclopntadienyl
CPMAS	Cross Polarization Magic Angle Spinning
CSTR	Continuous Stirred Tank Reactor
DEAC	chlorodiethyl aluminum
DOE	Design of Experiment
DRIFT	Diffuse reflectance infrared fourier transform
DSC	Differential Scanning Calorimetry
Et	Ethyl
EXAFS	Extended X-ray Absorption Fine Structure
fod	1,1,1,2,2,3,3-heptafluoro-7,7- dimethyl-4,6-octanedionate
FTIR	Fourier Transform Infrared
GC	Gas Chromatografy
GPC	Gel Permeation Chromatografy
HDPE	High Density Polyethylene
hi-PP	Hemi-isotactic Polypropylene
HLMI	High Load Melt Index
HT-SEC	High Temperature Size Exclusion Chromatography
i-Bu	Isobutyl
Ind	Indenyl
i-PP	Isotactic Polypropylene
IR	Infrared
LCB	Long Chain Branching
LDPE	Low Density Polyethylene

LLDPE	Linear Low Density Polyethylene
MAO	Methylalumoxane
MAS	Magic Angle Spinning
MCC	Mitsubishi Chamical Corporation
Me	Methyl
MI	Melt Index
MMD	Molar Mass Distribution
MMT	Montmorillonite
MVS	Melt Viscosity Standard
n-Bu	normal butyl
NMR	Nuclear Magnetic Resonance
NNDIMT	N,N-dimethyltoluidine
OMTS	octamethyltrisiloxane
PE	Polyethylene
PEHD	Polyethylene High Density
Ph	Phenyl
PO	Polyolefin
PP	Polypropylene
SA	Surface Area
SCB	Short Chain Branching
SEM	Scanning Electron Microscopy
sMAO	Solid MAO
SMAO	Supported MAO
SOMC	Surface Organometallic Chemistry
s-PP	syndiotactic polypropylene
SS-NMR	Solid State Nuclear Magnaetic Resonance
*t*Bu	tert-butyl
TCM	trichloromethane
THF	Tetrahydrofurane
TiBA	Triisobutyl aluminum
TMA	Trimethyl aluminum
tritox	tris-tert-butylmethoxide
UHMWPE	Ultra-High Molecular Weight Polyetylene

List of products

AS1	$[(\equiv SiO)_2Al(OC_6F_5)_2]^-[HNMe_2Et]^+$
AS2	$[(\equiv SiO)Al(OC_6F_5)_3]^-[HNMe_2Et]^+$
AS3	$[(\equiv SiO)_2Al(O_2C_{20}H_{12})]^-[HNMe_2Et]^+$
AS4	$[(\equiv SiO)_2Al(OC(CF_3)_2Ph)_2]^-[HNMe_2Et]^+$
AS5	$[(\equiv SiO)_2Al(O_2C_5HF_6)_2]^-[HNMe_2Et]^+$
AS6	$[(\equiv SiO)_2Al(O_2$P-binaphtol$)_2]^-[HNMe_2Et]^+$
AS7	$[(\equiv SiO)_2AlCl(OC_6F_5)]^-[HNEt_2Ph]^+$
AS8	$[(\equiv SiO)_2AlCl_2]^-[HNEtMe_2]^+$
AS9	$[(\equiv SiO)AlF(OC_6F_5)_2]^-[HNEtMe_2]^+$
AS10	$[(\equiv SiO)AlF(OC_6F_5)_2]^-[HNEtMe_2]^+$
AS11	$[(\equiv SiO)_2AlF(OC_6F_5)]^-[HNEtMe_2]^+$
AS12	$[(\equiv SiO)Y(OC_6F_5)_3]^-[HNMe_2(PhMe)]^+$
AS13	$[(\equiv SiO)_2Y(OC_6F_5)_2]^-[HNMe_2(PhMe)]^+$
AS14	$[(\equiv SiO)Y(OC_6F_5)_3]^-[HNMe_2Et]^+$
AS15	$[(\equiv SiO)_2Y(OC_6F_5)_2]^-[HNMe_2Et]^+$
Cat1	*rac*-$EtInd_2ZrCl_2$
Cat2	(n-$BuMeCp)_2ZrCl_2$
MCat1	*rac*-$EtInd_2ZrMe_2$
MCat2	(n-$BuMeCp)_2ZrMe_2$
P1	$(\equiv SiO)_2AlH(NEtMe_2)$
P2	$(\equiv SiO)AlH_2(NEtMe_2)$
P3	$(\equiv SiO)_2Al$*i*$Bu(Et_2O)$
P4	$(\equiv SiO)_2AlCl$
P5	$(\equiv SiO)AlF($*i*$Bu_2)(Et_2O)$
P6	$(\equiv SiO)AlF$*i*Bu_2
P7	$(\equiv SiO)_2[AlF($*i*$Bu)]_2$
P8	$(\equiv SiO)Y(CH_2PhNMe_2)_2$
P9	$(\equiv SiO)_2Y(CH_2PhNMe_2)$
P10	$(\equiv SiO)Y\{1,3\text{-}C_3H_3(SiMe_3)_2\}_2$
P11	$(\equiv SiO)_2Y\{1,3\text{-}C_3H_3(SiMe_3)_2\}$

P12	$[(\equiv SiO)Y\{1,3\text{-}C_3H_3(SiMe_3)_2\}]^+[B(C_6F_5)_4]^-$

IsoCat01	AS1/Cat1/TiBA
IsoCat02	AS1/Cat1/TiBA
IsoCat03	AS1/Cat1/TiBA
IsoCat04	AS1/Cat1/TiBA
IsoCatM1	AS1/MCat1 - toluene
IsoCatM2	AS1/MCat2 - toluene
IsoCatP	AS1/MCat1 - pentane
IsoCatL	AS1/MCat1 - labelled ^{13}C

Introduction

Why polyolefins?

Plastics, and consequently polyolefins (PO), are by now an indispensable feature in our everyday life. In 2015 the global plastic production consisted of 265 million of tons, of which 55% were polyolefins, PE and PP in all their grades.[1,2]

What made and still makes polyolefins the major class of polymers on the global market is their great versatility. In fact starting from the same two simple blocks, ethylene and propylene, more than 300 different polymer grades, with different mechanical and chemical properties, can and are produced worldwide for a wide range of applications: from food and drink containers, to tubes for gas and liquid transportation, to the medical and automobile sectors and many others.[3]

The fact that polyethylene and isotactic polypropylene (*i*-PP) are still so diffused nowadays is even more surprising if one considers the fact that their discovery traces back to the 1930s, for LDPE, and to the 1950s for HDPE, LLDPE and *i*-PP synthesized by coordination catalysis.[4] This great success is due to their versatility, as already hinted above, their low toxicity if compared with other plastic materials,[5] and, importantly, to the fact that they're one of the cheapest polymer classes on the global market.

Of the two more common classes of PO, polypropylene and polyethylene, the latter is the simplest with general formula $(\text{-}CH_2CH_2\text{-})_n$ (n = number of ethylene unit). Depending on the process used during the synthesis and the properties of the resins, it is possible to design three major polyethylene sub-categories: high density polyethylene (HDPE), low density polyethylene (LDPE) and linear low density polyethylene (LLDPE).

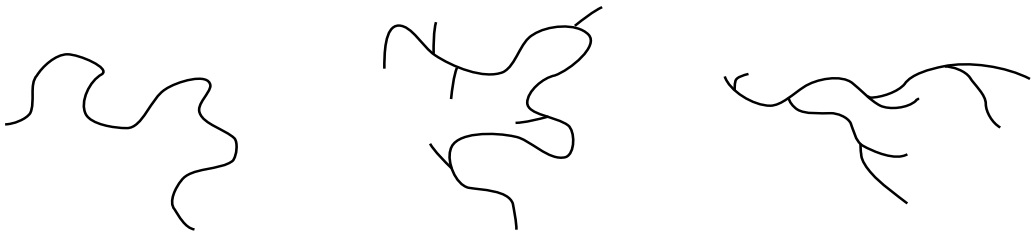

Figure 1 – simplified structure of the polymeric chains of the three different categories of polyethylene.

Of these three, HDPE and LLDPE are synthesized by coordination catalysis polymerization while LDPE by radical polymerization. The classification is based on the polymers' density, direct consequence of the chains' microstructure, and production process.

- HDPE resins have densities comprised between 945 and 970 Kg/m^3, the chains are highly linear with little to no branching, and the polymerization is promoted by coordination catalysis;
- LLDPE resins have densities in the order of 915 - 925 Kg/m^3. The lower density is due to the presence along the chain of controlled Short Chain Branching (SCB), obtained by incorporation of longer linear α-olefins (1-butene, 1-hexene and 1-ocetene) during the polymerization. To achieve this controlled insertion, the polymerization is performed by coordination catalysis;
- LDPE is characterized by densities of 910 - 940 Kg/m^3. Low density polyethylene is the only class of PE produced by radical processes, in conditions of very high temperatures and pressures. The macromolecules undergo a great number of side reactions, which results in a poor control of the polymer microstructure; the chains are in fact characterized by the presence of both SCB and Long Chain Branching (LCB).

The great difference in properties achievable starting by the same simple building block is what is more fascinating of polyolefins and of their great advantages.

How it began

The first process to be discovered and implemented for the production of polyethylene was the radical polymerization process for the synthesis of LDPE.[4] In 1937 the synthesis at high temperature (200-300°C) and elevated pressures (1000-4000 bar) of low density polyethylene was patented by Fawcett and Gibson, and in 1939 the industrial production of LDPE started, and the resin has begun to be used as an insulator.[6]

After the first discovery and industrial application of LDPE, great relevance was given to the development of a catalytic process for the production of polyethylene; and in the '50s two major discoveries consented the development of two processes for the synthesis of polyethylene in mild conditions.

Introduction

In 1951 Hogan and Banks at the Phillips Petroleum company reported that chromium oxides on silica-alumina surface were able to polymerize ethylene for producing HDPE.[7] Surprisingly after less than four years of fine tuning the process was already commercialized. The interesting aspects of Phillip's catalysts is the fact that they don't require any activation by any other agent than the monomer. Being heterogeneous catalysts, Phillip's catalysts present all the inconvenient of this class of catalysts: the presence of a multitude of different active sites on the surface impedes a fine tuning of the product, moreover it was very difficult to identify which was the structure but also the Cr oxidation state of the active site.[8] Due to the presence of different active site on the surface, the resins obtained with Phillips catalysts are characterized by a very broad molecular weight distribution (Đ ∼ 10) and present a small amount of LCB; these microstructural features give rise to good mechanical properties, such that HDPE produced by Cr catalysts still occupies 40-50% of the high density polyethylene production.[7,9–12]

Around the same time as the first development of the Phillips catalyst, in Germany, Ziegler discovered that by associating triethylaluminium with titanium tetrachloride it was possible to polymerize ethylene in high yield.[13] In 1954, in Italy, Natta used a Ziegler type catalyst to polymerize propylene in a stereoregular fashion.[14] All throughout the '60s and the '70s, a great effort was put in fine-tuning and exploiting the capabilities of Ziegler-Natta catalysts. The real step forward, though, was made when the crystalline form of titanium trichloride, β-$TiCl_3$, was abandoned for the δ-$TiCl_3$, causing a major gain in polymerization activity.[15] From that point onwards the technology behind Ziegler-Natta catalysis and process has only made steps forward increasing activity and product stereo- and regio-regularity, making it the catalyst of election for isotactic polypropylene and the second most used catalysts for HDPE. Ziegler Natta catalysts are nowadays currently widely used on the market for the production of various grades of LLDPE, by copolymerization of ethylene with linear α-olefins (e.g. 1-butene, 1-hexene, 1-octene…).

In the 1970s another breakthrough took place in the field of olefin coordination catalysis polymerization. Already since the late '50s titanocene complexes were used in combination with alkylaluminums in ethylene and propylene polymerization as models for the Ziegler-Natta catalysts.[16] These systems, though, presented very low activities. The situation completely changed when in 1976 Sinn and Kaminsky reported the discovery of a new activating agent,

methylaluminoxane, that would greatly enhance the activity of titanocene complexes.[17] Methylaluminoxane, MAO, was obtained by stoichiometric reaction of trimethylaluminium with water, forming cage-like structure of general formula (-Al-O-(Me)-)$_n$ with n = 5-20. Numerous studies have since been performed to elucidate the MAO's structure and it's interaction with the active sites,[18–20] it is in fact thanks to MAO that olefin polymerization catalysis promoted by metallocene has acquired an important stage in the polyolefin field.[21]

The development of molecular catalysts, flourished since the '80s thanks to the employment of MAO, not only consented to study the active site and mechanism involved in ethylene polymerization,[22,23] but pushed the development of more tailored and microstructurally controlled resins.

In fact, the greatest advantage presented by metallocenes and other 'single-site' catalysts resides in the possibility of precisely defining the ligand environment surrounding the active site, leading to a precise control of the microstructure of the produced polymer. Playing with the symmetry of the complexes it was possible to synthesize differently stereoregular resins:[24] isotactic polypropylene (*i*-PP), with a higher control on the degree of isotacticity, with respect to the resins obtained with ZN catalysts,[25,26] depending on the steric hindrance of the active site; syndiotactic[27] polypropylene (*s*-PP) or also hemi-isotactic[28] polypropylene (*hi*-PP).

For what concerns the ethylene polymerization catalysts, it was possible to favour or discourage the affinity of the active site for the comonomer by opening or closing the bite angle of the ligands on the metal centre. This led to the development of different complexes than the classic metallocenes of group 4 metals:[29,30] The *ansa*-cyclopentadienyl-amido complexes of titanium, also referred to as constrained geometry catalysts (CGC) are an example of these developments.[31–34] The openness of the active site favoured greatly the insertion of longer α-olefins, favouring the production of LLDPEs with a higher comonomer incorporation.[35]

As the development of new molecular catalysts became more and more important on the scientific scene, so was the push to find new molecular activators for 'single-site' systems. In 1990 the discovery made by Marks[36,37] and Ewen that the tris-pentafluorophenyl borane was an efficient activator for metallocenes, brought up the development of a new class of activators which didn't

need to be present in great excess with respect to the active species.[38] Notably the great efficiency obtained with boranes and even more with borates systems,[39,40] led to development of homologous systems based on different metal centres than Boron[41,42]

The development of molecular catalysis consented the synthesis of tailored polymer molecules with increasing performance capability,[43] thanks both to the possibility of controlling the ligand environment of the active site and to the 'single-site' nature of most molecular catalysts. But if this is true, why is the polyolefin market still dominated nowadays by Ziegler-Natta and Cr catalysts?

The answer is that, although a narrower molecular weight distribution avoids the presence in the final product of undesirable volatiles, at the same time the processing of the resins requires a dispersity larger than two, to lower the shear stress to which the polymer is subjected during the extrusion. This issue can be solved during the polymerization process, by operating the catalysts in two different reactors in two different conditions, obtaining thus a controlled enlargement of the molecular weight and chemical composition distributions of the resins.[43–47] At the same time, though, the synthesis of metallocene catalysts is more expensive than the classic heterogeneous catalysts and cannot be used in classical heterogeneous processes, gas or slurry phase, developed for the ZN and the Phillips systems. This makes 'single-site' catalysts unsuitable for the production of grades of low added value.

The obligation posed by molecular catalysts to use homogeneous solution processes, although some are still in use today (like "Dowlex" of the Dow Chemicals), creates numerous handling issues, from the lack of morphology of the final product to the fouling of reactors. To put aside this problem and gain all the advantages of heterogeneous catalysts, the scientific development focused on the immobilization of the 'single-site' catalysts on supports such as silica or $MgCl_2$. This approach would combine the advantages of both molecular and heterogeneous catalysts: on one side the ability of finely controlling the polymer characteristics and on the other the easier process handling of the catalyst and good morphology control of the polymer particles.[3,48,49]

Two are the approaches viable for the heterogenization of a molecular catalyst: binding directly the catalyst precursor to the surface of the support and the activator is then coordinated to it;

supporting the cocatalyst, generating a solid activator, and then support the catalyst by coordination to the supported cocatalyst. While binding directly the catalyst to the supports avoids risks of leaching, and thus loss of control of the process, the modification of the coordination environment of the active site could affect the final product's microstructure. In the case of solid activators, to avoid leaching of the active species, it is very important to insure a good coordination of the catalyst to the activator on the surface and an efficient supporting of the latter on the surface. But, generally, in this case the effect of the surface in the product's microstructure is little to none.

The literature on this topic is very reach and comprehend activators of very different nature the ones from the others. In the first chapter of this manuscript it is going to be presented a brief review of the most notable solid activators employed nowadays in industrial production and what are the factors to take into account when heterogenizing a molecular catalyst.

The obtained results during this work is going to be focussed on the development by Surface Organometallic Chemistry of new activating supports based on aluminium and yttrium for metallocene based Zr for ethylene polymerization. The study of the activating support based on Yttrium allowed us to discover an innovative supported yttrium based catalyst bearing allyl ligand that showed high activity in ethylene slurry polymerization.

Chapter II will discuss the synthesis and characterization of a bipodal aluminate activating support, AS1, of structure $[(\equiv SiO)_2Al(OC_6F_5)_2]^-[HNEtMe_2]^+$. The activator was then tested as cocatalyst at a lab scale for two zirconocene precursors, *rac*-$EtInd_2ZrCl_2$ and (*n*-$BuMeCp)_2ZrCl_2$, and at pre-industrial scale for *rac*-$EtInd_2ZrCl_2$ in slurry ethylene/1-hexene copolymerization. In a second section of the chapter is presented the isolation of formulated catalysts by reaction of *rac*-$EtInd_2ZrMe_2$ and (*n*-$BuMeCp)_2ZrMe_2$ with AS1, their characterization and application in both slurry and gas phase ethylene polymerization at lab scale. The stability of the active species on the formulated catalysts surface was also investigated by means of solid state NMR spectroscopy, DRIFT spectroscopy and mass balance analysis.

In Chapter III is presented the synthesis of five different activating supports obtained by the modification of the same grafted Al precursor, $(\equiv SiO)_2AlH(NEtMe_2)$, with five different ligands. All

the activating supports were tested as cocatalysts for *rac*-EtInd$_2$ZrCl$_2$ in slurry ethylene/1-hexene copolymerization. The aim is to investigate the effect of the nature of the ligand on the efficiency of the activating support.

Chapter IV is divided in two sections. In the first one is discussed the synthesis and characterization of Al-based activating support where the Al is bearing at least on Al-X bond, where X is an halogen atom, F or Cl. The obtained activating supports were tested as cocatalysts for *rac*-EtInd$_2$ZrCl$_2$ in ethylene/1-hexene slurry copolymerization. The aim was to increase the efficiency of the activating support by increasing the acidity of surface sites.[3,48] In the second section of Chapter IV is described the synthesis and characterization of four activating supports featuring an Y as metal centre. It was in fact seen, by Marks et al.,[41,42] that by using Y-based cocatalysts it was possible to reduce ligand transfer phenomena between the cocatalyst and the zirconocene active species, observed with Al-based cocatalysts. The Y-based activating supports obtained were tested in ethylene/1-hexene slurry copolymerization.

In Chapter V is instead presented the application in ethylene slurry polymerization of four grafted Y precursor, (≡SiO)Y(*o*-NMe$_2$toluidine)$_2$, (≡SiO)$_2$Y(*o*-NMe$_2$toluidine), (≡SiO)Y{1,3-C$_3$H$_3$(SiMe$_3$)$_2$}$_2$, (≡SiO)$_2$Y{1,3-C$_3$H$_3$(SiMe$_3$)$_2$}. The synthesis and characterization of these species was presented in Chapter IV as precursors for the Y-based activating supports. It is widely diffused in literature of Y neutral and cationic species as catalysts for ethylene polymerization[50–52], keeping this in mind the four obtained well-defined species were tested in slurry ethylene polymerization at lab scale and the monopodal (≡SiO)Y{1,3-C$_3$H$_3$(SiMe$_3$)$_2$}$_2$ was employed in pre-industrial scale polymerization. Moreover, in Chapter V is presented also the synthesis and of cationic Y species by reaction of the neutral precursors (≡SiO)Y{1,3-C$_3$H$_3$(SiMe$_3$)$_2$}$_2$ and (≡SiO)$_2$Y{1,3-C$_3$H$_3$(SiMe$_3$)$_2$} with [B(C$_6$F$_5$)$_4$]$^-$ [Ph$_3$C]$^+$, and their application in ethylene polymerization.

References

(1) Al-Ali AlMa'adeed, M.; Krupa, I. Introduction. In *Polyolefin Compounds and Materials*; Al-Ali AlMa'adeed, M., Krupa, I., Eds.; Springer International Publishing: Cham, 2016; pp 1–11. https://doi.org/10.1007/978-3-319-25982-6_1.

(2) Hutley, T. J.; Ouederni, M. Polyolefins—The History and Economic Impact. In *Polyolefin Compounds and Materials*; Al-Ali AlMa'adeed, M., Krupa, I., Eds.; Springer International Publishing: Cham, 2016; pp 13–50. https://doi.org/10.1007/978-3-319-25982-6_2.

(3) *Tailor-Made Polymers: Via Immobilization of Alpha-Olefin Polymerization Catalyst*; Severn, J., Ed.; Wiley-VCH: Weinheim, 2008.

(4) *Advances in Polyolefins*; Seymour, R. B., Cheng, T., Eds.; Springer US: Boston, MA, 1987. https://doi.org/10.1007/978-1-4757-9095-5.

(5) Tabone, M. D.; Cregg, J. J.; Beckman, E. J.; Landis, A. E. Sustainability Metrics: Life Cycle Assessment and Green Design in Polymers. *Environ. Sci. Technol.* **2010**, *44* (21), 8264–8269. https://doi.org/10.1021/es101640n.

(6) Utracki, L. A. *Polymer Blends*; Rapra review reports; Rapra Technology Ltd: Shawbury, Shrewsbury, 2000.

(7) Sailors, H. R.; Hogan, J. P. History of Polyolefins. *J. Macromol. Sci. Part - Chem.* **1981**, *15* (7), 1377–1402. https://doi.org/10.1080/00222338108056789.

(8) Brown, C.; Krzystek, J.; Achey, R.; Lita, A.; Fu, R.; Meulenberg, R. W.; Polinski, M.; Peek, N.; Wang, Y.; van de Burgt, L. J.; Profeta, S.; Stiegman, A. E.; Scott, S. L. Mechanism of Initiation in the Phillips Ethylene Polymerization Catalyst: Redox Processes Leading to the Active Site. *ACS Catal.* **2015**, *5* (9), 5574–5583. https://doi.org/10.1021/acscatal.5b00927.

(9) Hogan, J. P. Ethylene Polymerization Catalysis over Chromium Oxide. *J. Polym. Sci. [A1]* **1970**, *8* (9), 2637–2652. https://doi.org/10.1002/pol.1970.150080929.

(10) McDaniel, M. P. Supported Chromium Catalysts for Ethylene Polymerization. In *Advances in Catalysis*; Elsevier, 1985; Vol. 33, pp 47–98. https://doi.org/10.1016/S0360-0564(08)60258-8.

(11) McDaniel, M. P.; Rohlfing, D. C.; Benham, E. A. Long Chain Branching in Polyethylene from the Phillips Chromium Catalyst. *Polym. React. Eng.* **2003**, *11* (2), 101–132. https://doi.org/10.1081/PRE-120021071.

(12) Janzen, J.; Colby, R. H. Diagnosing Long-Chain Branching in Polyethylenes. *J. Mol. Struct.* **1999**, *485–486*, 569–583. https://doi.org/10.1016/S0022-2860(99)00097-6.

(13) Ziegler, K.; Holzkamp, E.; Breil, H.; Martin, H. Polymerisation von Äthylen Und Anderen Olefinen. *Angew. Chem.* **1955**, *67* (16), 426–426.

(14) Natta, G.; Pino, P.; Corradini, P.; Danusso, F.; Mantica, E.; Mazzanti, G.; Moraglio, G. CRYSTALLINE HIGH POLYMERS OF α-OLEFINS. *J. Am. Chem. Soc.* **1955**, *77* (6), 1708–1710. https://doi.org/10.1021/ja01611a109.

(15) Kissin, Y. V. *Alkene Polymerization Reactions with Transition Metal Catalysts*; Studies in surface science and catalysis; Elsevier: Amsterdam ; Boston, 2008.
(16) Breslow, D. S.; Newburg, N. R. BIS-(CYCLOPENTADIENYL)-TITANIUM DICHLORIDE — ALKYLALUMINUM COMPLEXLS AS CATALYSTS FOR THE POLYMERIZATION OF ETHYLENE. *J. Am. Chem. Soc.* **1957**, *79* (18), 5072–5073. https://doi.org/10.1021/ja01575a066.
(17) Andresen, A.; Cordes, H.-G.; Herwig, J.; Kaminsky, W.; Merck, A.; Mottweiler, R.; Pein, J.; Sinn, H.; Vollmer, H.-J. Halogen-Free Soluble Ziegler Catalysts for the Polymerization of Ethylene. Control of Molecular Weight by Choice of Temperature. *Angew. Chem. Int. Ed. Engl.* **1976**, *15* (10), 630–632. https://doi.org/10.1002/anie.197606301.
(18) Ghiotto, F.; Pateraki, C.; Tanskanen, J.; Severn, J. R.; Luehmann, N.; Kusmin, A.; Stellbrink, J.; Linnolahti, M.; Bochmann, M. Probing the Structure of Methylalumoxane (MAO) by a Combined Chemical, Spectroscopic, Neutron Scattering, and Computational Approach. *Organometallics* **2013**, *32* (11), 3354–3362. https://doi.org/10.1021/om4002878.
(19) Hirvi, J. T.; Bochmann, M.; Severn, J. R.; Linnolahti, M. Formation of Octameric Methylaluminoxanes by Hydrolysis of Trimethylaluminum and the Mechanisms of Catalyst Activation in Single-Site α-Olefin Polymerization Catalysis. *ChemPhysChem* **2014**, *15* (13), 2732–2742. https://doi.org/10.1002/cphc.201402298.
(20) Linnolahti, M.; Collins, S. Formation, Structure, and Composition of Methylaluminoxane. *ChemPhysChem* **2017**, *18* (23), 3369–3374. https://doi.org/10.1002/cphc.201700827.
(21) Kaminsky, W. The Discovery of Metallocene Catalysts and Their Present State of the Art. *J. Polym. Sci. Part Polym. Chem.* **2004**, *42* (16), 3911–3921. https://doi.org/10.1002/pola.20292.
(22) Jordan, R. F.; Dasher, W. E.; Echols, S. F. Reactive Cationic Dicyclopentadienyl Zirconium(IV) Complexes. *J. Am. Chem. Soc.* **1986**, *108* (7), 1718–1719. https://doi.org/10.1021/ja00267a068.
(23) Jordan, R. F.; Bajgur, C. S.; Willett, Roger.; Scott, Brian. Ethylene Polymerization by a Cationic Dicyclopentadienyl Zirconium(IV) Alkyl Complex. *J. Am. Chem. Soc.* **1986**, *108* (23), 7410–7411. https://doi.org/10.1021/ja00283a047.
(24) Corradini, P.; Guerra, G.; Cavallo, L. Do New Century Catalysts Unravel the Mechanism of Stereocontrol of Old Ziegler−Natta Catalysts? *Acc. Chem. Res.* **2004**, *37* (4), 231–241. https://doi.org/10.1021/ar030165n.
(25) Ewen, J. A. Mechanisms of Stereochemical Control in Propylene Polymerizations with Soluble Group 4B Metallocene/Methylalumoxane Catalysts. *J. Am. Chem. Soc.* **1984**, *106* (21), 6355–6364. https://doi.org/10.1021/ja00333a041.
(26) Kaminsky, W.; Külper, K.; Brintzinger, H. H.; Wild, F. R. W. P. Polymerization of Propene and Butene with a Chiral Zirconocene and Methylalumoxane as Cocatalyst. *Angew. Chem. Int. Ed. Engl.* **1985**, *24* (6), 507–508. https://doi.org/10.1002/anie.198505071.

(27) Ewen, J. A.; Jones, R. L.; Razavi, A.; Ferrara, J. D. Syndiospecific Propylene Polymerizations with Group IVB Metallocenes. *J. Am. Chem. Soc.* **1988**, *110* (18), 6255–6256. https://doi.org/10.1021/ja00226a056.

(28) Ewen, J. A.; Elder, M. J.; Jones, R. L.; Haspeslagh, L.; Atwood, J. L.; Bott, S. G.; Robinson, K. Metallocene/Polypropylene Structural Relationships: Implications on Polymerization and Stereochemical Control Mechanisms. *Makromol. Chem. Macromol. Symp.* **1991**, *48–49* (1), 253–295. https://doi.org/10.1002/masy.19910480121.

(29) Gielens, E. E. C. G.; Tiesnitsch, J. Y.; Hessen, B.; Teuben, J. H. Titanium Hydrocarbyl Complexes with a Linked Cyclopentadienyl−Alkoxide Ancillary Ligand; Participation of the Ligand in an Unusual Activation of a (Trimethylsilyl)Methyl Group †. *Organometallics* **1998**, *17* (9), 1652–1654. https://doi.org/10.1021/om970867e.

(30) Shapiro, P. J.; Bunel, E.; Schaefer, W. P.; Bercaw, J. E. Scandium Complex [{(.Eta.5-C5Me4)Me2Si(.Eta.1-NCMe3)}(PMe3)ScH]2: A Unique Example of a Single-Component .Alpha.-Olefin Polymerization Catalyst. *Organometallics* **1990**, *9* (3), 867–869. https://doi.org/10.1021/om00117a055.

(31) Cano, J.; Kunz, K. How to Synthesize a Constrained Geometry Catalyst (CGC) – A Survey. *J. Organomet. Chem.* **2007**, *692* (21), 4411–4423. https://doi.org/10.1016/j.jorganchem.2007.05.015.

(32) Cano, J.; Sudupe, M.; Royo, P. Synthesis and Reactivity of Di(Silylamido)Cyclopentadienyl Titanium and Zirconium Complexes. *J. Organomet. Chem.* **2007**, *692* (21), 4448–4459. https://doi.org/10.1016/j.jorganchem.2007.06.049.

(33) Chen, Y.-X.; Fu, P.-F.; Stern, C. L.; Marks, T. J. A Novel Phenolate “Constrained Geometry” Catalyst System. Efficient Synthesis, Structural Characterization, and α-Olefin Polymerization Catalysis. *Organometallics* **1997**, *16* (26), 5958–5963. https://doi.org/10.1021/om9707376.

(34) McKnight, A. L.; Waymouth, R. M. Group 4 *Ansa*- Cyclopentadienyl-Amido Catalysts for Olefin Polymerization. *Chem. Rev.* **1998**, *98* (7), 2587–2598. https://doi.org/10.1021/cr940442r.

(35) Braunschweig, H.; Breitling, F. M. Constrained Geometry Complexes—Synthesis and Applications. *Coord. Chem. Rev.* **2006**, *250* (21–22), 2691–2720. https://doi.org/10.1016/j.ccr.2005.10.022.

(36) Yang, X.; Stern, C. L.; Marks, T. J. Cation-like Homogeneous Olefin Polymerization Catalysts Based upon Zirconocene Alkyls and Tris(Pentafluorophenyl)Borane. *J. Am. Chem. Soc.* **1991**, *113* (9), 3623–3625. https://doi.org/10.1021/ja00009a076.

(37) Yang, X.; Stern, C. L.; Marks, T. J. Cationic Zirconocene Olefin Polymerization Catalysts Based on the Organo-Lewis Acid Tris(Pentafluorophenyl)Borane. A Synthetic,Structural, Solution Dynamic, and Polymerization Catalytic Study. *J. Am. Chem. Soc.* **1994**, *116* (22), 10015–10031. https://doi.org/10.1021/ja00101a022.

(38) Chen, E. Y.-X.; Marks, T. J. Cocatalysts for Metal-Catalyzed Olefin Polymerization: Activators, Activation Processes, and Structure−Activity Relationships. *Chem. Rev.* **2000**, *100* (4), 1391–1434. https://doi.org/10.1021/cr980462j.

(39) Chien, J. C. W.; Tsai, W. M.; Rausch, M. D. Isospecific Polymerization of Propylene Catalyzed by Rac-Ethylenebis(Indenyl)Methylzirconium Cation. *J. Am. Chem. Soc.* **1991**, *113* (22), 8570–8571. https://doi.org/10.1021/ja00022a081.

(40) Yang, Xinmin.; Stern, Charlotte.; Marks, T. J. Models for Organometallic Molecule-Support Complexes. Very Large Counterion Modulation of Cationic Actinide Alkyl Reactivity. *Organometallics* **1991**, *10* (4), 840–842. https://doi.org/10.1021/om00050a008.

(41) Metz, M. V.; Sun, Y.; Stern, C. L.; Marks, T. J. Weakly Coordinating Al-, Nb-, Ta-, Y-, and La-Based Perfluoroaryloxymetalate Anions as Cocatalyst Components for Single-Site Olefin Polymerization. *Organometallics* **2002**, *21* (18), 3691–3702. https://doi.org/10.1021/om020087s.

(42) Sun, Y.; Metz, M. V.; Stern, C. L.; Marks, T. J. Al-, Nb-, and Ta-Based Perfluoroaryloxide Anions as Cocatalysts for Metallocene-Mediated Ziegler−Natta Olefin Polymerization. *Organometallics* **2000**, *19* (9), 1625–1627. https://doi.org/10.1021/om990946l.

(43) Stürzel, M.; Mihan, S.; Mülhaupt, R. From Multisite Polymerization Catalysis to Sustainable Materials and All-Polyolefin Composites. *Chem. Rev.* **2016**, *116* (3), 1398–1433. https://doi.org/10.1021/acs.chemrev.5b00310.

(44) Ruff, M.; Paulik, C. Controlling Polyolefin Properties by In-Reactor Blending, 1-Polymerization Process, Precise Kinetics, and Molecular Properties of UHMW-PE Polymers. *Macromol. React. Eng.* **2012**, *6* (8), 302–317. https://doi.org/10.1002/mren.201200019.

(45) Ruff, M.; Paulik, C. Controlling Polyolefin Properties by In-Reactor Blending: 2. Particle Design. *Macromol. React. Eng.* **2013**, *7* (2), 71–83. https://doi.org/10.1002/mren.201200050.

(46) Ruff, M.; Lang, R. W.; Paulik, C. Controlling Polyolefin Properties by In-Reactor Blending: 3. Mechanical Properties. *Macromol. React. Eng.* **2013**, *7* (7), 328–343. https://doi.org/10.1002/mren.201200077.

(47) Mei, G.; Herben, P.; Cagnani, C.; Mazzucco, A. The Spherizone Process: A New PP Manufacturing Platform. *Macromol. Symp.* **2006**, *245–246* (1), 677–680. https://doi.org/10.1002/masy.200651395.

(48) Severn, J. R.; Chadwick, J. C.; Duchateau, R.; Friederichs, N. "Bound but Not Gagged"Immobilizing Single-Site α-Olefin Polymerization Catalysts. *Chem. Rev.* **2005**, *105* (11), 4073–4147. https://doi.org/10.1021/cr040670d.

(49) Severn, J. R.; Chadwick, J. C. Immobilisation of Homogeneous Olefin Polymerisation Catalysts. Factors Influencing Activity and Stability. *Dalton Trans.* **2013**, *42* (25), 8979. https://doi.org/10.1039/c3dt33098b.

(50) Schumann, Herbert.; Meese-Marktscheffel, J. A.; Esser, Lothar. Synthesis, Structure, and Reactivity of Organometallic .Pi.-Complexes of the Rare Earths in the Oxidation State Ln3+ with Aromatic Ligands. *Chem. Rev.* **1995**, *95* (4), 865–986. https://doi.org/10.1021/cr00036a004.

(51) Zeimentz, P. M.; Arndt, S.; Elvidge, B. R.; Okuda, J. Cationic Organometallic Complexes of Scandium, Yttrium, and the Lanthanoids. *Chem. Rev.* **2006**, *106* (6), 2404–2433. https://doi.org/10.1021/cr050574s.

(52) Le Roux, E.; Anwander, R. Surface Organolanthanide and -Actinide Chemistry. In *Modern Surface Organometallic Chemistry*; Basset, J.-M., Psaro, R., Roberto, D., Ugo, R., Eds.; Wiley-VCH Verlag GmbH & Co. KGaA: Weinheim, Germany, 2009; pp 455–512. https://doi.org/10.1002/9783527627097.ch12.

Chapter I:
Bibliographic review

Index

1. *Why the immobilization of the molecular catalysts?*

In the introduction it was briefly outlined how the supported metallocenes for polyethylene production present great interest from a commercial point of view. In fact immobilizing single-site molecular catalysts on a carrier would allow their utilization in slurry and gas-phase processes.[1]

As anticipated in the introduction, although some solution processes still exist, they present a number of inconveniencies.[1,2] Generally solution processes involve adiabatic reactions in hydrocarbon solvents at relatively high temperatures, 130-250°C, sufficient to keep the polymer in solution. At the end of the process the polymer separation from the solvent by vaporization and the recycling of the latter are high-energy-consuming stages of the overall process. One more inconvenience is that, since the polymer is kept in the solution phase, the viscosity of the medium increases rapidly with the molar mass, preventing the synthesis of high molar mass polymers.

Way more diffused is the use of heterogeneous processes such as slurry phase or gas phase processes.

In slurry processes[1,2] the heterogeneous catalyst is dispersed in an aliphatic hydrocarbon diluent. The original slurry phase processes were conducted in CSTR reactors at low temperatures, 70-90°C, and low ethylene pressures, 2-24 bar. One of the inconveniences of CSTR slurry processes is the limited range of grades achievable due to the high solvent-induced swelling that occurs with low density and low molar mass polyolefin grades. One of the crucial parameters in all olefin polymerization processes to take into account is heat removal. Olefin polymerization is in fact a very exothermic process, and if heat removal isn't optimal, in a slurry process specifically, the formation of 'hot spots' could occur, leading locally to softening of the polymer and agglomerate formation. These reactors are generally fitted with cooling jackets, and equipped with external heat exchangers and condensation units for the diluent.

Another important process for slurry-phase polymerization involves the use of slurry loop reactors,[3–7] which could have one or multiple loops in series in vertical or horizontal configuration; an example is the Phillips slurry loop process (Figure 1). In these reactors the heat-exchanging is way more efficient since there's a higher area-to-volume ratio for the cooling jackets surrounding

the pipes. In order to further ensure heat-exchange the conditions are chosen to operate in full liquid phase. Moreover, the solvent employed is isobutane, a light hydrocarbon, allowing to reduce the solubility and swelling problems encountered in the CSTR reactors, thus broadening the slate of grades achievable by the process. The temperatures employed vary between 85 and 110°C with pressures in the range 35-45 bars. The polymer is extracted in continuous and recovered by flashing of the diluent, which will then be recycled.

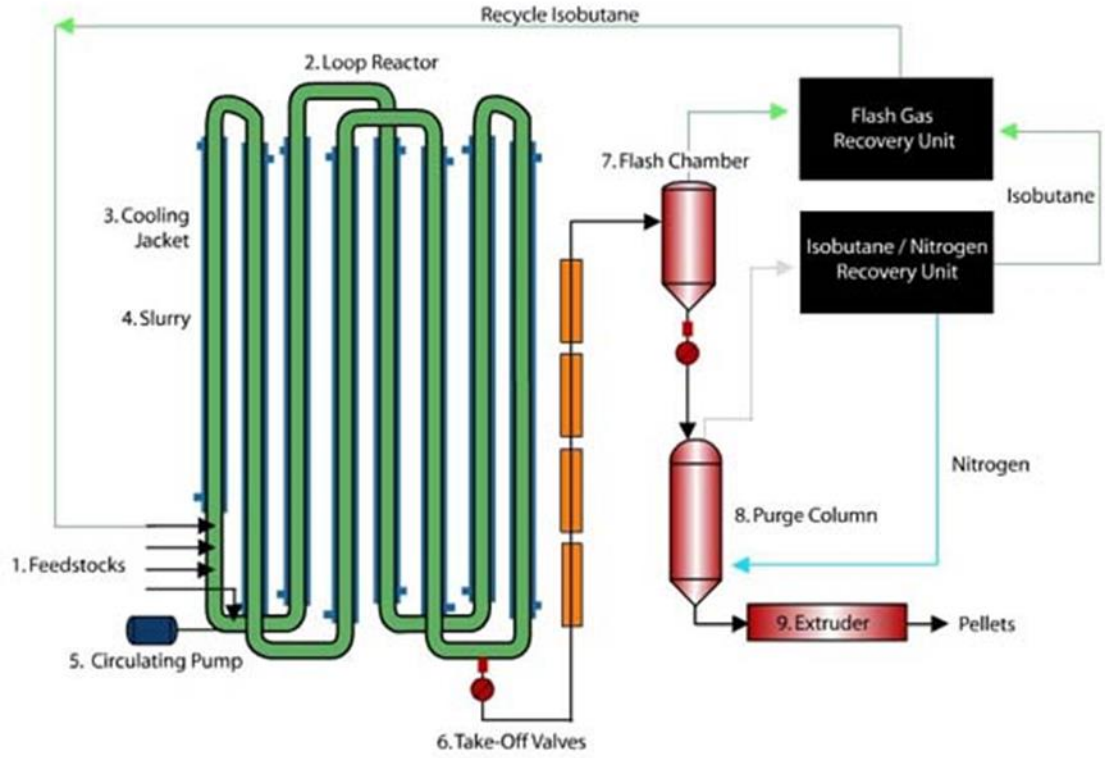

Figure 1 – Scheme of the Phillips slurry loop process.

For gas-phase processes are generally used vertical fluidized bed reactors, comprising a cylindrical reaction zone in which a polymer particle bed is suspended over a perforated grid by a carrier gas flow.[1,2,8–13] The carrier gas is composed by monomers and inert gases. It is clear that the velocity of the gas flow is a crucial parameter for the process: it has in fact has to be high enough to insure the suspension of the bed, but not such as to expel all of the particles out of the reactor. The catalysts employed are supported ones which can be fed in the reactor both in a continuous or semi continuous fashion. Like for the processes described previously it is fundamental to insure

the cooling of the reactor and an efficient heat-exchange, more difficult in this case given the absence of a diluent. In a fluidized bed process is the gas stream itself to serve as heat-exchanging medium. The gas exiting the reactor is recycled and fed again to the bed after having passed through a series of compressor and heat exchangers. If necessary it is possible to add additional cooling by feeding the reactor with a volatile hydrocarbon, like pentane. In the case of highly active catalysts, it possible to operate the reactors in "condensed" mode, where the monomers or other volatile hydrocarbons are injected in their condensed phase, and the heat of vaporization is used as added cooling agent. The typical operating temperatures in a fluidized bed process are between 70 and 115°C with pressures in the range of 20-30 bars. In Figure 2 is reported the scheme of the Unipol process.

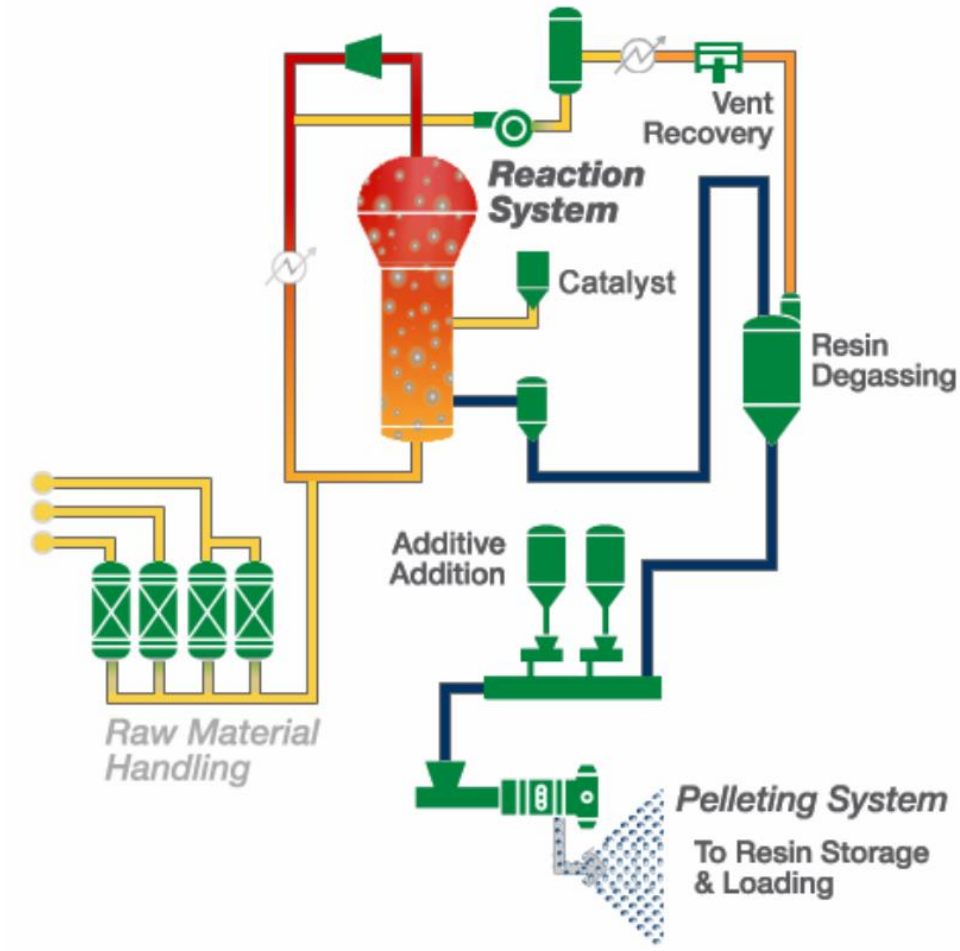

Figure 2 – Scheme of the Unipol gas-phase process.

Since the 1970s, a plethora of molecular complexes of different families have been synthesized and employed in ethylene polymerization.[14–18] Notably some have been employed commercially in renown processes, generally supported on silica/MAO. Unbridged metallocenes have been employed in both Mitsui Evolue gas phase process[19,20] and the Borealis Borstar loop/gas process.[21,22] Total employs bridged zirconocenes for the production of a great number of grades in the bimodal loop processes.[23–26] Dow Chemical, on the other hand developed its technology around CGC catalysts on silica-supported borates,[27–29] which are currently commercialized by INOES[30] for the application in LLDPE gas phase polymerization. The latest catalysts developed and commercialized are the "O_4"-based, bis-hyroxylarylaryloxy complexes, which have a huge structural flexibility, giving great marge to innovation. They have already been employed in different processes for the production of numerous products[31–35] and supported on both silica/MAO and anchored borate.[36,37]

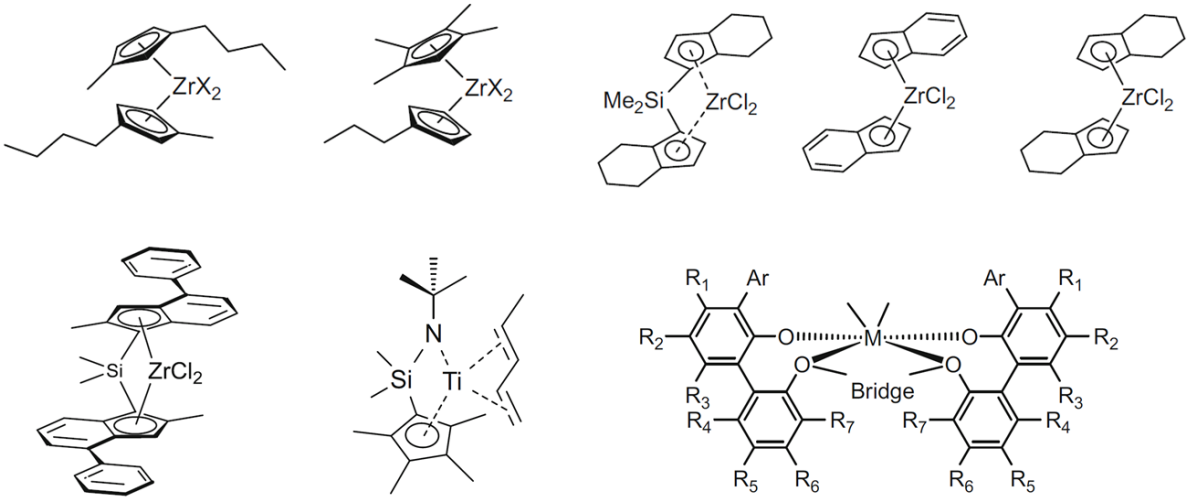

Figure 3 – Representation of some of the most common catalyst precursors for olefin polymerization.

All of the systems cited are currently applied in either gas-phase or slurry loop processes, which require the catalyst to be immobilized on a suitable support material, to prevent reactor fouling.[38] The heterogenization of the molecular catalysts for industrial application generally sees the chemical binding of the activator on a support and the immobilization of the active species by formation of an ion pair with the supported cocatalyst.[1] Silica/MAO is probably one of the most

common systems currently used, in this chapter we are going to discuss the advantages and disadvantages of this activator, as well as some other solid activators and their application.

Before plunging deep in the preparation of the support and the immobilization of the molecular catalysts, it is vital to understand what influence can have the immobilization itself on the activity and stability of the olefin polymerization catalysts.[38]

1.1 Chemical and physical effects of immobilization

Depending on the nature of both the catalyst precursor and the employed support for the catalyst preparation, it is possible to have opposite effects on the activity. It is renown that whether some catalysts show lower productivities after immobilizations,[1,39] other achieve a higher stability thanks to the support, not displaying thus the deactivation to which they are subjected in homogeneous processes.[40]

When immobilizing a catalyst, two are the possible methods involved: *physical impregnation* or *chemical tethering.* While physical impregnation of the catalyst or cocatalyst on a support has the advantage of simple synthetic procedures, it also presents great risks of leaching during the polymerization reaction. On the other hand, chemical binding of the catalyst or activator on the reactive sites of the support (SiOH groups in the case of silica, for example), highly reduces the risks of leaching of the active species, but at the same time it involves long and tricky synthetic procedures.[38]

In discussing the influence of the support on the catalyst's activity it is necessary to take into account two different effects: *chemical* and *physical,* which can influence both the stability of the catalyst and the polymer microstructure.

Chemical effects are the principal reason for which direct binding of active complexes on the surface of the supports is generally avoided, and why supporting MAO could generally increase its efficiency when combined with metallocenes.[41] During the reaction of methylaluminoxane with the silica surface, the silanols would preferentially react with the free TMA (trimethylaluminum) of MAO, which is the major responsible for the formation of bimetallic dormant species ($[Cp_2Zr(\mu\text{-}R)(\mu\text{-}Me)AlMe_2]^+$) blocking the coordination of the monomer.

Physical effects have a high impact, in case of ethylene polymerization, when the employed support in the synthesis of the catalysts has a low friability. The fact that the particle doesn't fragment according to the rate of polymer formation inside the pores, leads to diffusion limitations of the monomer.[42] So, it is necessary for the support to have a mechanical strength low enough to favour the particle's expansion during the polymerization, but high enough to avoid its complete disintegration of the particle in the first minutes of the reaction. In this case the presence of pores with a high diameter could favour the fragmentation process.[43] The monomer diffusion is highly influenced also by the crystalline nature of the polymer: the less crystalline the resin, the higher the monomer's diffusion rates.[44–46] It results evident than monomer diffusion is going to be a less limiting factor in LLDPE synthesis than HDPE.

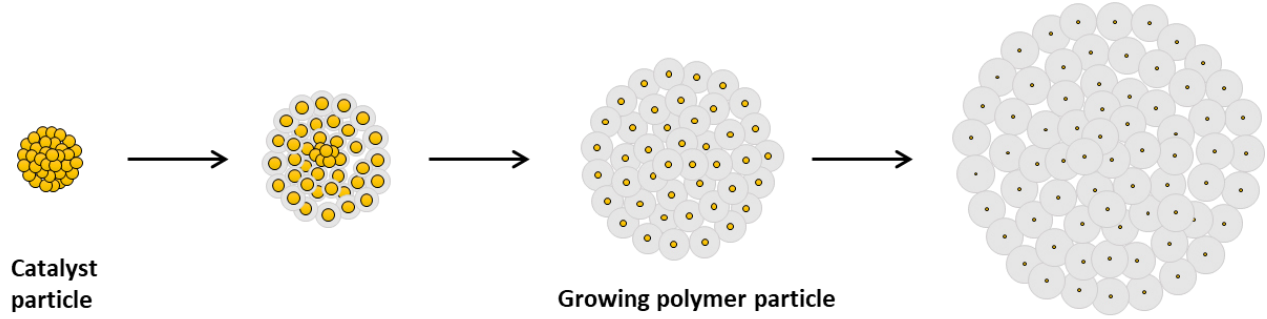

Figure 4 – Schematic representation of the fragmentation of a growing polymer particle.

Another phenomenon which was attributed to the fragmentation process, is a build-up of the activity in the first minutes of the polymerization with some supported metallocene catalysts on SiO_2/MAO.[47] At the very beginning of the polymerization, in fact, only the active sites on the surface of the support are involved in polymerization, while with the advancement of the particle's fragmentation new sites are revealed, increasing the activity until a plateau is reached when the catalyst's particle has fragmented completely.[48]

It is thus very important to define well the operating conditions, in order to limit the effects of physical limitations, which could also overshadow any chemical effects of the immobilization.

1.2 Catalyst stability

During the course of polymerization, metallocene catalysts are subjected to deactivation. Generally the order of stability is Zr > Hf > Ti and it strictly depends on the coordination sphere of

the metal center.[38] Immobilization of the catalyst on a support could either enhance or depress the catalyst stability, in dependence of the interaction that are created with the surface.

In the previous paragraph, it was cited as example the fact that grafting MAO on silica would "trap" the free TMA present in the system, inhibiting the formation of dormant bimetallic species and increasing the activity.[41] It is though necessary to take into account also the fact that the formation of bimetallic adduct protects the catalyst from deactivation, stabilizing the active species. Hindering the formation of bimetallic adducts while increasing the activity of the systems, at the same time causes also a rapid decay of the active centre.[49]

For some other metallocene systems, the high MAO concentration necessary to obtain a good catalyst activation,[50–53] favours bimetallic deactivation of the catalyst by formation of adducts such as [Zr]–CH_2–Al(CH_3)–O– with concomitant methane evolution.[54,55] In these cases, grafting MAO on silica impedes the catalyst's deactivation, stabilizing the activity throughout the polymerization.[56] Notably these systems are currently employed in the synthesis of LLDPE.[57]

It results evident that the immobilization effect on catalyst's stability and activity is strictly dependent on the studied complex.

1.3 Polymer structure

One of the main things to keep in mind when supporting a molecular catalyst is that it should retain its 'single site' nature and that the polymers produced in both homogeneous and heterogeneous phases have to present the same properties. Usually, in the case of solid activators these requirements are met, but it is not possible to define a general rule, the behavior of the catalyst after impregnation is strictly dependent on both the nature of the supported activator and of the active complex.[38]

It is very difficult to foresee the effects of the catalyst's immobilization on the polymer properties, because as said previously it is necessary to take into account the interaction of the active species with the surface of the support (the exact composition of which is sometimes very difficult to unveil) and the nature of the used support, but also the physical effects discussed earlier. For example, in an heterogeneous system, in conditions of mass transfer limitation, the monomer

concentration at the active site is lower than it would have been in homogeneous conditions, causing a drop in the molar mass of the produced resins.[58,59] In addition, gradient of monomer concentration in the polymer particles can lead to broadening of the molar mass distribution.[60]

At the same time the immobilization of the catalyst on a particle can be employed for the development of more complex and performing resins, in simple processes. For example, the immobilization of two catalysts with very different reactivities on the same support, could lead to the synthesis of bimodal resins with high comonomer incorporation in the high molar mass fraction in a one pot synthesis,[61] aim which is usually achieved in 'cascade' reactors by modifying the process conditions to which the catalyst is exposed in moving from on reactor to the second.[62] However the synthesis of such a catalyst is not so straightforward, it is in fact necessary to take into account not only the different reactivity of the two catalysts but also their responses to impurities, to the immobilization on the support and to the process operation.[38]

From all the considerations made up to this point it is clear that, although the immobilization of molecular catalysts is somewhat obliged for industrial application, it requires attention to a number of parameters not negligible.

In the following paragraphs are going to be presented some examples of supported activators currently used, starting from silica/MAO.

2. Activators: Silica/MAO

Undoubtedly methylaluminoxane, MAO, is what made possible the development and application of molecular catalysts.[63] Since its discovery MAO has been tested and studied as cocatalyst of a plethora of molecular catalyst precursors for both ethylene and propylene polymerization.[1] In presence of the precatalyst the MAO has a double role: generator and counter-anion of the active species.[64,65] However, despite its wide application, the very complex (and still partly obscure) structure of MAO makes it difficult to define exactly the mechanism with which this activation takes place.[55,66–69] It is mainly agreed upon that the activation proceeds by abstraction of the chlorides and methylation of the metallocene precursor[70] leading to the formation of a stable ionic couple between the $[MAO\text{-}X]^-$ anion and the active species.[71] What on the other side is not agreed

upon is what are the MAO species responsible of the activation, as well as why, to obtain an efficient catalyst activation, it is necessary to use MAO in a high excess (1000-10000 Al/M).[1]

Recently some studies were conducted to elucidate the structure by ESI-MS of the ions of ionic couple formed upon contacting MAO with a catalyst precursor in solution.[72] Trefz et al. studied the ions formed upon contacting MAO with three different compounds, $[Bu_4N]Cl$, OMTS (octamethyltrisiloxane) and Cp_2ZrMe_2 in perfluorobenzene. Interestingly the study revealed that at low reactant concentration the same anion was formed in solution, regardless of the reactant, characterized by a major peak at 1853 m/z, corresponding to the anion of structure $[Al_5O_8(MeAlO)_{15}(AlMe_3)_{10}]^-$ which can also be represented as $[(MeAlO)_{23}(AlMe_3)_7Me]$-.[72] It is important to stress out the fact that the same ions are formed regardless of the reactant, moreover chlorination of the species occurs only at high concentration of salt in mixtures MAO/$[Bu_4N]Cl$, with the formation of differently chlorinated ions, which in turn can easily generate $AlMe_2Cl$ species. In presence of the zirconocene the major cationic species present was the bimolecular adduct $[Cp_2Zr(\mu\text{-}Me)_2AlMe_2]^+$ [73–76] at 307 m/z. At high reactant concentration on the other side it was possible to observe ion-pair aggregation with cluster formation. This phenomenon could be due to the fact that, while at low reactant concentration just the most reactive components of MAO interact with the reactant, at higher concentration of the reactant more solvated ions are formed, some of which could also support higher negative charges. When the concentration exceeds a certain value, then, it is possible to see the formation of an aggregated ionic phase. This study would suggest that one of the main role of MAO is as source of $[AlMe_2]^+$,[77–79] which is the most reactive species Lewis acid in the mixture investigated, in turn the addition of $[Bu_4N]Cl$ causes chlorination of the species with formation of $AlMe_2Cl$ and weakly coordinated $[Bu_4N][MAO]$. At high concentration of the chlorinating agent, redistribution reactions occur between the species.

The formation of different ion pair adducts at varying Al:Zr ratios can explain why it is necessary to work at more than 500:1 Al:Zr in order to have high activities in solution olefin polymerization.[80] Another study investigated the effect on polymerization activity and polymer molar masses of using as catalyst precursor either Cp_2ZrCl_2 or Cp_2ZrMe_2, activated by MAO in toluene, at different Al:Zr ratios.[81] The two complexes showed the same behavior from a productivity point of view but

very different molar masses and molar mass distribution. Moreover, the article evidenced how, although the catalyst efficiency of the system highly depends on the Al:Zr ratio in the polymerization medium, it is really the [Zr] which dictates the polymerization behavior. It is assumed that at high Zr concentration, ion quadruples and other aggregates can form by reversible association of unhindered ion pairs, and that at this association state, deactivation processes can actively take place.

The situation gets even more tricky when MAO is supported on silica. It is in fact necessary to remember that the majority of the processes for the production of polyolefins relies on solid catalyst particle which could create discrete polymer particles, assuring the good operability of the plants and the absence of fouling.[1,39] It follows that homogeneous 'single-site' catalysts require heterogenization, to be applied in such gas or slurry/loop phase processes.[61] At the same time, as discussed in the previous paragraph, the retention of the 'single-site' nature of the catalyst is tricky after its immobilization on a support, and it requires lots of precautions at the moment of the catalyst's synthesis.

2.1 Immobilization of MAO on SiO_2

Given the great complexity of structures which compose MAO, it becomes challenging to have an insight on how it reacts with the surface of a support like silica.[61] Many studies have been performed to clarify which are the preferential pattern of interaction between MAO and SiO_2.

Upon contacting the two reactants, the silanols present on the surface would preferentially react with the free TMA of MAO.[82,83] Different structures are obtained depending if the trimethylaluminium is in its monomeric or dimeric form. In the first case the aluminium species on the surface would be tri-coordinated and highly reactive Lewis acids,[82] apt to activate the catalyst precursor. On the other side, the surface structures found by Scott et al. are believed to be the result of the reaction between SiO_2 and dimeric TMA, with 4-coordinated aluminium species.[83]

Further studies proposed that the surface SiOH groups would first react with the free TMA and successively with the MAO cages.[84] Surface studies at different loading of MAO show that for Al loadings in the range 0.1-6.0 wt% some silanols are free on the support, and are completely

consumed for higher Al contents, 8.0-24 wt%.[85] Moreover it was demonstrated that for loadings of Al higher than 12 wt%, the MAO is only physisorbed, and thus more 'leachable'. However, this study was performed on only one type of silica treated at one temperature, so the values reported for the Al loading have to be considered cautiously.

2.2 Catalyst preparation

The immobilization of a molecular catalyst (in this work it will be discussed principally of metallocene catalysts) can be achieved in multiple ways;[1,61] of this multitude, three are the main approaches utilized nowadays for the preparation of industrial catalysts. As always it is necessary to keep in mind that the more efficient procedure for the synthesis of a determinate catalyst, strictly depends on the metallocene precursor selected, and that it is very difficult to foresee which is going to be the best approach before the actual synthesis.

- Approach 1 is a two-step process in which the MAO is first impregnated on the silica, and then the metallocene precursor is immobilized on the SiO_2/MAO;
- Approach 2 sees the metallocene activation by MAO in solution prior to the immobilization on the silica surface;
- In approach 3, the metallocene precursor is contacted with the support and then activated in a second time with the MAO.

It is important to point out that the third approach presents many inconveniences, of which the predominant is the fact that the catalyst precursor can easily react in an undesired fashion with the silica surface, resulting in a deterioration of the active species. The second approach, although being the most convenient, isn't always a valid choice. It is in fact possible that the catalyst precursor deactivates after a prolonged contact with MAO.[61]

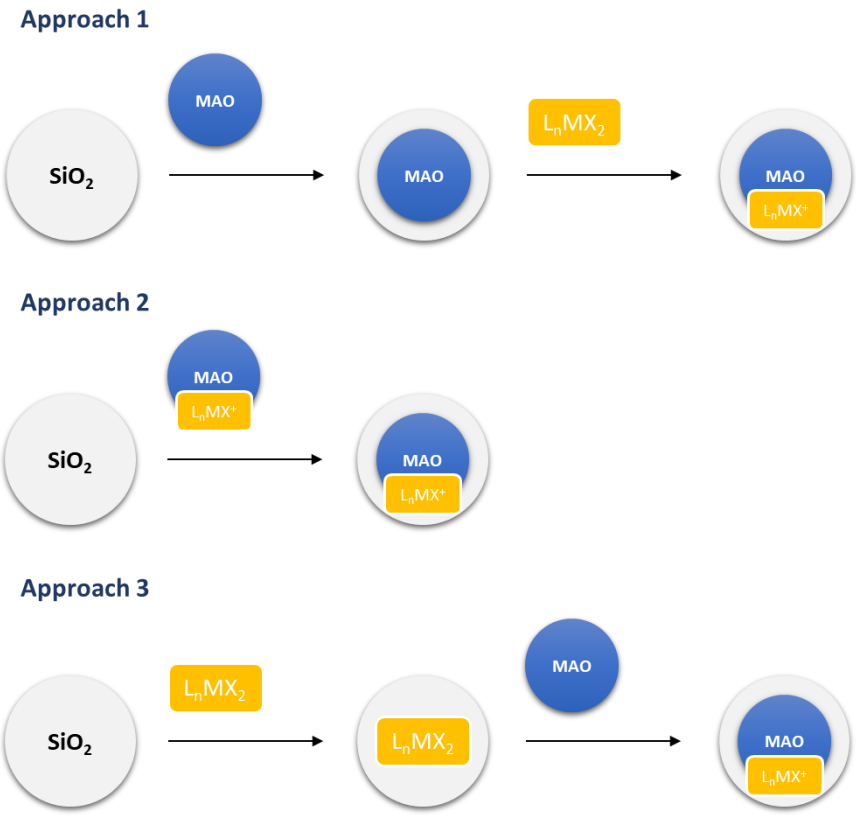

Figure 5 – Possible approaches for the synthesis of a catalyst on SiO_2/MAO.

The first approach was the first reported for the synthesis of this kind of catalysts,[86,87] and it is still used nowadays for the synthesis of commercial catalysts, which are employed in slurry and gas-phase processes.[1]

For this kind of procedure it is very important for the MAO to be strongly anchored to the surface to avoid leaching phenomena; to this aim a heat treatment during the MAO impregnation revealed to be very effective.[88,89] On the other side, low temperatures are preferable during the metallocene immobilization phase to obtain high productivities.

Just like in the case of free MAO, SiO_2/MAO is able to activate both chlorinated and alkylated catalyst precursors, however what is still not certain is which are the actual species on the surface responsible for the activation.[90] Two are the possible species involved: Lewis acid sites or $AlMe_2^+$;[41,69,77,91–94] many studies were performed demonstrating the role of both strong Lewis acid sites[91] and $AlMe_2^+$ (by formation of a bimetallic adduct with zirconocene)[69,77,93] in the formation of the active species. A recent study performed by Weckhuysen et al.[90] demonstrated, by

characterization studies of different Zr/MAO/SiO_2 catalysts at different MAO loadings, that the species majorly involved in the zirconocene activation are the $AlMe_2^+$ generated form the weak Lewis site on the surface of the activator, and that their number is a direct function of the MAO loading on the surface.

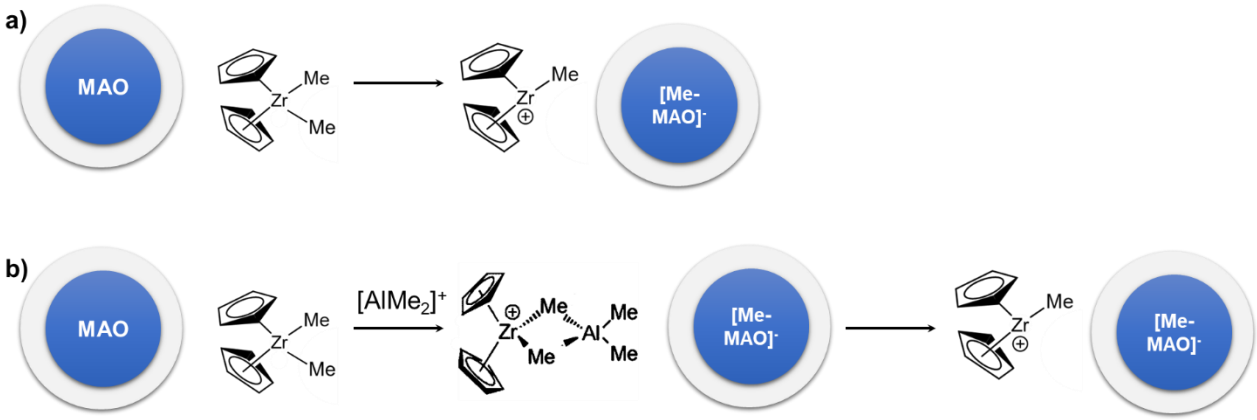

Figure 6 – Possible activation patterns in presence of supported MAO: a) by methyl abstraction b) formation of a bimetallic adduct by interaction with $[AlMe_2]^+$.

It is clear that even though free MAO and SiO_2/MAO have been around for quite a few years now, there is still much to understand about these activators and the intrinsic way in which they work.

2.3 Modified SiO_2/MAO supports

It was seen that functionalizing the surface silica before or after reaction with MAO had incredibly positive effects on the final catalyst's activity.[18,61] The role of chemically modifying the support is three-fold: remove the silanols groups from the silica surface, generating a more uniform surface and increasing the amount of Lewis and Brønsted acid sites on the surface.

The modifiers most commonly used were chloro- or alkoxy-silanes,[95–97] as well as fluorinating agents such as NaF;[18,61] other inorganic salts of anions such as SO_4^{2-},[98,99] NO_3^{2-} and SiF_6^{2-},[100–102] were also employed to functionalize the support prior to the addition of MAO, with incredibly boosting effects on the activity in polymerization. Researchers at Albemarle, additionally showed that also post-modifications of SiO_2/MAO supports can increase the efficiency of the activator up to twice its initial value.[103]

2.4 Solid MAO

Another interesting approach towards the synthesis of immobilized molecular catalysts is the generation of solid MAO/catalyst precursor particles free of support.[18] The first system of the kind to be developed was the Syrius catalyst commercialized by Borealis. In their procedure the catalyst precursor is pre-contacted with MAO in solution and then mixed with a perfluorinated surfactant.[104–107] A perfluorocarbon solvent is then added to the solution, at low temperature, in order to obtain a dispersed emulsion which is then solidified by contacting it with an excess of perfluorocarbon at high temperature. The toluene is extracted in the perfluorocarbon and the catalyst particles are recovered by filtration at high temperature. In order to be operated, these catalytic systems have to be pre-polymerized.[108]

The method introduced by Borealis was then modified either by the addition of an additional boron cocatalyst to the MAO,[109,110] or by the use of clathered MAO.[111–113] Moreover solidification of the latter in absence of perfluorocarbon generates highly compact spherical polymer particle, with very high activity.[18,114–116]

The synthesis and application of solid methylaluminoxane was studied also by O'Hare et al.[117–120] In 2016[119] they investigated the synthesis of sMAO by controlled reaction of TMA with benzoic acid.

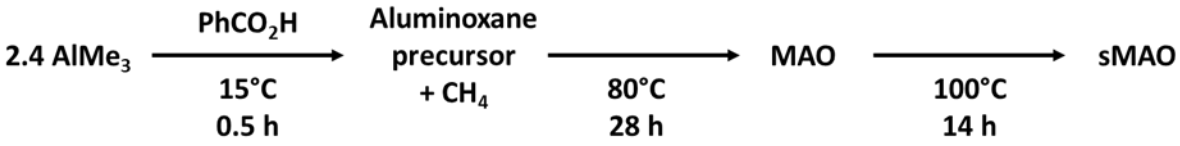

Figure 7 – Protocol followed by O'Hare et al. in the synthesis of sMAO.

The influence on the sMAO performance of the different reaction parameters, Al:O ratio, reaction temperature, was studied; it was found that a maximum of performance of the support as activator of metallocene was reached for Al:O 1.2. Moreover, it was seen that the employed temperature in the second step of the synthesis influenced the final surface area (SA) of the support: increasing the temperature caused an increase in the SA of the solid MAO. The support was tested as activator for two different zirconocenes, *meso*-Et(Me_7Ind)$_2$Zr(CH_2Ph)$_2$ and *meso*-Et(Me_7Ind)$_2$Zr($CH_2{}^t$Bu)Cl, in ethylene polymerization.[117] The sMAO was efficient in the activation

of the chosen precursors showing activities of up to 5000 kg_{PE} mol_{Zr}^{-1} h^{-1} bar^{-1} for *meso*-$Et(Me_7Ind)_2Zr(CH_2Ph)_2$, even though the displayed activity were lower than the results obtained by combining the same zirconocene precursosrs with silica-supported MAO.[121]

In 2020[120] O'Hare et al. reported the study of sMAO systems modified with pentafluorophenol as activators for zirconocene precursors of structure $Me_2Si(Cp)(Me_7Ind)ZrX_2$ (X = Cl, Me, CH_2Ph) in ethylene/1-hexene copolymerization. The study showed that, although pentafluophenol modification would increase the sMAO performance as activator, it would affect badly polymer morphology, with the formation of agglomerates.

In parallel to the development of silica/MAO and solid MAO ran that of methyaluminoxane-free solid supports for molecular catalysts.

3. Solid acids supports

In the previous paragraph it was introduced how, modifying the surface of the support prior to the MAO's immobilization, it was possible to increase the efficiency of the solid activator in combination with a metallocene;[18] similarly it is reported in the literature the development of a great number of solid acid supports by simply increasing the acid character of the surface by functionalization with different anions.[122]

3.1 Activating supports based on modified solid oxide

The presence of Lewis, or Brønsted, acids on the surface of a solid activator is fundamental for the activation of molecular catalysts. On the surface of solid oxides generally used as supports (silica, alumina, mixed silica/alumina supports), surface's acidity can be achieved by heat treatment.[122] Interestingly, it was seen that the intrinsic acidity of the solid oxide wasn't sufficient to efficiently activate metallocene precursors. It was necessary to modify the surface with strongly electron-withdrawing anions. A study on the development of solid activators by modification of solid oxides with electron-withdrawing anions was extensively reported by McDaniel in 2008.[122]

From the data showed in the work, silica/alumina (13 wt% of alumina) appeared to be the most efficient solid activator, even more so if treated with anions. Although SiO_2/Al_2O_3 was treated with

a certain number of anionic species, the best results were obtained when fluoride or triflate were used.

Whatever the employed fluoriding agent, the reported activities were higher than 10000 g g_{cat}^{-1} h^{-1} at 90°C and 40 bars of ethylene. The reported method previewed an initial modification of the surface of the solid oxide with the chosen fluoriding agent and successive calcination of the support. Different loadings and calcination temperatures were tested. It was found that increasing the calcination temperature would increase the activity of the final catalyst until a maximum was reached for a given temperature, beyond which the activator would lose its efficiency. The same behaviour was observed for all the F^- loading tested. It was though observed that higher the fluoride loading on the surface, lower was the calcination temperature necessary to obtain the maximum of the activity for the support. The reason behind this behaviour isn't clear yet; it could be assumed that, if the activity was mainly due to the presence of Bronsted sites on the surface, the presence of fluoride would increase of acid sites, but a too high loading of anion would consume the OH groups. A similar consideration could be done for the heat treatment of the support: while treatment at high temperatures favours the formation of Bronsted acid sites, at too high temperatures their number starts decreasing due to condensation.[122]

Another example of fluorinated solid acid activators was reported in 2013 by Boisson et al.[123] In this work was investigated the efficiency in activating a metallocene of aluminium fluoride species supported on the silica surface. Two different approaches were employed to generate the desired A-F groups on the surface: the partially dehydroxylated silica support was either reacted directly with an aluminium fluoride compound such as $AlEt_2F$, or it was first contacted with an alkylaluminium compound (e.g. $AlEt_3$) and then the grafted adducts were functionalized by reaction with HF. The hydrofluoric acid was generated by decomposition of $(NH_4)_2SiF_6$ at 450°C.

$$[NH_4]_2SiF_6 \xrightarrow[450\ °C]{\Delta} 2\ NH_3 + SiF_4 + 2\ HF$$

Scheme 1 - Thermal decomposition of $(NH_4)_2SiF_6$ to HF.

The paper, moreover, reported that the generation of Al-F species on the surface of the support wasn't sufficient to obtain an efficient activation of the metallocene precursor; it was in fact necessary to generate some aluminium oxide species prior to the fluorination. This was achieved by a combustion of the support after the grafting of the triethylaluminium. In Scheme 2 are reported the two methods described for the synthesis of the solid activators.

The paper furtherly investigated the effect of fluoride loading on the efficiency of the activator. The F loading on the support ranged between 1.2 and 5.3 wt%. The systems were tested as cocatalysts for *rac*-$EtInd_2ZrCl_2$ in ethylene/1-hexene slurry copolymerization in heptane at 80°C and 4 bars of ethylene. Al(*i*Bu)$_3$ was employed as scavenger and alkylating agent. The study

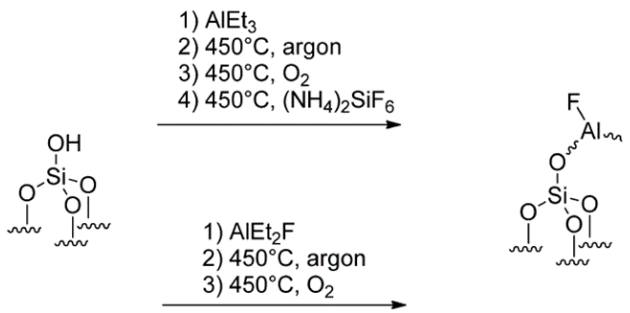

Scheme 2 – Synthetic procedures for the synthesis of fluorinated solid acids.

reported that, at the same loading of 1-hexene, the highest productivity was obtained with the maximum fluoride loading, 5.3 wt%, and was of 750 g g_{AS}^{-1}.

In the work of McDaniel similar trends to those observed with the fluoride anion can be seen when SiO_2/Al_2O_3 is reacted with triflic acid.[61] In this case the activity of the resulting catalysts is mainly attributed to the triflic acid on the surface., As in the case of the fluoride treatment, it is enhanced by heat treatment of the support at increasing temperatures up to 450°C after which triflate decomposition phenomena start occurring.

One of the major inconveniences of these supports is that, given the synthesis process, it is very difficult to know exactly the structure of the species present on the surface of the solid activator, which as a consequence makes it tricky to understand how the catalyst precursor interacts with the support.

3.2 Clay as activating support for molecular catalysts

Clays are layered minerals constituted of silicates and aluminosilicates; the internal structure and the type of ions trapped in between the layers can differ greatly, generating a huge variety of clays, such as: montmorillonite, hectorite, vermiculite, hydrotalcitite, smectite, mica, or kaolin. Many, if not all, of these have been used as support for molecular catalysts in olefin polymerization. At Tosoh, clays impregnated with quaternary ammonium were used to activate different metallocene complexes.[124–126] The use of aluminoxane-modified clays for the activation of zirconocenes was also reported.[127,128]

Another interesting system for the activation and immobilization of homogeneous catalysts is acid-treated montmorillonite (MMT). It was first developed as a solid activator in the 1990s by Mitsubishi Chemical Corporation (MCC).[129,130] For these kind of activators two key factors to the activation have been addressed: understanding the location of the active species in the layered structure and what are the requirements of the clay to consent the activation. The localization of the active sites is still object of discussion. Weiss et al.[131] propose that the metallocene is activated on the alkyaluminium sites fixated to the OH groups at the end of silicate layers, formed by aluminum extraction. Another hypothesis is that the activation occurs in between the layers, because it is there that the doping of clays commonly takes place.[132] A third theory proposes that the metallocene activation is located at the clay's surface, since the acid treatment, necessary for the activation, takes place at the surface.[133,134]

For what concerns the reasons behind the metallocene activation, many studies have been done for both the wet and dry systems. In the wet system, efficient support systems were prepared by reacting a clay containing water with $AlMe_3$, generating surface MAO species.[135] Further studies have demonstrated that acidic character of the mineral enhances the efficiency of the support.[136] On the other side, the dry system demonstrated activating abilities also in absence of alkylaluminum treatment.[130] This is due to the presence of the support of Lewis acid sites, which are able to activate polymerization catalyst precursors.[137]

Two recent works have studied deeply the acid activation of the clay surface and how it influences the metallocene activation, to try and localize the active species on the support. Murata et al.[138]

studied the morphological and acidic properties of different montmorillonites treated with H_2SO_4 to generate acid sites by Al abstraction. When tested in propylene polymerization as activators of *rac*-dimethylsilylenebis[1,1-{2-methyl-4-(4-chlorophenyl)-4-hydroazulenyl}]zirconium dichloride ($AzuZrCl_2$), the activities appeared to be strictly dependent on the acidic properties of the support: the systems showing the best activity were those presenting strong acid sites. Moreover, it was found that the acidity of the support was strictly correlated to the Al abstraction, it was in fact found that strong acid sites were immediately formed by Al elimination. On the other side a too drastic extraction of aluminum from the support causes a modification of the morphology of the clay, with a conversion of small pores to large ones. It is known that strong acid sites are predominantly located in small pores, while large ones host weak acid sites; it is consequent, though, that high Al extractions are detrimental to the activity of the system. The acid treatment had also a huge effect on the morphology of the clay, it was in fact possible to observe a broadening of the edge's thickness and the formation of small pores, where the acid sites are localized. In a previous work on similar systems, Murata et al.[139] also demonstrated that the interlayer distance of the clay wasn't in anyway influenced by the activation treatment, forcing the metallocene catalysts to be located on the borders of the particles.

4 Surface Organometallic Chemistry (SOMC), an approach

From the examples of solid activators presented above in this chapter one concept was recurrent in almost all of them: once the solid activator is obtained, it is not possible to confirm with certainty the structure of the species on the surface, which of them are active participants in the activation of the catalyst and what kind of interactions take place once the active ionic couple is formed. One of the reasons behind this is that opening a window that could allow to put into focus the surface composition and structure is no easy task, moreover surfaces aren't homogeneous, and thus react in multiple ways in presence of a compound, resulting in a mixture of final products.

Surface organometallic chemistry is a relatively new approach for the development of well-defined heterogeneous catalysts.[140,141] It is based on the controlled grafting of organometallic complexes on the surface of solid oxides, with the formation of a complex chemically bound to the surface. The final species are well-defined grafted complexes[142–145] and their coordination sphere

comprises both the bonds formed with the surface and those still present with the coordination ligands.

The key to the successful synthesis of well-defined grafted species is a precise control of the reactive sites on the surface of the supports, the nature of which is going to influence the number of bonds the organometallic complex is going to create with the surface, and the structure of the final product. Depending on the treatment the support underwent to, and consequently what reactive groups are left on the surface, the grafted species can be mono-, bi- or tri-podal, in relation to the number of bonds created between the metal centre and the surface (respectively one, two or three bonds with the support). The characterization is performed by different techniques, including EXAFS, IR, solid state NMR, mass balance analysis of the species on the surface (by elemental analysis) and those released at the moment of the grafting or by hydrolysis of the product (by gas chromatography). The obtained grafted species can be either used directly as catalysts or be furtherly modified to obtain the desired catalyst. In Figure 8 is reported a schematic representation of the SOMC approach.

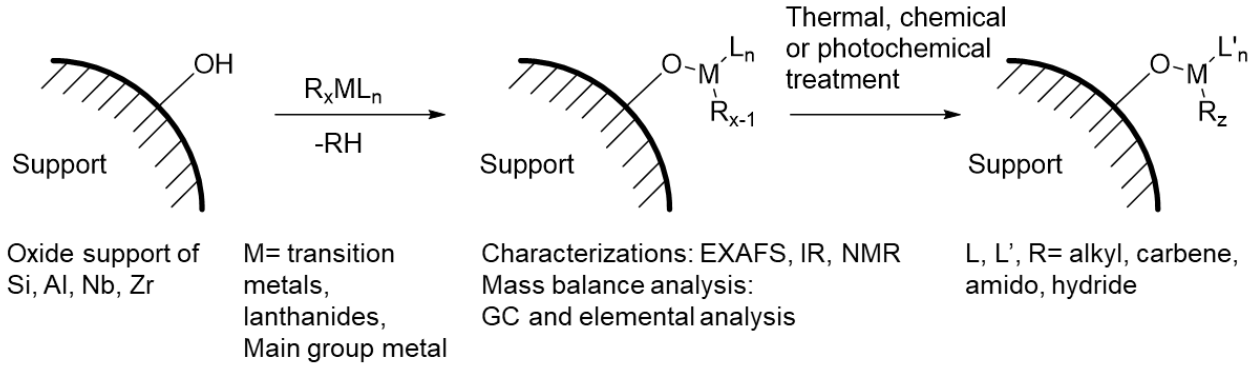

Figure 8 – Schematic representation of the SOMC approach.

The synthesised catalysts using this approach present multiple advantages. Being heterogeneous species, they possess all the perks of this class of catalysts (ease of separation from the product and recyclability) and, at the same time, all the advantages of the homogeneous catalysts, since the grafted species are well-defined (higher selectivities, possibility of studying the reaction mechanisms). Moreover, the fact that the species possess low mobility, avoids unwanted side-reaction that can take place in solution, such as bimolecular reactions.[146]

The SOMC approach presents almost infinite possibilities for the development of new catalytic systems, given the possibility of playing on both the support (nature of the oxide, pre-treatment of the surface),[147–150] the grafted complexes and the post-functionalization of the grafted complexes. This wide range of possibilities has permitted the synthesis of a huge amount of catalysts for a plethora of applications.[141]

Of the great variety of supports accessible for SOMC, silica is one of the most widely used, and is the support employed for the synthesis of all the activating supports and catalysts presented in this work. In the next paragraph we are going to discuss its structure and the possible surface reactive sites and their evolution with thermal treatment.

4.1 Silica

The bulk of the silica particles is composed of tetrahedral units of SiO_4, inaccessible to the reactant. The surface composition of the silica, on the other side, presents a mixture of species quite complex: physisorbed water, isolated, geminal and vicinal silanol groups, and siloxane bridges (≡SiOSi≡) forming six- or four-membered rings with the SiO_4 of the bulk.[151] These are the sites principally involved in the reaction with organometallic complexes.

It is the type and distribution of the reactive sites on the surface of the silica which regulates the structure (and reactivity) of the grafted products after the reaction. In order to control the grafting fashion of the organometallic complexes, it is possible to tune the distribution of silanols and siloxane bridges (and eliminate the physisorbed water) on the surface, by treating the support at high temperatures under controlled atmospheres (vacuum, dry air…) for a certain period of time. The evolution of the species on the surface is reported in Figure 10 at different partial dehydroxylation temperatures.[151]

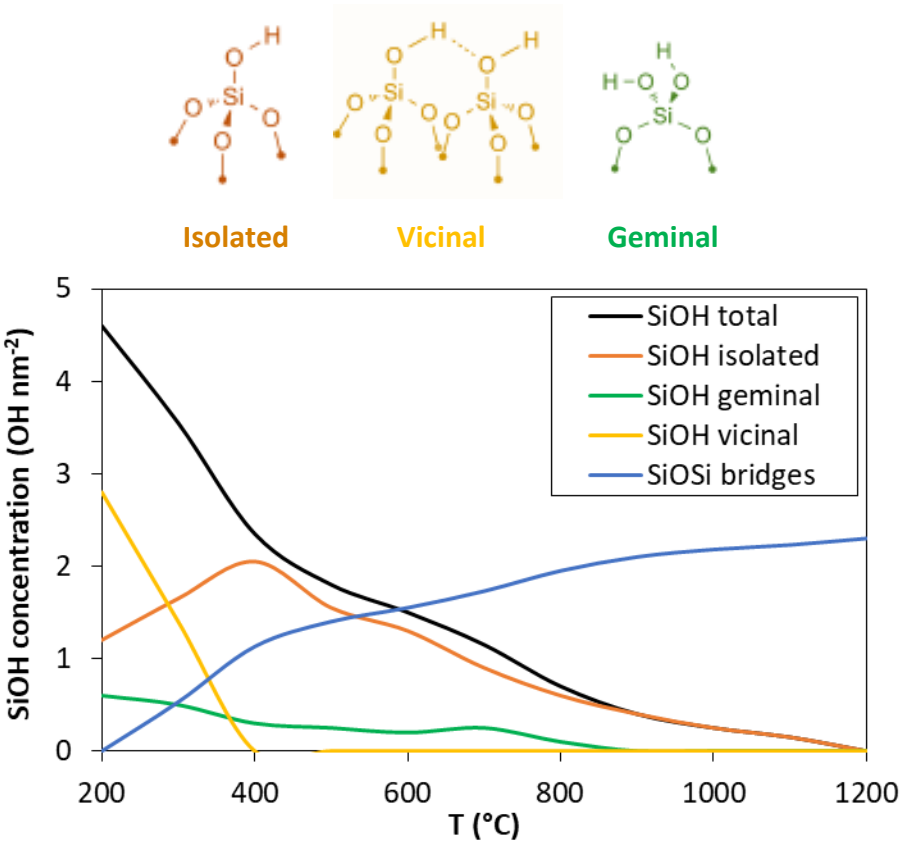

Figure 9 – Evolution of silanols and siloxane bridge distribution at increasing dehydroxylation temperatures.

It is possible to see how, after treatment at 200°C, all three kinds of silanols are still present on the surface, and that the majority is composed of vicinal bridging silanols, which rapidly disappear if the dehydroxylation temperature is increased to 400°C. At this temperature, and higher, the condensation of vicinal silanols favours the formation of isolated silanols and siloxane bridges, which constitute the main species. The increase of the treatment temperature has a duplex effect: diminishing the amount of SiOH and increasing the siloxane bridges' amount, until at 1200 °C practically all silanols on the surface are consumed.

The types of silanols on the surface can be studied by means of different techniques, such as IR spectroscopy,[152,153] solid state NMR[154] and reactivity studies.[155] The amount of SiOH groups present on the surface at room temperature is strictly dependent on the structure of the silica and how it was synthesized.

For the synthesis of the grafted species performed in this thesis work, two dehydroxylation temperatures were employed: 200 and 700°C. The difference in composition of the surface, after treatment at the two temperatures, is reflected in the structure of the grafted complexes.

In Figure 11 is reported a representation of the DRIFT spectra of Grace silica Sylopol 2408 after partial dehydroxylation at 200 and 700°C.

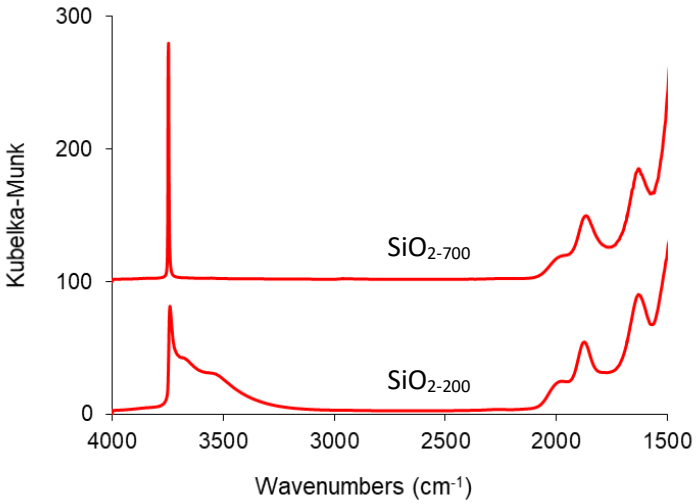

Figure 10 – DRIFT spectra of Grace silica Sylopol 2408 partially dehydroxylated at 200 °C (bottom) and at 700 °C (top).

From the DRIFT spectra it is clear how the surface of the silica dehydroxylated at 200°C ($SiO_{2\text{-}200}$) is more complex than that treated at 700°C ($SiO_{2\text{-}700}$). In fact, where $SiO_{2\text{-}700}$ presents one sharp peak at 3743 cm^{-1} for the O-H stretching of the isolated silanols, $SiO_{2\text{-}200}$ shows two additional bands at 3680 and 3530 cm^{-1} for the vicinal silanols.

4.2 Grafted borate activators

One of the classes of supported activators having great success nowadays are supported borate anions, generally on silica. Perfluorinated aryl complexes of metals from Group 13 are efficient cocatalysts for molecular catalysts in the homogeneous phase.[92,156–170] The main advantages presented by these activators, putting aside the great efficiency, are the fact that low cocatalyst/metal ratio are sufficient to reach good performances and that they're discreet molecules, allowing a precise characterization of the ionic couple formed upon activation.[171] it is exactly these properties that has pushed towards the development of solid activators presenting discreet borates (or other metallates of Groups 13) on the silica surface.[1]

4.2.1 Grafting of borane compounds

In this kind of solid activators the metal is directly bound to the surface of the support. The first grafted B-based activators were obtained by reacting *tris*-pentafluorophenyl borane on the silica surface.[172–174]

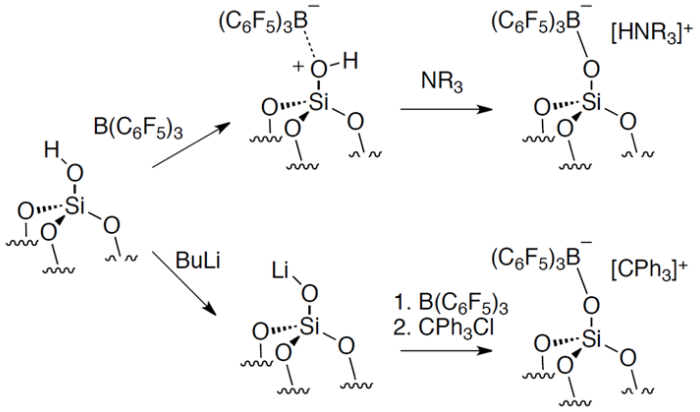

Scheme 3 – Synthetic pathways to the synthesis of silica grafted borate activators.

The structures obtained, $(\equiv SiOH)^{\delta+}[B(C_6F_5)_3]^{\delta-}$,[172,173] $[(\equiv SiO)B(C_6F_5)_3]^{-}[HNR_3]^{+}$,[172–175] $[(\equiv SiO)B(C_6F_5)_3]^{-}[CPh_3]^{+}$,[174–178] proved to be efficient activators for dimethyl metallocene catalysts, their interaction was in fact deeply investigated and the species formed reported.

It was found that contacting Cp_2ZrMe_2 with $(\equiv SiOH)^{\delta+}[B(C_6F_5)_3]^{\delta-}$ causes the cleavage of the boron-siloxy ligand, proved by the presence in solution of $MeB(C_6F_5)_2$ after the reaction, and the formation of a grafted zirconocene species.[179]

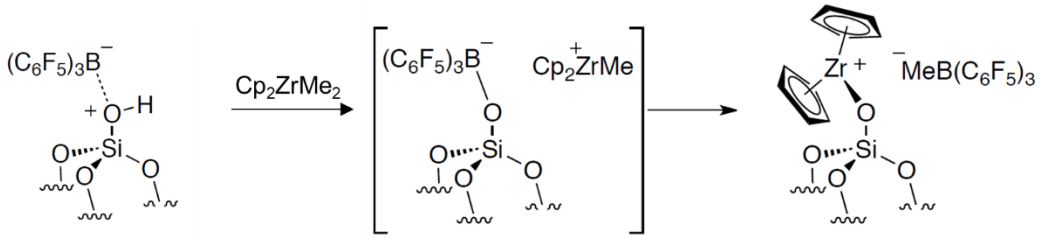

Scheme 4 – Reaction between Cp_2ZrMe_2 and $(\equiv SiOH)^{\delta+}[B(C_6F_5)_3]^{\delta-}$

Successively, Gulari et al. stated that when Cp_2ZrCl_2 was reacted with $(\equiv SiOH)^{\delta+}[B(C_6F_5)_3]^{\delta-}$ in presence of an excess of TiBA as alkylating agent, would not lead to the leaching of the borane but to the formation of the active species $[(\equiv SiO)B(C_6F_5)_3]^-[\ Cp_2ZrR]^+$.[176]

The elucidation on the structures formed by reaction of the catalyst precursors with the grafted borate species is due to their discreet nature and thus the possibility of fully characterize them.[180–182] Structure investigations also showed that the choice of the counter ion for the grafted borate is very important for the final structure of the active species. Basset et al. reported that in presence of $[HNEt_2Ph]^+$ as stabilizing cation for $[(\equiv SiO)B(C_6F_5)_3]^-$, two possible ionic couple are formed on the

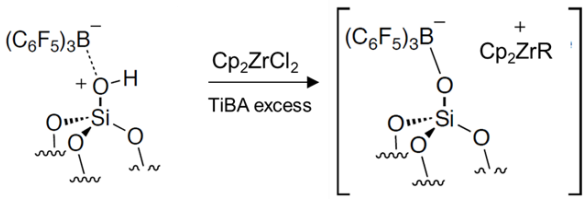

Scheme 5 – Formation of the active species by interaction of Cp_2ZrCl_2 with $(\equiv SiOH)^{\delta+}[B(C_6F_5)_3]^{\delta-}$ in presence of an excess of TiBA.

surface, which will interact differently with the catalyst precursor, forming two different species. The possible pathways are reported in Scheme 6.[183]

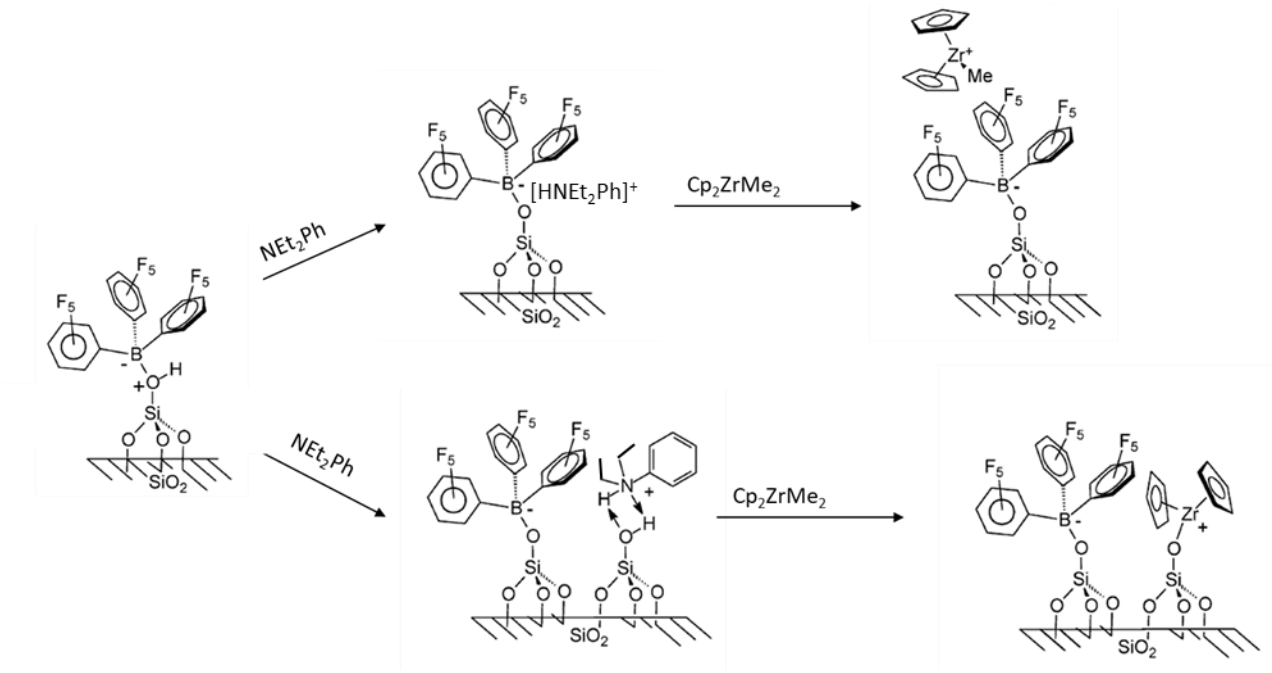

Scheme 6 – Possible structures formed by interaction of a grafted borate with diethylaniline, and their reaction with Cp_2ZrMe_2.

4.2.2 Tethering of borate complexes

Another successful approach to the synthesis of solid activators for molecular catalysts is the tethering of the co-catalyst. The difference with the activators presented in the previous paragraph is the presence of a spacer between the surface of the support and metal centre of the cocatalyst. Tethered borate cocatalysts have been deeply studied in literature and are nowadays used industrially as supports for molecular catalysts in different processes.

The first tethering of a perfluorophenylborate was disclosed in 1995,[184] but the first application of such species as solid activators of catalysts for olefin polymerization was only disclosed in 1997 by Fritze et al. at Basell GmbH.[185] In this work the employed spacer for the tethering of the boron complex was either a chlorosilyl or an ethoxysilyl group (Scheme 7). The species reported in the patent, even though they resulted to be successful in activating the molecular catalysts, led to low activities.

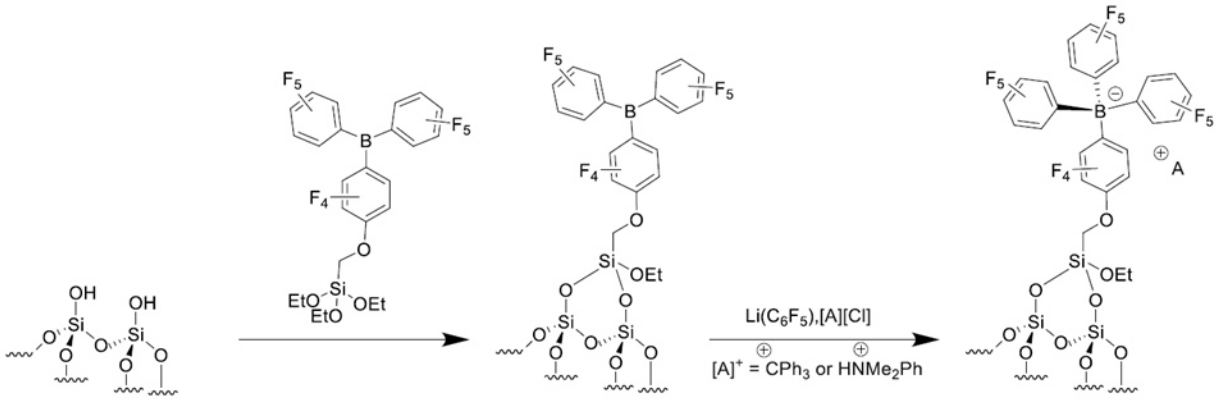

Scheme 7 – Tethering of a borate species to the silica surface as described by Fitze et al.

Higher activities were obtained when a hydroxyl-containing borate species was tethered on a support previously treated with an alkylaluminium (Scheme 8). The procedure was first disclosed in 1998 by Dow Chemical Company and W.R. Grace. The presence of the hydroxyl group on the borate renders the complex highly reactive towards the grafted Al species on the surface of the support, favouring the formation of the desired species. Such cocatalysts were and are still employed in the activation of metallocene and constrained geometry catalysts for industrial applications.[186,187]

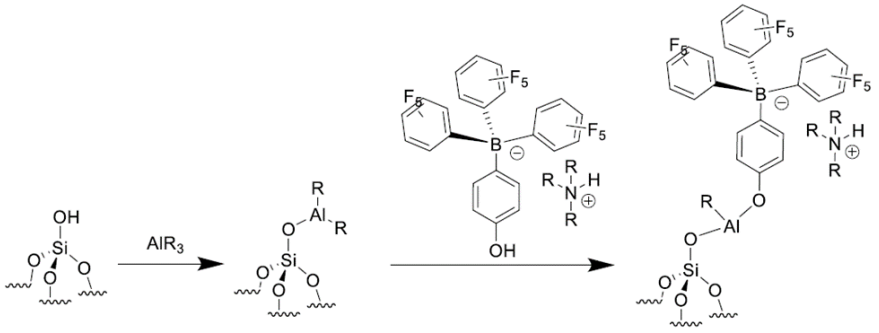

Scheme 8 – Tethering of a borate complex to an alkylaluminium treated silica.

These systems have been deeply studied for their application in both slurry and gas phase processes, by collaboration ventures of Dow Chemical with either Asahi Chemical or British Petroleum (today INEOS) respectively.[188–191] However it is worth noting that the exact structure of the tethered borates is still unresolved, mainly because it is very difficult to elucidate the exact structure of the grafted aluminium species on the support's surface. This, though doesn't impede their wide industrial application.

4.3 Synthesis of an aluminate activating support

Recently in our group, SOMC was successfully employed in the synthesis of an aluminate activating support grafted on silica particles.[192] The procedure followed was a two-step synthesis where firstly triisobutylaluminum was grafted in Et_2O on the surface of a silica partially dehydroxylated at 700°C, and successively the grafted aluminium species were functionalized with pentafluorophenol and diethylaniline.

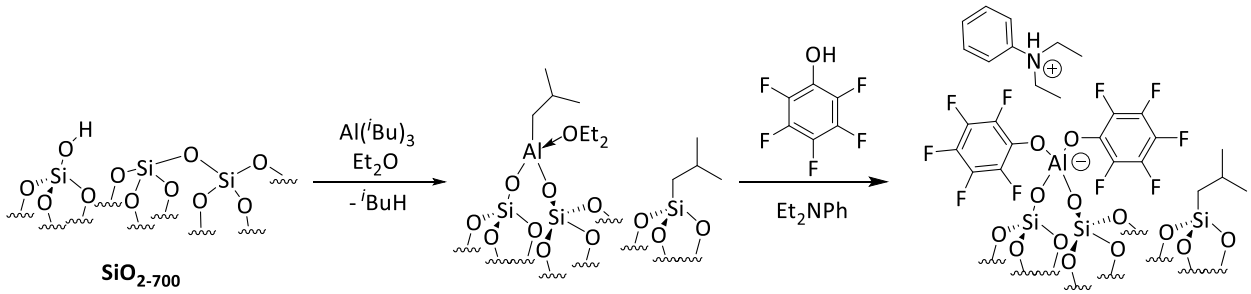

Scheme 9 – Synthesis of $[(\equiv SiO)_2Al(OC_6F_5)_2]^-[HNEtPh]^+$.

The synthesis of a similar activating support was previously disclosed Luo et al. at Albemarle Corporation.[193] In their patent it is described the synthesis of an aluminate species by functionalization of TEA-passivated silica surface; the obtained species, although being active cocatalysts for zirconocene catalysts in ethylene copolymerization, weren't structurally defined, due to the complex way with which TEA reacts with the silica surface.

In the work of Sauter et al.[192] it is described the synthesis of a well-defined aluminate species. TiBA was chosen as alkylaluminium precursor for its lower tendency to create dimers in solution. To further favour the monomer form was employed a coordinating solvent such as Et_2O. The reaction of TiBA with the silica surface forces the opening of highly stained siloxane bridges on the surface, causing the formation of bipodal isobutylaluminum species.[194]

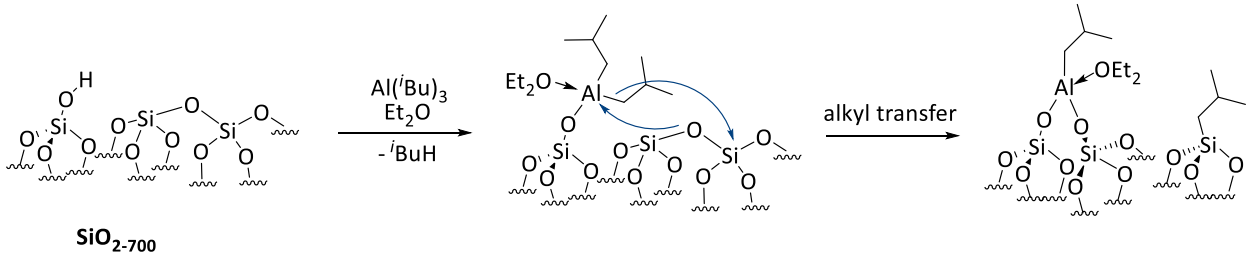

Scheme 10 – Grafting of TiBA on $SiO_{2\text{-}700}$ in diethyl ether.

The successive reaction of the grafted alkyl precursor with 2 equivalents of pentafluorophenol and diethylaniline resulted in the synthesis of a well-defined bipodal aluminate of structure $[(\equiv SiO)_2Al(OC_6F_5)_2]^-[HNEt_2Ph]^+$.

The activating support was then tested in ethylene/1-hexene slurry copolymerization as activator of two zirconocene complexes $(n\text{-BuCp})_2ZrCl_2$ and *rac*-$EtInd_2ZrCl_2$. The polymerizations were conducted at 4 bars of ethylene pressure and 80°C. The obtained activities for the two systems were fairly high, 133 g g_{cat}^{-1} h^{-1} for $[(\equiv SiO)_2Al(OC_6F_5)_2]^-[HNEt_2Ph]^+$/$(n\text{-BuCp})_2ZrCl_2$ and 656 g g_{cat}^{-1} h^{-1} for $[(\equiv SiO)_2Al(OC_6F_5)_2]^-[HNEt_2Ph]^+$/*rac*-$EtInd_2ZrCl_2$. The obtained resins exhibited a good particle morphology, proving that the active species are tightly coordinated to the surface of the support.

5 *Summary and aim of the work*

The discovery of molecular catalysts active in the polymerization of olefins, and most importantly the implement of activators, such as MAO, which allowed their efficient activation was one of the major breakthroughs in the field of ethylene and propylene polymerization. It is though necessary to remind that molecular catalysts started being properly diffused in the industrial processes once immobilized on a support. The reason for and the difficulties behind the heterogenisation of molecular catalysts was amply discussed in this chapter, even though much has been inevitably left out.

One of the greatest problem surrounding the immobilization of a catalyst precursor on a solid activator is that it is not possible to foresee the way in which the former is going to interact with the surface, and how this interaction will affect its productivity and the properties of the produced polymer resins. Most of the times it is due to the fact that the structure of the supported activator

is not well-defined, either because of the employed precursor (e.g. MAO) or for the procedure used in the synthesis of the solid activators (e.g. halogenated solid acids).

This PhD thesis work intends to face this issue proposing the synthesis of well-defined activating supports for metallocenes and their application in ethylene/1-hexene slurry or gas phase copolymerization. It is in fact our opinion that by following a controlled grafting, such as the SOMC school teaches, for the synthesis of the activator, we will successfully obtain well-defined structures apt to activate metallocene precursors. In the following chapters it is going to be presented the synthesis of 15 activating supports and their application in polymerization as cocatalysts for *rac*-$EtInd_2ZrCl_2$.

More specifically in Chapter II is discussed the synthesis and characterization of a bipodal aluminate activating support, its application in polymerization at both laboratory and pre-industrial scale and its employment in the isolation of formulated catalysts with *rac*-$EtInd_2ZrMe_2$ and (*n*-$BuMeCp)_2ZrMe_2$.

Chapter III investigates the effects of ligand structure on the efficiency of the activating supports as cocatalyst. Starting from the same bipodal aluminium precursor, $(\equiv SiO)_2AlH(NMe_2Et)$, four well-defined activators were synthesized by functionalization with diversely functionalized ligands.

Chapter IV is divided in two sections: in the first is presented the synthesis of activators by functionalization of halogenated grafted aluminum precursors, mono- and bi-podal; in the second is presented the synthesis of four activating supports featuring as metal centre an Y atom at the place of the Al, with the aim of strengthening the stability of the catalyst's ionic couple.

Chapter V focuses on topic that differs slightly from what is presented in Chapters II to IV. The second section of Chapter IV describes the synthesis of four grafted Y precursors on both $SiO_{2\text{-}700}$ and $SiO_{2\text{-}200}$. that are used for preparation of solid activators. However, molecular yttrium based catalysts are renown for a long time for their activity towards olefin and diene polymerization.[195,196] This drove us to investigate these well-defined supported yttrium complexes. In Chapter V it is studied the activity of these species as catalysts in ethylene polymerization. Before discussing the obtained results during this thesis, Chapter V will briefly

review the literature existing on olefin polymerization promoted by molecular rare-earth metal catalysts and on the grafting of rare-earth metal complexes.

References

(1) Severn, J. R.; Chadwick, J. C.; Duchateau, R.; Friederichs, N. "Bound but Not Gagged"Immobilizing Single-Site α-Olefin Polymerization Catalysts. *Chem. Rev.* 2005, *105* (11), 4073–4147. https://doi.org/10.1021/cr040670d.

(2) Polyolefin Reactors and Processes. In *Polyolefin Reaction Engineering*; John Wiley & Sons, Ltd, 2012; pp 87–129. https://doi.org/10.1002/9783527646944.ch4.

(3) Phillips Petroleum Co. Slurry Loop Process. *Int. J. Hydrocarb. Eng.* 1998, *3* (10), 76–80.

(4) Kufeld, S. E.; Reid, T. A.; Tait, J. H.; Burns, D. H.; Verser, D. W.; Hensley, H. D.; Przelomski, D. J.; Cymbaluk, T. H.; Franklin, R. K. I.; Perez, E. P.; Hottovy, J. D. United States Patent Application: 0030229187 - Slurry Polymerization Reactor Having Large Length / Diameter Ratio, and Process of Polymerizing Polyolefins in Such a Reactor. 20030229187, A1.

(5) Kendrick, J. A.; Towles, T. W.; Roger, S. T. United States Patent Application: 0020173598 - Continuous Slurry Polymerization Process and Apparatus. 20020173598, A1.

(6) Iwasaki, S.; Yamamoto, T. Loop Reactor for Polymerization of Olefin. JPS6213408 (A).

(7) Martin, J. L.; Bergmeister, J. J.; Hsieh, E. T.-Y.; Mcdaniel, M. P.; Benham, E. A.; Secora, S. J. Olefin Polymerization Processes and Products Thereof. EP0909769 (A2).

(8) Samples, P. K.; Matthews, W. a; Parrish, J. R.; Hartley, I. J.; Lee, K. H. Process Control in the Presence of Chromium Based Catalyst. EP0866077 (A1).

(9) Chinh, J.-C. Polymerisation Process. EP0803519 (A1).

(10) Chinh, J.-C. Polymerisation Process. EP0824114 (A1).

(11) Chinh, J.-C.; Power, M. B. Polymerisation Process. EP0824116 (A1).

(12) Polymerisation Process. EP0824115 (A1).

(13) Jauniaux, M. Continuous Process for Obtaining Propylene Polymers. WO9855519 (A1).

(14) Resconi, L.; Chadwick, J. C.; Cavallo, L. Olefin Polymerizations with Group IV Metal Catalysts. In *Comprehensive Organometallic Chemistry III*; Elsevier, 2007; pp 1005–1166. https://doi.org/10.1016/B0-08-045047-4/00065-0.

(15) *Polyolefins: 50 Years after Ziegler and Natta II: Polyolefins by Metallocenes and Other Single-Site Catalysts*; Kaminsky, W., Ed.; Advances in Polymer Science; Springer Berlin Heidelberg: Berlin, Heidelberg, 2013; Vol. 258. https://doi.org/10.1007/978-3-642-40805-2.

(16) Baier, M. C.; Zuideveld, M. A.; Mecking, S. Post-Metallocenes in the Industrial Production of Polyolefins. *Angew. Chem. Int. Ed.* 2014, *53* (37), 9722–9744. https://doi.org/10.1002/anie.201400799.

(17) *Late Transition Metal Polymerization Catalysis*, 1st ed.; Rieger, B., Baugh, L. S., Kacker, S., Striegler, S., Eds.; Wiley, 2003. https://doi.org/10.1002/3527601805.

(18) Severn, J. R. Recent Developments in Supported Polyolefin Catalysts: A Review. In *Multimodal Polymers with Supported Catalysts*; Albunia, A. R., Prades, F., Jeremic, D., Eds.; Springer

International Publishing: Cham, 2019; pp 1–53. https://doi.org/10.1007/978-3-030-03476-4_1.

(19) Tohi, Y.; Yoshitsugu, K.; Akiyama, N.; Fujita, T.; Chinaka, M. Method for Producing Olefin Polymer. US8445609B2, May 21, 2013.

(20) Takahashi, M.; Todo, A.; Ikeyama, S.; Tsutsui, T.; Matsunaga, S.; Kaneshige, N. Ethylene Copolymer Composition. US6894120B2, May 17, 2005.

(21) Kokko, E.; Pakkanen, A.; Vahteri, M.; Palmlof, M.; Oderkerk, J. Cross-Linkable Polyethylene Resin for Pipes Made by a Single-Site Catalyst. US20110262670A1, October 27, 2011.

(22) Helland, I.; Skar, M. Multimodal Medium Density Polyethylene Polymer Composition. US8314187B2, November 20, 2012.

(23) Miserque, O.; Michel, J.; Dupire, M.; Siberdt, F.; Costa, J.-L.; Bettonville, S.; Rouyer, V.; Damme, E. Polyethylene Pipe Resins and Production Thereof. US6946521B2, September 20, 2005.

(24) Slawinski, M. Process for the Preparation of a Particulate Bimodal Polyethylene Product. US8445607B2, May 21, 2013.

(25) Michel, J.; Slawinski, M.; Debras, G. Process for Preparing a Polyethylene Resin in a Double Loop Reactor with a Mixture of Bis-Indenyl and Bis-Tetrahydroindenyl. US8153734B2, April 10, 2012.

(26) Belloir, P.; Bertrand, C. Resin and Pipes for Transporting Water Containing Chlorine Dioxide. US8691354B2, April 8, 2014.

(27) Jacobsen, G. B.; Matsushita, F.; Spencer, L.; Wauteraerts, P. L. Ethylene Copolymer Compositions. US6506866B2, January 14, 2003.

(28) Jacobsen, G. B.; Loix, P. H. H.; Stevens, T. J. P. Catalyst Component Dispersion Comprising an Ionic Compound and Solid Addition Polymerization Catalysts Containing the Same. US6271165B1, August 7, 2001.

(29) Arriola, D. J.; Timmers, F. J.; Devore, D. D.; Redwine, O. D. Alpha-Olefin Based Branched Polymer. US7193024B2, March 20, 2007.

(30) Chai, C. K. Copolymers and Films Thereof. US7968659B2, June 28, 2011.

(31) Hermel-Davidock, T. J.; Demirors, M.; Hayne, S. M.; Cong, R. Ethylene-Based Polymer Compositions. US8729200B2, May 20, 2014.

(32) Karjala, T. P.; Ewart, S. W.; Eddy, C. R.; JR, A. E. V.; Demirors, M.; Munjal, S.; Yau, W. W. Process to Make Long Chain Branched (LCB), Block, or Interconnected Copolymers of Ethylene. US8722817B2, May 13, 2014.

(33) Konze, W. V.; Stevens, J. C.; VanderLende, D. D. High Efficiency Solution Polymerization Process. US8202953B2, June 19, 2012.

(34) Ewart, S. W.; Munjal, S.; JR, A. E. V.; Karjala, T. P.; Demirors, M. Processes to Prepare Ethylene-Based Polymer Compositions. US9045628B2, June 2, 2015.

(35) Hustad, P. D.; Szuromi, E.; Timmers, F. J.; Carnahan, E. M.; Clark, T. P.; Roof, G. R.; Klamo, S. B.; Arriola, D. J. Comb Architecture Olefin Block Copolymers. US8907034B2, December 9, 2014.
(36) Diamond, G. M.; Leclerc, M. K.; Zhu, G. Method for Producing Very-High or Ultra-High Molecular Weight Polyethylene. US8637618B2, January 28, 2014.
(37) Robert, D.; Hufen, J.; Lüdtke, K.; Ehlers, J. Process for Producing High Molecular Weight Polyethylene. US9034999B2, May 19, 2015.
(38) Severn, J. R.; Chadwick, J. C. Immobilisation of Homogeneous Olefin Polymerisation Catalysts. Factors Influencing Activity and Stability. *Dalton Trans.* 2013, *42* (25), 8979. https://doi.org/10.1039/c3dt33098b.
(39) Hlatky, G. G. Heterogeneous Single-Site Catalysts for Olefin Polymerization. *Chem. Rev.* 2000, *100* (4), 1347–1376. https://doi.org/10.1021/cr9902401.
(40) Leeuwen, P. W. N. M. van; Chadwick, J. C. *Homogeneous Catalysts: Activity, Stability, Deactivation*; Wiley -VCH: Weinheim, Germany, 2011.
(41) Panchenko, V. N.; Semikolenova, N. V.; Danilova, I. G.; Paukshtis, E. A.; Zakharov, V. A. IRS Study of Ethylene Polymerization Catalyst SiO2/Methylaluminoxane/Zirconocene. *J. Mol. Catal. Chem.* 1999, *142* (1), 27–37. https://doi.org/10.1016/S1381-1169(98)00275-1.
(42) Hammawa, H.; Wanke, S. E. Influence of Support Friability and Concentration of α-Olefins on Gas-Phase Ethylene Polymerization over Polymer-Supported Metallocene/Methylaluminoxane Catalysts. *J. Appl. Polym. Sci.* 2007, *104* (1), 514–527. https://doi.org/10.1002/app.25527.
(43) Hassan Nejad, M.; Ferrari, P.; Pennini, G.; Cecchin, G. Ethylene Homo- and Copolymerization over MgCl2-TiCl4 Catalysts: Polymerization Kinetics and Polymer Particle Morphology. *J. Appl. Polym. Sci.* 2008, *108* (5), 3388–3402. https://doi.org/10.1002/app.27964.
(44) Tait, P. J. T.; Berry, I. G. 5. Rata Enhancement Effects in the Prepolymerization and Copolymerization of Ethylene and α-Olefins. In *Studies in Surface Science and Catalysis*; Elsevier, 1994; Vol. 89, pp 55–72. https://doi.org/10.1016/S0167-2991(08)63021-9.
(45) Kou, B.; McAuley, K. B.; Hsu, C. C.; Bacon, D. W.; Yao, K. Z. Gas-Phase Ethylene/Hexene Copolymerization with Metallocene Catalyst in a Laboratory-Scale Reactor. *Ind. Eng. Chem. Res.* 2005, *44* (8), 2443–2450. https://doi.org/10.1021/ie049067b.
(46) Zakharov, V. A.; Bukatov, G. D.; Barabanov, A. A. Recent Data on the Number of Active Centers and Propagation Rate Constants in Olefin Polymerization with Supported ZN Catalysts. *Macromol. Symp.* 2004, *213* (1), 19–28. https://doi.org/10.1002/masy.200450903.
(47) Bonini, F.; Fraaije, V.; Fink, G. Propylene Polymerization through Supported Metallocene/ MAO Catalysts: Kinetic Analysis and Modelling. *J. Polym. Sci. Part Polym. Chem.* 1995, *33* (14), 2393–2402. https://doi.org/10.1002/pola.1995.080331412.

(48) McKenna, T. F. L.; Di Martino, A.; Weickert, G.; Soares, J. B. P. Particle Growth During the Polymerisation of Olefins on Supported Catalysts, 1 - Nascent Polymer Structures. *Macromol. React. Eng.* **2010**, *4* (1), 40–64. https://doi.org/10.1002/mren.200900025.

(49) Schröder, L.; Brintzinger, H.-H.; Babushkin, D. E.; Fischer, D.; Mülhaupt, R. *R Ac* -Me $_2$ Si(2-Me-4- *t*- Bu-C $_5$ H $_2$) $_2$ ZrMe $^+$: An Alkyl Zirconocenium Cation Stabilized by Steric Shielding against Interaction with Ancillary Ligands. *Organometallics* **2005**, *24* (5), 867–871. https://doi.org/10.1021/om049139z.

(50) Jüngling, S.; Mülhaupt, R. The Influence of Methylalumoxane Concentration on Propene Polymerization with Homogeneous Metallocene-Based Ziegler-Natta Catalysts. *J. Organomet. Chem.* **1995**, *497* (1–2), 27–32. https://doi.org/10.1016/0022-328X(95)00106-Z.

(51) Coevoet, D.; Cramail, H.; Deffieux, A. Activation of Rac-Ethylenebis(Indenyl)Zirconium Dichloride with a Low Amount of Methylaluminoxane (MAO) for Olefin Polymerizations. *Macromol. Chem. Phys.* **1996**, *197* (3), 855–867. https://doi.org/10.1002/macp.1996.021970308.

(52) Koltzenburg, S. The Influence of Methylalumoxane (MAO) on the Isoselective Propene Polymerization with the Homogeneous Metallocene Me2Si(Benz[e]Ind)2ZrCl2. *J. Mol. Catal. Chem.* **1997**, *116* (3), 355–363. https://doi.org/10.1016/S1381-1169(96)00370-6.

(53) Kleinschmidt, R.; van der Leek, Y.; Reffke, M.; Fink, G. Kinetics and Mechanistic Insight into Propylene Polymerization with Different Metallocenes and Various Aluminium Alkyls as Cocatalysts. *J. Mol. Catal. Chem.* **1999**, *148* (1–2), 29–41. https://doi.org/10.1016/S1381-1169(99)00055-2.

(54) Kaminsky, W.; Steiger, R. Polymerization of Olefins with Homogeneous Zirconocene/Alumoxane Catalysts. *Polyhedron* **1988**, *7* (22–23), 2375–2381. https://doi.org/10.1016/S0277-5387(00)86355-X.

(55) Kaminsky, W.; Bark, A.; Steiger, R. Stereospecific Polymerization by Metallocene/Aluminoxane Catalysts. *J. Mol. Catal.* **1992**, *74* (1–3), 109–119. https://doi.org/10.1016/0304-5102(92)80228-9.

(56) Kaminsky, W.; Strübel, C. Hydrogen Transfer Reactions of Supported Metallocene Catalysts. *J. Mol. Catal. Chem.* **1998**, *128* (1–3), 191–200. https://doi.org/10.1016/S1381-1169(97)00172-6.

(57) Bamberger, R. L.; German, P. M.; Malpass, G. D. J.; Locke, L. K. Ethylene Copolymers Having Narrow Composition Distribution, Their Production and Use. WO9426816 (A1), November 24, 1994.

(58) Arrowsmith, D.; Kaminsky, W.; Laban, A.; Weingarten, U. Comparison of the Polymerization of Propene by Homogeneous and Heterogeneous Metallocene/MAO-Catalysts under Different Polymerization Conditions. *Macromol. Chem. Phys.* **2001**, *202* (11), 2161–2167. https://doi.org/10.1002/1521-3935(20010701)202:11<2161::AID-MACP2161>3.0.CO;2-J.

(59) Frediani, M.; Kaminsky, W. Propene Polymerisation Withrac-[Me2Si(2-Me-4-(α-Naphthyl)-1-Ind)2]ZrCl2 as a Highly Active Catalyst: Influence of Monomer Concentration, Polymerisation Temperature and a Heterogenising Support. *Macromol. Chem. Phys.* 2003, *204* (16), 1941–1947. https://doi.org/10.1002/macp.200350062.

(60) Bashir, M. A.; Monteil, V.; Boisson, C.; McKenna, T. F. L. Experimental Proof of the Existence of Mass-Transfer Resistance during Early Stages of Ethylene Polymerization with Silica Supported Metallocene/MAO Catalysts. *AIChE J.* 2017, *63* (10), 4476–4490. https://doi.org/10.1002/aic.15806.

(61) *Tailor-Made Polymers: Via Immobilization of Alpha-Olefin Polymerization Catalyst*; Severn, J., Ed.; Wiley-VCH: Weinheim, 2008.

(62) Alt, F. P.; Böhm, L. L.; Enderle, H.-F.; Berthold, J. Bimodal Polyethylene – Interplay of Catalyst and Process. *Macromol. Symp.* 2001, *163* (1), 135–144. https://doi.org/10.1002/1521-3900(200101)163:1<135::AID-MASY135>3.0.CO;2-7.

(63) Sinn, H.; Kaminsky, W.; Vollmer, H.-J.; Woldt, R. "Living Polymers" on Polymerization with Extremely Productive Ziegler Catalysts. *Angew. Chem. Int. Ed. Engl.* 1980, *19* (5), 390–392. https://doi.org/10.1002/anie.198003901.

(64) Resconi, L.; Cavallo, L.; Fait, A.; Piemontesi, F. Selectivity in Propene Polymerization with Metallocene Catalysts. *Chem. Rev.* 2000, *100* (4), 1253–1346. https://doi.org/10.1021/cr9804691.

(65) Reddy, S. Homogeneous Metallocene-Methylaluminoxane Catalyst Systems for Ethylene Polymerization. *Prog. Polym. Sci.* 1995, *20* (2), 309–367. https://doi.org/10.1016/0079-6700(94)00035-Z.

(66) Giannetti, E.; Nicoletti, G. M.; Mazzocchi, R. Homogeneous Ziegler–Natta Catalysis. II. Ethylene Polymerization by IVB Transition Metal Complexes/Methyl Aluminoxane Catalyst Systems. *J. Polym. Sci. Polym. Chem. Ed.* 1985, *23* (8), 2117–2134. https://doi.org/10.1002/pol.1985.170230805.

(67) Cam, D.; Giannini, U. Concerning the Reaction of Zirconocene Dichloride and Methylalumoxane: Homogeneous Ziegler-Natta Catalytic System for Olefin Polymerization. *Makromol. Chem.* 1992, *193* (5), 1049–1055. https://doi.org/10.1002/macp.1992.021930502.

(68) Chien, J. C. W.; Wang, B.-P. Metallocene–Methylaluminoxane Catalysts for Olefin Polymerization. I. Trimethylaluminum as Coactivator. *J. Polym. Sci. Part Polym. Chem.* 1988, *26* (11), 3089–3102. https://doi.org/10.1002/pola.1988.080261117.

(69) Ghiotto, F.; Pateraki, C.; Tanskanen, J.; Severn, J. R.; Luehmann, N.; Kusmin, A.; Stellbrink, J.; Linnolahti, M.; Bochmann, M. Probing the Structure of Methylalumoxane (MAO) by a Combined Chemical, Spectroscopic, Neutron Scattering, and Computational Approach. *Organometallics* 2013, *32* (11), 3354–3362. https://doi.org/10.1021/om4002878.

(70) Coates, G. W. Precise Control of Polyolefin Stereochemistry Using Single-Site Metal Catalysts. *Chem. Rev.* 2000, *100* (4), 1223–1252. https://doi.org/10.1021/cr990286u.

(71) Bochmann, M. Kinetic and Mechanistic Aspects of Metallocene Polymerisation Catalysts. *J. Organomet. Chem.* 2004, *689* (24), 3982–3998. https://doi.org/10.1016/j.jorganchem.2004.07.006.

(72) Trefz, T. K.; Henderson, M. A.; Wang, M. Y.; Collins, S.; McIndoe, J. S. Mass Spectrometric Characterization of Methylaluminoxane. *Organometallics* 2013, *32* (11), 3149–3152. https://doi.org/10.1021/om400256f.

(73) Babushkin, D. E.; Semikolenova, N. V.; Zakharov, V. A.; Talsi, E. P. Mechanism of Dimethylzirconocene Activation with Methylaluminoxane: NMR Monitoring of Intermediates at High Al/Zr Ratios. *Macromol. Chem. Phys.* 2000, *201* (5), 558–567. https://doi.org/10.1002/(SICI)1521-3935(20000301)201:5<558::AID-MACP558>3.0.CO;2-N.

(74) *Organometallic Catalysts and Olefin Polymerization: Catalysts for a New Millennium*; Blom, R., Follestad, A., Rytter, E., Tilset, M., Ystenes, M., Eds.; Springer-Verlag: Berlin Heidelberg, 2001. https://doi.org/10.1007/978-3-642-59465-6.

(75) Pédeutour, J.-N.; Cramail, H.; Deffieux, A. Influence of X Ligand Nature in the Activation Process of RacEt(Ind)2ZrX2 by Methylaluminoxane. *J. Mol. Catal. Chem.* 2001, *176* (1), 87–94. https://doi.org/10.1016/S1381-1169(01)00260-6.

(76) Tritto, I.; Donetti, R.; Sacchi, M. C.; Locatelli, P.; Zannoni, G. Dimethylzirconocene−Methylaluminoxane Catalyst for Olefin Polymerization: NMR Study of Reaction Equilibria. *Macromolecules* 1997, *30* (5), 1247–1252. https://doi.org/10.1021/ma9608986.

(77) Luo, L.; Sangokoya, S. a; Wu, X.; Diefenbach, S. P.; Kneale, B. Aluminoxane Catalyst Activators Derived from Dialkylaluminum Cation Precursor Agents, Processes for Making Same, and Use Thereof in Catalysts and Polymerization of Olefins. WO2009029857 (A1), March 5, 2009.

(78) Kim, K.-C.; Reed, C. A.; Long, G. S.; Sen, A. Et2Al+ Alumenium Ion-like Chemistry. Synthesis and Reactivity toward Alkenes and Alkene Oxides. *J. Am. Chem. Soc.* 2002, *124* (26), 7662–7663. https://doi.org/10.1021/ja0259990.

(79) Klosin, J.; Roof, G. R.; Chen, E. Y.-X.; Abboud, K. A. Ligand Exchange and Alkyl Abstraction Involving (Perfluoroaryl)Boranes and -Alanes with Aluminum and Gallium Alkyls. *Organometallics* 2000, *19* (23), 4684–4686. https://doi.org/10.1021/om000573k.

(80) Möhring, P. C.; Coville, N. J. Homogeneous Group 4 Metallocene Ziegler-Natta Catalysts: The Influence of Cyclopentadienyl-Ring Substituents. *J. Organomet. Chem.* 1994, *479* (1), 1–29. https://doi.org/10.1016/0022-328X(94)84087-3.

(81) Collins, S.; Linnolahti, M.; Zamora, M. G.; Zijlstra, H. S.; Rodríguez Hernández, M. T.; Perez-Camacho, O. Activation of Cp_2ZrX_2 (X = Me, Cl) by Methylaluminoxane As Studied by Electrospray Ionization Mass Spectrometry: Relationship to Polymerization Catalysis.

Macromolecules 2017, *50* (22), 8871–8884. https://doi.org/10.1021/acs.macromol.7b00933.

(82) Bartram, M. E.; Michalske, T. A.; Rogers, J. W. A Reexamination of the Chemisorption of Trimethylaluminum on Silica. *J. Phys. Chem.* 1991, *95* (11), 4453–4463. https://doi.org/10.1021/j100164a054.

(83) Scott, S. L.; Church, T. L.; Nguyen, D. H.; Mader, E. A.; Moran, J. An Investigation of Catalyst/Cocatalyst/Support Interactions in Silica-Supported Olefin Polymerization Catalysts Based on Cp*TiMe3*. *Top. Catal.* 2005, *34* (1–4), 109–120. https://doi.org/10.1007/s11244-005-3804-6.

(84) Talsi, E. The Metallocene/Methylaluminoxane Catalysts Formation: EPR Spin Probe Study of Lewis Acidic Sites of Methylaluminoxane. *J. Mol. Catal. Chem.* 1999, *139* (2–3), 131–137. https://doi.org/10.1016/S1381-1169(98)00194-0.

(85) Haag, M. C.; Krug, C.; Dupont, J.; de Galland, G. B.; dos Santos, J. H. Z.; Uozumi, T.; Sano, T.; Soga, K. Effects of Al/Zr Ratio on Ethylene–Propylene Copolymerization with Supported-Zirconocene Catalysts. *J. Mol. Catal. Chem.* 2001, *169* (1–2), 275–287. https://doi.org/10.1016/S1381-1169(01)00045-0.

(86) Welborn, H. C. Jr. Supported Polymerization Catalyst. US4808561A, February 28, 1989.

(87) Takahashi, T. Process for Producing Ethylene Copolymers. US5026797A, June 25, 1991.

(88) Razavi, A.; Debras, G. L. G. Process for Producing Polyolefins and Polyolefin Catalyst. US5719241A, February 17, 1998.

(89) Tian, J.; Gauthier, W.; Rauscher, D.; Henry, S. Polyolefin Production with a High Performance Support for a Metallocene Catalyst System. US20030236365A1, December 25, 2003.

(90) Velthoen, M. E. Z.; Muñoz-Murillo, A.; Bouhmadi, A.; Cecius, M.; Diefenbach, S.; Weckhuysen, B. M. The Multifaceted Role of Methylaluminoxane in Metallocene-Based Olefin Polymerization Catalysis. *Macromolecules* 2018, *51* (2), 343–355. https://doi.org/10.1021/acs.macromol.7b02169.

(91) Zakharov, V. A.; Panchenko, V. N.; Semikolenova, N. V.; Danilova, I. G.; Paukshtis, E. A. IRS Study of Ethylene Polymerization Catalyst SiO 2 /MAO/Zirconocene. *Polym. Bull.* 1999, *43* (1), 87–92. https://doi.org/10.1007/s002890050537.

(92) Chen, E. Y.-X.; Marks, T. J. Cocatalysts for Metal-Catalyzed Olefin Polymerization: Activators, Activation Processes, and Structure–Activity Relationships. *Chem. Rev.* 2000, *100* (4), 1391–1434. https://doi.org/10.1021/cr980462j.

(93) Hirvi, J. T.; Bochmann, M.; Severn, J. R.; Linnolahti, M. Formation of Octameric Methylaluminoxanes by Hydrolysis of Trimethylaluminum and the Mechanisms of Catalyst Activation in Single-Site α-Olefin Polymerization Catalysis. *ChemPhysChem* 2014, *15* (13), 2732–2742. https://doi.org/10.1002/cphc.201402298.

(94) Imhoff, D. W.; Simeral, L. S.; Sangokoya, S. A.; Peel, J. H. Characterization of Methylaluminoxanes and Determination of Trimethylaluminum Using Proton NMR. *Organometallics* 1998, *17* (10), 1941–1945. https://doi.org/10.1021/om980046p.

(95) Soga, K.; Shiono, T.; Kim, H. J. Activation of SiO2-supported Zirconocene Catalysts by Common Trialkylaluminiums. *Makromol. Chem.* 1993, *194* (12), 3499–3504. https://doi.org/10.1002/macp.1993.021941227.

(96) Chao, C.; Pratchayawutthirat, W.; Praserthdam, P.; Shiono, T.; Rempel, G. L. Copolymerization of Ethylene and Propylene Using Silicon Tetrachloride-Modified Silica/MAO with Et[Ind]2ZrCl2 Metallocene Catalyst. *Macromol. Rapid Commun.* 2002, *23* (12), 672–675. https://doi.org/10.1002/1521-3927(20020801)23:12<672::AID-MARC672>3.0.CO;2-I.

(97) Jongsomjit, B.; Kaewkrajang, P.; Wanke, S. E.; Praserthdam, P. A Comparative Study of Ethylene/ -Olefin Copolymerization with Silane-Modified Silica-Supported MAO Using Zirconocene Catalysts. *Catal. Lett.* 2004, *94* (3/4), 205–208. https://doi.org/10.1023/B:CATL.0000020547.69383.e6.

(98) Gao, X.; Santos, B. G.; Hoang, P. P. M.; Jones, A. M.; Shaw, B. M.; Jobe, I. R. Reactor Continuity. US8298978B2, October 30, 2012.

(99) Lam, P.; Ker, V.; Carter, C. A. G.; Shaw, B. M.; Baar, C. R.; Kazakov, A.; McKay, I. D.; Jeremic, D. Polyethylene Film. US8829137B2, September 9, 2014.

(100) Gao, X.; Chisholm, P. S.; Kowalchuk, M. G.; Donaldson, R. D. Catalyst for Olefin Polymerization. US6734266B2, May 11, 2004.

(101) Speca, A. N. Highly Active Supported Catalyst Compositions. US6368999B1, April 9, 2002.

(102) Farley, J. M.; Adetunji, P. A.; Mirams, S. J.; Beckton, G. L. Hafnocene Catalyzed Polyethylene Films Having Rapid Cling Development. WO2014144397 (A2), September 18, 2014.

(103) Luo, L.; Sangokoya, S. A.; Wu, X.; Diefenbach, S. P.; Kneale, B. Aluminoxane Catalyst Activators Derived from Dialkylaluminum Cation Precursor Agents, Processes for Making Same, and Use Thereof in Catalysts and Polymerization of Olefins. US8354485B2, January 15, 2013.

(104) Denifl, P.; Van, P. E.; Bartke, M.; Oksman, M.; Mustonen, M.; Garoff, T.; Pesonen, K. Production of Olefin Polymerisation Catalysts. WO03051934 (A2).

(105) Bartke, M.; Oksman, M.; Mustonen, M.; Denifl, P. A New Heterogenization Technique for Single-Site Polymerization Catalysts. *Macromol. Mater. Eng.* 2005, *290* (4), 250–255. https://doi.org/10.1002/mame.200400288.

(106) Tynys, A.; Saarinen, T.; Bartke, M.; Löfgren, B. Propylene Polymerisations with Novel Heterogeneous Combination Metallocene Catalyst Systems. *Polymer* 2007, *48* (7), 1893–1902. https://doi.org/10.1016/j.polymer.2007.02.020.

(107) Heiskanen, H.; Denifl, P.; Hurme, M.; Pitkänen, P. Novel Preparation and Properties of Microspheres Involving a Hydrocarbon-Perfluorocarbon Solvent Extraction Process. *Chem. Eng. Technol.* 2010, *33* (4), 682–691. https://doi.org/10.1002/ceat.200900371.

(108) Aumo, J.; Matikainen, P.; Bartke, M.; Elovirta, T.; Vijay, S.; Lylykangas, M.; Elo, P.; Huhtanen, L. Process for Olefin Polymerization. US8501881B2, August 6, 2013.

(109) Kallio, K.; Mustonen, M.; Huhtanen, L.; Severn, J.; Castro, P.; Virkkunen, V.; Hongell, A.-L.; Lehtiniemi, I. Catalyst for the Polymerisation of Olefins. EP2722345 (A1).

(110) Kallio, K.; Mustonen, M.; Elo, P.; Severn, J.; Denifl, P. Preparation of a Solid Catalyst System. US8828901B2, September 9, 2014.

(111) Sangokoya, S. A. 54) LIQUID CLATHRATE ALUMNOXANE COMPOSITIONS. 8.

(112) Sangokoya, S. A. Liquid Clathrate Aluminoxane Compositions as Co-Catalysts with Transition Metal Catalyst Compounds. US5922631A, July 13, 1999.

(113) Elo, P.; Severn, J.; Denifl, P.; Rautio, S.; Mustonen, M.; Hongell, A.-L. Process for the Preparation of an Unsupported, Solid Metallocene Catalyst System and Its Use in Polymerization of Olefins. US8420562B2, April 16, 2013.

(114) Kallio, K.; FI; Mustonen, M.; FI; Elo, P.; FI; Severn, J.; FI; Denifl, P.; FI. United States Patent: 8828901 - Preparation of a Solid Catalyst System. 8828901, September 9, 2014.

(115) Valonen, J.; Mustonen, M. Process for the Preparation of a Solid Metallocene Catalyst System and Its Use in Polymerisation of Olefins. US8822365B2, September 2, 2014.

(116) Reznichenko, A.; Ajellal, N.; Castro, P.; Saeed, I. Solid Single Site Catalysts with High Polymerisation Activity. WO2015062936 (A1).

(117) Arnold, T. A. Q.; Turner, Z. R.; Buffet, J.-C.; O'Hare, D. Polymethylaluminoxane Supported Zirconocene Catalysts for Polymerisation of Ethylene. *J. Organomet. Chem.* 2016, *822*, 85–90. https://doi.org/10.1016/j.jorganchem.2016.08.015.

(118) Lamb, J. V.; Buffet, J.-C.; Turner, Z. R.; O'Hare, D. Group 4 Permethylindenyl Complexes for Slurry-Phase Polymerisation of Ethylene. *Polym. Chem.* 2019, *10* (11), 1386–1398. https://doi.org/10.1039/C8PY01796D.

(119) Kilpatrick, A. F. R.; Buffet, J.-C.; Nørby, P.; Rees, N. H.; Funnell, N. P.; Sripothongnak, S.; O'Hare, D. Synthesis and Characterization of Solid Polymethylaluminoxane: A Bifunctional Activator and Support for Slurry-Phase Ethylene Polymerization. *Chem. Mater.* 2016, *28* (20), 7444–7450. https://doi.org/10.1021/acs.chemmater.6b03009.

(120) Lamb, J. V.; Buffet, J.-C.; Turner, Z. R.; O'Hare, D. Ethylene Polymerization Using Zirconocenes Supported on Pentafluorophenyl-Modified Solid Polymethylaluminoxane. *Macromolecules* 2020, *53* (3), 929–935. https://doi.org/10.1021/acs.macromol.9b02146.

(121) Buffet, J.-C.; Arnold, T. A. Q.; Turner, Z. R.; Angpanitcharoen, P.; O'Hare, D. Synthesis and Characterisation of Permethylindenyl Zirconium Complexes and Their Use in Ethylene Polymerisation. *RSC Adv.* 2015, *5* (106), 87456–87464. https://doi.org/10.1039/C5RA20465H.

(122) *Tailor-Made Polymers: Via Immobilization of Alpha-Olefin Polymerization Catalyst*; Severn, J., Ed.; Wiley-VCH: Weinheim, 2008.

(123) Prades, F.; Broyer, J.-P.; Belaid, I.; Boyron, O.; Miserque, O.; Spitz, R.; Boisson, C. Borate and MAO Free Activating Supports for Metallocene Complexes. *ACS Catal.* 2013, *3* (10), 2288–2293. https://doi.org/10.1021/cs400655y.

(124) Yano, A.; Sato, M. Olefin Polymerization Catalyst and Olefin Polymerization Process. US5830820A, November 3, 1998.

(125) Kaneko, T.; Yano, A. Olefin Polymerisation Catalysts and Processes for Producing Olefin Polymers. EP0849292A1, June 24, 1998.

(126) Hamura, S.; Yasuda, H.; Yoshida, T.; Sato, M. Catalyst for Polymerization of an Olefin, and Method for Producing an Olefin Polymer. US5906955A, May 25, 1999.

(127) Wei, L.; Tang, T.; Huang, B. Synthesis and Characterization of Polyethylene/Clay–Silica Nanocomposites: A Montmorillonite/Silica-Hybrid-Supported Catalyst and in Situ Polymerization. *J. Polym. Sci. Part Polym. Chem.* 2004, *42* (4), 941–949. https://doi.org/10.1002/pola.11053.

(128) Liu, C. Zirconocene Catalyst Well Spaced inside Modified Montmorillonite for Ethylene Polymerization: Role of Pretreatment and Modification of Montmorillonite in Tailoring Polymer Properties. *J. Catal.* 2004, *221* (1), 162–169. https://doi.org/10.1016/j.jcat.2003.08.013.

(129) Suga, Y.; Maruyama, Y.; Isobe, E.; Suzuki, T.; Shimizu, F. Catalyst for Polymerizing an Olefin and Method for Producing an Olefin Polymer. US5308811A, May 3, 1994.

(130) Suga, Y.; Uehara, Y.; Maruyama, Y.; Isobe, E.; Ishihama, Y.; Sagae, T. Catalyst for Polymerizing an Olefin and Method for Polymerizing the Olefin. US5928982A, July 27, 1999.

(131) Weiss, K.; Wirth-Pfeifer, C.; Hofmann, M.; Botzenhardt, S.; Lang, H.; Brüning, K.; Meichel, E. Polymerisation of Ethylene or Propylene with Heterogeneous Metallocene Catalysts on Clay Minerals. *J. Mol. Catal. Chem.* 2002, *182–183*, 143–149. https://doi.org/10.1016/S1381-1169(01)00481-2.

(132) Kurokawa, H.; Morita, S.; Matsuda, M.; Suzuki, H.; Ohshima, M.; Miura, H. Polymerization of Ethylene Using Zirconocenes Supported on Swellable Cation-Exchanged Fluorotetrasilicic Mica. *Appl. Catal. Gen.* 2009, *360* (2), 192–198. https://doi.org/10.1016/j.apcata.2009.03.017.

(133) Nakano, H.; Takahashi, T.; Uchino, H.; Tayano, T.; Sugano, T. 4 - Polymerization Behavior with Metallocene Catalyst Supported by Clay Mineral Activator. In *Studies in Surface Science and Catalysis*; Shiono, T., Nomura, K., Terano, M., Eds.; Progress in Olefin Polymerization Catalysts and Polyolefin Materials; Elsevier, 2006; Vol. 161, pp 19–24. https://doi.org/10.1016/S0167-2991(06)80428-3.

(134) Angaji, M. T.; Zinali, A. Z.; Qazvini, N. T. Study of Physical, Chemical and Morphological Alterations of Smectite Clay upon Activation and Functionalization via the Acid Treatment. *World J. Nano Sci. Eng.* 2013, *3* (4), 161–168. https://doi.org/10.4236/wjnse.2013.34019.

(135) Novokshonova, L. A.; Kovaleva, N. Yu.; Ushakova, T. M.; Meshkova, I. N.; Krasheninnikov, V. G.; Ladygina, T. A.; Leipunskii, I. O.; Zhigach, A. N.; Kuskov, M. L. Partially Hydrolyzed Alkylaluminums as the Active Heterogenized Components of Metallocene Catalysts. *Kinet. Catal.* 2005, *46* (6), 853–860. https://doi.org/10.1007/s10975-005-0147-z.

(136) Camejo-Abreu, C.; Tabernero, V.; Alba, M. D.; Cuenca, T.; Terreros, P. Enhanced Activity of Clays and Its Crucial Role for the Activity in Ethylene Polymerization. *J. Mol. Catal. Chem.* 2014, *393*, 96–104. https://doi.org/10.1016/j.molcata.2014.05.030.

(137) Sano, T.; Niimi, T.; Miyazaki, T.; Tsubaki, S.; Oumi, Y.; Uozumi, T. Effective Activation of Metallocene Catalyst with AlMCM-41 in Propylene Polymerization. 6.

(138) Tayano, T.; Uchino, H.; Sagae, T.; Yokomizo, K.; Nakayama, K.; Ohta, S.; Nakano, H.; Murata, M. Effect of Acid Treatment of Montmorillonite on "Support-Activator" Performance to Support Metallocene for Propylene Polymerization Catalyst. *Macromol. React. Eng.* 2017, *11* (2), 1600017. https://doi.org/10.1002/mren.201600017.

(139) Tayano, T.; Uchino, H.; Sagae, T.; Ohta, S.; Kitade, S.; Satake, H.; Murata, M. Locating the Active Sites of Metallocene Catalysts Supported on Acid-Treated Montmorillonite. *J. Mol. Catal. Chem.* 2016, *420*, 228–236. https://doi.org/10.1016/j.molcata.2016.04.016.

(140) Copéret, C.; Chabanas, M.; Petroff Saint-Arroman, R.; Basset, J.-M. Homogeneous and Heterogeneous Catalysis: Bridging the Gap through Surface Organometallic Chemistry. *Angew. Chem. Int. Ed.* 2003, *42* (2), 156–181.

(141) Copéret, C.; Allouche, F.; Chan, K. W.; Conley, M. P.; Delley, M. F.; Fedorov, A.; Moroz, I. B.; Mougel, V.; Pucino, M.; Searles, K.; Yamamoto, K.; Zhizhko, P. A. Bridging the Gap between Industrial and Well-Defined Supported Catalysts. *Angew. Chem. Int. Ed.* 2018, *57* (22), 6398–6440. https://doi.org/10.1002/anie.201702387.

(142) Basset, J. M.; Candy, J. P.; Choplin, A.; Nédez, C.; Quignard, F.; Santini, C. C.; Théolier, A. From Clusters and Surfaces to Clusters on Surfaces: An Opening toward Surface Organometallic Chemistry. *Mater. Chem. Phys.* 1991, *29* (1–4), 5–32. https://doi.org/10.1016/0254-0584(91)90003-D.

(143) Basset, J. M.; Candy, J. P.; Choplin, A.; Didillon, B.; Quignard, F.; Theolier, A. Surface Organometallic Chemistry on Oxides, on Zeolites and on Metals. In *Perspectives in Catalysis*; Thomas J M, Z. K. I., Ed.; Vol.; Blackwell Scientific Publisher, 1992; pp 125–145.

(144) Scott, S. L.; Basset, J.-M. Coordination Chemistry on Surfaces: A New Method To Graft Rhenium(VII) Oxide on Highly Dehydroxylated Oxides. *J. Am. Chem. Soc.* 1994, *116* (26), 12069–12070. https://doi.org/10.1021/ja00105a064.

(145) Lefebvre, F.; Thivolle-Cazat, J.; Dufaud, V.; Niccolai, G. P.; Basset, J.-M. Oxide Supported Surface Organometallic Complexes as a New Generation of Catalysts for Carbon–Carbon Bond Activation. *Appl. Catal. Gen.* 1999, *182* (1), 1–8. https://doi.org/10.1016/S0926-860X(98)00420-7.

(146) Lopez, L. P. H.; Schrock, R. R.; Müller, P. Dimers That Contain Unbridged W(IV)/W(IV) Double Bonds. *Organometallics* **2006**, *25* (8), 1978–1986. https://doi.org/10.1021/om050961s.

(147) *Modern Surface Organometallic Chemistry*; Basset, J.-M., Ed.; Wiley-VCH: Weinheim, 2009.

(148) Surface Organometallic Chemistry of Tin: Grafting Reaction of Sn(CH3)4 in HY Zeolite Supercage | Chemistry Letters https://www-journal-csj-jp.docelec.univ-lyon1.fr/doi/10.1246/cl.2000.1164 (accessed Dec 18, 2019).

(149) Ryndin, Yu. A.; Candy, J. P.; Didillon, B.; Savary, L.; Basset, J. M. Surface Organometallic Chemistry on Metals Applied to the Environment: Hydrogenolysis of AsPh3 with Nickel Supported on Alumina. *J. Catal.* **2001**, *198* (1), 103–108. https://doi.org/10.1006/jcat.2000.3116.

(150) Deghedi, L.; Basset, J.-M.; Bergeret, G.; Candy, J.-P.; Valero, M. C.; Dalmon, J.-A.; De Mallmann, A.; Dubreuil, A.-C.; Fischer, L. Preparation of Nanosized Bimetallic Ni-Sn and Ni-Au/SiO2 Catalysts by SOMC/M. Correlation between Structure and Catalytic Properties in Styrene Hydrogenation. In *Studies in Surface Science and Catalysis*; Gaigneaux, E. M., Devillers, M., Hermans, S., Jacobs, P. A., Martens, J. A., Ruiz, P., Eds.; Scientific Bases for the Preparation of Heterogeneous Catalysts; Elsevier, 2010; Vol. 175, pp 617–620. https://doi.org/10.1016/S0167-2991(10)75121-1.

(151) Zhuravlev, L. T. The Surface Chemistry of Amorphous Silica. Zhuravlev Model. *Colloids Surf. Physicochem. Eng. Asp.* **2000**, *173* (1–3), 1–38.

(152) Lataste, E.; Demourgues, A.; Leclerc, H.; Goupil, J.-M.; Vimont, A.; Durand, E.; Labrugère, C.; Benalla, H.; Tressaud, A. Access to Highly Fluorinated Silica by Direct F_2 Fluorination: Chemical Compositions and FTIR Investigations. *J. Phys. Chem. C* **2008**, *112* (29), 10943–10951. https://doi.org/10.1021/jp710790e.

(153) Morrow, B. A.; McFarlan, A. J. Infrared and Gravimetric Study of an Aerosil and a Precipitated Silica Using Chemical and Hydrogen/Deuterium Exchange Probes. *Langmuir* **1991**, *7* (8), 1695–1701. https://doi.org/10.1021/la00056a022.

(154) Millot, N.; Santini, C. C.; Lefebvre, F.; Basset, J.-M. Surface Organometallic Chemistry: A Route to Well-Defined Boron Heterogeneous Co-Catalyst for Olefin Polymerisation. *Comptes Rendus Chim.* **2004**, *7* (8–9), 725–736. https://doi.org/10.1016/j.crci.2004.03.011.

(155) Morrow, B. A.; McFarlan, A. J. Chemical Reactions at Silica Surfaces. *J. Non-Cryst. Solids* **1990**, *120* (1–3), 61–71. https://doi.org/10.1016/0022-3093(90)90191-N.

(156) E. Piers, W.; Chivers, T. Pentafluorophenylboranes: From Obscurity to Applications. *Chem. Soc. Rev.* **1997**, *26* (5), 345–354. https://doi.org/10.1039/CS9972600345.

(157) Bochmann, M. Cationic Group 4 Metallocene Complexes and Their Role in Polymerisation Catalysis: The Chemistry of Well Defined Ziegler Catalysts. *J. Chem. Soc. Dalton Trans.* **1996**, No. 3, 255–270. https://doi.org/10.1039/DT9960000255.

(158) Turner, H. W.; Hlatky, G. G.; Eckman, R. R. Ionic Metallocene Catalyst Compositions. US5198401A, March 30, 1993.

(159) Ewen, J. A.; Elder, M. J. Preparation of Metallocene Catalysts for Polymerization of Olefins. US5387568A, February 7, 1995.

(160) Chien, J. C. W.; Tsai, W. M.; Rausch, M. D. Isospecific Polymerization of Propylene Catalyzed by Rac-Ethylenebis(Indenyl)Methylzirconium Cation. *J. Am. Chem. Soc.* 1991, *113* (22), 8570–8571. https://doi.org/10.1021/ja00022a081.

(161) Yang, X.; Stern, C. L.; Marks, T. J. Cation-like Homogeneous Olefin Polymerization Catalysts Based upon Zirconocene Alkyls and Tris(Pentafluorophenyl)Borane. *J. Am. Chem. Soc.* 1991, *113* (9), 3623–3625. https://doi.org/10.1021/ja00009a076.

(162) Lancaster, S. J.; Walker, D. A.; Thornton-Pett, M.; Bochmann, M. New Weakly Coordinating Counter Anions for High Activity Polymerisation Catalysts: [(C6F5)3B–CN–B(C6F5)3]− and [Ni{CNB(C6F5)3}4]2−. *Chem. Commun.* 1999, No. 16, 1533–1534. https://doi.org/10.1039/a903788h.

(163) Zhou, J.; Lancaster, S. J.; Walker, D. A.; Beck, S.; Thornton-Pett, M.; Bochmann, M. Synthesis, Structures, and Reactivity of Weakly Coordinating Anions with Delocalized Borate Structure: The Assessment of Anion Effects in Metallocene Polymerization Catalysts. *J. Am. Chem. Soc.* 2001, *123* (2), 223–237. https://doi.org/10.1021/ja002820h.

(164) LaPointe, R. E.; Roof, G. R.; Abboud, K. A.; Klosin, J. New Family of Weakly Coordinating Anions. *J. Am. Chem. Soc.* 2000, *122* (39), 9560–9561. https://doi.org/10.1021/ja002664e.

(165) Kehr, G.; Roesmann, R.; Fröhlich, R.; Holst, C.; Erker, G. Protonation of the Heterocyclic Cp-Anion Equivalent [Pyrrolyl-B(C6F5)3]Li − Formation of a Useful Neutral Brønsted Acid for the Generation of Homogeneous Metallocene Ziegler Catalysts. *Eur. J. Inorg. Chem.* 2001, *2001* (2), 535–538. https://doi.org/10.1002/1099-0682(200102)2001:2<535::AID-EJIC535>3.0.CO;2-6.

(166) Blackwell, J. M.; Piers, W. E.; Parvez, M.; McDonald, R. Solution and Solid-State Characteristics of Imine Adducts with Tris(Pentafluorophenyl)Borane. *Organometallics* 2002, *21* (7), 1400–1407. https://doi.org/10.1021/om011086n.

(167) Focante, F.; Camurati, I.; Nanni, D.; Leardini, R.; Resconi, L. Synthesis and Reactivity of *N* -Heterocycle-B(C_6F_5)$_3$ Complexes. 3. Generation of *N* -Methylpyrrol-2-Yl and *N* -Methylindol-2-Yl Borate Zwitterions with Acidic Sp^3 Carbons. *Organometallics* 2004, *23* (22), 5135–5141. https://doi.org/10.1021/om0499308.

(168) Siedle, A. R.; Newmark, R. A.; Lamanna, W. M.; Huffman, J. C. Structure of a Zirconoxyborane Having a Zirconium-Fluorine-Carbon Bridge. *Organometallics* 1993, *12* (5), 1491–1492. https://doi.org/10.1021/om00029a002.

(169) Elder, M. J.; Ewen, J. A. Cationic Metallocene Catalysts Based on Triphenylcarbenium Aluminum. EP0573403 (A2), December 8, 1993.

(170) Sun, Y.; Metz, M. V.; Stern, C. L.; Marks, T. J. Al-, Nb-, and Ta-Based Perfluoroaryloxide Anions as Cocatalysts for Metallocene-Mediated Ziegler−Natta Olefin Polymerization. *Organometallics* 2000, *19* (9), 1625–1627. https://doi.org/10.1021/om990946l.

(171) Pédeutour, J.-N.; Radhakrishnan, K.; Cramail, H.; Deffieux, A. Reactivity of Metallocene Catalysts for Olefin Polymerization: Influence of Activator Nature and Structure. *Macromol. Rapid Commun.* 2001, *22* (14), 1095–1123. https://doi.org/10.1002/1521-3927(20011001)22:14<1095::AID-MARC1095>3.0.CO;2-R.

(172) Walzer, J. F. Jr. Supported Ionic Catalyst Composition. US5972823A, October 26, 1999.

(173) Walzer, J. F. Jr. Supported Ionic Catalyst Composition. US5643847A, July 1, 1997.

(174) Ward, D. G.; Carnahan, E. M. Supported Catalytic Activator. US5939347A, August 17, 1999.

(175) Bochmann, M.; Pindado, G. J.; Lancaster, S. J. The Versatile Chemistry of Metallocene Polymerisation Catalysts: New Developments in Half-Sandwich Complexes and Catalyst Heterogenisation. *J. Mol. Catal. Chem.* 1999, *146* (1–2), 179–190. https://doi.org/10.1016/S1381-1169(99)00064-3.

(176) Charoenchaidet, S.; Chavadej, S.; Gulari, E. Borane-Functionalized Silica Supports. *J. Mol. Catal. Chem.* 2002, *185* (1–2), 167–177. https://doi.org/10.1016/S1381-1169(02)00002-X.

(177) Charoenchaidet, S.; Chavadej, S.; Gulari, E. Methylaluminoxane-Free Ethylene Polymerization within Situ Activated Zirconocene Triisobutylaluminum Catalysts and Silica-Supported Stabilized Borate Cocatalysts. *J. Polym. Sci. Part Polym. Chem.* 2002, *40* (19), 3240–3248. https://doi.org/10.1002/pola.10410.

(178) Charoenchaidet, S.; Chavadej, S.; Gulari, E. Improving the Performance of Heterogeneous Borane Cocatalysts by Pretreatment of the Silica Support with Alkylaluminum Compounds. *Macromol. Rapid Commun.* 2002, *23* (7), 426–431. https://doi.org/10.1002/1521-3927(20020401)23:7<426::AID-MARC426>3.0.CO;2-3.

(179) Tian, J.; Wang, S.; Feng, Y.; Li, J.; Collins, S. Borane-Functionalized Oxide Supports: Development of Active Supported Metallocene Catalysts at Low Aluminoxane Loading. *J. Mol. Catal. Chem.* 1999, *144* (1), 137–150. https://doi.org/10.1016/S1381-1169(98)00341-0.

(180) Millot, N.; Cox, A.; Santini, C. C.; Molard, Y.; Basset, J.-M. Surface Organometallic Chemistry of Main Group Elements: Selective Synthesis of Silica Supported [$\equiv$ Si- OB (C6F5) 3]-[HNEt2Ph]+. *Chem.- Eur. J.* 2002, *8* (6), 1438–1442.

(181) Millot, N.; Santini, C. C.; Baudouin, A.; Basset, J.-M. Supported Cationic Complexes: Selective Preparation and Characterization of the Well-Defined Electrophilic Metallocenium Cation [≡SiO–B(C_6F_5)$_3$]$^-$ [Cp*ZrMe_2(Et_2NPh)]$^+$ Supported on Silica. *Chem Commun* 2003, No. 16, 2034–2035. https://doi.org/10.1039/B304047J.

(182) Millot, N.; Santini, C. C.; Lefebvre, F.; Basset, J.-M. Surface Organometallic Chemistry: A Route to Well-Defined Boron Heterogeneous Co-Catalyst for Olefin Polymerisation. *Comptes Rendus Chim.* 2004, *7* (8–9), 725–736. https://doi.org/10.1016/j.crci.2004.03.011.

(183) Panchenko, V. N.; Danilova, I. G.; Zakharov, V. A.; Paukshtis, E. A. Silica-Supported Zirconocene/(Perfluorophenyl)Borate Catalyst for Propylene Polymerization. *J. Mol. Catal. Chem.* 2005, *225* (2), 271–277. https://doi.org/10.1016/j.molcata.2004.07.006.

(184) Turner, H. W. United States Patent: 5427991 - Polyionic Transition Metal Catalyst Composition. 5427991, June 27, 1995.

(185) Fritze, C.; Küber, F.; Bohnen, H. Covalently Supported Chemical Compound Which Can Be Neutral or Ionic in the Claims. US6329313B1, December 11, 2001.

(186) Carnahan, E. M.; Carney, M. J.; Neithamer, D. R.; Nickias, P. N.; Shih, K.-Y.; Spencer, L. Supported Catalyst Containing Tethered Cation Forming Activator. WO1997019959A1, June 5, 1997.

(187) Shih, K.-Y. Supported Bidentate and Tridentate Catalyst Compositions and Olefin Polymerization Using Same. US6184171B1, February 6, 2001.

(188) Jacobsen, G. B.; Dun, J. J. V.; Chum, P.-W. S.; Meiske, L. A.; Matsushita, F.; Miyamoto, A. Process for Preparing Copolymers and Blend Compositions Containing the Same. WO1997043323A1, November 20, 1997.

(189) Jacobsen, G. B.; Kimberley, B. S.; Mastroianni, S.; Taylor, M. J.; Garcia, E.; Lacane, G. Supported Polymerisation Catalysts. WO2004018530A1, March 4, 2004.

(190) Chum, P. S.; Swogger, K. W. Olefin Polymer Technologies—History and Recent Progress at The Dow Chemical Company. *Prog. Polym. Sci.* 2008, *33* (8), 797–819. https://doi.org/10.1016/j.progpolymsci.2008.05.003.

(191) Burkhardt, T. J.; Murata, M.; Brandley, W. B. Method for Making and Using a Supported Metallocene Catalyst System. US5240894A, August 31, 1993.

(192) Sauter, D. W.; Popoff, N.; Bashir, M. A.; Szeto, K. C.; Gauvin, R. M.; Delevoye, L.; Taoufik, M.; Boisson, C. The Design of a Bipodal Bis(Pentafluorophenoxy)Aluminate Supported on Silica as an Activator for Ethylene Polymerization Using Surface Organometallic Chemistry. *Chem. Commun.* 2016, *52* (26), 4776–4779. https://doi.org/10.1039/C6CC00060F.

(193) Luo, L.; Wu, K.; Diefenbach, S. P. Catalyst Activators, Processes for Making Same, and Use Thereof in Catalysts and Polymerization of Olefins. US7928172B2, April 19, 2011.

(194) Popoff, N.; Espinas, J.; Pelletier, J.; Szeto, K. C.; Thivolle-Cazat, J.; Delevoye, L.; Gauvin, R. M.; Taoufik, M. Design and Application of a Hybrid Material Featuring Well-Defined, Tuneable Grafting Sites for Supported Catalysis. *ChemCatChem* 2013, *5* (7), 1971–1977. https://doi.org/10.1002/cctc.201200850.

(195) Schumann, Herbert.; Meese-Marktscheffel, J. A.; Esser, Lothar. Synthesis, Structure, and Reactivity of Organometallic .Pi.-Complexes of the Rare Earths in the Oxidation State Ln3+ with Aromatic Ligands. *Chem. Rev.* 1995, *95* (4), 865–986. https://doi.org/10.1021/cr00036a004.

(196) Zeimentz, P. M.; Arndt, S.; Elvidge, B. R.; Okuda, J. Cationic Organometallic Complexes of Scandium, Yttrium, and the Lanthanoids. *Chem. Rev.* 2006, *106* (6), 2404–2433. https://doi.org/10.1021/cr050574s.

CHAPTER II:

Development and application of $[(\equiv SiO)_2Al(OC_6F_5)_2]^-[HNMe_2Et]^+$ as activating support for metallocenes

Index

Introduction

As discussed in the introduction, the aim of this experimental work is the development by SOMC of Activating Supports (AS) for molecular catalysts and their application in ethylene polymerization.

Solid activators obtained by the reaction of organometallic aluminium precursors with a support (namely silica) treated at different temperatures, proved to be very efficient co-catalysts for metallocenes in ethylene polymerization. In the majority of the cases, though, none or very little importance was given to the study and deep characterization of the structures formed on the surface after the immobilization reaction of the Aluminium complexes on the surface.[1,2]

It is in this aspect that the SOMC approach applied by our group shows its great advantages. Recently in our group was successfully synthesised a well-defined activating support, **1**, following the pathway reported in Scheme 1.[3]

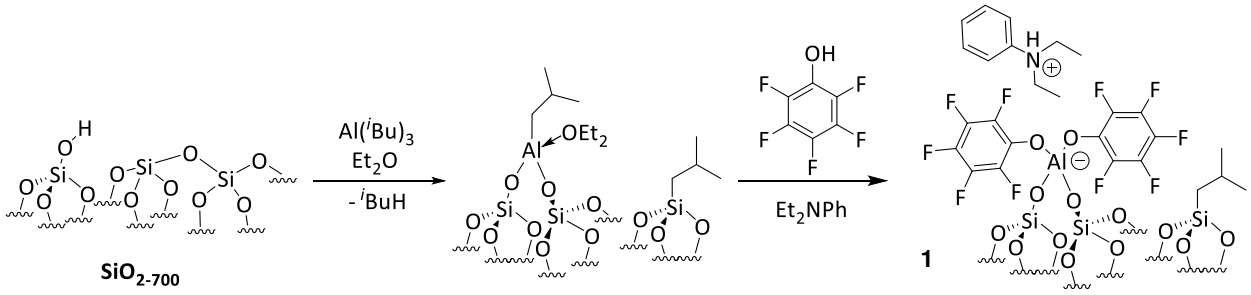

Scheme 1 – Synthetic pathway for the synthesis of **1** well-defined activating support for molecular catalysts.[3]

This activating support, **1**, showed discreet efficiency when tested as co-catalyst for *rac*-$EtInd_2ZrCl_2$ in ethylene/1-hexene copolymerization in presence of an excess of TiBA , 656 $g_{PE}\ g_{cat}^{-1}\ h^{-1}$, 22500 $Kg_{PE}\ mol_{Zr}^{-1}\ h^{-1}$.

The moderate activity obtained by the system **1**/rac-$EtInd_2ZrCl_2$/TiBA could be ascribed to a not efficient separation of the ionic couple (cationic Zirconium complex and anionic aluminate).

Recent studies in the field of olefin metathesis have shown the great influence of the treatment of the support on the activity of Mo or W based catalysts.[4] These studies demonstrated that the amplitude of the (≡SiO-M-OSi≡) bite angle has a direct impact on the catalyst's performances.

In order to investigate the effect of the treatment of the support also in the case of olefin polymerization, we devised a different synthetic pathway to obtain a bipodal aluminate activating support on silica dehydroxylated at 200°C.[5] The pathway followed is depicted in Scheme 2.

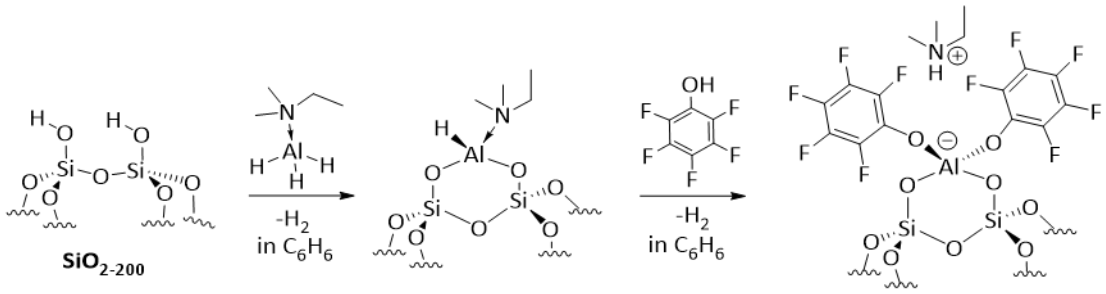

Scheme 2 – Synthetic pathway for AS1.

Using silica treated at lower temperatures will ideally generate bipodal aluminate species with a different (≡SiO-M-OSi≡) bite angle and a different coordinating ability than **1**, which will then reflect on its efficiency as a cocatalyst for metallocenes in ethylene polymerization.

1. Synthesis of $[(\equiv SiO)_2Al(OC_6F_5)_2]^-[HNMe_2Et]^+$, AS1

1.1 Silica treatment, dehydroxylation at 200°C, $SiO_{2\text{-}200}$

The silica chosen for the synthesis of the activating supports developed in this work is the Sylopol 2408 from Grace Davidson. This silica presents a specific area of 300 $m^2 g^{-1}$, a Pore Volume of 1.55 mL g^{-1} and particle size of 40 µm, and was selected for its good fragmentation behaviour during the polymerization.[5]

Before the reaction the support was partially dehydroxylated for 14 hours under dynamic high vacuum (1 mPa) at 200°C, in order to remove all the water and partially condensate the silanols on the surface.

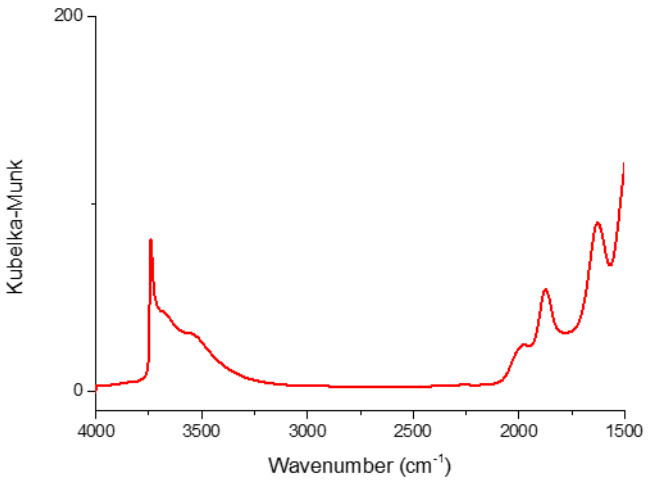

Figure 1 – DRIFT spectrum for $SiO_{2\text{-}200}$.

The DRIFT spectrum (Figure 1) of the surface of the support showed a peak at 3743 cm^{-1} proper of the O-H stretching of the isolated silanols and two overlapping bands at 3680 and 3570 cm^{-1} characteristic of vicinal and geminal groups.

The amount of silanols (SiOH) on the surface, determined by titration by reaction with CH_3MgBr, was 1.62 mmol g^{-1}.

1.2 Grafting of $AlH_3(NEtMe_2)$ on $SiO_{2\text{-}200}$, P1

In order to synthetize the bipodal activating support AS1, we first generated the bipodal aluminium precursor. 1.2 eq. of AlH_3NMe_2Et per 2 eq. of SiOH were put to react in benzene for two hours to obtain $(\equiv SiO)_2AlH(NMe_2Et)$, P1 (Scheme 3).

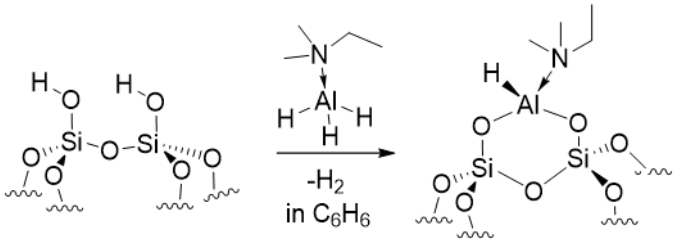

Scheme 3 – Grafting $AlH_3(NMe_2Et)$ on $SiO_{2\text{-}200}$ in C_6H_6 at room temperature

Material P1 was characterized by DRIFT spectroscopy. In Figure 2 are reported the spectra before and after the reaction.

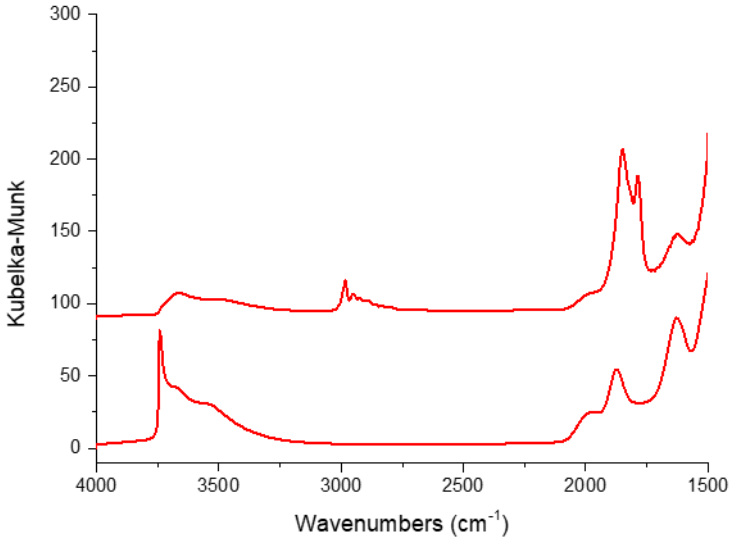

Figure 2 – DRIFT spectra of $SiO_{2\text{-}200}$ before the grafting (bottom) and after the grafting of the aluminium hydride, $(\equiv SiO)_2AlH(NMe_2Et)$ (top).

The disappearance of the signal at 3747 cm^{-1} and the decreasing of the intensity of the bands at 3570 and 3680 cm^{-1}, signifies that all the accessible SiOH groups on the surface reacted with the $AlH_3.NMe_2Et$.

Between 2700 and 2900 cm^{-1} fall the peaks of the C-H bond stretching of the amine's alkyl fragments, while at 1850 and 1800 cm^{-1} appear the peaks of the Al-H bond stretching of the

aluminium hydride (this assignment is in agreement with what is reported by Humphries et al. for free alane).[6] The amount of H_2 released by the hydrolysis of P1 was quantified, and reported in Table 1 with the elemental analysis quantifications for the grafted adduct.

Table 1 – Elemental analysis and GC results for $(\equiv SiO)_2AlH(NMe_2Et)$.

wt% Al	wt% C	wt% N	wt% H	C/N	C/Al	N/Al	H/Al	Al mmol g^{-1}	H_2/Al Hydrolysis
2.69	4.71	1.45	1.12	3.8 (th. 4)	4.4 (th. 4)	1.1 (th. 1)	12.5 (th. 12)	1.0	1.1 (th. 1)

The presence of 2.69 wt% of aluminium on the surface is coherent with 1.0 mmol g^{-1} of grafted Al. The 4.4 C/Al and 1.1 N/Al ratios are close to the theoretical values, respectively 4 and 1, confirming the formation of bipodal $(\equiv SiO)_2AlH(NMe_2Et)$ species. This is furthermore corroborated by the quantification of the H_2 released by the hydrolysis of the product: 1.1 mmol(H_2) g^{-1} were evolved during the reaction, resulting in a H_2/Al ratio of 1.1 very close to the theoretical value of 1 for a bipodal aluminium hydride.

In Figure 3 are reported the ^1H MAS and ^{13}C CP/MAS-NMR spectra for P1, they reveal signals attributed to the methyl and ethyl groups bound to the nitrogen atom.

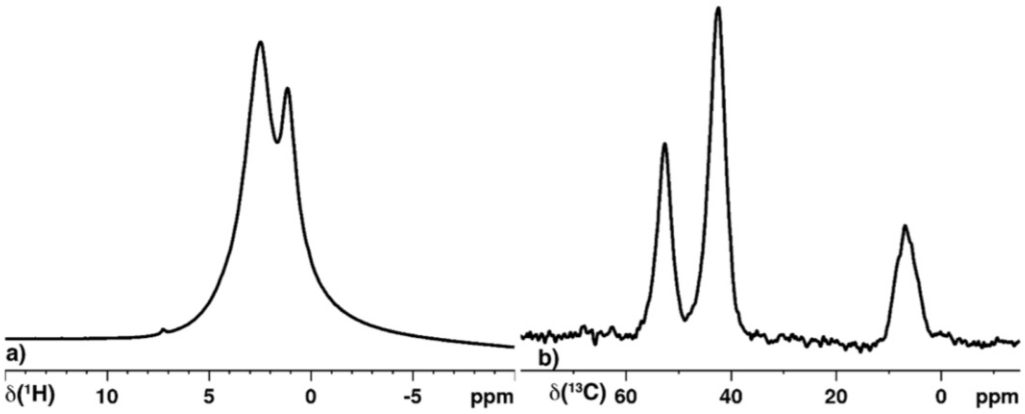

Figure 3 – a) ^1H MAS and b) ^{13}C CP-MAS NMR spectra for P1.

In the ^1H spectrum, the chemical shift at 1.3 ppm corresponds to the resonance of the methyl group from the NCH_2CH_3 fragment, whereas the signal at 2.7 ppm is attributed to the methyl and methylene groups bound to the nitrogen atom (Figure 3a). The signal for the hydride directly

bound to the Al cannot be seen because it falls underneath the peaks of the amine, around 3.9 ppm.[7]

The ^{13}C spectrum (Figure 3b) shows a broad peak at 6 ppm assigned to methyl group of the NCH_2CH_3 fragment, an intense signal at 42.3 ppm corresponding to the NCH_3 groups, and a signal at 52.2 ppm proper to the methylene of the ethyl group.

1.3 Modification of $(\equiv SiO)_2AlH(NMe_2Et)$ with pentafluorophenol, AS1

2.2 eq. of C_6F_5OH per eq. of Al were put to react with P1 in benzene. The reaction was left to proceed overnight to obtain the $[(\equiv SiO)_2Al(OC_6F_5)_2]^-[HNMe_2Et]^+$ ionic couple, according to the reaction reported in Scheme 4.

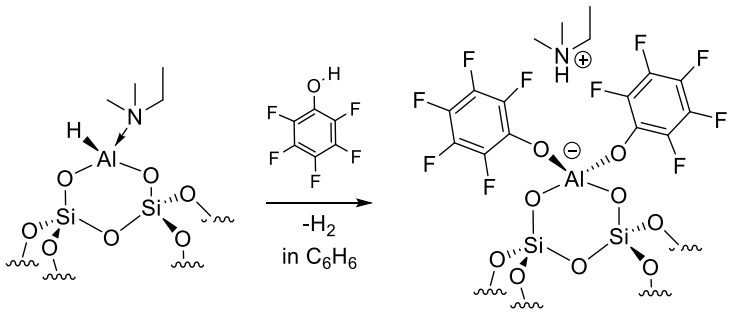

Scheme 4 – Synthesis of AS1 from P1.

The powder obtained was characterized by DRIFT spectroscopy. In Figure 4 are reported the DRIFT spectra for P1 (below) and AS1 (above).

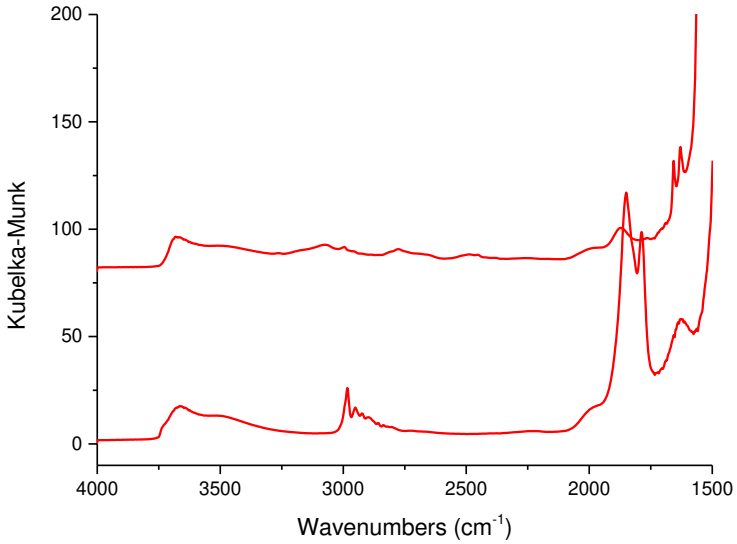

Figure 4 - DRIFT spectra $(\equiv SiO)_2AlH(NMe_2Et)$, P1 (bottom) and $[(\equiv SiO)_2Al(OC_6F_5)_2]^-[EtMe_2NH]^+$, AS1 (top).

The DRFT spectrum for AS1 shows the disappearance of the peaks at 1850 and 1800 cm^{-1} attributed to the Al-H bond stretching, indicating that all the hydrides on the surface reacted with the pentafluorophenol. The peak at 3070 cm^{-1}, proper of the N-H stretching of the ammonium, indicates the formation of the desired ionic couple, while below 3000 cm^{-1} there are broad signals of the C-H stretching.

In Table 2 are reported the elemental analysis results for AS1 and the quantification of the hydrogen evolved by the grafting reaction.

Table 2 – Elemental analysis and hydrogen quantification results for AS1.

wt% Al	wt% C	wt% N	C/N	C/Al	N/Al	Al mmol g^{-1}	H_2/Al Grafting
1.4	11.4	0.9	14.1 (th. 16)	18.2 (th. 16)	1.3 (th. 1)	0.55	0.8 (th. 1)

The amounts of 11.4 wt% C, 0.9 wt% N and 1.4 wt% Al on the surface, give a ratio C/Al and N/Al respectively of 18.2 and 1.3, very close to the theoretical value for the $[(\equiv SiO)_2Al(OC_6F_5)_2]^-[HNMe_2Et]^+$ ionic couple, 16 and 1 respectively. Also, the amount of hydrogen evolved by the reaction is compatible with the complete reaction of P1 with protic substrate C_6F_5OH to give the desired aluminate complex on the surface.

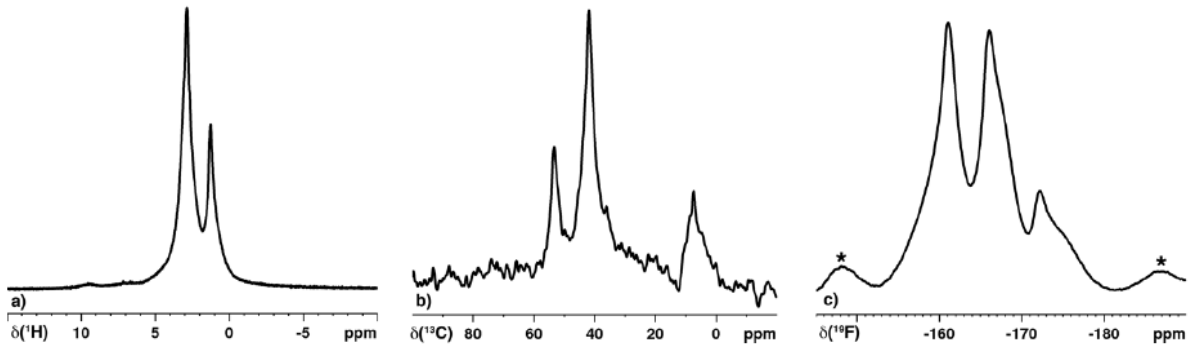

Figure 5 – Solid-state NMR spectra of AS1: a) ^1H MAS; b) ^{13}C CPMAS; c) ^{19}F MAS (asterisks indicate spinning side bands).

The ^1H and ^{13}C solid state NMR spectra for AS1 are very similar to those acquired for P1, in fact the protonation of the amine to ammonium doesn't affect much the chemical shift of the alkyl fragments bound to the N.

The ^{1}H spectrum shows at 1.3 ppm the resonance of the methyl fragment of the NCH_2CH_3 and at 2.9 ppm the signal of the NCH_3 and methylene group bound to the nitrogen atom.

The ^{13}C CPMAS NMR spectrum shows three signals at 7.4, 41.9 and 53.2 ppm respectively corresponding to the chemical shift of the methyls and the methylene of the NCH_2CH_3, and the NCH_3.

In both the ^{1}H and ^{13}C solid state NMR spectra the signals shifted slightly downfield, probably due to a shielding caused by the ionic character of AS1.

The presence of the $[(\equiv SiO)_2Al(OC_6F_5)_2]^-$ anion can be further confirmed by ^{19}F solid state NMR. The spectrum of AS1 shows three signals around -161, -166 and -173 ppm (Figure 5c). The intensities and chemical shifts of these three signals are characteristics of the ortho, meta and para fluorine atoms respectively, on the $[(\equiv SiO)_2Al(OC_6F_5)_2]^-$ anion, in agreement with literature data.[3,8]

AS1 was furtherly characterized by ^{27}Al MAS solid state NMR. The acquired spectrum is reported in Figure 6 in comparison with the ^{27}Al spectrum of activating support **1** obtained by functionalization of grafted bipodal Al-isobutyl, as shown in Scheme 1, and prepared in our laboratory facilities.[3]

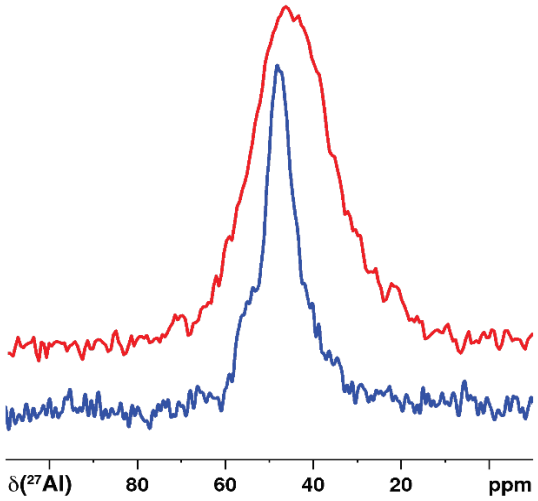

Figure 6 – ^{27}Al MAS NMR spectra of activating supports **1** (blue plot) and AS1 (red plot).

The comparison of the spectra acquired for the two activating supports **1** and AS1 reveals two signals of different shape and chemical shift. The signal of **1** is centered around 58 ppm and presents a line shape characteristic of quadrupolar coupling; the quadrupolar coupling constant (C_Q = 7.7 MHz) and asymmetry parameter (η= 0.8) are typical of aluminum centers in tetrahedral configuration, with a distorted AlO_4 coordination sphere. The fact that the spectrum can be modeled with only line broadening and no advanced distribution function (Czjzeck-type), proves that the species on the surface have a rather well-defined structure.[9] On the other hand, the ^{27}Al signal of AS1 features a chemical shift of 47.5 ppm, corresponding to a shift at the lower end of the AlO_4 region, or upper end of AlO_5 region.[10] In this case a Czjzeck-type distribution is necessary to model the signal, given its non-symmetric nature (it is broader than **1**), meaning that the Al centers in AS1 feature distribution of both chemical shift and quadrupolar coupling constant. Thus, the quadrupolar coupling constant of the AS1 signal (CQ = 4.2 MHz) is indicative of a slightly distorted environment. In addition, the chemical shift of this Al species present a Gaussian distribution of 18 ppm. These elements indicate that compared to **1**, the aluminum sites in AS1 are less uniform and feature a structure that is much less defined. This can be seen with the wide chemical shift distribution, which encompasses the AlO_4 and AlO_5 structures, that is with or without coordinated siloxane on the aluminate center. Thus, the difference between both NMR signals reveals differences in terms of the structure of both Al centers, even though their raw formula are similar. They both display a tetrahedral configuration but the distortion of this

geometry is not the same for both supported species. This difference in term of distortion could be explained by the differences in terms of synthesis ($SiO_{2\text{-}700}$ vs. $SiO_{2\text{-}200}$, grafting of TiBA vs. grafting of aluminum hydride, diethylaniline vs. dimethylethylamine for **1** and AS1, respectively). The different thermal treatments of silica lead to a different nature of the surface of silica which introduces geometrical and electronical differences in the structure of the resulting bipodal species. Based on these differences it would not be surprising that **1** and AS1 exhibit a different (≡SiO-Al-OSi≡) bite angle, or different degree of (≡Si-O-Si≡) coordination.

From the characterizations performed on AS1 it is possible to confirm the successful synthesis of the ionic couple $[(\equiv SiO)_2Al(OC_6F_5)_2]^-[HNMe_2Et]^+$, by grafting of an aluminium hydride on $SiO_{2\text{-}200}$ and successive modification of the bipodal hydride thus obtained with pentafluorophenol.

The activating support AS1 was then tested as cocatalyst for two different metallocenes in ethylene/1-hexene slurry co-polymerization.

2. Test in slurry polymerization of AS1 as cocatalyst for rac-$EtInd_2ZrCl_2$ and $(MeCpBu)_2ZrCl_2$

AS1 was tested as activator for two different zirconocene precursors, *rac*-$EtInd_2ZrCl_2$, Cat1, and (*n*-$BuCpMe)_2ZrCl_2$, Cat2, (Scheme 5) in presence of alkylating agent TiBA in ethylene/1-hexene slurry copolymerization.

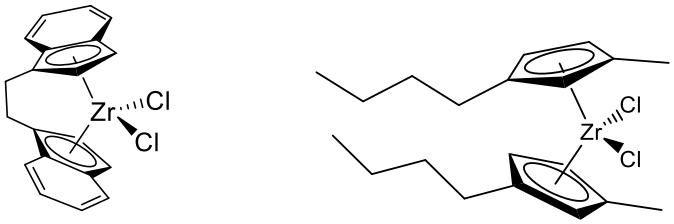

Scheme 5 – Structure for rac-$EtInd_2ZrCl_2$ (left) and (n-$BuCpMe)_2ZrCl_2$ (right)

The polymerization conditions used during the tests were the same for the two catalytic precursors. The polymerizations were conducted in 300 mL of heptane, at 80°C and 4 bars of

ethylene pressure for 30 minutes. The total concentration of [Zr] was 2 µM and TiBA was used as scavenger and alkylating agent in concentration 1 mM. The zirconocene precursor was activated right before the start of the polymerization by contacting it with the activating support in presence of TiBA, as alkylating agent.

The polymerization results for the two different catalytic systems, AS1/Cat1 and AS1/Cat2, are reported in Table 3.

Table 3 – Polymerization results obtained with the systems AS1/Cat1 and AS1/Cat2. General conditions: 80°C; 4 bars C_2H_4; 30 minutes; 300 mL heptane; [TiBA] 1 mM.

run	Catalyst	m mg	Zr µmol	$Zr/Al_{surface}$	Zr loading Wt%	C6 mol%	Yield g	Activity $g\ g^{-1}_{cat}\ h^{-1}$
1	AS1/*Cat1*	20.6	0.68	0.06	0.31	19.2	10.7	1111
2	AS1/*Cat2*	20.3	0.64	0.06	0.29	19.3	10.0	982

The polymerization tests showed high polymerization productivities for both systems, 1111 $g\ g_{cat}^{-1}\ h^{-1}$ for Cat1 and 982 $g\ g_{cat}^{-1}\ h^{-1}$ for Cat2, proving AS1 to be a highly efficient activating support for molecular catalysts. The two systems, though, showed a very different behaviour from a kinetic point of view. In Figure 7 are reported the kinetic profiles during the polymerization for runs 1 and 2.

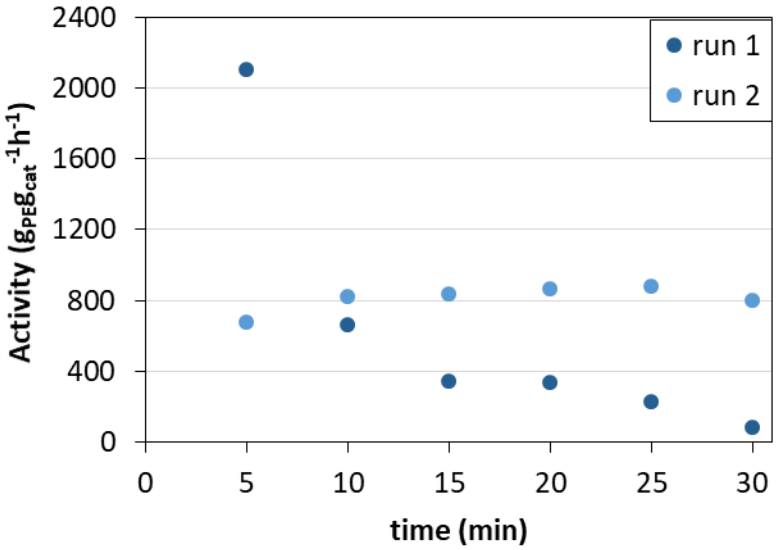

Figure 7 – Kinetic profiles for the polymerization tests performed with AS1/Cat1 and AS1/Cat2.

While AS1/Cat1 shows a very high boost in activity in the very first minutes of the polymerization followed by a rapid deactivation pattern, AS1/Cat2 presents a more stable activity throughout the polymerization time.

The great differences in the kinetic behaviour are certainly due to the intrinsic nature of the two zirconocenes, but it can also be attributed to possible deactivation phenomena occurring during the polymerization itself, more favourably for Cat1 than for Cat2.

In order to investigate if the activity shown by AS1/Cat2 remains stable even at longer polymerization times, a second polymerization test was performed with this system. The same polymerization conditions of run2 were used, but the polymerization lasted 60 minutes instead of 30. The results for run 3 are reported in Table 4 and the kinetic profile in Figure 8, in comparison with those of run 2.

Table 4 – Polymerization results obtained with the system AS1/Cat2. General conditions: 80°C; 4 bars C_2H_4; 300 mL heptane; [TiBA] 1 mM

run	Catalyst	m mg	Zr µmol	$Zr/Al_{surface}$	Zr loading Wt%	C6 mol%	time min	Yield g	Activity $g\ g^{-1}_{cat}\ h^{-1}$
2	AS/*Cat2*	20.3	0.64	0.06	0.29	19.3	30	10.0	982
3	AS/*Cat2*	21.2	0.68	0.06	0.29	19.2	60	16.7	788

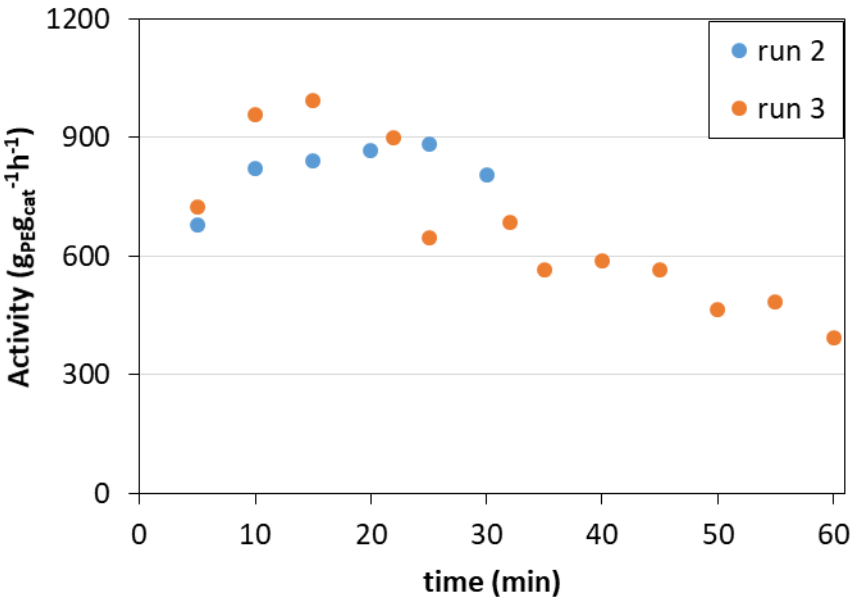

Figure 8 – Kinetic profiles for the polymerization tests performed with AS1/Cat2.

How it is shown in Figure 8, after the first 30 minutes of polymerization, system AS1/Cat2 starts to undergo to a slow deactivation pattern, although keeping a good overall stability throughout the polymerization, furthermore confirming that the kinetic profile of the test performed with AS1/Cat1 is characteristic of the zirconocene complex and not induced by the activating support.

The polymers obtained in run 1-3 were characterized by DSC and HT-SEC and IR spectroscopy. The amount of comonomer incorporated in the polymer chain was evaluated either by ^{13}C NMR or IR spectroscopy.

Table 5 – DSC, HT-SEC characterization comonomer incorporation quantification results for the polymers obtained in runs 1-3.

run	time min	Activity $g\ g^{-1}_{cat}\ h^{-1}$	$X_{1\text{-hexene}}$ (mol%)	Tf2 °C	Crystallinity %	M_n $g\ mol^{-1}$	M_w $g\ mol^{-1}$	Đ
1	30	1111	1.8	117	41	22000	60700	2.7
2	30	982	0.99	125	55	95000	213000	2.2
3	60	788	0.94	125	44	89300	204300	2.3

The polymers' characterization results show that the two catalysts differ not only in the polymerization kinetics but also for the type of resins produced at similar reaction conditions. Cat1 demonstrated a better incorporation ability than Cat2: at same co-monomer feed the amount of 1-hexene incorporated in the chain produced by AS1/Cat1 is almost double that of the resins produced in runs 2 and 3. The higher comonomer content of resin 1 is reflected in a lower melting temperature, 117°C, than those of the polymers obtained in runs 2-3, 125°C.

The products differ also in molar mass and molar mass distribution. While *rac*-$EtInd_2ZrCl_2$ produces resins with a fairly low M_w and broad dispersity (M_w 60 Kg mol^{-1} and Đ of 2.7), (*n*-$BuCpMe)_2ZrCl_2$ produces higher molecular weight polymer chains with a narrower molar mass distribution, closer to that expected for single-site catalysts (M_w of around 200 Kg mol^{-1}, Đ close to 2).

The narrow distribution obtained with Cat2 proved the single site nature of the catalyst during the polymerization. The molar mass distribution found for the polymer produced by Cat2, although larger than that predicted for a single-site catalyst, was already reported in literature for this

system,[2,11–13] and it could be attributed to the interaction of the zirconocene with the surface of the support.

The fluffs were then furtherly characterized by SEM microscopy, to evaluate the morphology of the resins produced. In Figures 9 and 10 are respectively reported the images acquired for run 1 and 2 respectively.

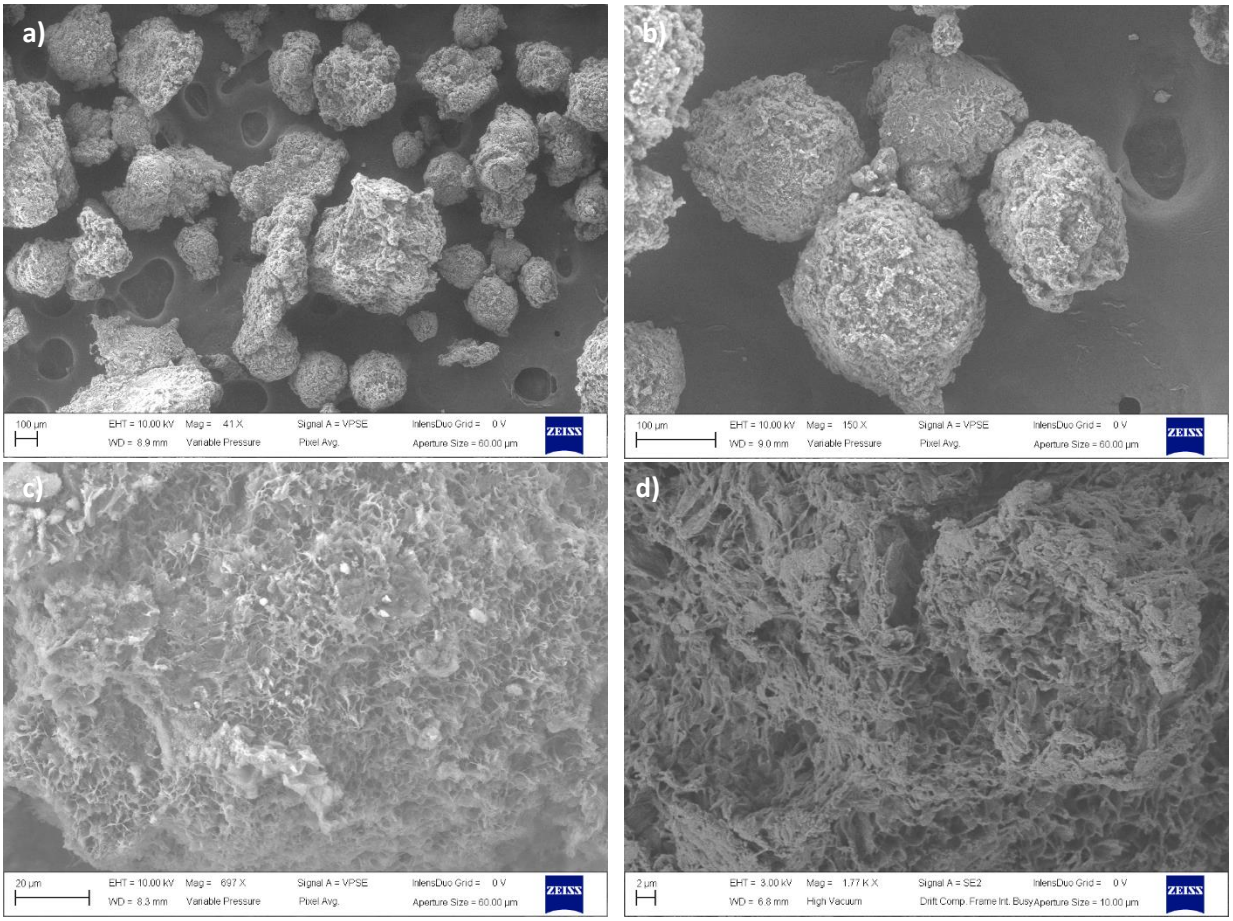

Figure 9 – SEM Images of the resins obtained with AS1/Cat1 at different magnifications: a) 40x; b) 150x; c) 700x; 1.77Kx.

In Figure 9 are depicted the SEM images acquired for the polymer obtained with the catalytic system AS1/Cat1 in run 1. From the general pictures it is possible to see the spherical particles proper of resins obtained in heterogeneous slurry polymerization processes such as the one used in this work. What is also possible to see from the pictures is the absence of undesirable fines. From the images at higher magnification is then possible to see the style of growth of the polymer.

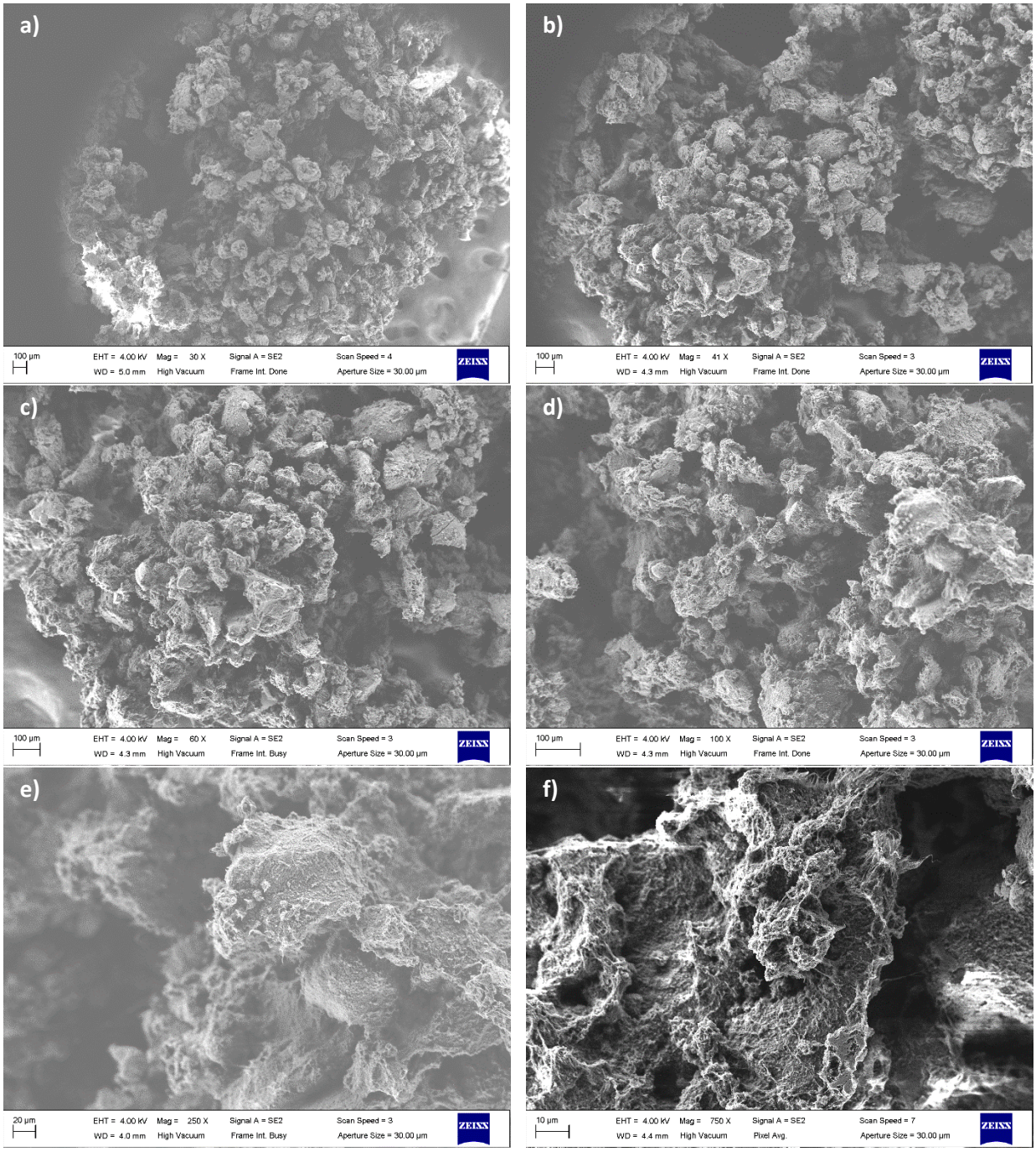

Figure 10 – SEM images acquired for the resin obtained with AS1/Cat2 at different magnifications: a)30x; b) 40x ; c) 60x; d) 100x; e) 250x; f) 750x.

In Figure 10 are depicted the SEM images acquired for the resin obtained with the catalytic system AS1/Cat2 in run 2. From the general pictures it is possible to see small agglomerates of spherical particles, results of the heterogeneous slurry polymerizations systems. It is not possible to say if these agglomerates were formed during the polymerization or, most probably, during the

recovering and drying of the product. What is though interesting to note, like for the case of Cat1, is the absence of fines. From the images acquired at higher magnifications, c), d), e), f), it is possible to see polymer's growth structure.

Both the activity and polymer characterization results indicate AS1 as a highly performing activating support for homogeneous catalysts in slurry ethylene/1-hexene copolymerization.

Given the promising results obtained at the laboratory scale, one of the two active systems investigated were tested at a pre-industrial scale in the INEOS Company's facilities.

3. Scale-up of the system AS1/rac-EtInd$_2$ZrCl$_2$ at pre-industrial scale

As stated in the previous paragraph, the slurry polymerization tests performed at the laboratory scale with $[(\equiv SiO)_2Al(OC_6F_5)_2]^-[HNMe_2Et]^+$ in combination with (*n*-BuCpMe)$_2$ZrCl$_2$ and *rac*-EtInd$_2$ZrCl$_2$ lead to promising results from both an activity and final product point of view. In order to ensure that the technology transfer from lab to pre-industrial scale for these systems was possible, we selected AS1/Cat1 to perform some tests in slurry polymerization in pre-industrial reactors at INEOS facilities in Brussels.

The procedure followed during the testing of the catalyst was first to find the best conditions in which to test AS1/Cat1 (e.g. feed composition, amount of catalyst to inject…) to have a well-behaved and controlled process, and then to study the effect of the Zr loading on the catalyst's activity and on the product's microstructure.

The tests were performed in 5L autoclaves in 1.5L of isobutane as solvent, at 80°C, 10 bars of ethylene and 0.15 mol% H_2/C_2 ratio. The polymerizations lasted one hour.

AS1 was pre-contacted with Cat1 right before being injected in the reactor. TiBA was used as both scavenger and alkylating agent for rac-EtInd$_2$ZrCl$_2$. The total TiBA/Zr vised for the polymerization was 100; 50% of the scavenger was directly injected in the reactor prior to the polymerization and 50% was used during the catalyst pre-contact to alkylate the zirconocene bis-chloride complex.

Based on the results obtained at the lab scale, a ratio of 0.06 Zr/Al$_{surf}$ was selected for the first reference tests. Also, based on the activities recorded, it was decided to inject 100 mg of catalyst

in the reactor. AS1/Cat1 was tested at two different comonomer feed's compositions, 25 and 60 g of 1-hexene were used respectively in the first two polymerization tests. In Table 6 are reported the results for the first tests performed in Brussels.

Table 6 – Polymerization tests with AS1 and *rac*-EtInd$_2$ZrCl$_2$. Conditions: 1.5L isobutane, 80°C, 10 bars ethylene, 0.15 mol% H_2/C_2, 1 hour, 100 $(TiBA/Zr)_{tot}$, 50 $(TiBA/Zr)_{prec}$.

runs	m sup	nZr	Wt%	$Zr/Al_{(surf)}$	1-hexene	C6/C2 real	Yield	Activity
	mg	µmol	Zr		g	%mol	g	g g_{cat}^{-1} h^{-1}
4	100	3	0.27	0.06	25	0.39	442	4420
5	100	3	0.27	0.06	60	0.91	435	4350

The activity recorded for AS1/Cat1 during run 4 and 5 was close to four times higher than that recorded previously, moreover the initial activity was so high that it was not possible to control the process efficiently. In Figure 11 are reported the activity profiles for run 4 and 5.

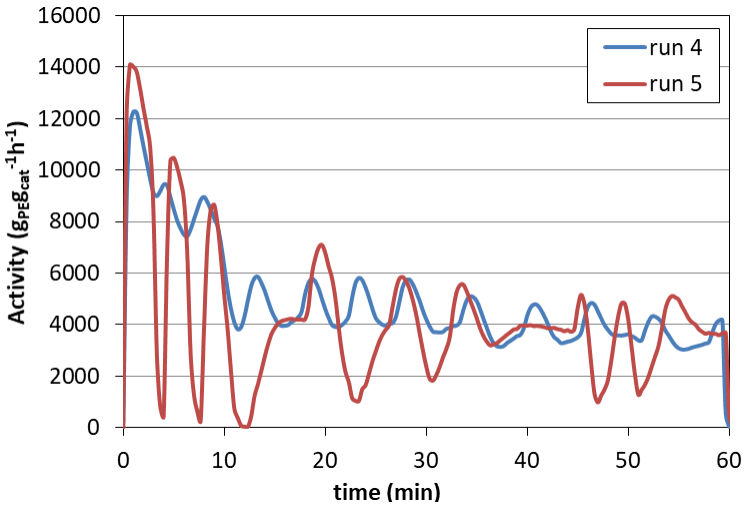

Figure 11 – Activity profiles for run 4 and 5 performed with AS1/Cat1 at pre-industrial scale.

The plot shows clearly the difficulty encountered during run 4, but more importantly during run 5, in controlling the polymerization process. The high boost in activity occurring at the very beginning of the polymerization reaction caused the occurrence of exotherms of 30°C and 50°C degrees respectively for run 4 and 5. This caused a complete loss of morphology control on the final polymer particles.

The amount of catalyst injected in run 4-5 was definitely too much, considering the gain in activity observed at pre-industrial scale. It was thus decided to reduce to one-third the amount of powder injected in the reactor.

Table 7 – Polymerization tests with AS1 and *rac*-EtInd$_2$ZrCl$_2$. Conditions: 1.5L isobutane, 80°C, 10 bars ethylene, 0.15 mol% H_2/C_2, 1 hour, 100 $(TiBA/Zr)_{tot}$, 50 $(TiBA/Zr)_{prec}$.

runs	m sup	nZr	Wt%	Zr/Al(surf)	1-hexene	C6/C2 real	Yield	Activity
	mg	µmol	Zr		g	%mol	g	g g_{cat}^{-1} h^{-1}
6	33	1	0.28	0.06	25	0.75	135	4091
7	33	1	0.28	0.06	60	1.25	244	7394

In Table 7 are reported the results for the tests performed using 33 mg of catalyst instead of 100. What it is interesting to notice is that, while at a lower comonomer loading, run 6, it was possible to have a good control of the polymerization process, in run 7 controlling the polymerization resulted to be harder than in run 5. Figure 12 depicts the kinetic profiles for both run 6 and 7

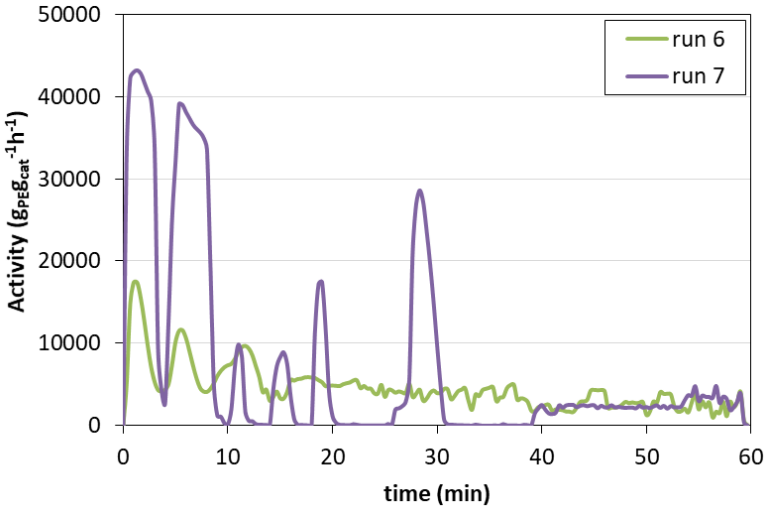

Figure 12 – Activity profiles for run 6 and 7 done with AS1/Cat1 at pre-industrial scale.

The plot in Figure 11 shows clearly how the high boost in activity was such to make impossible a control of the polymerization process. Whereas run 6 showed a kinetic profile stable throughout the polymerization. This difference in behavior suggests that the amount of catalyst used in tests 6 and 7 is right to obtain a good control of the polymerization process at low comonomer concentrations, but that *rac*-EtInd$_2$ZrCl$_2$ is too sensitive to the amount of comonomer used during

the reaction, and that 60 g is probably a too high initial amount of 1-hexene to consent a control of the polymerization, in these operating conditions.

It was devised to lower initial comonomer feed (40 g) with successive addition of 1-hexene aliquots during the polymerization in order to vise a constant C_6/C_2 ratio throughout the polymerization. The C_6/C_2 ratio was monitored by GC analysis of the gas phase in the reactor.

Having established the conditions in which to operate the catalyst, it was decided to investigate the effect of the Zr loading on the catalyst's activity. In Table 8 are reported the polymerization results obtained.

Table 8 - Polymerization tests with AS1 and *rac*-$EtInd_2ZrCl_2$, at different Zr loadings. Conditions: 1.5L isobutane, 80°C, 10 bars ethylene, 0.15 mol% H_2/C_2, 1 hour, 100 $(TiBA/Zr)_{tot}$, 50 $(TiBA/Zr)_{prec}$.

runs	m sup mg	nZr µmol	Wt% Zr	Zr/Al(surf)	1-hexene g	C6/C2 real %mol	Yield g	Activity g g_{cat}^{-1} h^{-1}
8	33	1	0.28	0.06	40+10	1.33	194	5879
9	66	1	0.14	0.03	40+10+10	1.28	343	5197
10	100	1	0.09	0.02	40+10+10	1.23	196	1960
11	20	1	0.46	0.10	40	1.20	93	4650

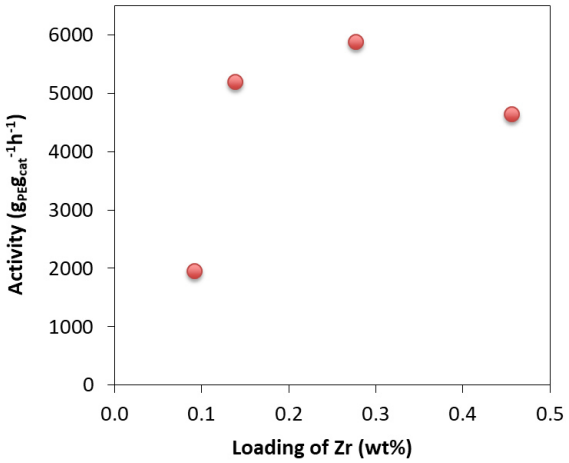

Figure 13 – Productivity in function of the Zr loading on the activating support for the system AS1/Cat1, as resulted from runs 8-11.

In Table 8 are reported the polymerization results for runs 8-11. How it is possible to see from the overall productivity values reported in Table 8 and from the plot depicted in Figure 13, the system AS1/Cat1 reaches a maximum of productivity in polymerization for 0.28wt% of Zr on the surface (0.06 Zr/Al_{surf} ratio). Either increasing or decreasing the wt% of metallocene on the support causes a drop in acivity. This kind of relationship between the metallocene loading and the overall activity has already been discussed in literature regarding different kinds of metallocenes and solid activators.[1] The reason for this behavior could be imputed to the fact that, at a too high concentration of active species on the surface, possible interaction between the metal centers start to take place, affecting the activity. On this note, it could be interesting to remark that the evolution of the absolute yield in function of the Zr loading doesn't match perfectly the activity one. Explaining this phenomenon is no easy task, but it is without question that form an industrial production point of view the parameter to take into consideration is the productivity, and that is why we focused on studying its evolution in relation to the zirconium concentration on the surface of the support.

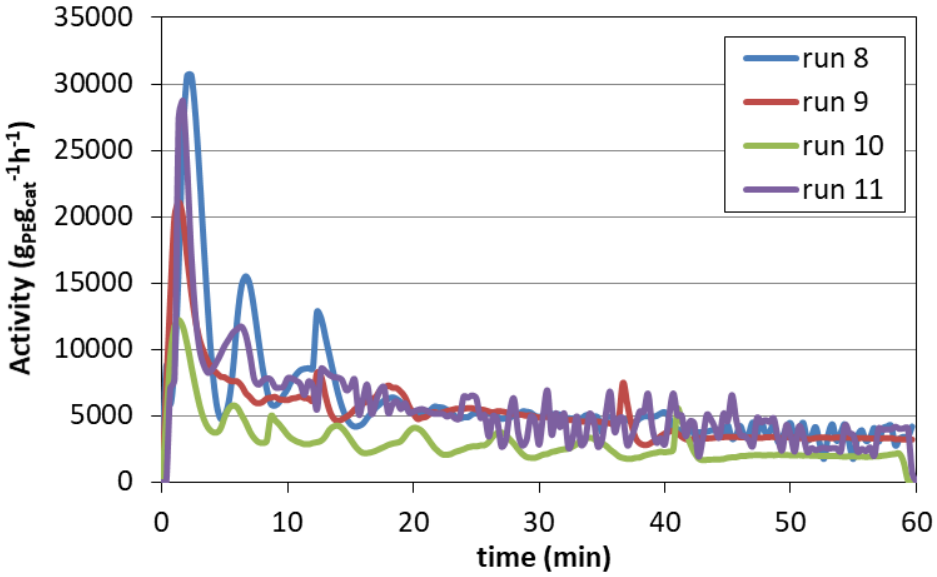

Figure 14 - Kinetic profiles for the polymerization runs performed with AS1/Cat1 at different Zr loading.

Figure 14 depicts the kinetic profiles for runs 8-11, in all the runs there was an initial activity boost followed by a rapid drop in activity after the first five minutes of polymerization, to then stabilize on a more or less stable value for the rest of the run (reproducing the kinetic profile already

observed in run 1 at laboratory scale). In order to validate the method of subsequent comonomer addition as able not only to stabilize the ratio C_6/C_2 throughout one single polymerization reaction, but also to keep the C_6/C_2 comparable between the four different runs, in Figure 15 is reported the GC response for C_6/C_2 in runs 8-11, clearly showing that the four polymerizations proceeded at the same comonomer feed composition.

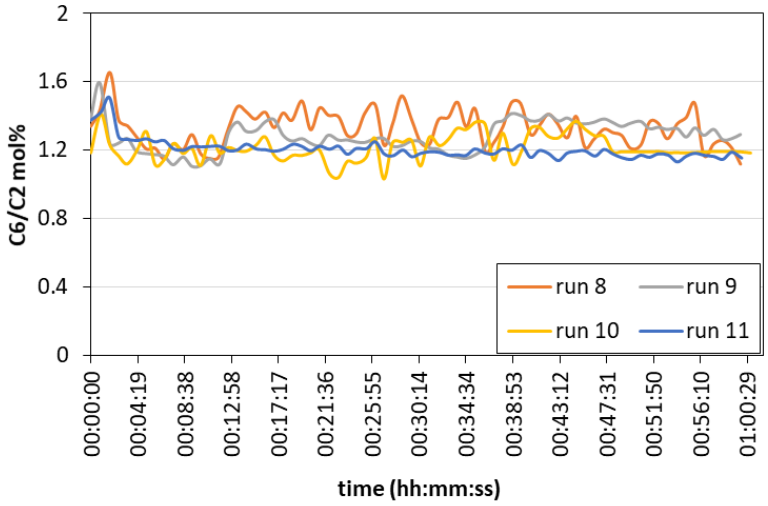

Figure 15 – GC response for the C6/C2 ratio during runs 8-11.

The resins obtained where then characterized by GPC, DSC, IR, Melt Index, Bulk Density and MVS. The results are reported in Table 9 and 10.

Table 9 – Characterization results for the resins obtained with AS1/Cat1 in run 4-11 in pre-industrial scale. Results for the DSC, GPC and IR characterizations.

run	Wt% Zr	1-hexene g	Activity g $g_{cat}^{-1}h^{-1}$	T_{f2} °C	Crystallinity %	M_n g mol^{-1}	M_w g mol^{-1}	Đ	Comonomer mol%
4	0.27	25	4420	125	56.8	15500	84400	5.5	1.5
5	0.27	60	4350	121	42.7	17800	84500	4.8	3.2
6	0.28	25	4091	124	57.8	10300	69200	6.7	1.4
7	0.28	60	7394	115	37.4	20300	85700	4.2	4.7
8	0.28	40+10	5879	118	46.2	16200	99800	6.2	2.4
9	0.14	40+20	5197	117	43.2	26100	149600	5.7	2.5
10	0.09	40+20	1960	115	42.8	23100	135100	5.9	2.5
11	0.46	40	4650	120	50.1	14600	94300	6.4	1.9

From the first set of characterization results reported in Table 9 it is possible to evince a certain amount of information regarding the resins obtained at a pre-industrial scale.

Firstly, if we focus on the results for run 4 and run 6, which were conducted in conditions similar to run 1 from the point of view of the C6/C2 ratio, we find that the products show molar masses and co-monomer incorporations similar to run 1. The molar mass distributions found are broad, as typical for the system. It is interesting though how the melting temperatures of runs 4 and 6 are slightly higher than what expected for the level of comonomer incorporation. This may be due to a drift in the feed composition for the two runs, and the temperature peak observed is the one of the chains produced towards the end of the reaction. The results, anyhow, confirmed, also from the product point of view, that the scale up of the system AS1/Cat1 was successfully achieved.

If we then focus on the characterization results of runs 8-11, we can notice that these polymers present lower melting temperatures due to higher comonomer incorporation, as expected given the higher amount of 1-hexene used during the polymerization. Moreover, it looks like that the loading of Zr on the catalyst has an influence on the Mw of the resins produced. It is very clear from the GPC-FTIR traces reported in Figure 16.

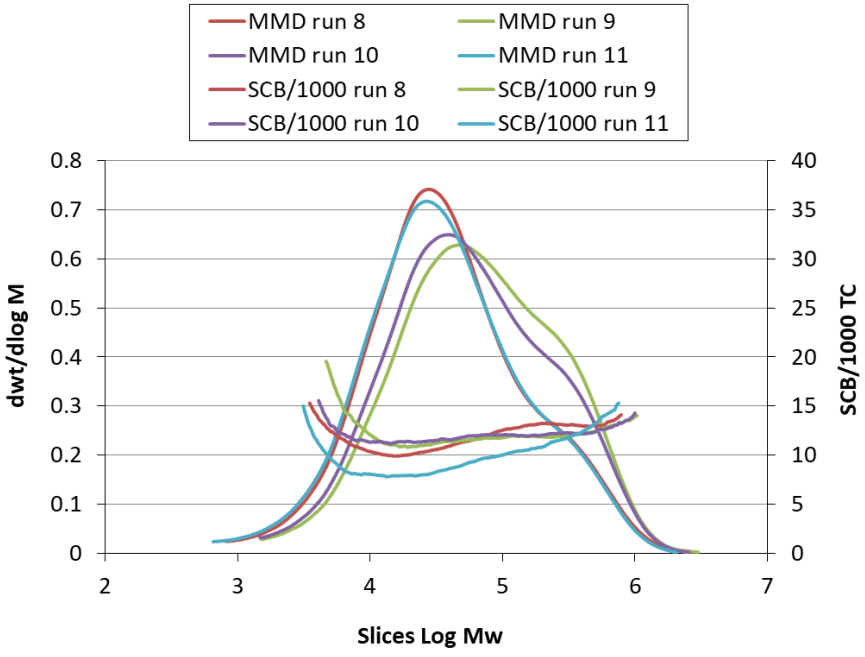

Figure 16 – GPC-IR traces for the resins obtained in run 8-11.

From the plot depicted in Figure 16, results evident the bimodal behaviour of all the resins but also that the polymers synthesized at lower Zr/Al_{surf} ratio (run 9 and 10) show higher M_w. The reason behind the different polymers' microstructure at different Zr loadings on the catalyst is not yet clear. It could be due to different type of interactions of the zirconocene with the activating support's surface taking place at different Zr concentrations on the surface.

Table 10 – Characterization results for the resins obtained with AS1/Cat1 in run 4-11 in pre-industrial scale. Results for the Bulk density, Melt Index and Standard Volumic Mass characterizations.

run	Wt% Zr	1-hexene g	Activity $g\ g_{cat}^{-1}\ h^{-1}$	BD kg/m^3	MVS kg/m^3	MI2 g/10min	HLMI g/10min
4	0.27	25	4420	297	935	5.98	206
5	0.27	60	4350	321	921	4.02	143
6	0.28	25	4091	272	939	10.9	too fluid
7	0.28	60	7394	428	916	3.50	90.4
8	0.28	40+10	5879	367	926	3.32	149
9	0.14	40+20	5197	365	921	0.13	12.6
10	0.09	40+20	1960	330	922	0.27	21.9
11	0.46	40	4650	293	931	2.83	138

The density and Melt Index results reported in Table 10 are in agreement with the characterization results in Table 9. In fact, the MI values found for run 8-11 differ depending on the Zr loading in the catalyst, following the same trend already discussed for the molar masses. The resins obtained presented varying values of bulk densities across the table; this parameter is very important from a processing point of view, it in fact gives an idea of the packing efficiency inside the reactor during the polymerization process; the values obtained are overall acceptable and in the cases of runs 8 and 9 in line with what is industrially expected.

Finally, an analysis of the particle size distribution was performed for the resins obtained during well controlled polymerization processes, run 6, 8-11. The results are reported in Table 11.

Table 11 – Particle size distributions for the runs 6, 8-11 conducted on a pre-industrial scale with AS1/Cat1.

run	Mean µm	Median µm	d10 µm	d50 µm	d90 µm	Span
6	259	240	52	240	486	1.8
8	354	325	93	325	643	1.7
9	341	300	108	300	584	1.6
10	501	314	94	314	1304	3.9
11	303	283	69	283	554	1.7

In Figure 17 is reported as example the plot of the particle size distribution for run 8.

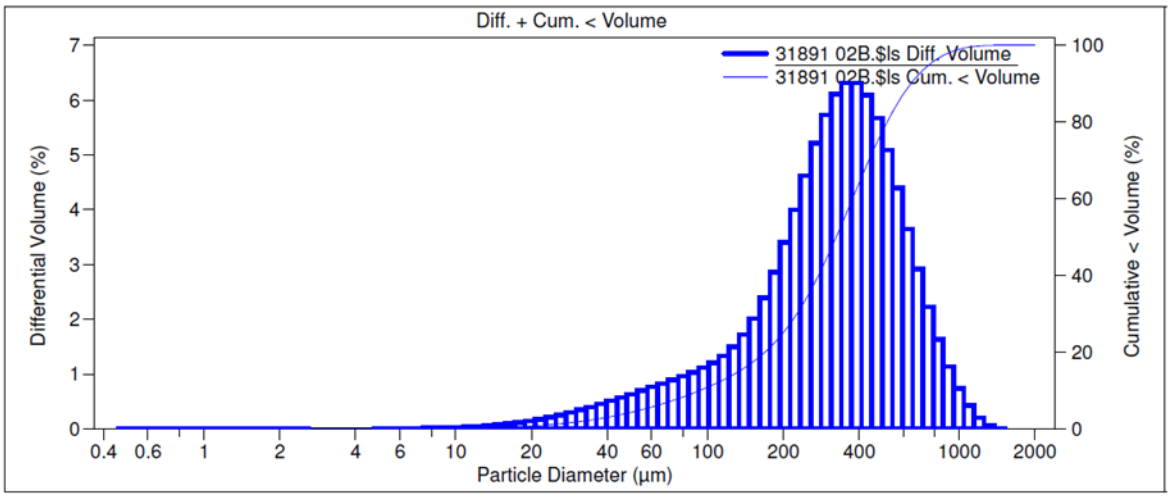

Figure 17 – Particle size distribution for the polymer synthesized in run 8 with AS1/Cat1.

The data reported in Table 11 show a consistent behaviour of the particle size distribution among the five different runs. It is though worth highlighting the fact that the span of the particle distribution profile is higher than the desired value of one, it is in fact possible to see in the plot in Figure 16 a shoulder around low particle diameters. This would suggest a not perfectly controlled fragmentation of the particles during the polymerization reactions.

But, even considering the not ideal particle size distribution, the results obtained with AS1/Cat1 at pre-industrial scale are promising and encouraging. We thus decided to proceed with the isolation of a formulated 'dry' catalyst using AS1 as activator and support and *rac*-EtInd$_2$ZrCl$_2$ as catalyst precursor.

4. Formulation of an isolated 'dry' pre-catalyst ($[(\equiv SiO)_2Al(OC_6F_5)_2]^-[HNMe_2Et]^+$/*rac*-$EtInd_2ZrCl_2$

4.1 Isolation of the zirconocene on the surface in presence of TiBA and polymerization tests

The ideal aim of this thesis work is the isolation of an active catalyst by coordination of a molecular catalyst to the surface of an innovative activating support. As shown in the previous paragraphs two systems have been studied ($[(\equiv SiO)_2Al(OC_6F_5)_2]^-[HNMe_2Et]^+$/*rac*-$EtInd_2ZrCl_2$ and $[(\equiv SiO)_2Al(OC_6F_5)_2]^-[HNMe_2Et]^+$/(n-BuMeCp)$_2ZrCl_2$) which have revealed great application potential.

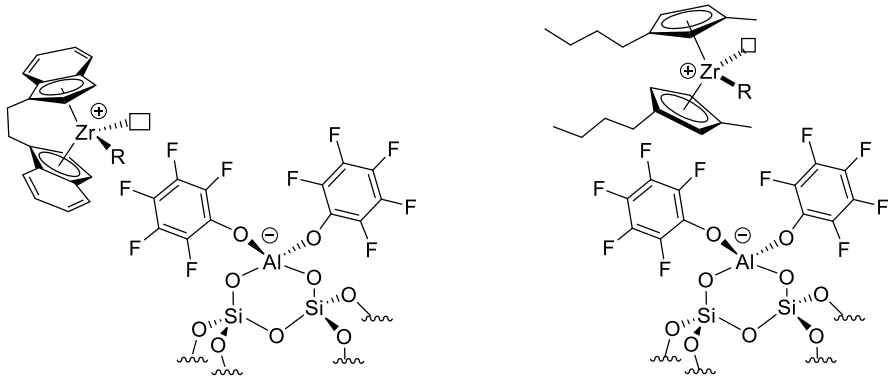

Scheme 6 – Structure of the two efficient catalytic systems tested.

In order to see if it was possible to isolate the catalyst and if the active species is stable on the surface, we proceeded to the formulation of an isolated catalyst.

The first zirconocene studied under this perspective was *rac*-$EtInd_2ZrCl_2$.

A ratio Zr/Al_{surf} of 0.06 was devised for the formulated catalyst, derived from the study shown in the previous paragraph. The coordination of the Zr on the surface was conducted in presence of TiBA as alkylating agent, in order to create a Zr-C bond. The ratio TiBA/Zr was 50, the same used for the test done at INEOS's facilities.

3 g of AS1 and 89 µmol of Cat1 were contacted in toluene in presence of TiBA and left to react for one hour at 50°C under stirring. At the end of the reaction the surnatant was still deeply yellow, indicating that the zirconocene didn't coordinate fully to the AS surface. After washing the product once with toluene and twice with hexane the powder was dried.

Table 12 – Zr content real vs target for IsoCat.

run	Zr target wt%	Zr/Al target	Zr real wt%	Zr/Al real
IsoCat	0.28	0.06	0.06	0.007

Table 12 reports the Zr content found for IsoCat by elemental analysis in comparison to the targeted one. It is evident that the most part of the zirconocene did not coordinate on the surface. This could have been the results of many reasons, most probably due to the procedure followed during the supporting reaction.

Nonetheless, IsoCat was tested in the INEOS facilities in ethylene/1-hexene copolymerization. The polymerization was conducted in 1.5L of isobutane as diluent, at 80°C, 10 bars of ethylene and in presence of 0.5 mmol of TiBA as scavenger. The results of the polymerization are reported in Table 13 and in Figure 18 is depicted the kinetic profile.

Table 13 – Results of the polymerization test performed with IsoCat at INEOS facilities. Conditions: 1.5L isobutane, 80°C, 10 bars ethylene, 0.15 mol% H_2/C_2, 1 hour.

run	m cat mg	nZr µmol	1-hexene g	TiBA mmol	Yield g	Activity $g\ g_{cat}^{-1}\ h^{-1}$
IsoCat	66	0.25	40	0.5	20	303

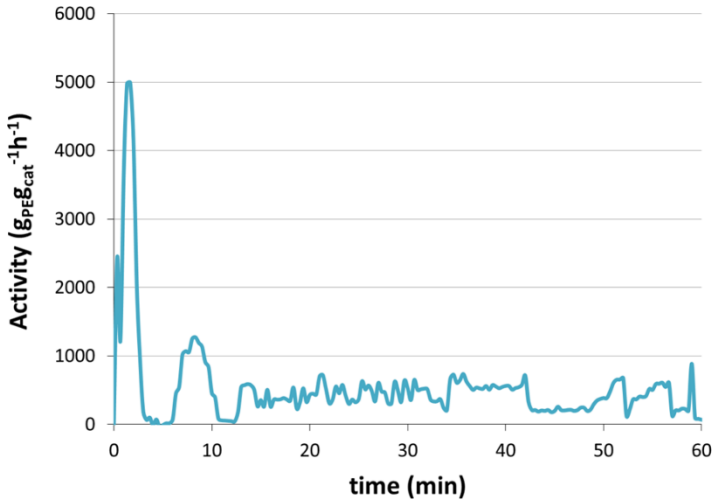

Figure 18 – Kinetic profile of the polymerization test performed at INEOS with IsoCat.

The activity obtained, 303 $g_{PE}\, g_{cat}^{-1}\, h^{-1}$, was one order of magnitude lower than what was obtained previously with the pre-contact method. This isn't very surprising given the very low amount of zirconocene present on the catalyst's surface. The real issue in the low activity obtained with IsoCat is the fact that the targeted Zr/Al ratio on the surface was not met.

In order to solve this problem the protocol of synthesis of the catalyst was modified at the lab scale: the catalyst suspension was left to react under stirring in the glovebox for one hour at room temperature, 25°C. In Table 14 are reported the results for the synthesis of two different formulated catalysts

Given the difficulties in reaching the target amount of Zr on the catalyst surface, it was devised to contact Cat1 and AS1 in a higher Zr/Al ratio, 0.12, during the reaction. Moreover IsoCat02 was prepared in presence of 1-hexene, in the hope that a small amount of polyhexene produced during the catalyst's synthesis could stabilize the active species on the surface.

Table 14 – Reaction conditions and real surface composition for the formulated catalysts IsoCat01 and IsoCat02.

	Reaction conditions			Surface					
	Zr/Al_{surf}	TiBA/Zr	1-hex/Zr	Al wt%	Zr wt%	n Al mmol g^{-1}	n Zr mmol g^{-1}	Zr/Al_{AS}	Zr/Al_{tot}
IsoCat01	0.12	50	-	2.76	0.11	1.02	0.012	0.022	0.012
IsoCat02	0.12	50	12	2.31	0.12	0.86	0.013	0.023	0.018

In the case of IsoCat01 and 02, the amount of zirconocene effectively immobilized on the silica was lower with respect to the target value. Presence of 1-hexene didn't affect the zirconocene coordination in any noticeable way. The elemental analysis results also showed that a large amount of the TiBA used for the alkylation of the zirconocene chloride stays coordinated on the surface after the washings of the catalyst (the number of moles of Al found on the support rose from 0.55 $mmolg^{-1}$ in AS1 to 1.02 mmol g^{-1} in IsoCat01 and to 0.86 mmol g^{-1} in IsoCat02). It was not possible, though, to establish if the TiBA was coordinated directly to the zirconocene, affecting the active species, or to the silica surface.

Both catalysts were characterized by DRIFT and solid state ^{1}H MAS and ^{13}C CP-MAS NMR. The spectra of the two catalysts look very similar.

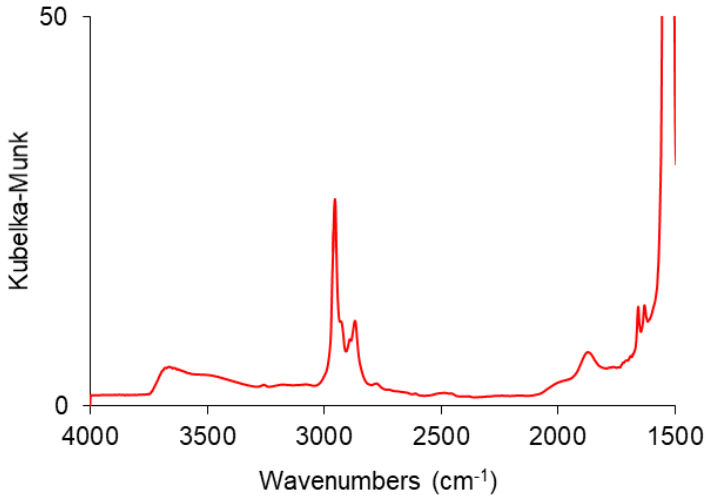

Figure 19 – DRIFT spectrum of the formulated catalyst IsoCat01.

As a title of example Figure 19 depicts the DRIFT spectrum for IsoCat01. The plot reveals an intense group of peaks below 3000 cm^{-1}, frequency characteristic of the C-H stretching. The presence of peaks in this area of the spectrum is in agreement with the presence on the surface of both the zirconocene and a considerable amount of Al*i*Bu_3.

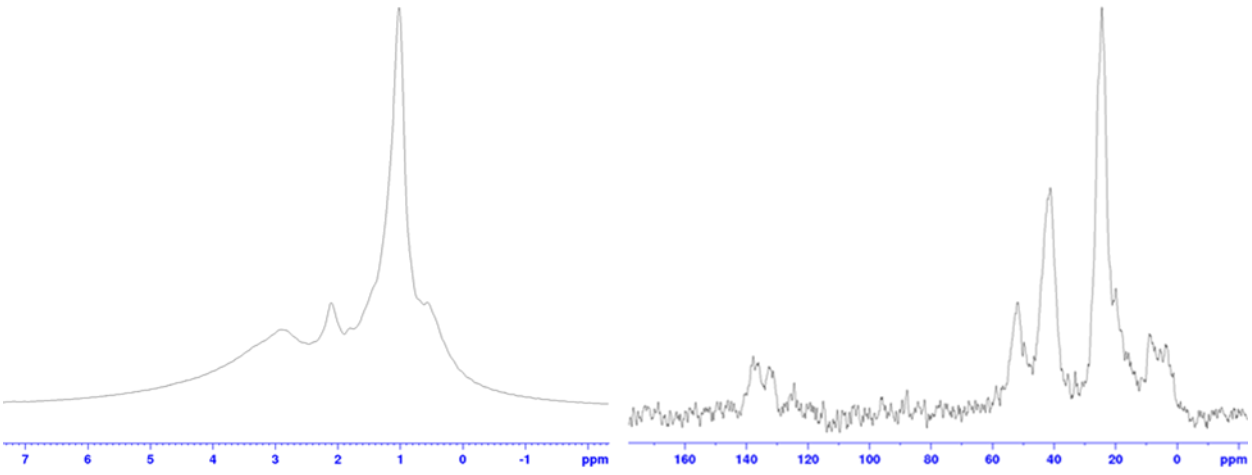

Figure 20 – ^{1}H MAS (left) and ^{13}C CPMAS (right) NMR spectra of IsoCat01.

The NMR spectra of Figure 20 also show the presence of coordinated TiBA on the surface. Moreover, the amount of zirconocene coordinated to the AS is so little that it is not possible to

see the signal of the indenyl rings at the ^{1}H spectrum, while at the ^{13}C it generates a large peak of small intensity around 130 ppm.

At the ^{1}H NMR spectrum is possible to see five peaks at 0.56, 1.01, 1.79, 2.10 and 2.91 ppm corresponding respectively to the methylene group bonded to the Al, the methyl moiety of the NCH_2CH_3, methyls and methyne groups of Al*i*Bu, and at last the resonance of the methylene of the NCH_2CH_3 and the methyl directly bound to the N of the ammonium.

In the ^{13}C NMR spectra are depicted at 6.0 ppm the resonance of the methyl fragment of the NCH_2CH_3, at 19.9 and 24.4 ppm the signals of the methylene and of the methyne and methyls of the Al*i*Bu group. At 41.2 ppm and at 51.7 ppm resonate the methyls directly bound to the N and the methylene groups of the NCH_2CH_3 respectively.

Even though the Zr content on the two formulated catalysts was lower than the desired value, they were tested in ethylene/1-hexene slurry copolymerization.

The polymerizations were run in 300 mL of heptane at 80°C and under 4 bars of ethylene, TiBA was used as scavenger. In Table 15 are reported the polymerization results.

Table 15 – Polymerization results obtained with IsoCAt01 and IsoCat02 in slurry copolymerization. General conditions: 80°C; 4 bars C_2H_4; 300 mL heptane; [TiBA] 1mM.

Run	Catalyst	M mg	Zr mmol g^{-1}	Zr µmol	$Zr/Al_{surface}$	Zr Wt%	C6 mol%	Yield g	Activity g g_{cat}^{-1} h^{-1}
1	AS1/*Cat1*	20.6	-	0.68	0.06	0.31	19.2	10.7	1111
12	IsoCat01	18.5	0.012	0.22	0.022	0.11	19.8	0.95	103
13	IsoCat02	29.2	0.013	0.38	0.023	0.12	19.8	2.63	180

The results are reported in comparison with those obtained with the pre-contact method for the system AS1/Cat1, in the same conditions. The activity recorded for both formulated catalysts is low with respect to the reference, as clearly depicted also in Figure 21.

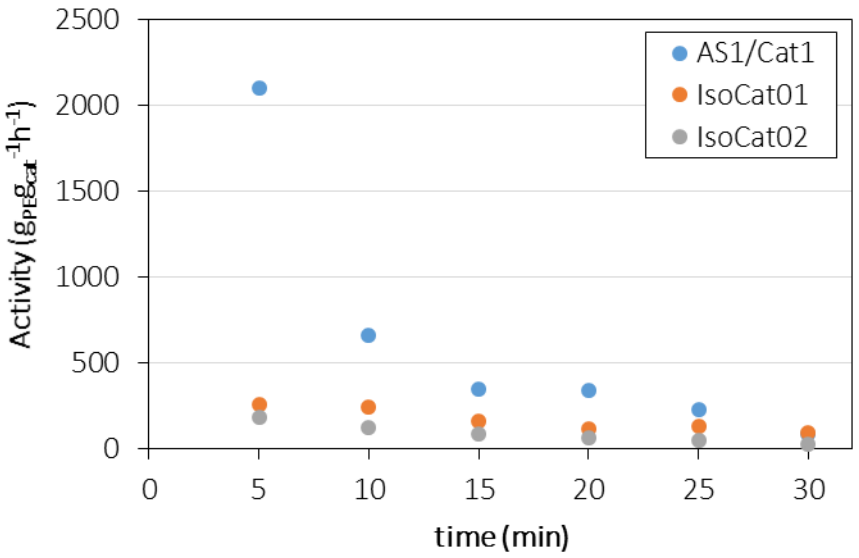

Figure 21 – Kinetic profiles for the polymerization runs conducted with the system AS1/Cat1, IsoCAt01 and IsoCat02.

As in the case of IsoCat, also for IsoCat01 and 02 the real issue consists in the low amount of Zr present on the surface, affecting the productivity of the catalyst. When the product was recovered, it was possible to see the formation of small aggregates of particles, but it was not possible to understand if they were formed during the polymerization or were the result of the polymer recovering process.

In order to tackle the issue of the zirconocene coordination to the surface of the activating support, the protocol followed for the synthesis of the 'dry' catalyst was modified, in order to try and force the coordination. The amount of toluene used during the synthesis was reduced to 2 mL (2.6 times the pore volume of the silica) just enough to solubilize Cat1. The catalyst's washing step was removed: after leaving the catalyst react for one hour, the solvent was removed by drying under vacuum.

In this third batch of formulated catalysts the TiBA/Zr ratio was varied during the immobilization reaction, to investigate its effect on the activity.

Table 16 – Surface composition of IsoCAt03 and IsoCat04.

	Zr wt%	n Zr mmol g^{-1}	Zr/Al_{surf}	TiBA/Zr
IsoCat03	0.3	0.036	0.07	50
IsoCat04	0.4	0.044	0.08	3

Table 16 reports the surface composition of the formulated catalysts IsoCat03 and IsoCat04, obtained at different TiBA/Zr ratios. The impact of the TiBA/Zr ratio was immediately discernible, in fact, as soon as the reaction was started, the suspension of IsoCat04 turned from a yellow colour (characteristic of the bis-indenyl zirconocene complex) to dark green. At the end of the reaction the product was dried and characterized by DRIFT and solid state NMR.

While the DRIFT spectra for IsoCat03 and 04 resemble on any account the one reported in Figure 19, it is worthwhile to consider the ^{1}H MAS and ^{13}C CP-MAS solid state NMR spectra for IsoCat04.

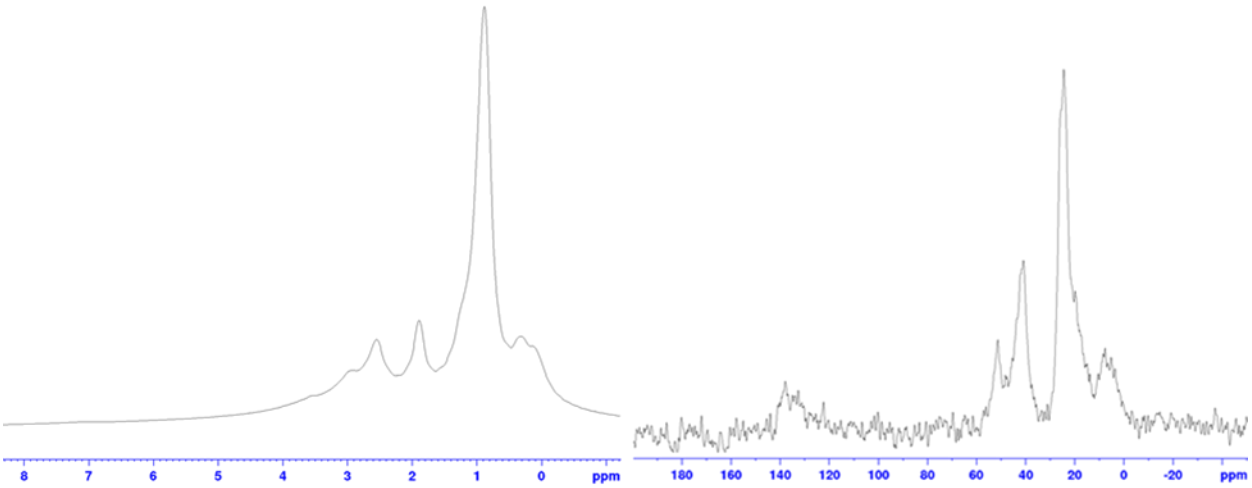

Figure 22 – ^{1}H MAS (left) and ^{13}C CPMAS (right) NMR spectra of IsoCat01.

The ^{13}C NMR spectrum for IsoCat04 presents itself to be very similar to the one of IsoCat01 depicted in Figure 19, with at 7.6 ppm the resonance of the methyl fragment of the NCH_2CH_3, at 19.9 and 24.5 ppm the signals of the methylene and of the methyne and methyls of the Al*i*Bu group. At 40.9 ppm resonate the methyls directly bound to the N and at 51.3 ppm the methylene groups of the ammonium. On the other side the ^{1}H NMR shows a higher number of signals, in fact besides the peaks at 0.31, 0.87, 1.88, 2.54 and 2.92 ppm corresponding respectively to the

methylene group bound to the Al, the methyl moiety of the NCH_2CH_3, the methyls and methyne of the Al*i*Bu, and the methylene of the NCH_2CH_3 and the methyl directly bound to the N of the ammonium, there's two additional bands at 0.13 and 3.55 ppm that could be due to differently coordinated TiBA moieties.

The formulated catalysts IsoCat03 and IsoCat04 were then tested in ethylene/1-hexene slurry copolymerization. The polymerizations were run in 300 mL of heptane at 80°C and under 4 bars of ethylene, TiBA was used as scavenger. In Table 17 are reported the polymerization results.

Table 17 – Polymerization results obtained with IsoCat03 and IsoCat04 in slurry ethylene copolymerization. General conditions: 80°C; 4 bars C_2H_4; 300 mL heptane; [TiBA] 1mM.

run	Catalyst	Time* days	m mg	Zr mmol g^{-1}	Zr µmol	Zr/Al_{surf}	Zr Wt%	C6 mol%	Yield g	Activity g g_{cat}^{-1} h^{-1}
14	IsoCat03	-	21.1	0.036	0.76	0.065	0.33	19.8	2.65	251.5
15	IsoCat04	1	38.6	0.044	1.70	0.08	0.40	19.8	21.1	1090
16	IsoCat04	4	26.0	0.044	1.15	0.08	0.40	19.8	9.41	725
17	IsoCat04	5	21.6	0.044	0.95	0.08	0.40	20.2	5.88	545
18	IsoCat04	21	26.1	0.044	1.15	0.08	0.40	19.8	3.25	250

*Time elapsed since the synthesis. Runs 15-18 were conducted over a period of two-three weeks, giving to the catalyst time to age.

As expected IsoCat03 resulted to be more active than IsoCat01 or IsoCat02 given the higher loading of Zr on the surface, but still the productivity wasn't very high. On the other side, lowering the TiBA/Zr ratio during the synthesis had a very positive effect productivity-wise.

In fact, the catalyst was so active that in run 15 it was not possible to control the temperature during the polymerization. The exotherm was such to bring the temperature of the system to 90°C from the set-point of 80°C, additionally it was necessary to stop the polymerization after 23 minutes.

In order to have a better control of the process, in the following tests the amount of catalyst was reduced. In Figure 23 are reported the kinetic profiles for run 14-18.

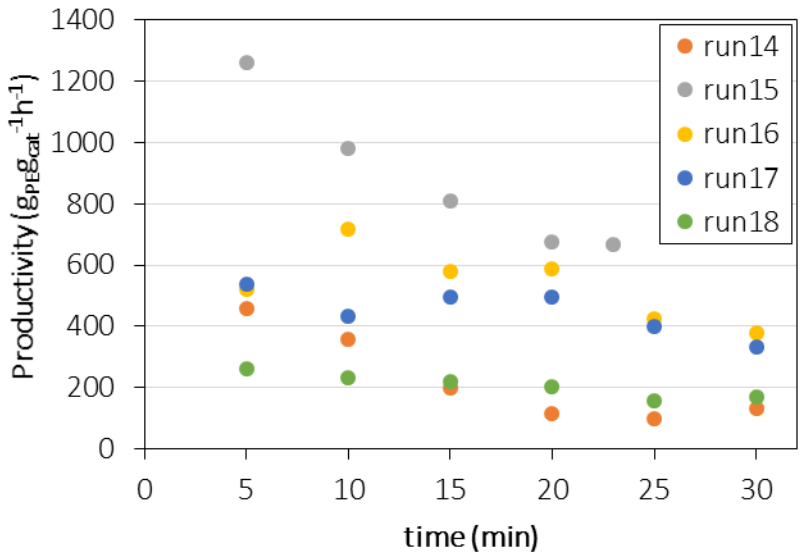

Figure 23 – Kinetic profiles for the polymerization tests performed with IsoCat03 and isoCat04, run 14-18.

Both Table 17 and Figure 23 show a clear trend of IsoCat04 to deactivate over time during storage, in fact the activity drops from 725 to 250 $g_{PE}\ g_{cat}^{-1}\ h^{-1}$, meaning that, at room temperature, the active species are unstable on the surface and evolve over time.

The deactivation of the active species could be due either to a transfer of a phenoxy group from the activator to the zirconocene,[8] or to a side reaction of either the aluminate or the zirconocene with the TiBA coordinated to the surface. For example, it is possible for TiBA to react with one Al-OC_6F_5 fragment on the surface, the alkylation would result in an anionic $[(\equiv SiO)_2AliBu(OC_6F_5)]^-$ species and a not efficient separation of the ionic couple on the surface. This considered, given the great gain in activity obtained in reducing the TiBA/Zr ratio during the preparation of the catalyst, it could be assumed that TiBA is one of the main causes for the loss in activity. To avoid this problem, we decided to proceed to the synthesis of a formulated catalyst in absence of TiBA.

The polymers obtained with IsoCat03 and IsoCat04 were characterized by DSC, HT-SEC and IR. The results for the characterization are reported in Table 18.

Table 18 – DSC, HT-SEC and comonomer content characterization results for the polymer synthesized by IsoCat03 and IsoCat04.

run	Catalyst	Activity g g_{cat}^{-1} h^{-1}	*T*f2 °C	Crystallinity %	M_n g mol^{-1}	M_w g mol^{-1}	Đ
14	IsoCat03	251.5	122	38.5			
15	IsoCat04	1090	120	43.7	48100	153400	3.2
16	IsoCat04	725	121	40.5			
17	IsoCat04	545	122	44.8	20000	226000	11.3
18	IsoCat04	250	123	44.9	30300	130600	4.3

The melting temperatures and crystallinity fractions found for runs 14-18 are comparable with what already observed for the system AS1/Cat1. The resins present again the same large molecular weights distributions typical of this catalyst, while overall higher M_w where found than those obtained by pre-contact activation of the catalyst. This could be one other effect of the modifications of the active site caused by the presence of a great amount of TiBA on the surface.

As said previously to eliminate the use of the alkylating TiBA during the synthesis of the isolated catalysts, we proceeded to the methylation of the zirconocene chloride pre-catalyst, and then to its coordination on AS1.

4.2 Methylation of *rac*-$EtInd_2ZrCl_2$ to *rac*-$EtInd_2ZrMe_2$, MCat1

The synthesis of *rac*-$EtInd_2ZrMe_2$ was done by methylation of *rac*-$EtInd_2ZrCl_2$ with $LiCH_3$ according to the reaction reported in Scheme 7.

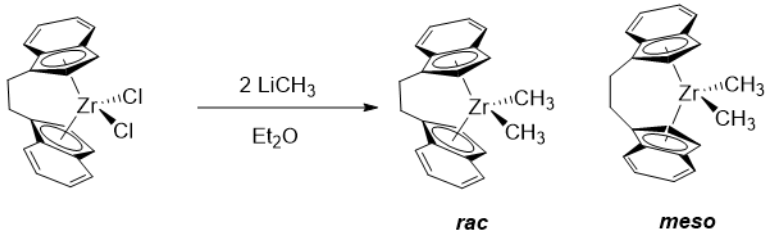

Scheme 7 – Methylation reaction of *rac*-$EtInd_2ZrCl_2$.

The product was characterized by ^1H solution NMR in C_6D_6. The spectrum is reported in Figure 23.

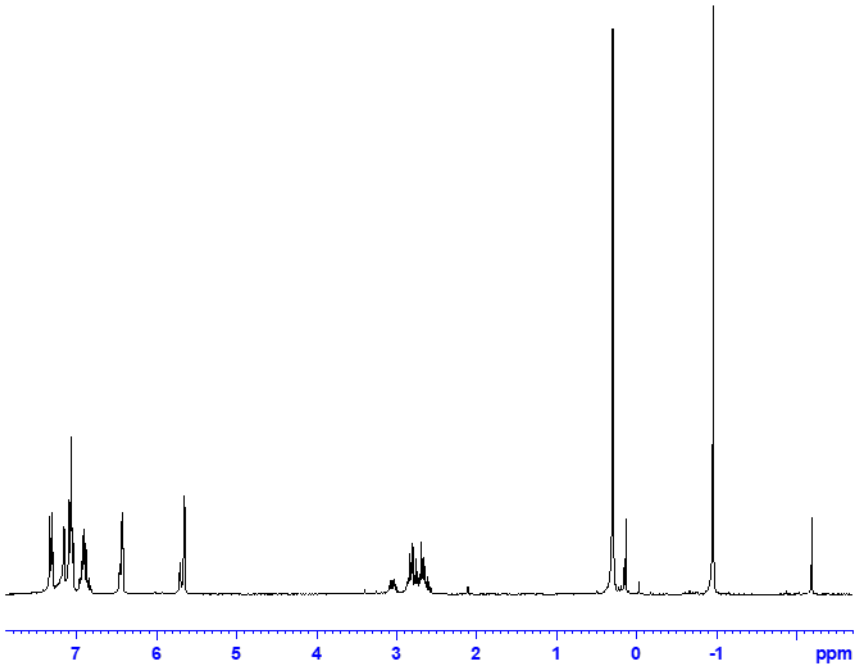

Figure 24 – ^{1}H NMR spectrum of MCat1 in C_6D_6.

The ^{1}H NMR spectrum shows that during the methylation reaction a partial racemization of the zirconocene occurred. From the integration of the peaks of the methyls it was possible to evince that the ratio *meso:rac* was 28:72. The assignation of the peaks for the two isomers was done according to the literature.[14] The methyls resonate at -2.19 and 0.14 ppm for the meso isomer, and at -0.95 ppm for the rac. Between 2.5 and 3.2 ppm are located the multiplets of the ethyl bridge for both species. The two doublets of the Cp ring are located at 5.66 and 6.43 ppm for the rac (J=3.30 Hz) and at 5.71 and 6.46 ppm for the meso (J= 3.30 Hz). Between 6.8 and 7.4 ppm resonate the aromatics of both isomers. The intense peak at 0.3 ppm was due to impurities of the deuterated benzene.

4.3 Isolation of a formulated catalyst from MCat1 and AS1

MCat1 was used to synthesize two different isolated 'dry' catalysts by reaction with AS1, IsoCatM1 and IsoCatP. The difference between the two catalysts resides in the solvent used for their synthesis; in fact IsoCatM1 was obtained in toluene while IsoCatP in pentane. In Table 19 is reported the surface composition for the two.

Table 19 – Surface composition for IsoCatM1 and IsoCatP.

	Zr wt%	n Al mmol g^{-1}	n Zr mmol g^{-1}	Zr/Al_{surf}
IsoCatM1	0.3	0.55	0.035	0.07
IsoCatP	0.6	0.55	0.07	0.12

The two catalysts were tested in ethylene slurry polymerization in the same conditions as the previous dry catalysts.

- Test in slurry polymerization with IsoCatM1

The polymerizations were run in 300 mL of heptane at 80°C and under 4 bars of ethylene, TiBA was used as scavenger. The results obtained for IsoCatM1 and IsoCatP are going to be discussed separately. In Table 20 are reported the polymerization results for IsoCatM1.

Table 20 – Polymerization results obtained with IsoCatM1 in slurry ethylene copolymerization. General conditions: 80°C; 4 bars C_2H_4; 300 mL heptane; [TiBA] 1mM.

run	Time* days	m mg	Zr mmol g^{-1}	Zr µmol	$Zr/Al_{surface}$	Zr loading Wt%	C6 mol%	Yield g	Activity g g_{cat}^{-1} h^{-1}
19	1	23.2	0.034	0.79	0.07	0.31	8.16	3.83	330
20	3	9.0	0.034	0.31	0.06	0.31	15.0	1.88	420
21	2	22.7	0.034	0.77	0.06	0.31	20.0	21.4	1888
22	4	12.5	0.034	0.43	0.06	0.31	20.2	8.45	1350
23	11	12.4	0.034	0.42	0.06	0.31	20.2	5.24	850
24	18	17.4	0.034	0.59	0.06	0.31	19.5	2.21	255

*Time elapsed since the synthesis. Runs 19-24 were conducted over a period of two-three weeks, giving to the catalyst time to age.

From the results reported in Table 20 three important information about IsoCatM1 can be evinced.

Firstly, the hypothesis that TiBA was detrimental for the activity of the catalyst was confirmed. In fact, if we compare run 21 from Table 20 with run 15 in Table 17, we can see that the first is almost twice as active as the latter. So much so, that in run 21 it was not possible to control the temperature of the reaction at 80°C, but it rose to 90°C, making it impossible to run the polymerization past 25 minutes of reaction time.

It was necessary to reduce the amount of catalyst injected for the following tests. Figure 25 reports the kinetic profiles for run 19-24, showing even more evidently the high activities obtained.

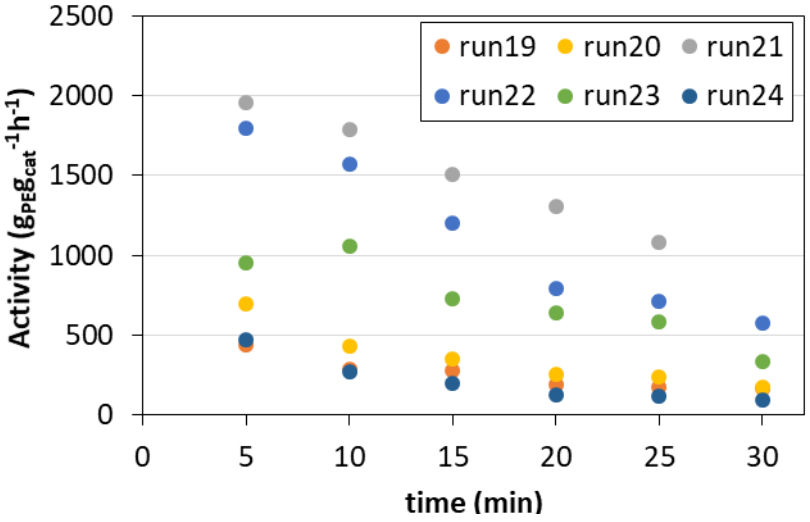

Figure 25 – Kinetic profiles for the slurry polymerization tests performed with IsoCatM1.

The second characteristic that can be evinced by looking at runs 19-21 is the great effect of the feed's tenure in comonomer on the catalyst's activity. In fact, increasing the concentration of 1-hexene from 8 to 20 mol%, causes a huge spike in the productivity of the catalyst, as depicted in Figure 26.

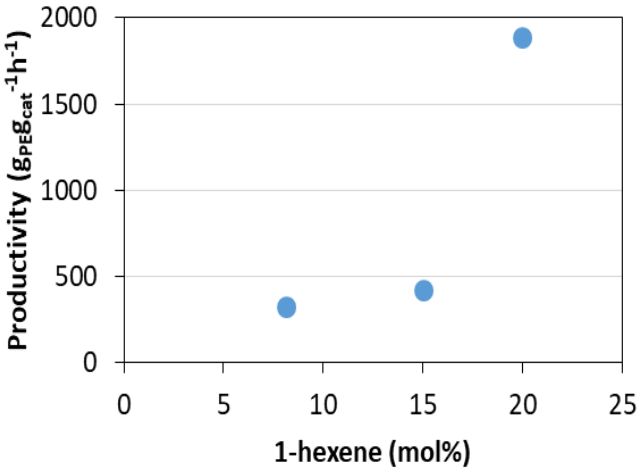

Figure 26 – Comonomer effect on the productivity of IsoCatM1.

Nonetheless, runs 22-24 show that even though the presence of TiBA adsorbed on the surface of the catalyst had negative effect on the activity, it was not the only cause for the catalyst deactivation over time at room temperature. After 20 days from its synthesis in fact the productivity of IsoCatM1 dropped from 1350 to 255 g g_{cat}^{-1} h^{-1}. The deactivation has then to be imputed to a side reaction occurring between the zirconocene and the activating support.

The polymers obtained with IsoCatM1 were then characterized by DSC, HT-SEC and IR. In Table 21 are reported the results.

Table 21 – DSC, HT-SEC and comonomer content characterization results for the polymer synthesized by IsoCatM1.

run	C6	Activity	*T*f2	Crystallinity	M_n	M_w	Đ	Comonomer
	mol%	g g_{cat}^{-1} h^{-1}	°C	%	g mol^{-1}	g mol^{-1}		mol%
19	8.16	330	127	46.7	63700	146500	2.3	0.8
20	15.0	420	118	51.6	45800	151300	3.3	1.2
21	20.0	1888	119	46.2	24500	54800	2.2	1.9
22	20.2	1350	118	41.4	26500	100500	3.8	2.0
23	20.2	850	117	52.2	35100	159500	4.5	1.7
24	19.5	255	115	42.0	51000	171300	3.4	1.7

All the samples produced by IsoCatM1 reveal the same large molecular weight distribution proper of *rac*-EtInd$_2$ZrCl$_2$, with the exception of run 21. In fact, this resin not only has a PD close to two but also a M_w lower than the other samples. This could be imputed to the higher polymerization temperature at which the sample was produced. This could have had, in fact, some effect on the performance of the active site. This is even clearer when observing the SEC traces for the samples reported in Figure 27.

The plot of the GPC traces evidences clearly the difference between run 21 and runs 22-23. Since the only difference consists in the temperature reached during the reaction, it could be safe to assume that the shrinking in the molecular weight and molecular weight distribution witnessed at 90°C, is in fact due to the higher temperature.

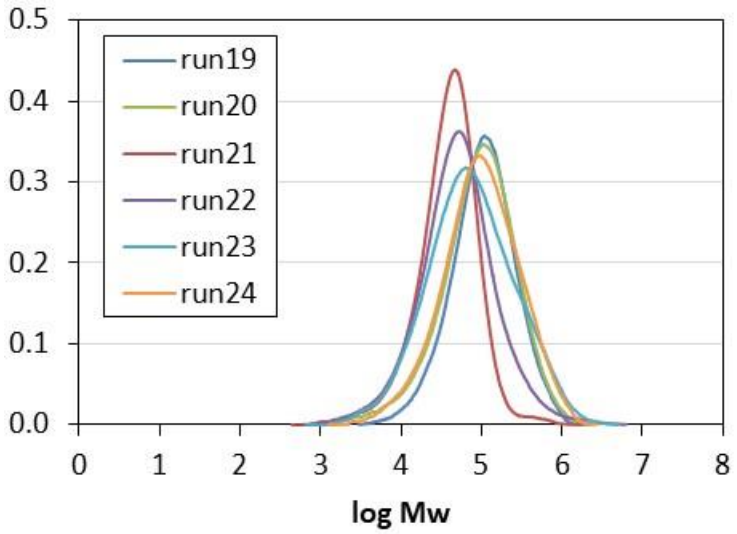

Figure 27 – SEC traces of the resins obtained with IsoCAtM1.

Table 21 also reports the comonomer content of runs 19-24. As expected the amount to α-olefin incorporated grows from run 19 to 21 as a consequence of the increase of the tenure in C6 of the reaction feed. The degree of branching found is in agreement with what previously seen with other resins produced with Cat1 and is well reflected in the melting temperatures reported in Table 21 for the polymers.

- Test in slurry polymerization with IsoCatP

The same polymerization conditions applied for IsoCatM1 were used for IsoCatP. The polymerizations were run in 300 mL of heptane at 80°C and under 4 bars of ethylene pressure, TiBA was used as scavenger. In Table 22 are reported the polymerization results for IsoCatP.

Table 22 – Polymerization results obtained with IsoCatP in slurry ethylene copolymerization. General conditions: 80°C; 4 bars C_2H_4; 300 mL heptane; [TiBA] 1mM.

run	*N of days**	*T* °C	m mg	Zr µmol	$Zr/Al_{surface}$	Zr loading Wt%	C6 mol%	Yield g	Activity g g_{cat}^{-1} h^{-1}
25	8	80	12.6	0.82	0.12	0.59	19.5	5.03	800
26	22	80	10.1	0.66	0.12	0.59	19.0	3.12	615
27	1	90	19.5	1.27	0.12	0.59	19.8	21.8	3030
28	20	90	19.0	1.23	0.12	0.59	19.8	21.9	2310
29	23	95	11.5	0.74	0.12	0.59	21.8	19.8	3300

*At room temperature.

The tests performed with IsoCatP show a lower activity at 80°C with respect to IsoCatM1 as could have been expected after the study performed in paragraph 3 of the Chapter for a Zr/Al ratio higher than 0.06 on the surface of the catalyst. Moreover, the tests reported in Table 22 show how the catalyst's activity is highly responsive not only to the C6/C2 ratio in the reactor, but also to the temperature of the polymerization. The activity plots reported in Figure 28 make this observation even more evident.

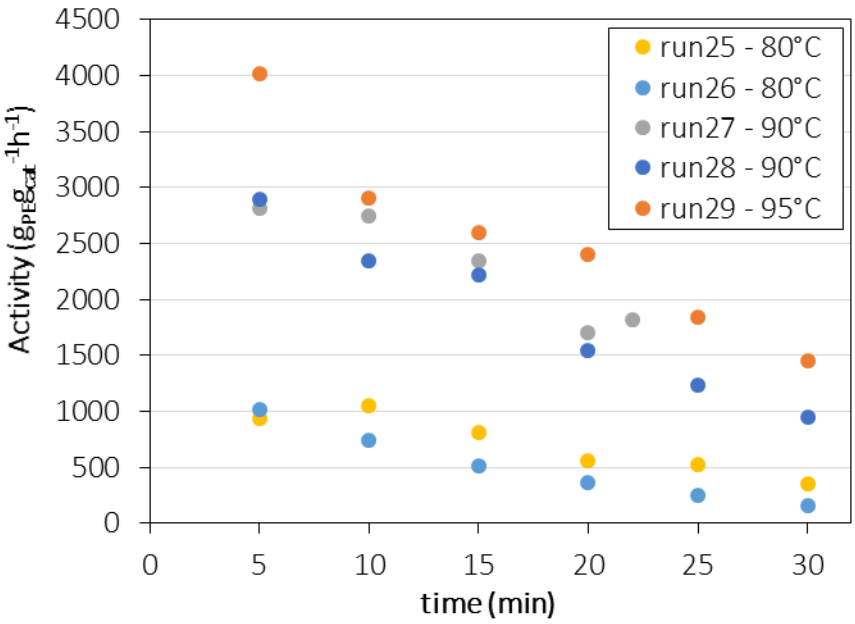

Figure 28– Kinetic profiles for the slurry polymerization tests performed with IsoCatM1.

The effect of the temperature on the catalyst's performance was impressive, the productivity rose from 800 to 3030 g g_{cat}^{-1} h^{-1} in going from 80°C to 90°C. Independently of the temperature at which the polymerizations were run, though, also IsoCatP, like the other isolated catalysts, was subject to a deactivation phenomenon over time under storage at ambient temperature in the glove box: activity at 80°C dropped from 800 to 650 g g_{cat}^{-1} h^{-1}, while at 90°C the productivity passed from 3030 to 2310 g g_{cat}^{-1} h^{-1} in 20 days.

In order to check if the temperature had an effect also on the structure of the polymer and not only the productivity, the resins obtained were analyzed by DSC, HT-SEC and IR. The results are reported in Table 23

Table 23 – DSC, HT-SEC and comonomer content characterization results for the polymer synthesized by IsoCatP.

run	N of days	*T* °C	Activity g g_{cat}^{-1} h^{-1}	Tf2 °C	Crystallinity %	M_n g mol^{-1}	M_w g mol^{-1}	Đ	Comonomer mol%
25	8	80	800	122	37.8	19700	133800	6.8	1.5
26	22	80	615	117	45.9	39300	158800	4.0	1.6
27	1	90	3030	122	40.3	18300	49000	2.7	1.6
28	20	90	2309	120	36.5	25900	63000	2.4	1.5
29	23	95	3455	119	29.7	21100	50600	2.4	1.7

*At room temperature.

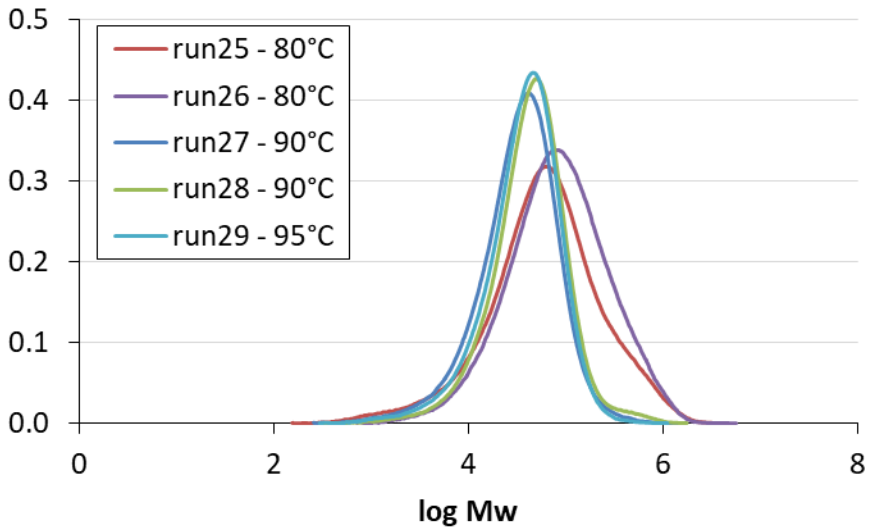

Figure 19 – HT-SEC traces of the resins obtained with IsoCatM1.

From the HT-SEC results it is clear that the temperature has an effect on the molecular weight and distribution of the resins. While the polymers synthesized at 80°C have a Đ higher than 4 and an M_w above 130000 g mol^{-1}, the resins obtained at 90°C have shorter chains and narrower molar mass distributions, M_w around 50000 g mol^{-1} and Đ close to 2. The plot of the SEC traces in Figure 29 exemplifies it very clearly. It isn't easy to prove the exact effect of the temperature on the catalyst and on the polymer particles; it could either influence directly the interaction between the zirconocene and the activator on the surface, or merely have a more physical effect on the growing particle dynamics.

This temperature effect is interesting from a product tailoring point of view. In fact, by controlling the temperature of polymerization it could be possible to control the properties of the final resins.

It was not possible to perform a characterization of the morphology of the resins obtained with this catalyst due to the formation of aggregates at the time of the filtration to recover the product.

- Ethylene polymerization tests in gas phase with IsoCatM1

Once confirmed the well-behaviour of the formulated catalysts in slurry polymerization, IsoCatM1, the most performing of the isolated catalysts synthesized, was employed in gas phase ethylene polymerization. The aim of this test was to check the behaviour of the catalyst also in gas phase from both an activity and product performance point of view.

Moreover, the performance of IsoCatM1 was compared, in similar conditions, to that of two INEOS industrial references. The polymerizations were conducted in a 2.5 L turbosphere reactor, under 7 bars of ethylene pressure for one hour, 70-100 g of salt were used to disperse the catalyst and TiBA was employed as scavenger. In Table 24 are reported the polymerization tests' results.

Table 24 – Polymerization results for the gas phase polymerization tests performed with IsoCatM1 and INEOS references. General conditions: 2.5L; 7 bars C2; 1 hour; 70-100 g salt; TiBA as scavenger.

catalyst	T	m cat	Zr	Ti	TiBA	Yield	Productivity
	°C	mg	wt%	wt%	mmol	g	$g_{PE}\, g_{cat}^{-1}\, h^{-1}$
INEOS1	72	100	-	0.22	0.8	18.0	180
INEOS2	85	100	0.48	-	1.0	51.0	510
IsoCatM1	75	12.7	0.31	-	1.0	3.62	285

From the data reported in Table 24 the productivity of IsoCatM1 is in the same order of magnitude as the industrial references, even higher than INEOS1. In Figure 28 are reported the kinetic profiles for the three catalysts.

The plot depicts clearly that although the three catalysts present a very different behaviour and kinetics one from the other, the overall activity is in the same range. The fact that the activities recorded with IsoCatM1 are in the same range of those of industrial catalysts is once more a proof that the activating support AS1 has the same level of efficiency of supported activators currently used in industrial production.

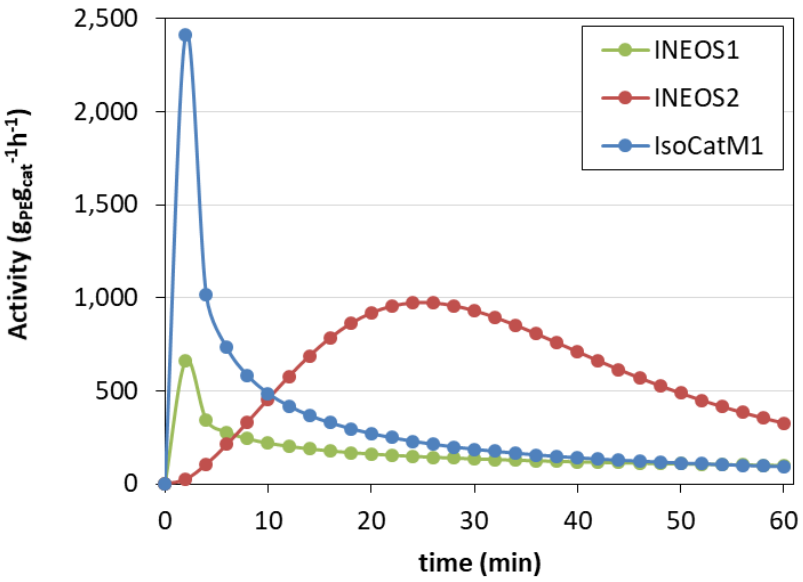

Figure 30 – Kinetic profiles for the gas phase polymerization test performed with IsoCatM1 confronted with two industrial references.

It is worth noticing that the productivity recorded for IsoCatM1 in gas phase, 285 $g_{PE}\, g_{cat}^{-1}\, h^{-1}$, is lower than the maximum one recorded in slurry polymerization, 1350 $g_{PE}\, g_{cat}^{-1}\, h^{-1}$, but it is to be expected considering that the reaction in gas phase was conducted in homopolymerization conditions, and that it was stated before that the comonomer concentration in the feed has a huge effect on the catalyst's activity.

The polymer obtained with IsoCatM1 in gas phase was characterized by DSC and HT-SEC, the results are reported in Table 25.

Table 25 – DSC and HT-SEC characterization results for the polymer synthesized by IsoCatM1 in gas phase homopolymerization.

run	Activity $g\, g_{cat}^{-1}\, h^{-1}$	Tf2 °C	Crystallinity %	M_n $g\, mol^{-1}$	M_w $g\, mol^{-1}$	PD
IsoCatM1	285	130.8	54.0	46300	108800	2.4

As expected, considering that the run was conducted in homopolymerization conditions, the DSC characterization of the fluff evidenced a high melting temperature, 130°C, and a high crystallinity fraction, 54%, confirming the HDPE nature of the resin.

For what concerns, on the other side, the HT-SEC characterization, the molar mass of the polymer resulted to be in line with what already observed for IsoCatM1 in runs 19-24. But instead of what we were used to observe with polymers obtained with *rac*-$EtInd_2ZrCl_2$, the polydispersity in this case is narrower, 2.4 instead of 3.0 or higher. The narrowing of the polydispersity could be simply due to the absence of comonomer; in fact IsoCatM1, but also AS1/Cat1, were never tested in homopolymerization conditions in slurry. A second reason for the narrower molar mass distribution could be found in a change in the process, passing from slurry to gas phase polymerization, could affect also the microstructure of the final polymer.

The morphology of the powder obtained was observed by SEM microscopy. The images acquired are reported in Figure 31. From the general pictures (Figure 30a and 30b), we observed the absence of undesirable fine amongst the polymer particles, confirming once more the good behaviour of the catalytic system. In the the images acquired at higher magnifications, c), d), e), f), the polymer's growth structure.

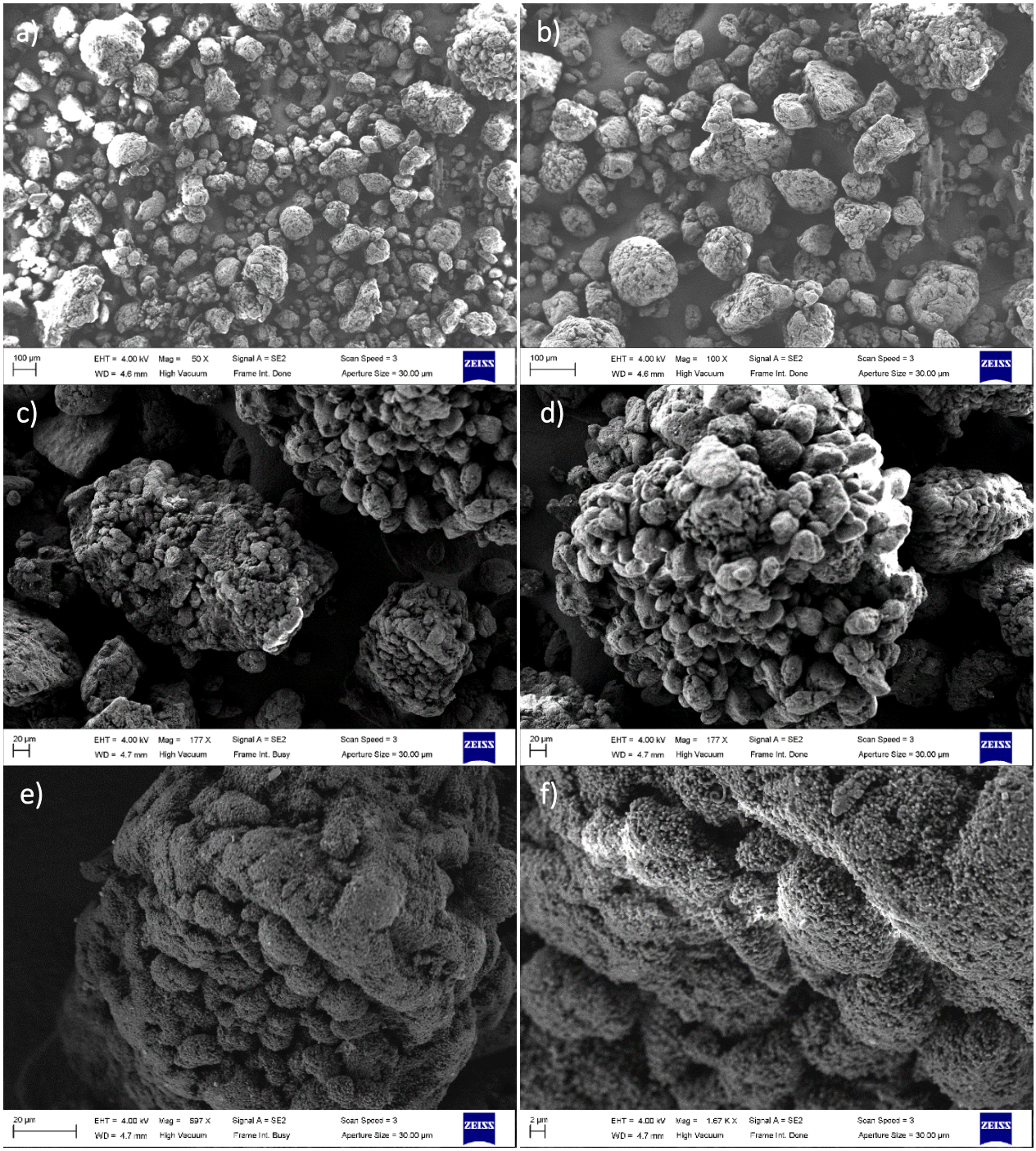

Figure 31 – SEM images acquired for the resin obtained with IsoCatM1 in gas phase at different magnifications: a)50x; b) 100x ; c) 177x; d) 177x; e) 557x; f) 1.77Kx.

Given the good results obtained with *rac*-EtInd$_2$ZrMe$_2$ in the isolation of a formulated catalyst, we decided to isolate a 'dry' catalyst also with (*n*-BuMeCp)$_2$ZrCl$_2$.

4.4 Synthesis of (*n*-BuMeCp)$_2$ZrMe$_2$, MCat2

For the isolation of the formulated catalyst based on (*n*-BuMeCp)$_2$ZrCl$_2$, it was decided to use the complex, (*n*-BuMeCp)$_2$ZrMe$_2$, MCat2, that can react directly with AS1, in order to avoid the problems observed with IsoCat01-04 in presence of TiBA.

The procedure followed for the synthesis of (*n*-BuMeCp)$_2$ZrMe$_2$ was the same used for MCat1. (*n*-BuMeCp)$_2$ZrCl$_2$ was reacted with 2 eq. of CH_3Li in Et_2O overnight, then the product was extracted in pentane and dried to give a white powder. In Scheme 8 is reported the reaction pathway.

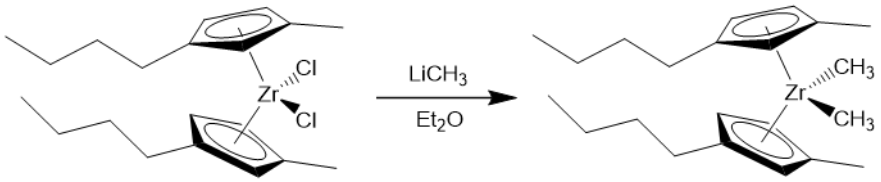

Scheme 8 – Synthesis of (n-BuMeCp)$_2$ZrMe$_2$, MCat2.

The product was characterized by ^{1}H solution NMR in C_6D_6. The acquired spectrum is reported in Figure 32 and shows the successful methylation of the zirconocene.

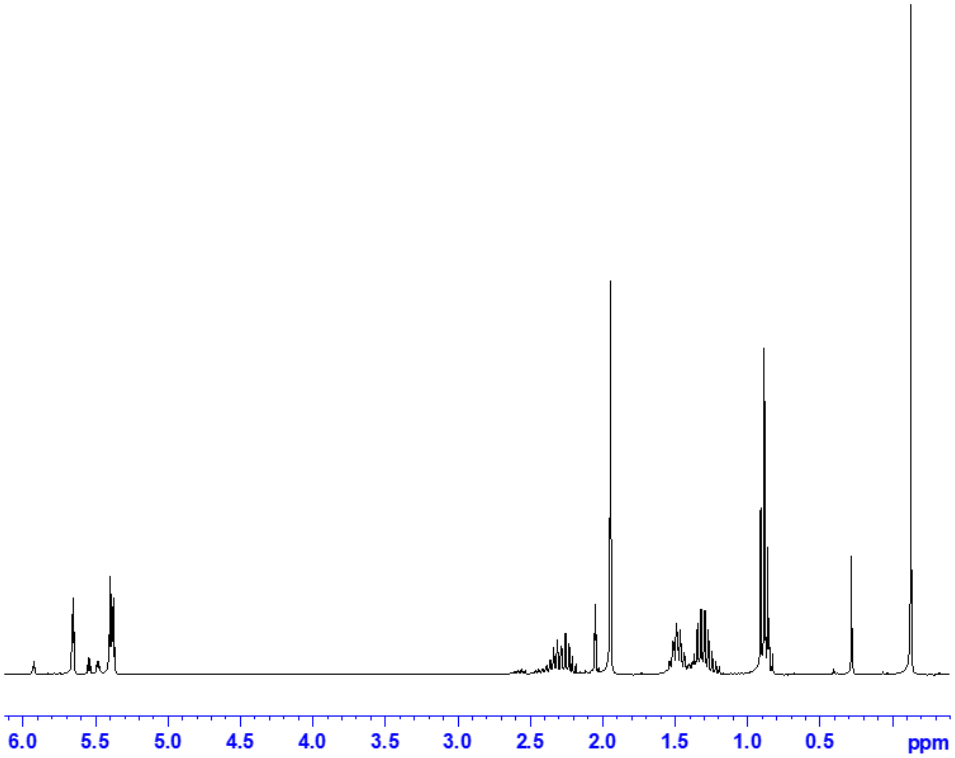

Figure 32 – ^{1}H NMR spectrum of (n-BuMeCp)$_2$ZrMe$_2$ in benzene-d$_6$.

The spectrum appears clean with the signals proper of MCat2. At -0.13 ppm can be seen in fact the singlet of the Zr-CH_3 moiety and at 0.89 ppm the triplet of the methyl of the butyl group. At 1.3 ppm and 1.5 ppm resonate respectively the CpC_2H_4-C***H₂***-Me and the $CpCH_2$-C***H₂***-C_2H_5 as multiplets. The singlet of the methyl group directly bonded to the Cp rings falls at 1.95 ppm and at 2.29 ppm there's a multiplet assigned to Cp-C***H₂***-C_3H_7. The protons of the cyclopentadienyl ring resonate at 5.40 and 5.66 ppm as a multiplet and triplet respectively.

- Synthesis of IsoCatM2

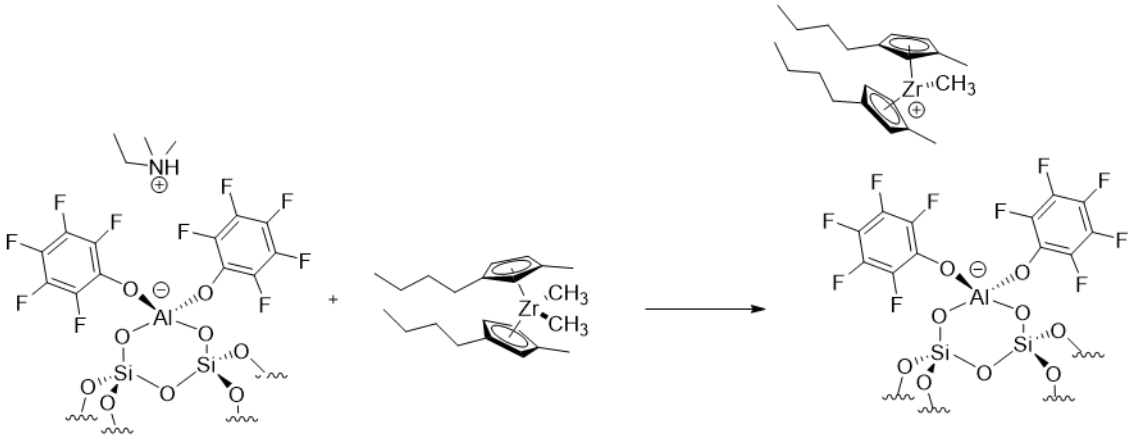

Scheme 9 – Synthesis of the 'dry' catalyst IsoCatM2.

MCat2 thus obtained was reacted in hexane with AS1 for 1 hour to synthesize the 'dry' catalyst IsoCatM2. The Zr/Al ratio targeted was very close to the one used for the reference runs 2 and 3. In Table 26 is reported the surface composition for IsoCatM2.

Table 26 – Surface composition of IsoCatM2.

	Zr wt%	n Al mmol g^{-1}	n Zr mmol g^{-1}	Zr/Al_{surf}
IsoCatM2	0.33	0.72	0.036	0.05

The product was characterized by DRIFT and ^{1}H MAS and ^{13}C CPMAS solid state NMR. In Figure 33 is reported the DRIFT spectrum of the catalyst.

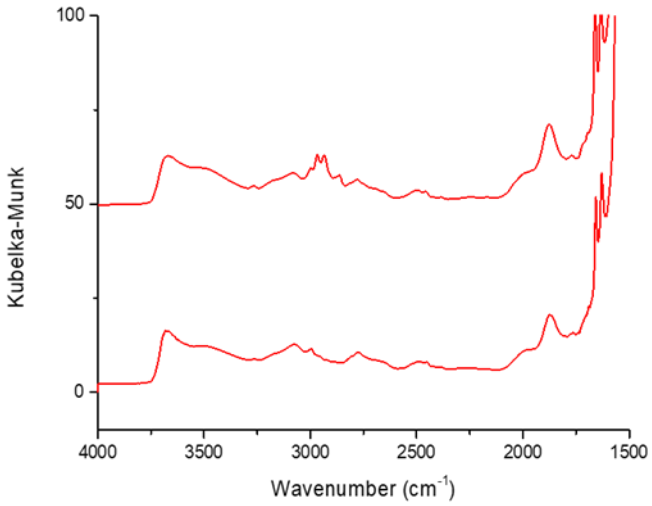

Figure 20 – DRIFT spectra of AS1 (bottom) and IsoCatM2 (top).

Upon reaction of MCat2 with the surface of AS1 the main change to the DRIFT spectrum is the increase in intensity of the bands relative to the CH stretching at 3000 cm^{-1}. The peak at 3070 cm^{-1} of the N-H stretching of the ammonium is still present, but this is was to be expected considering the low amount of zirconocene introduced with respect to the ammonium on the surface.

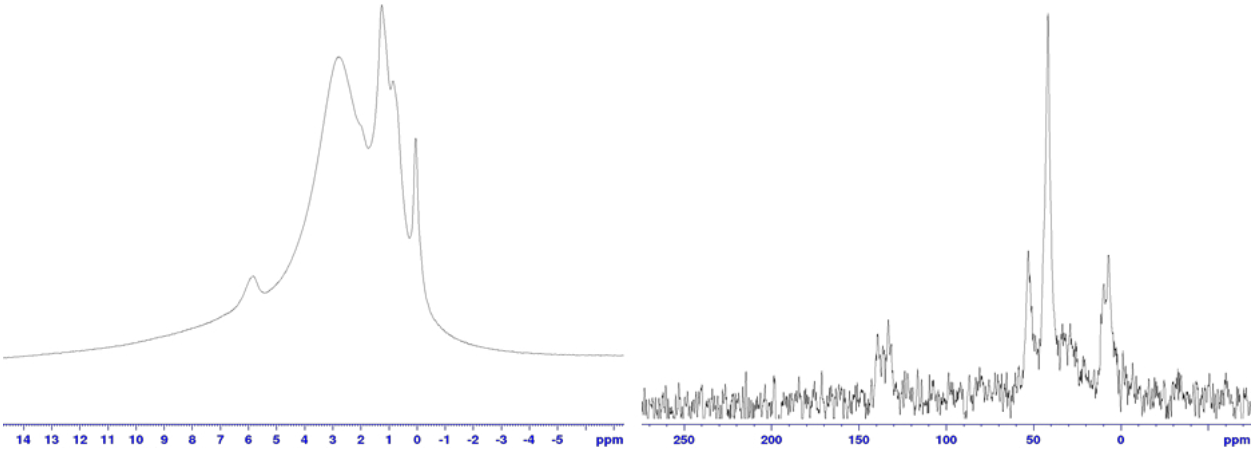

Figure 34 – ^{1}H MAS (left) and ^{13}C CPMAS (right) NMR spectra of IsoCat01.

The ^{1}H spectrum clearly shows the signals for the zirconocene complex coordinated on the surface. At 5.83 ppm resonate the protons of the Cp ring, the shoulder at 1.98 ppm can be attributed to the methyl group directly bonded to the Cp, while at 1.25 and 0.85 ppm there's the signal of the methylenes and of the methyls of the butyls moieties, respectively. Underneath the

same large peak resonate the methyl of the NCH_2CH_3 and at 2.79 ppm the NCH_3 and the methylene bonded to the N. The peak at 0.04 ppm could be due to grease residues; given the very low Zr/Al ratio, it is not possible to individuate the Zr-CH_3 signal.

At the ^{13}C NMR are present five peaks at 140.1, 133.2, 53.6, 41.8 and 8 ppm. The peaks at 140.1 and 133.2 ppm are assigned to the Cp ring of the zirconocene, at 53.6 ppm resonate the methylene of the ethyl bonded to the N, at 41.8 ppm is the signal of the NCH_3 group and at 8 ppm the methyl of the ethyl bonded to the N. Underneath these large peaks fall also the signals of the aliphatic groups of the zirconocene.

- Test in slurry polymerization with IsoCatM2

IsoCatM2 was then tested in ethylene/1-hexene slurry copolymerization. The same polymerization conditions applied for IsoCatM1 and IsoCatP were used also for IsoCatM2. The polymerizations were run in 300 mL of heptane at 80°C and under 4 bars of ethylene, TiBA was used as scavenger.

In Table 27 are reported the polymerization results for IsoCatM2.

Table 27 – Polymerization results obtained with IsoCatM2 in slurry ethylene copolymerization. General conditions: 80°C; 4 bars C_2H_4; 300 mL heptane; [TiBA] 1mM.

run	time	m	Zr	$Zr/Al_{surface}$	Zr loading	C6	Yield	Activity
	min	mg	µmol		Wt%	mol%	g	$g\ g^{-1}_{cat}\ h^{-1}$
30	30	16.0	0.58	0.05	0.33	19.3	3.47	435
31	30	33.2	1.20	0.05	0.33	20.5	9.93	600
32	60	23.5	0.85	0.05	0.33	19.8	8.42	360
33	30	22.0	0.79	0.05	0.33	20.2	1.10	100

In Figure 35 are depicted the Kinetic profiles for runs 30-33.

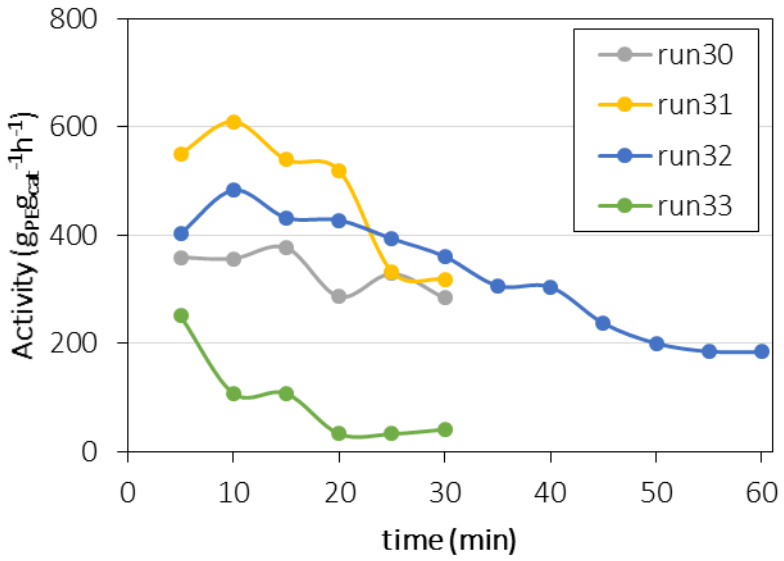

Figure 35 – Kinetic profiles for the slurry polymerization tests performed with IsoCatM1.

IsoCatM2 showed lower productivities than IsoCatM1 and IsoCatP, but also lower than the ones during run 2 and 3. However, the same kinetic profile recorded with the pre-contact method, was found also in the case of IsoCatM2.

The greater stability showed during the polymerization time could have suggested also a higher stability of the active species on the silica surface over time, at room temperature. Instead, run 33, conducted one month after run30 and 31, and showed a deep drop in productivity (from 600 $g_{PE}\, g_{cat}^{-1}\, h^{-1}$ to 100 $g_{PE}\, g_{cat}^{-1}\, h^{-1}$).

The polymers obtained with IsoCatM2 were characterized by DSC, HT-SEC and IR. The results are reported in Table 28.

Table 28 – DSC, HT-SEC and comonomer content characterization results for the polymer synthesized by IsoCatM2.

run	time	Activity	*T*f2	Crystallinity	M_n	M_w	Đ	Comonomer
	min	$g\, g_{cat}^{-1} h^{-1}$	°C	%	$g\, mol^{-1}$	$g\, mol^{-1}$		mol%
30	30	435	127.6	48.1	54900	113500	2.1	0.7
31	30	600	123.7	44.1	46700	104100	2.2	0.9
32	60	360	126.8	45.3	55900	114800	2.1	0.7
33	30	100	127.0	46.4	70000	135100	1.9	0.7

The characterization of the resins obtained in runs 30-33 show some coherence with the results obtained with runs 2 and 3. In fact from both the comonomer content and the melting temperature it is possible to see how IsoCatM2 has a lower tendency to incorporate 1-hexene than IsoCatM1 and IsoCatP, mirroring what was observed for the tests performed by pre-contacting AS1 with Cat1 and Cat2.

The results obtained by HT-SEC are on the other side more surprising. In fact, while as expected the molar mass distribution of all four resins reported in Table 28 are narrow (all close to 2), in line with what observed previously in runs 2 and 3, the molar masses are lower than expected (100 Kg mol^{-1} instead of the 200 Kg mol^{-1} found previously). This could be either due to the methylation of the catalyst or a different interaction of the same with the surface of AS1 following the isolation, which causes the formation of different active species on the surface.

The instability of the active species on the surface of AS1, independently of the zirconocene employed for the synthesis of the catalysts, suggests an inherent tendency of the aluminate anion grafted on the silica to react with the active zirconocene to deactivate it.

In order to better understand the evolution of the ionic couple on the surface, a labelled zirconocene, *rac*-$EtInd_2Zr(^{13}CH_3)_2$, was reacted with AS1, and the species evolution was observed over time.

5. Active species evolution on the silica surface

In order to better observe by NMR the evolution of the species on the surface and possible transfers of ligands between the surface of the activating support and the zirconocene, *rac*-$EtInd_2ZrMe_2$ was enriched in ^{13}C at the methyl positons during the methylation reaction.

To do so a batch of CH_3Li 60% enriched in ^{13}C was prepared by reaction of $^{13}CH_3I/^{12}CH_3I$ in 60:40 ratio with *n*-BuLi.

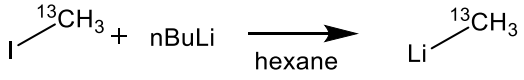

Scheme 10 – Synthesis of $^{13}CH_3Li$.

The product was characterized by solution ^{1}H and ^{13}C NMR in THF-d_8. The spectra are reported in Figure 36.

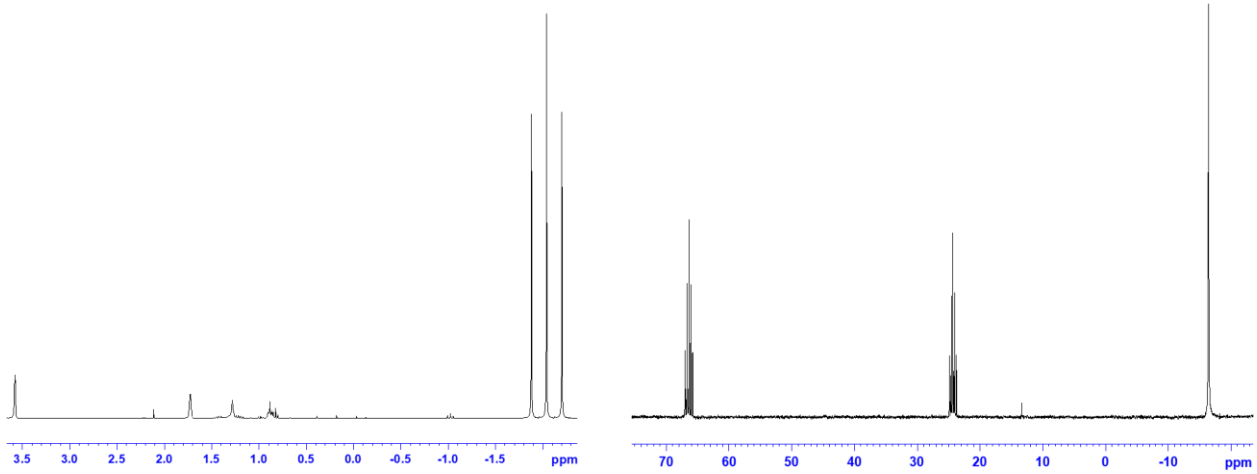

Figure 36 – ^{1}H and ^{13}C solution NMR for $^{13}CH_3Li$ in THF-d_8.

The NMR spectra confirm the ^{13}C enrichment of the methyllithium synthesized. The ^{1}H NMR spectrum displays two signals, a singlet at -2.04 ppm assigned to the methyl of $^{12}CH_3Li$, and a doublet centred at -2.04 ppm, due to the coupling between ^{13}C and ^{1}H (J=97 Hz), assigned to $^{13}CH_3Li$. The integration of the two signals confirm the ratio 60:40 between $^{13}CH_3Li$ and $^{12}CH_3Li$. The ^{13}C NMR spectrum shows one intense peak at -16.4 ppm for the $^{13}CH_3Li$.

The methyllitium thus synthesized was used for the synthesis of *rac*-$EtInd_2ZrMe_2$ enriched in ^{13}C at the methyl positions. The reaction followed was the same described in paragraph 4.2. The product was then analysed by ^{1}H and ^{13}C solution NMR in benzene-d_6. The spectra are reported in Figure 37.

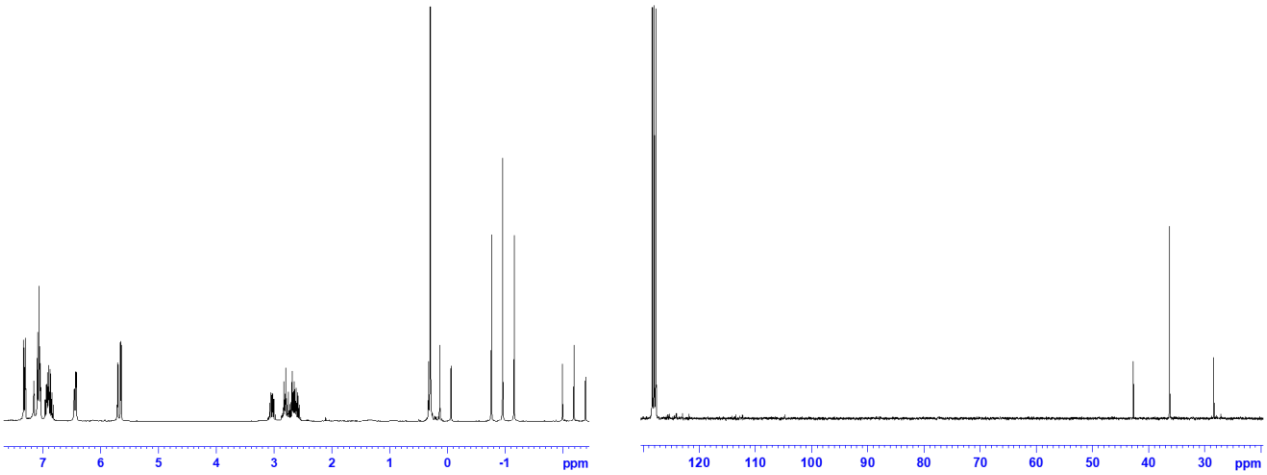

Figure 37 – ^{1}H and ^{13}C NMR for labelled rac-$EtInd_2ZrMe_2$ in benzene-d_6.

Like in the case of the non-labelled complex, upon methylation of *rac*-$EtInd_2ZrCl_2$, a partial isomerization of the zirconocene from the *rac* to the *meso* form occurred. The spectra also show the enrichment in ^{13}C of the complex. For what concerns the *rac* isomer in the methyl area of the ^{1}H spectrum are present two signals, a singlet at 0.95 ppm, assigned to the Zr-$^{12}CH_3$, and a doublet centred at 0.95 ppm, due to the coupling between ^{13}C and ^{1}H (J = 117.7 Hz), assigned to Zr-$^{13}CH_3$. A similar situation is found for the *meso* isomer. In this case the two methyls resonate at two different chemical shift, at -2.19 ppm are located the first singlet and doublet (J = 118.8 Hz), and at 0.14 ppm the singlet and the doublet (J = 116.6 Hz) for the second methyl of the *meso* isomer. The relative integration of the peaks shows a 60:40 ratio *meso/rac*-$EtInd_2Zr(^{13}CH_3)_2$: *meso/rac*-$EtInd_2Zr(^{12}CH_3)_2$, and a 62:38 ratio *meso*:*rac.*

The ^{13}C spectrum exhibits three signals at 28.4, 36.6 and 42.7 ppm. The signal at 36.6 ppm is assigned to the labelled methyls of the *rac* isomer while the signal at 28.4 and 42.7 ppm to the two methyls of the *meso* isomer.

The zirconocene was then supported on the surface of AS1 and the IsoCatL thus obtained was characterized by solid state NMR. The amount of zirconocene used in the reaction was higher than target set for the previous catalyst synthesises to facilitate the characterization of the surface species. In Table 28 is reported the surface composition of IsoCatL.

Table 28 – Surface composition of IsoCatL.

	Zr wt%	n Al mmolg^{-1}	n Zr mmolg^{-1}	Zr/Al$_{surf}$
IsoCatL	0.6	0.55	0.065	0.12

The catalyst was characterized by ^{1}H MAS and ^{13}C CPMAS solid state NMR a first time right after the synthesis and then a second time two weeks later, so as to evaluate if the spectra evolved over time.

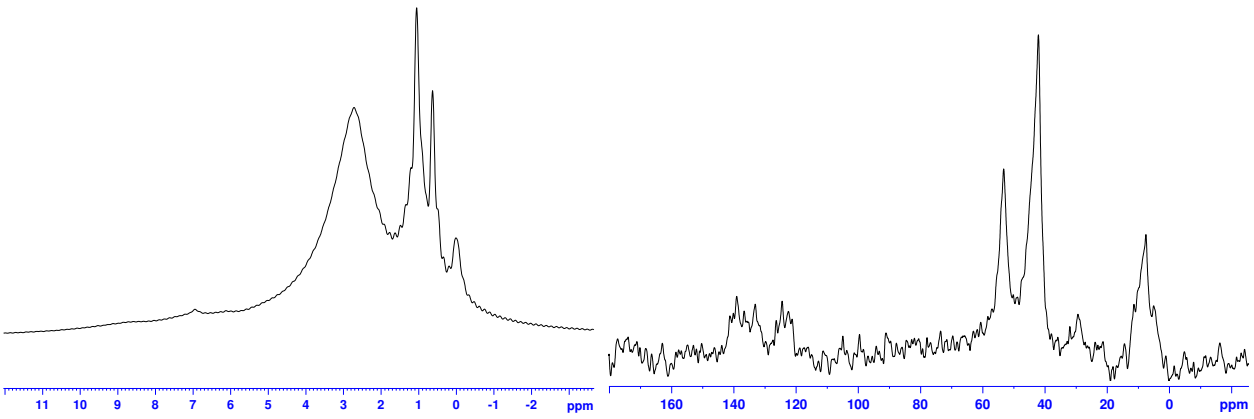

Figure 38 – ^{1}H MAS (left) and ^{13}C CPMAS (right) NMR spectra for IsoCatL soon after the synthesis.

The spectra reported in Figure 38 where acquired right after the synthesis of IsoCatL. The ^{1}H spectrum shows clearly the coordination of the zirconocene to the aluminate on the surface, the peaks at 0.63 and 1.06 ppm can be assigned to the Zr-CH_3 signals respectively of the [*meso*-$EtInd_2ZrCH_3$]$^+$ and [*rac*-$EtInd_2ZrCH_3$]$^+$, underneath these two peaks fall also the methyl signal of the NCH_2CH_3 moiety of the ammonium still present on the surface, and at 2.72 ppm is the peak relative to the methylene of the NCH_2CH_3 and to the methyls directly bound to the nitrogen. At 6.95 ppm is also possible to see a small shoulder for the protons of the indenyl ligand.

At the ^{13}C NMR are present the peaks for the ammonium ion at 7.6, 42.1 and 53.3 ppm assigned, as previously discussed, to the methyl of the NCH_2CH_3, the methyls bound to the N and the methylene of the NCH_2CH_3 respectively. Between 118 and 146 ppm is visible a large band assigned to the indenyl ring and at 29.4 ppm the signal of the methylene carbons of the ethyl bridge. Due to the large nature of the peaks at the solid state NMR and the low amount of zirconocene on the

surface, it is not possible to see the signals of the methyls bound to the zirconium, that should have fallen in the same area of the NCH_2 and NCH_3.

A 2D spectrum of IsoCatL was acquired to better understand the surface.

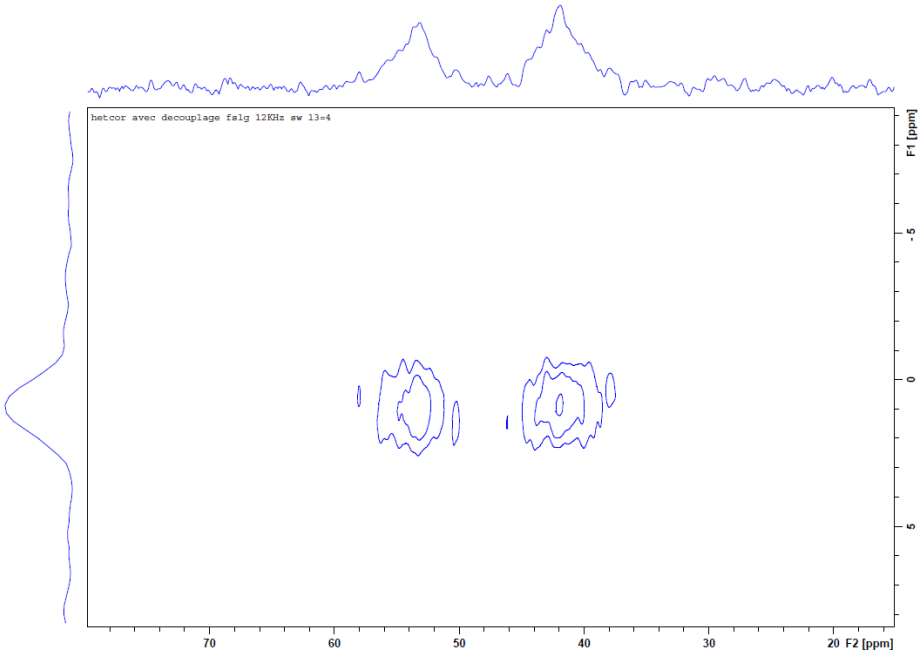

Figure 39 – HETCOR 2D solid state NMR spectrum of IsoCatL.

The HETCOR spectrum shows two signals centred at 41.8 and 53.1 ppm at the ^{13}C and 1 ppm at the ^{1}H. These two signals are clearly assignable to the methyls bound to the Zr of [*rac*-$EtInd_2ZrCH_3$]$^+$ and [*meso*-$EtInd_2ZrCH_3$]$^+$. The information derived from the NMR characterization of IsoCatL confirms the formation of the active species at the moment of the isolation, successively a number of side reaction could occur.

In Scheme 11 are reported some of the side reaction possible on the surface.

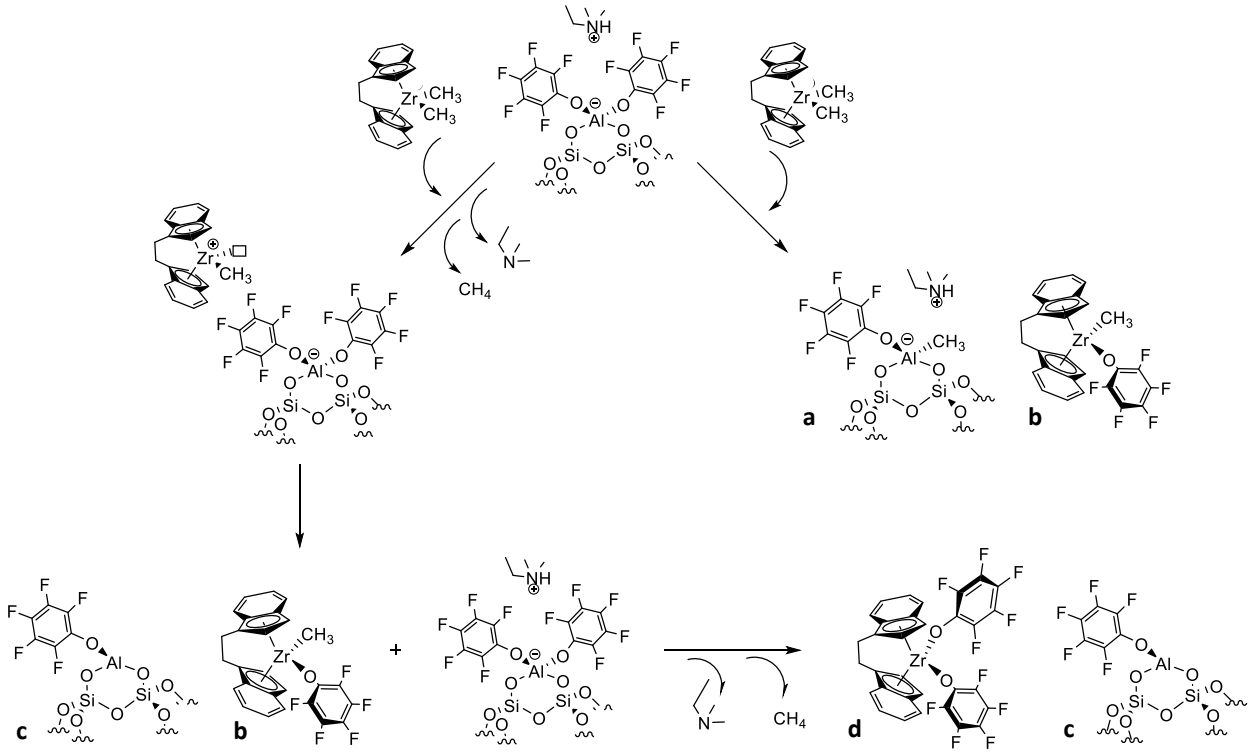

Scheme 11 – Deactivation patterns possible for IsoCat.

Upon first reaction of MCat1 on AS1 two main events could occur, the formation of the active species (left in Scheme 11) or a transfer of ligands between the aluminate and the zirconocene (right in Scheme 11), generating an aluminate with an Al-CH_3 bond, **a**, and a zirconocene featuring a phenoxy group as ligand, $EtInd_2ZrMeOC_6F_5$, **b.** This pattern would be very easy to detect because the methyl bound to the aluminium has a very characteristic chemical shift at the ^{13}C NMR, around -10 ppm.

If the active species is obtained on the surface, it could also be subjected to a ligand transfer between the zirconocene and the aluminate. This would give as product the zirconocene **b** and a neutral bipodal aluminium $(SiO)_2AlOC_6F_5$, **c**. The same **b** though could react again with second $[(SiO)Al(OC_6F_5)]^-[HNEtMe_2]^+$, present in great excess with respect to the zirconocene. This second ligand transfer would generate a second **c** species and $EtInd_2Zr(OC_6F_5)_2$, **d**. The detection of these species could be not as straightforward as the formation of **a**, but still achievable.

After two weeks from the synthesis of IsoCatL the catalyst was characterized by solid state NMR, the conditions used for the spectra acquisition was the same in both cases. The ^{1}H and ^{13}C NMR spectra acquired are reported in Figure 40.

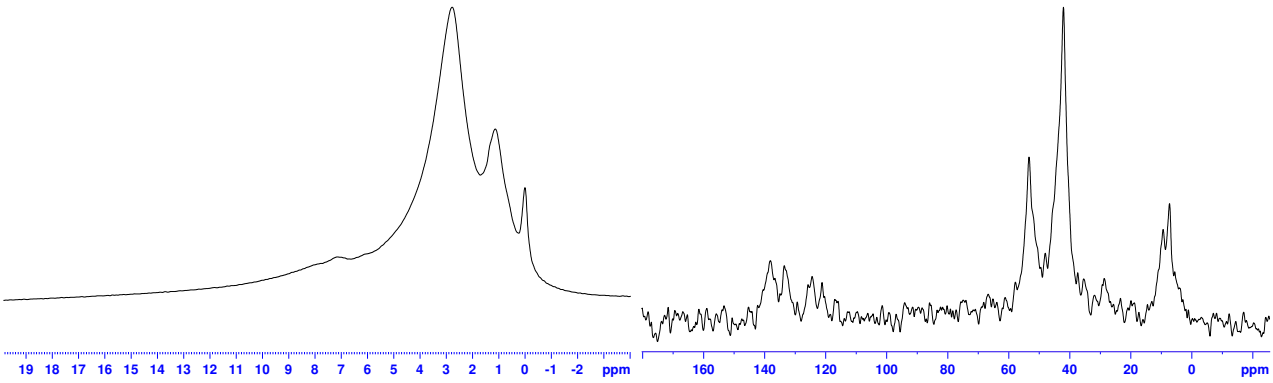

Figure 40 – ^{1}H MAS (left) and ^{13}C CPMAS (right) NMR spectra for IsoCatL two weeks after the synthesis.

The ^{1}H MAS NMR spectrum shows immediately an evolution of the catalyst. In fact, the peaks at 0.63 and 1.06 ppm that were assigned to the methyls bound to the Zr have disappeared, revealing the signal of the methyl of the NCH_2CH_3 moiety. At 2.72 ppm then there's the peak relative to the methylene of the NCH_2CH_3 and to the methyls directly bonded to the nitrogen. At 7.14 ppm is also possible to see a small shoulder for the protons of the indenyl ligand.

The ^{13}C spectrum hasn't really changed over time, it is still possible to see prevalently the signals relative to the ammonium. At 7.29 ppm resonates the methyl of the NCH_2CH_3, the methyls bound to the N resonate at 42.1 ppm while the methylene of the NCH_2CH_3 at 53.3 ppm. It is though clear the absence of any peak at -10 ppm, significant of the fact that no Al-C bond was formed over time, excluding the right side of Scheme 11 from the possible deactivation pathways.

The same reasoning done for the ^{13}C, can be done for the HETCOR spectrum acquired, and reported in Figure 41.

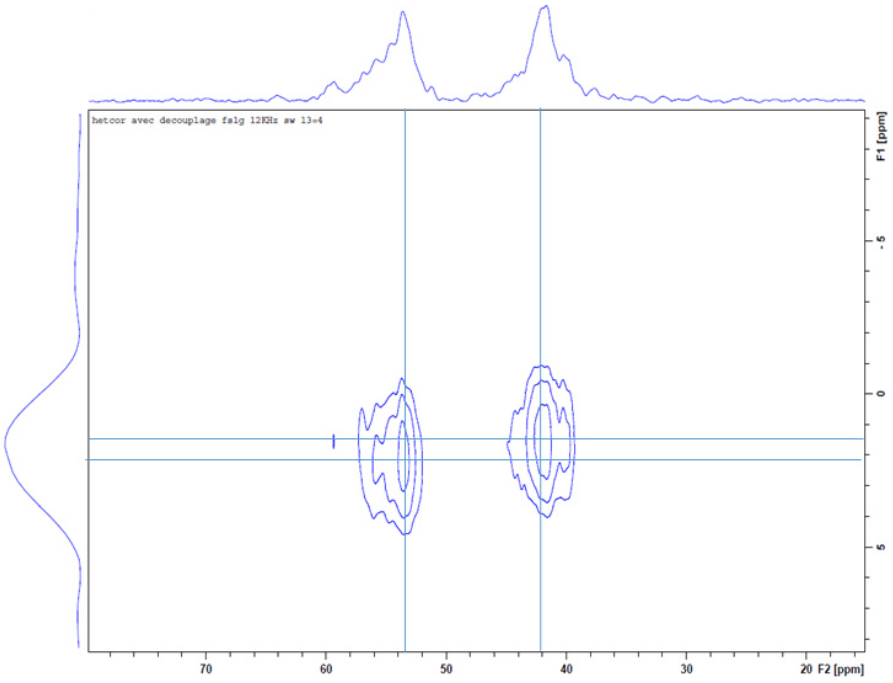

Figure 41 – HETCOR 2D solid state NMR spectrum of IsoCatL after two weeks from the synthesis.

The spectrum presents itself very similar to the one reported in Figure 38. The fact that the methyls of the two zirconocene isomers resonate at two different chemical shifts makes the interpretation of the HETCOR spectrum of the evolved species tricky. The signal for the methyl of a –ZrMe(OC_6F_5) species falls around 54 ppm according to the literature.[15] The spectrum reported in Figure 41 shows two peaks at 41.7 and 53.7 ppm, this together with the 1D ^{1}H spectrum could suggest the presence on the surface of two zirconocene species, one neutral, $EtInd_2Zr(Me)OC_6F_5$, generated by the reaction with the surface, and the other, the cationic active species.

Unfortunately the low amount of Zr present on the surface doesn't allow us to discern precisely the deactivation pattern taken by the active species. Nonetheless, it is possible to hypothesize, based on the literature, that the deactivation proceeds through the transfer of the phenoxy ligand. Further studies at higher Zr/Al ratios are anyway necessary to confirm this hypothesis.

Conclusions

In this chapter it was presented the synthesis, characterization and application of a bipodal aluminate activating support, AS1. The support was tested in ethylene/1-hexene slurry copolymerization as cocatalysts for two different zirconocene precursors, *rac*-EtInd$_2$ZrCl$_2$ (Cat1) and (*n*-BuMeCp)$_2$ZrCl$_2$, (Cat 2) in presence of TiBA as activating support.

Both systems showed good activities, 1111 $g_{PE}\ g_{cat}^{-1}\ h^{-1}$ for the system AS1/Cat1/TiBA and 980 $g_{PE}\ g_{cat}^{-1}\ h^{-1}$ for AS1/Cat2/TiBA. The resins obtained were well controlled from a morphology point of view and their microstructure was in agreement with what previously observed in the literature for these catalyst's precursors. Considering the promising results, the system AS1/Cat1/TiBA was scaled up to pre-industrial scale.

The scale-up of the technology was successful, higher activities than at lab-scale were found, between 5000 and 6000 $g_{PE}\ g_{cat}^{-1}\ h^{-1}$. The study at pre-industrial scale was also used to determine the optimal value of Zr/Al on the surface, to obtain a maximum in the activity. The value found, 0.06 Zr/Al, was also vised for the isolation of a formulated 'dry' catalyst.

Two different approaches were employed for the isolation of the active species on the surface: the first approach saw the reaction of Cat1 and AS1 in presence of TiBA as alkylating agent; the presence of the alkyl, though, appeared to have detrimental effects on the activity. It was so decided to react AS1 with methylated catalyst precursors *rac*-EtInd$_2$ZrMe$_2$ and (*n*-BuMeCp)$_2$ZrMe$_2$. The catalysts obtained resulted to be highly active but subjected to deactivation over a short period of time (20 days) at room temperature. Following a first study of the evolution of the active species on the surface and what is reported in literature for similar systems, it was hypothesized that the decay of the active species was possibly due to a transfer of a ligand from the activating support surface species to the zirconocene cation. Further studies are though necessary to confirm this theory.

References

(1) *Tailor-Made Polymers: Via Immobilization of Alpha-Olefin Polymerization Catalyst*; Severn, J., Ed.; Wiley-VCH: Weinheim, 2008.

(2) Prades, F.; Broyer, J.-P.; Belaid, I.; Boyron, O.; Miserque, O.; Spitz, R.; Boisson, C. Borate and MAO Free Activating Supports for Metallocene Complexes. *ACS Catal.* 2013, *3* (10), 2288–2293. https://doi.org/10.1021/cs400655y.

(3) Sauter, D. W.; Popoff, N.; Bashir, M. A.; Szeto, K. C.; Gauvin, R. M.; Delevoye, L.; Taoufik, M.; Boisson, C. The Design of a Bipodal Bis(Pentafluorophenoxy)Aluminate Supported on Silica as an Activator for Ethylene Polymerization Using Surface Organometallic Chemistry. *Chem. Commun.* 2016, *52* (26), 4776–4779. https://doi.org/10.1039/C6CC00060F.

(4) Howell, J. G.; Li, Y.-P.; Bell, A. T. Propene Metathesis over Supported Tungsten Oxide Catalysts: A Study of Active Site Formation. *ACS Catal.* 2016, *6* (11), 7728–7738. https://doi.org/10.1021/acscatal.6b01842.

(5) Sauter, D. W.; Chiari, V.; Aykac, N.; Bouaouli, S.; Perrin, L.; Delevoye, L.; Gauvin, R. M.; Szeto, K. C.; Boisson, C.; Taoufik, M. Preparation of Monopodal and Bipodal Aluminum Surface Species by Selective Protonolysis of Highly Reactive [$AlH_3(NMe_2Et)$] on Silica. *Dalton Trans.* 2017, *46* (35), 11547–11551. https://doi.org/10.1039/C7DT02575K.

(6) Humphries, T. D.; Munroe, K. T.; Decken, A.; McGrady, G. S. Lewis Base Complexes of AlH3: Prediction of Preferred Structure and Stoichiometry. *Dalton Trans.* 2013, *42* (19), 6965. https://doi.org/10.1039/c3dt00047h.

(7) Mazoyer, E.; TrØbosc, J.; Baudouin, A.; Boyron, O.; Pelletier, Jø.; Basset, J.-M.; Vitorino, M. J.; Nicholas, C. P.; Gauvin, Rø. M.; Taoufik, M.; et al. Heteronuclear NMR Correlations To Probe the Local Structure of Catalytically Active Surface Aluminum Hydride Species on G-Alumina*. *Angew Chem Int Ed* 2010, 5.

(8) Metz, M. V.; Sun, Y.; Stern, C. L.; Marks, T. J. Weakly Coordinating Al-, Nb-, Ta-, Y-, and La-Based Perfluoroaryloxymetalate Anions as Cocatalyst Components for Single-Site Olefin Polymerization. *Organometallics* 2002, *21* (18), 3691–3702. https://doi.org/10.1021/om020087s.

(9) Khosravi M., M.; Andrus, M. B.; Burt, S. R.; Woodfield, B. F. Generalized Preparation Method and Characterization of Aluminum Isopropoxide, Aluminum Phenoxide, and Aluminum n-Hexyloxide. *Polyhedron* 2013, *62*, 18–25. https://doi.org/10.1016/j.poly.2013.06.019.

(10) Decken, A.; Jenkins, H. D. B.; Nikiforov, G. B.; Passmore, J. The Reaction of $Li[Al(OR)_4]$ R = $OC(CF_3)_2Ph$, $OC(CF_3)_3$ with NO/NO_2 Giving $NO[Al(OR)_4]$, $Li[NO_3]$ and N_2O. The Synthesis of $NO[Al(OR)_4]$ from $Li[Al(OR)_4]$ and $NO[SbF_6]$ in Sulfur Dioxide Solution. *Dalton Trans* 2004, No. 16, 2496–2504. https://doi.org/10.1039/B405715E.

(11) Chu, K.-J.; Soares, J. B. P.; Penlidis, A. Effect of Hydrogen on Ethylene Polymerization Using In-Situ Supported Metallocene Catalysts. *Macromol. Chem. Phys.* 2000, *201* (5), 552–557.

https://doi.org/10.1002/(SICI)1521-3935(20000301)201:5<552::AID-MACP552>3.0.CO;2-A.

(12) Tisse, V. F.; Boisson, C.; McKenna, T. F. L. Activation and Deactivation of the Polymerization of Ethylene over *Rac* -EtInd $_2$ ZrCl $_2$ and (*n* BuCp) $_2$ ZrCl $_2$ on an Activating Silica Support. *Macromol. Chem. Phys.* 2014, *215* (14), 1358–1369. https://doi.org/10.1002/macp.201400023.

(13) Haag, M. C.; Krug, C.; Dupont, J.; de Galland, G. B.; dos Santos, J. H. Z.; Uozumi, T.; Sano, T.; Soga, K. Effects of Al/Zr Ratio on Ethylene–Propylene Copolymerization with Supported-Zirconocene Catalysts. *J. Mol. Catal. Chem.* 2001, *169* (1–2), 275–287. https://doi.org/10.1016/S1381-1169(01)00045-0.

(14) Balboni, D.; Camurati, I.; Prini, G.; Resconi, L.; Galli, S.; Mercandelli, P.; Sironi, A. Group 4 Dimethylmetallocenes: Improved Synthesis and Reactivity Studies. *Inorg. Chem.* 2001, *40* (26), 6588–6597. https://doi.org/10.1021/ic010018q.

(15) Popoff, N.; Gauvin, R. M.; De Mallmann, A.; Taoufik, M. On the Fate of Silica-Supported Half-Metallocene Cations: Elucidating a Catalyst's Deactivation Pathways. *Organometallics* 2012, *31* (13), 4763–4768. https://doi.org/10.1021/om3003224.

(16) Amor, J. I.; Burton, N. C.; Cuenca, T. Synthesis and Characterization of New Alkoxide and Aryloxide Derivatives of Titanium and Zirconium. X-Ray Molecular Structure of [ZrCp 2(OC6 2]. 8.

(17) Perrotin, P.; El-Zoghbi, I.; Oguadinma, P. O.; Schaper, F. Replacing Chloride by Alkoxide: Cp2Zr(H)OR, Searching for Alternatives to Schwartz's Reagent. 11.

CHAPTER III:

Activating supports with chelating or sterically hindered ligands on the Al centre

Index

Introduction

In Chapter II it was presented the synthesis, characterization and application of $[(\equiv SiO)_2Al(OC_6F_5)_2]^-[HNMe_2Et]^+$, AS1 (Scheme 1), in ethylene slurry polymerization as a cocatalyst for the two zirconocenes *rac*-$EtInd_2ZrCl_2$ and (*n*-$BuMeCp)_2ZrCl_2$. The two systems showed very good potential from a productivity and resins' morphology point of view. So much so that the catalyst AS1/*rac*-$EtInd_2ZrCl_2$ was tested at a pre-industrial scale showing high activities up to about 6000 $g_{PE}\, g_{cat}^{-1}\, h^{-1}$.

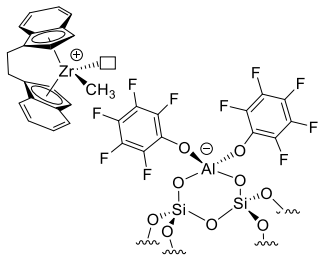

Scheme 1 – Structure of the catalyst AS1/rac-$EtInd_2ZrCl_2$.

Although the excellent activities obtained, a recurrent problem was found for the catalysts synthesized and isolated using AS1: the active species on the surface, although stable at low temperatures (-20 °C), at room temperature decay rapidly. In fact, for all the catalysts synthesized, in the span of two weeks, the activity in lab conditions dropped from over 1000 $g_{PE}\, g_{cat}^{-1}\, h^{-1}$ to 200 $g_{PE}\, g_{cat}^{-1}\, h^{-1}$, or lower.

It was proved that at room temperature a transfer of ligand occurs between the activator and the zirconocene, making the catalyst less active (Scheme 2).

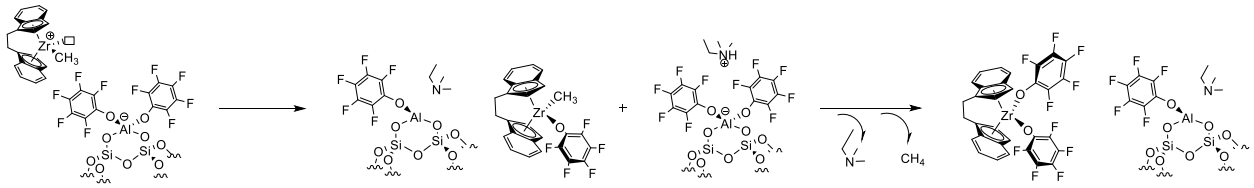

Scheme 2 – Possible catalyst deactivation pattern.

The same problem was reported by Marks et al. in 2002[1] for molecular activators homologous to AS1. They tackled the issue by increasing the steric hindrance of the ligands of the cocatalyst, impeding thus kinetically the occurring of the transfer (Scheme 3).

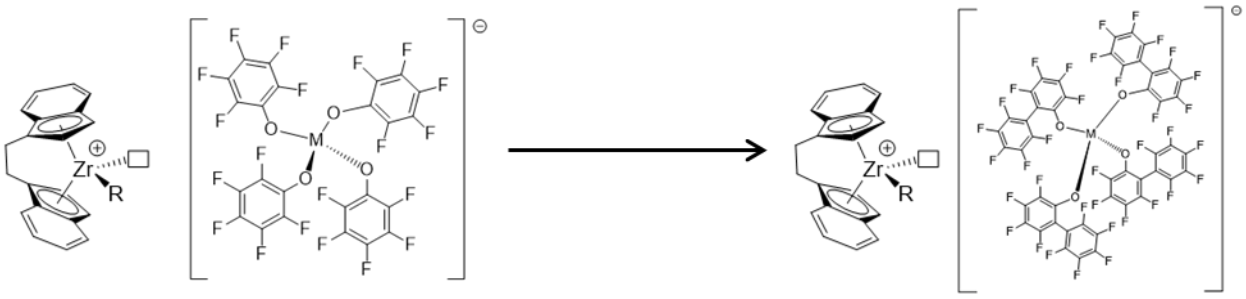

Scheme 3 – Structure of the molecular activators with differently sterically hindered ligands reported by Marks.

In the same frame of mind, we decided to solve the issue by making the Al centre less accessible for a transfer, by either increasing the steric hindrance of the ligands employed during the functionalization or by increasing their chelating ability.

In this chapter is presented the synthesis of five different activating supports with different chelating or sterically hindered ligands, and their test in ethylene/1-hexene slurry copolymerization in combination with *rac*-EtInd$_2$ZrCl$_2$.

1. Synthesis of $[(\equiv SiO)Al(OC_6F_5)_3]^-[HNMe_2Et]^+$, AS2

In Chapter II the effect on the activity of the heat treatment of the support, and consequently the amount and type of anionic activator based on Al on its surface, was discussed.[2] It was seen in fact how passing from grafting a bipodal aluminate, $[(\equiv SiO)_2Al(OC_6F_5)_2]^-[HNEt_2Ph]^+$, on a silica dehydroxylated at 700°C to supporting it on one dehydroxylated at 200°C, increased of at least twice the efficiency of the activator (in combination with *rac*-$EtInd_2ZrCl_2$ the activity in ethylene/1-hexene slurry copolymerization rises from 656 to 1111 $g_{PE}\, g_{cat}^{-1}\, h^{-1}$ in passing from $SiO_{2\text{-}700}$ to $SiO_{2\text{-}200}$ as support).

AS2 was synthesized by grafting $AlH_3.NEtMe_2$ on $SiO_{2\text{-}700}$ and then modifying the grafted species with pentafluorophenol, to obtain the activating support.

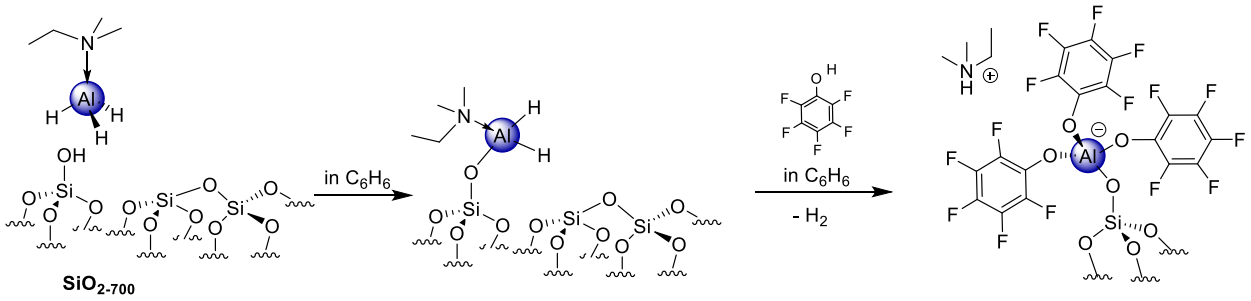

Scheme 4 – Synthesis of $[(\equiv SiO)Al(OC_6F_5)_3]^-[HNMe_2Et]^+$, AS2.

The aim behind the synthesis of AS2 was to investigate the efficiency of a monopodal activating support in comparison to the bipodal AS1.

1.1 Silica's treatment, dehydroxylation at 700°C, $SiO_{2\text{-}700}$

As in the case of AS1 the selected silica for the synthesis of AS2 was Grace silica Sylopol 2408. The support was treated under high vacuum for 14 hours at 700°C, in order to remove all the physisorbed water and favour the condensation of vicinal silanols to have just isolated silanols on the surface.[3]

The surface was characterized by DRIFT spectroscopy after treatment. The spectrum is reported in Figure 1.

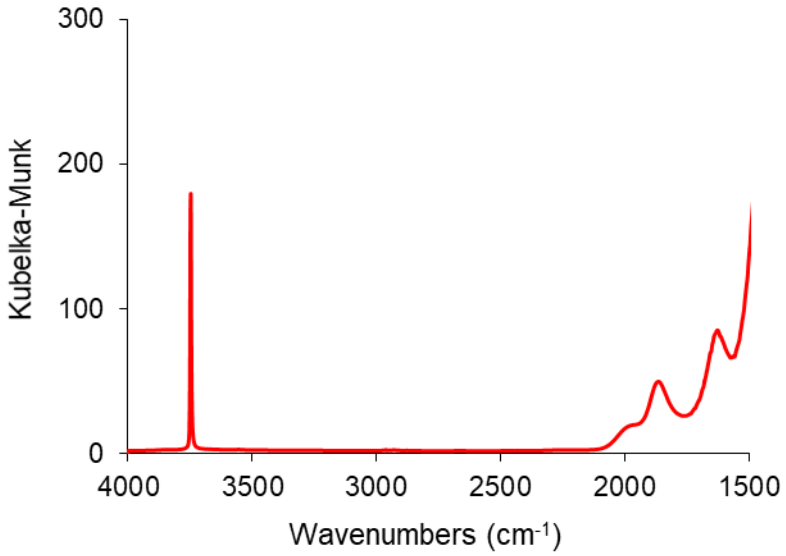

Figure 1 – DRIFT spectrum of $SiO_{2\text{-}700}$.

The spectrum exhibits one sharp peak at 3743 cm^{-1} characteristic of the O-H stretching of the isolated silanols. By titration with Al*i*Bu_3 was determined that 0.58 mmol g^{-1} of SiOH groups were present on the surface.

1.2 Grafting of $AlH_3(NEtMe_2)$ on $SiO_{2\text{-}700}$, P2

In order to synthetize the activating support AS2, it was first generated on the silica surface the grafted aluminium hydride precursor. 1.2 eq. of AlH_3NMe_2Et per eq. of SiOH were put to react in benzene for two hours to obtain (≡SiO)$AlH_2(NMe_2Et)$, P2.[4] Scheme 2 shows the reaction and the structure for P2.

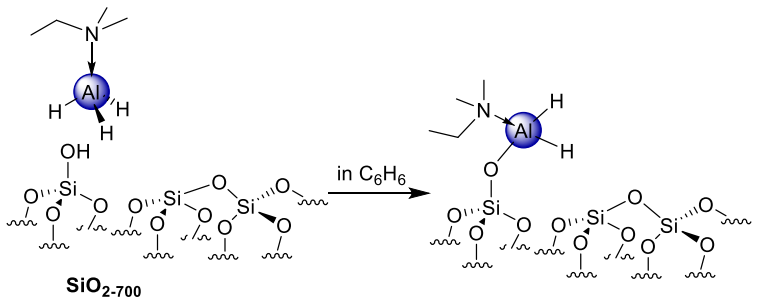

Scheme 5 – Grafting of $AlH_3.NEtMe_2$ on $SiO_{2\text{-}700}$.

The resulting material was characterized by DRIFT spectroscopy. Figure 2 depicts the DRIFT spectra of the support before and after the reaction with the alane.

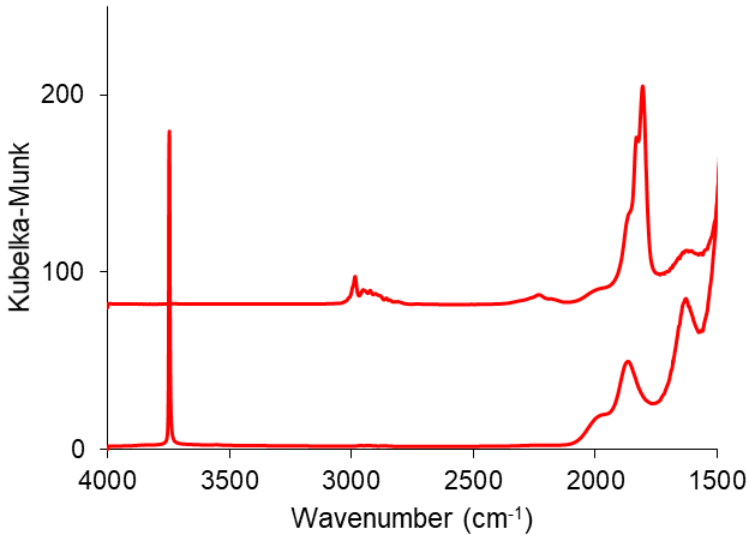

Figure 2 – DRIFT spectra of $SiO_{2\text{-}700}$ (bottom) and P2 (top).

Upon reaction of $AlH_3(NEtMe_2)$ with $SiO_{2\text{-}700}$ all the silanols were consumed, as indicated by the disappearance of the peak at 3743 cm^{-1}. A set of peaks appears below 3000 cm^{-1} assigned to the C-H stretching of the alkyl groups of the amine. The three peaks at 1865, 1831 and 1805 cm^{-1} are due to the Al-H stretching, the wavelength of the stretching is in agreement with what is reported in literature for the free alane.[5] An additional peak resonates at 2234 cm^{-1}, this wavelength is characteristic of Si-H stretching, indicating that during the grafting of the alane on the silica surface an opening of siloxane bridges occurred with consequent transfer of an hydride to the silica.[4]

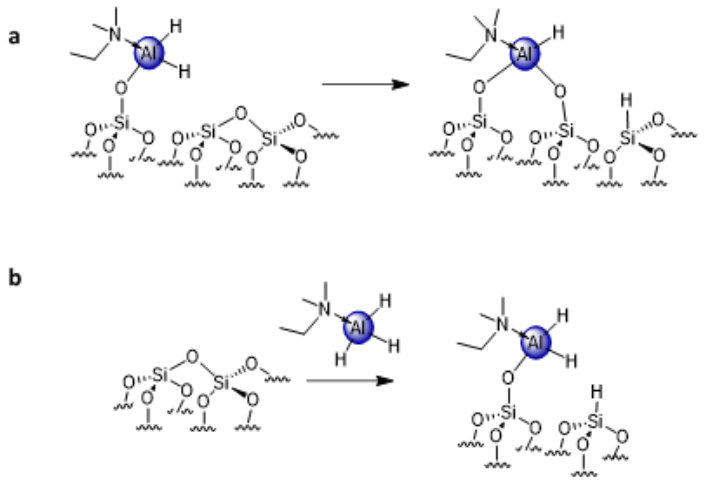

Scheme 6 – Possible ways of formation of a Si-H bond. (a) transfer of hydride after protonolysis ; (b) transfer of hydride upon opening of a siloxane bond.

As shown in Scheme 6, the opening of the siloxane bridge can occur either by direct reaction of the free alane with the siloxane, route **b** in Scheme 6, or by reaction of the bridge with the monopodal (≡SiO)$AlH_2(NMe_2Et)$, obtained from the reaction of the alane with the SiOH groups, route, **a** in Scheme 6. The opening of the siloxane bridges as described by pattern, **a**, has as consequence the formation of a fraction of bipodal species on the surface of the support.

In order to better understand the species' composition on the surface, the H_2 evolved by the grafting reaction and upon hydrolysis of P2 was quantified. The quantifications' results are reported in Table 1 with the results of the elemental analysis for P2.

Table 1 – Elemental analysis and H_2 quantification results for P2.

wt% Al	wt% C	wt% N	wt% H	C/N	C/Al	N/Al	H/Al	Al mmol g^{-1}	H_2/Al Grafting	H_2/Al Hydrolysis
1.89	3.03	1.19	0.83	3.0 (th. 4)	3.6 (th 4)	1.2 (th. 1)	11.8 (th. 13)	0.7	0.8 (th. 1)	1.5 (th. 2)

The quantification of the elements found 0.7 mmol g^{-1} of aluminium on the surface of P2. The amount of N and C recovered, 1.19 and 3.03 wt% respectively, is close to the theoretical value for the presence of one amine coordinated per aluminium, the ratios C/Al and N/Al are in fact 3.6 and 1.2 respectively. It is worth to notice more aluminium than the amount of surface silanols (0.58 mmol g^{-1}) was found grafted on the surface of $SiO_{2\text{-}700}$, proving that a fraction of the alane reacted directly with the siloxane bridges, as described by pattern **b** in Scheme 6.

Concerning the hydrogen quantification, the amount of H_2 evolved per Al during the grafting reaction, 0.8 H_2/Al, is close to the theoretical value of one for a monopodal aluminium hydride on the surface (also considering that the reaction leading to monopodal species from direct opening of siloxane bridges would not release any H_2). The quantification of the hydrogen evolved by the hydrolysis of P1, then, showed that just 1.5 H_2 per Al were evolved, proving that 50% of the grafted species are bipodal.

This requires a modification of the reaction Scheme for the synthesis of P2, to include both species on the surface.

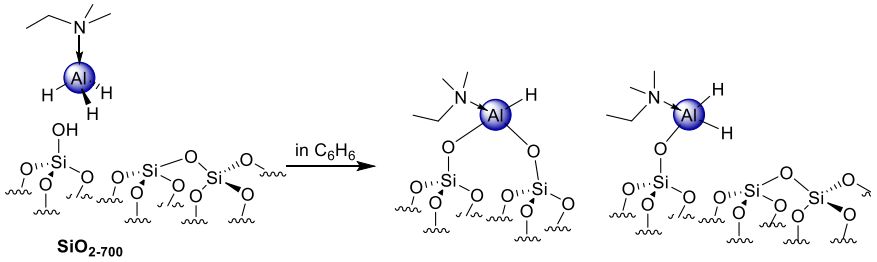

Scheme 7 – Synthesis of P2.

P1 was then characterized by solid state ^{1}H MAS and ^{13}C CPMAS solid state NMR.

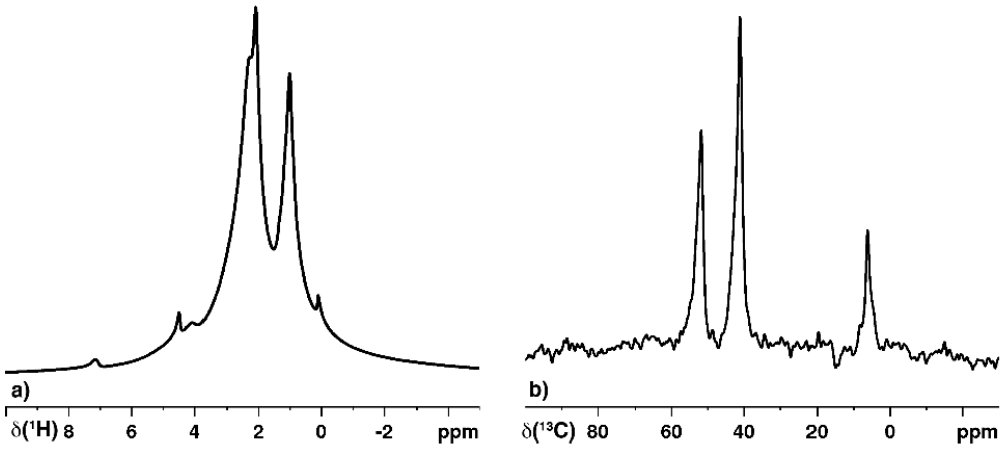

Figure 3 – a) ^{1}H and b) ^{13}C solid state NMR spectra of P2.

The ^{1}H spectrum reveals two intense signals relative to the amine. At 0.9 ppm resonate the methyl group of the $NCH_2\underline{CH_3}$ fragments and the signal around 2.1 ppm is assigned to the methylene of the $N\underline{CH_2}CH_3$ fragments and the methyl directly bound to the N. At 4.2 ppm there is a feeble peak assigned to the SiH proton.[4] As already stated in Chapter II for P1, it is not possible to see the signal relative to the proton bound to the Al, because it is hidden by the signals of the amine.[6]

The ^{13}C spectrum shows three peaks assigned to the alkyls of the amine. At 6.2 ppm resonates the methyl group of the NCH_2CH_3 fragment, at 41.1 ppm the methyls directly bound to the N, and at 51.9 ppm the methylene group of the NCH_2CH_3 moiety.

The characterizations performed on P2 confirmed the presence on the surface of a mixture of mono- and bi-podal aluminum hydride species in ratio 50:50. This grafted precursor was then used in the synthesis of the activating support AS2.

1.3 Synthesis of AS2 by reaction of P2 with pentafluorophenol

In order to obtain the desired activating support AS2, P2 was reacted with 3 eq. of pentafluorophenol overnight in benzene. Given the composition of the surface of P2, upon reaction with pentafluorophenol both monopodal and bipodal aluminate species are going to be grafted on the silica surface, as shown in Scheme 8.

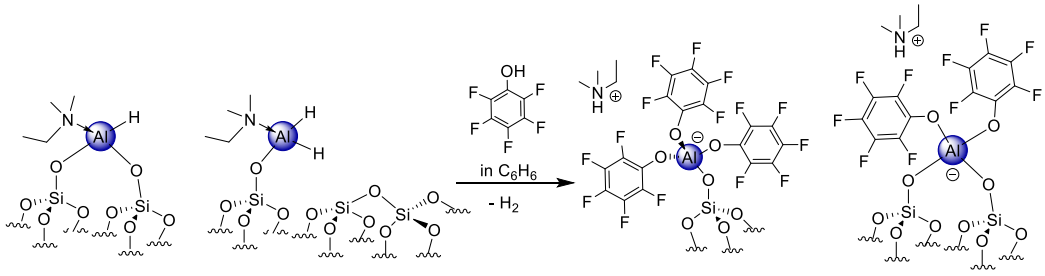

Scheme 8 – Synthesis of AS2.

The activating support was characterized by DRIFT, ^{1}H and ^{13}C solid state NMR and elemental analysis.

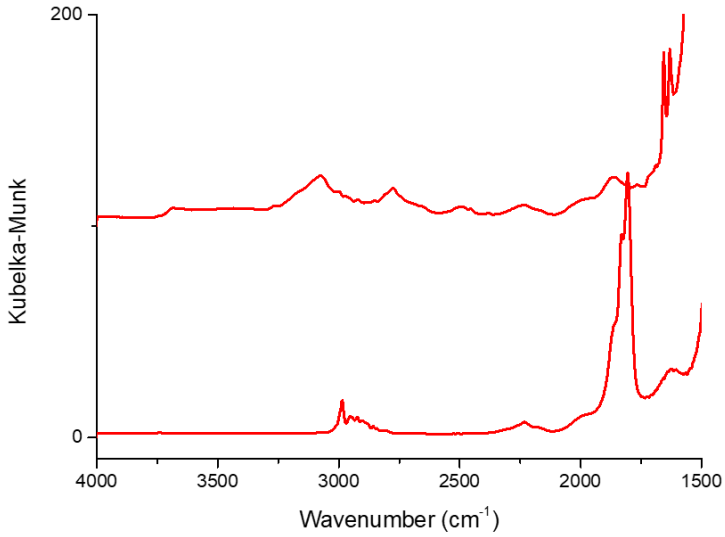

Figure 4 – DRIFT spectra of P2 (below) and AS2 (above).

In Figure 4 are reported the DRIFT spectra of P2 and AS2. After the reaction with pentafluorophenol, the peaks around 1831 cm^{-1} assigned to the Al-H stretching disappear, confirming that all the aluminium hydrides were consumed, at 3070 cm^{-1} then appears an intense peak characteristic of the N-H stretching attributed to the ammonium ion. The presence of the latter peak confirms the formation of the desired ionic couple on the surface. To better prove the structure of the species on the surface, an elemental analysis quantification was performed on AS2. The results are reported in Table 2.

Table 2 – Elemental analysis and hydrogen quantification for AS2.

wt% Al	wt% C	wt% N	wt% H	C/N	C/Al	N/Al	Al mmol g^{-1}	H_2/Al Grafting
1.25	9.32	0.74	0.55	14.7 (th. 19)	16.8 (th. 19)	1.1 (th. 1)	0.46	1.4 (th. 1.5)

The amount of hydrogen released per Al is in agreement with what observed at the DRIFT, that all the hydrides have reacted. Moreover, the amount of C per Al present on the surface, 16.8 C/Al, is in agreement with the formation of the ionic couples (C/Al th. 19).

AS2 was then characterized by ^{1}H MAS, ^{13}C CPMAS and ^{19}F MAS solid state NMR. The spectra are reported in Figure 5.

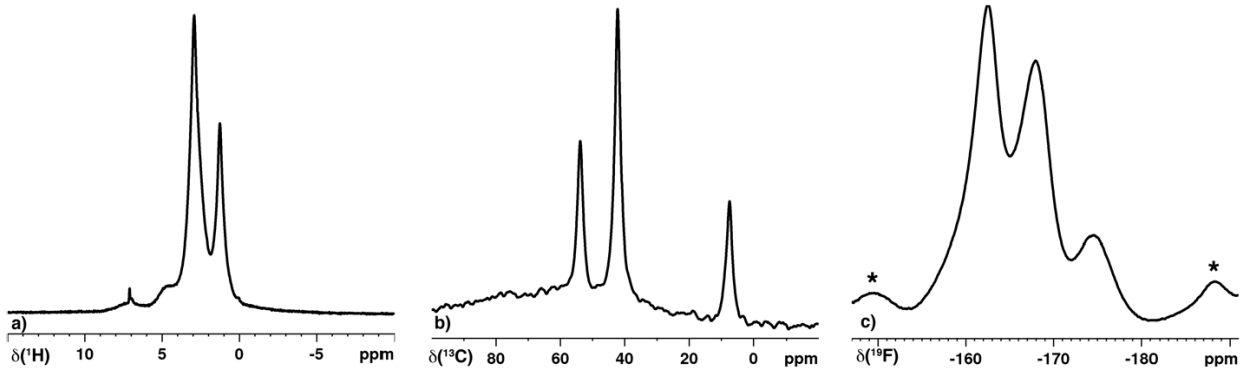

Figure 5 – a) ^{1}H MAS, b) ^{13}C CPMAS and c) ^{19}F MAS NMR spectra of AS2.

The functionalization of P2 with pentafluorophenol to generate AS2 didn't cause many changes to the ^{1}H MAS and ^{13}C CPMAS NMR spectra in relation to P2. The ^{1}H spectrum shows two intense

peaks at 1.3 and 2.9 ppm assigned, the first, to the methyl of the $NCH_2\underline{CH_3}$ fragment and the second to the methyls directly bound to the N and the methylene of the $N\underline{CH_2}CH_3$ fragment. It is still present the peak at 4.2 ppm relative to the SiH proton bound to the surface of the support. The ^{13}C NMR spectrum shows at 7.1 ppm the signal relative to the methyl of the NCH_2CH_3 fragment, at 42.5 ppm resonate the methyls directly bound to the N and at 53.7 ppm the methylene of the NCH_2CH_3 fragment. The ^{19}F spectrum shows the signals of the pentafluorophenoxy ligands of AS2 at -162, -168 and -174 ppm respectively assigned to the fluorines in ortho, meta and para of the aryl group.[1,7]

The characterizations performed on the solid confirmed that upon functionalization of P2 with pentafluorophenol activating support AS2 was obtained, the surface of which was composed in 50:50 ratio of monopodal $[(\equiv SiO)Al(OC_6F_5)_3]^-[HNMe_2Et]^+$ and bipodal $[(\equiv SiO)_2Al(OC_6F_5)_2]^-[HNMe_2Et]^+$. The activating support was then tested in polymerization.

1.4 Test in ethylene polymerization in combination with *rac*-EtInd$_2$ZrCl$_2$

AS2 was tested in ethylene/1-hexene slurry copolymerization as co-catalyst for *rac*-EtInd$_2$ZrCl$_2$, Cat1. The system AS2/Cat1 was tested in exactly the same conditions than that used for AS1/Cat1 in run1 (see chapter II).

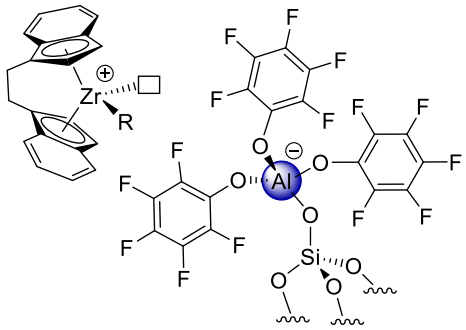

Scheme 9 – Structure of the catalyst AS2/Cat1.

The polymerizations were conducted in 300 mL of heptane, at 80°C and 4 bars of ethylene pressure for 30 minutes. The total [Zr] was 2 µM and TiBA was used as scavenger in concentration 1 mM. The zirconocene precursor was activated right before the start of the polymerization by contacting it with the activating support in presence of TiBA, as alkylating agent.

The polymerization results for AS2/Cat1 are reported in comparison with those of AS1/Cat1 in Table 3.

Table 3 – Polymerization results obtained with the systems AS1/Cat1 and AS2/Cat1. General conditions: 80°C; 4 bars C_2H_4; 30 minutes; 300 mL heptane; [TiBA] 1mM.

run	Catalyst	m mg	Zr µmol	$Zr/Al_{surface}$	Zr loading Wt%	C6 mol%	Yield g	Activity $g\ g_{cat}^{-1}\ h^{-1}$
1	AS1/*Cat1*	20.6	0.68	0.06	0.31	19.2	10.7	1111
2	AS2/*Cat1*	20.0	1.01	0.11	0.45	17.5	3.7	370

The productivity of AS2/Cat1 is three times lower than that exhibited by AS1/Cat1. The difference is even more evident when looking at the kinetic profiles reported in Figure 6.

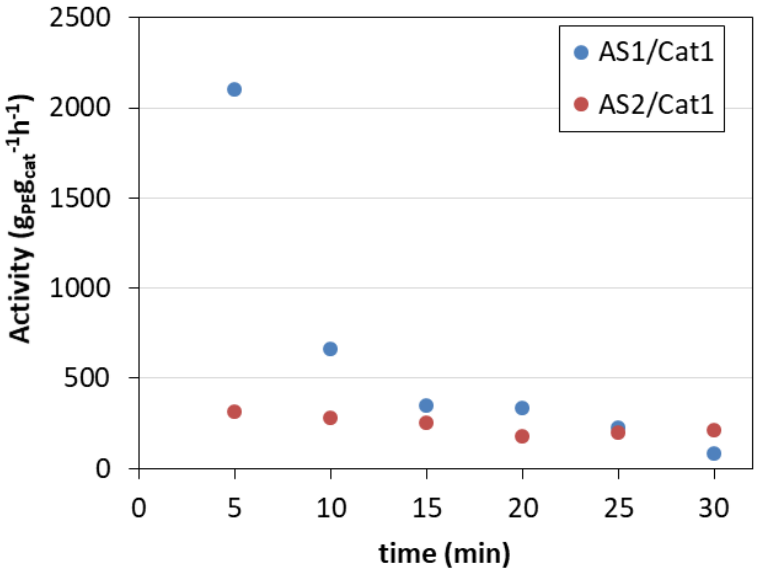

Figure 6 – Kinetic profiles for AS1/Cat1 and AS2/Cat1 in ethylene/1-hexene slurry copolymerization.

The plot reported in Figure 6 shows the different behaviour, activity-wise, of the two catalytic systems at the beginning of the polymerization. AS1/Cat1 has a way higher activity than AS2/Cat1, to then deactivate to reach the same value in the last 15 minutes of polymerization.

The activity displayed by AS2/Cat1 is also lower than that reported for the bipodal activator $[(\equiv SiO)Al(OC_6F_5)_3]^-[HNEt_2Ph]^+$ on $SiO_{2\text{-}700}$ in combination with Cat1, reported by Sauter et al. in 2016.[7] This suggests not only that a bipodal activator on $SiO_{2\text{-}700}$ is less efficient than the

homologous on $SiO_{2\text{-}200}$, for surface effects,[2] but also that the compresence of mono and bipodal surface species is negative for the activity. Most probably because the monopodal species is a less efficient counter-anion than the bipodal aluminate.

The produced polymer was characterized by HT-SEC, DSC and ^{13}C NMR, the results are reported in Table 4.

Table 4 – DSC and HT-SEC characterization results for the polymers obtained in runs 1 and 2.

run	Catalyst	Activity $g\ g_{cat}^{-1}\ h^{-1}$	$X_{1\text{-hexene}}$ (mol%)	T_{m2} °C	Crystallinity %	M_n Da	M_w Da	Đ
1	AS1/*Cat1*	1111	1.8	117	41	22000	60700	2.7
2	AS2/*Cat1*	370	1.4	116	39	-	-	-

The polymers obtained with the two different catalytic systems behaved very similarly, they present in fact similar melting temperatures and crystalline fraction.

The results obtained with AS2 were not as satisfying as expected, the activity obtained was lower than with AS1 and, even though it is difficult to see from Figure 6, AS2/Cat1 was subject to deactivation during the polymerization time. This phenomenon is due to the transfer of ligand from Al to Zr giving inactive neutral species more favourable in the case of AS2 than AS1. In order to avoid the ligand transfer from the surface to the active species, new activating supports were synthesized by using more sterically hindered or chelating ligands.

2. Synthesis of activating supports with ligands alternative to pentafluorophenol

2.1 Choice of the grafted Al precursor

For the synthesis of the activating supports described in this paragraph, the same supported aluminium material was used, $(\equiv SiO)_2AlH(NMe_2Et)$, P1.

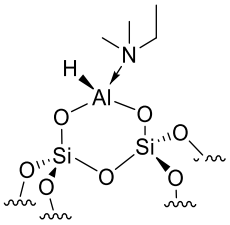

Scheme 10 – Structure of P1.

The choice was made primarily because P1 was easy to synthesize and the species on the surface are well-defined, and then because, using the same grafted Al precursor employed in the synthesis of AS1 for other activating supports with different ligands, would facilitate a comparison of their efficiency in polymerization.

The synthesis and characterization of P1 were already discussed in Chapter II and will not be described here.

The nature of the chosen ligands differed a lot. In Scheme 11 are reported the selected ligands.

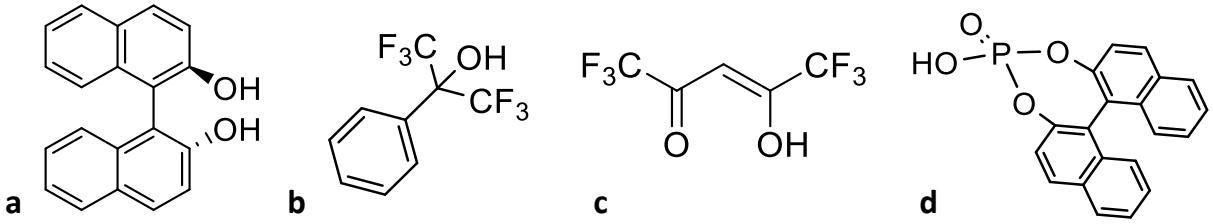

Scheme 11 – Alternative ligands employed for the synthesis of activating supports. a) binaphtol; b) sterically hindered benzyl alcool; c) acetyl acetonate; d) binaphthyl diyl hydrogenphosphate.

The choice was done based on the ligand ability of complexating the Al to give a stable aluminate.[8–10]

2.2 Synthesis of $[(\equiv SiO)_2Al(O_2C_{20}H_{12})]^-[HNMe_2Et]^+$, AS3

- Synthesis and characterization

The activating support AS3 was synthesized by functionalization of P1 with 1.2 eq. of rac-binaphtol per eq. of Al on the surface. The reaction was conducted in toluene for two hours, the product was then washed and dried under high vacuum.

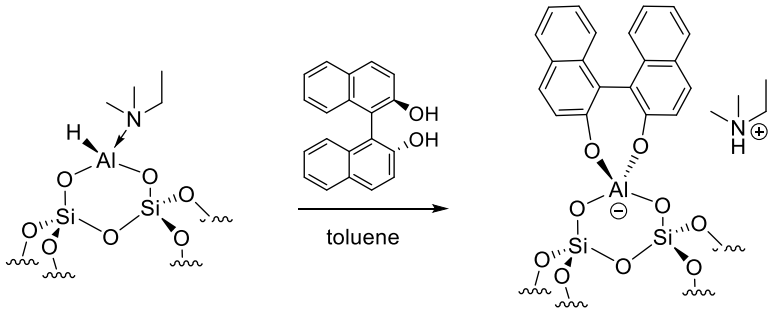

Scheme 12 – Synthesis of $[(\equiv SiO)_2Al(O_2C_{20}H_{12})]^-[HNMe_2Et]^+$, AS3.

The idea behind the choice of the rac-binaphtol as ligand, is that its chelating and bulky nature around Al centre would avoid its transfer from the surface to the zirconocene.

After functionalization of P1 by rac-binaphtol the resulting material, AS3, was characterized in order to establish the expected structure $[(\equiv SiO)_2Al(O_2C_{20}H_{12})]^-[HNMe_2Et]^+$. In Figure 7 is reported the DRIFT spectrum.

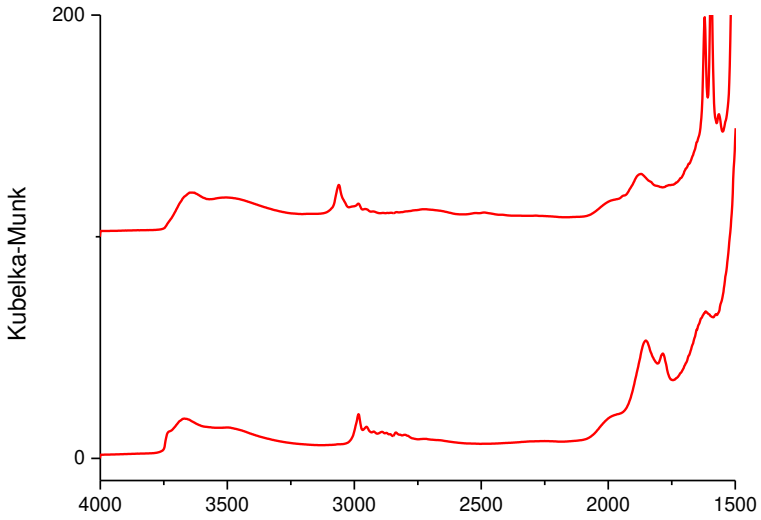

Figure 7 – DRIFT spectrum of P1 (bottom) and AS3 (top).

The DRIFT characterization of AS3 shows that upon reaction with the binaphtol, all the Al-H on the surface reacted: the peaks at 1850 and 1800 cm^{-1} in the spectrum of P1 were completely consumed in AS3. The peak at 3070 cm^{-1} characteristic of the N-H stretching of the ammonium, indicates the formation of the ionic couple. Between 1500 and 1600 cm^{-1} appear then two sharp signals assigned to the C=C stretching of the aromatic rings.

Table 5 – Elemental analysis results for AS3.

wt% Al	wt% C	wt% N	wt% H	C/N	C/Al	N/Al	Al mmol g^{-1}
0.88	11.0	0.67	1.11	19.1 (th.24)	28.6 (th. 24)	1.5 (th. 1)	0.33

The amount of 0.88 wt% of aluminium found on the surface of AS3 counts for 0.33 mmol g^{-1} of Al. Moreover, the ratios 28.6 C/Al and 1.5 N/Al recovered from the analysis are in agreement with the presence of one rac-binaphtol bound per Al with an ammonium counter ion.

From both the DRIFT and Elemental analysis' results, it is possible to affirm confidently that upon reaction of P1 with the binaphtol an ionic couple was obtained on the surface.

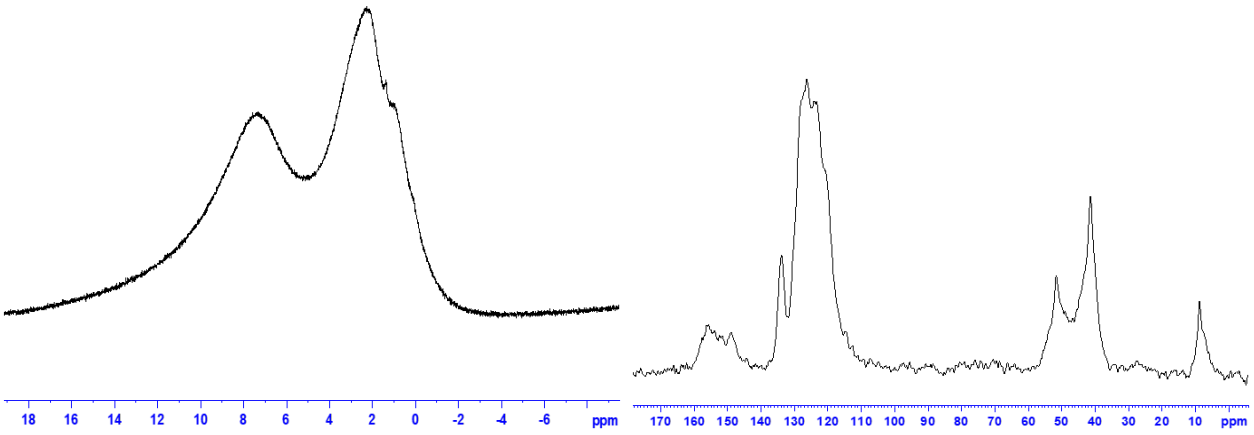

Figure 8 – ^{1}H MAS (right) and ^{13}C CPMAS (left) solid state NMR spectra for AS3.

In Figure 8 are reported the ^{1}H MAS and ^{13}C CPMAS solid state NMR spectra for AS3. The ^{1}H spectrum appears very broad and not resolved signals, only two main peaks at 7.38 and 2.38 ppm and a shoulder at 0.98 ppm are observed; the peak at 7.38 ppm is assigned to aromatic protons

of the binaphtol, at 2.38 ppm resonate the methylene of the $N\underline{CH_2}CH_3$ and the methyls directly bound to the N of the ammonium ion, the shoulder at 0.98 ppm can be attributed to the methyl of the $NCH_2\underline{CH_3}$ fragment. The ^{13}C spectrum shows six broad peaks, at 9.1, 41.6, 51.7, 126.4, 134.0 and 153.2 ppm. The peaks in the aliphatic region are assigned to the alkyl fragments on the ammonium ion, while the peaks in the aromatic region are attributed to the rac-binaphtol ligand. At 9.1 ppm resonates the methyl of the $NCH_2\underline{CH_3}$, the methyls directly bound to the N resonate at 41.6 ppm, while the peak at 51.7 ppm is assigned to the methylene directly bound to the N of the NCH_2CH_3 fragment. The peak at 153.2 ppm is the signal relative to the carbons bonded to the O of the binaphtol ligand, the two other peaks at 134.0 and 153.2 ppm are assigned to the remaining aromatic carbons of the binaphtol.

The characterizations performed on AS3, proved that upon reaction of P1 with the binaphtol it was possible to obtain an ionic couple featuring an aluminate with one bound binaphtol ligand and an ammonium as counter-ion. The activating support was tested in ethylene/1-hexene slurry copolymerization in combination with *rac*-$EtInd_2ZrCl_2$.

- Test in ethylene polymerization in combination with *rac*-$EtInd_2ZrCl_2$

AS3 was tested in ethylene/1-hexene slurry copolymerization as co-catalyst for *rac*-$EtInd_2ZrCl_2$, Cat1. The system AS3/Cat1 was tested in exactly the same conditions than that used for AS1/Cat1 and AS2/Cat1.

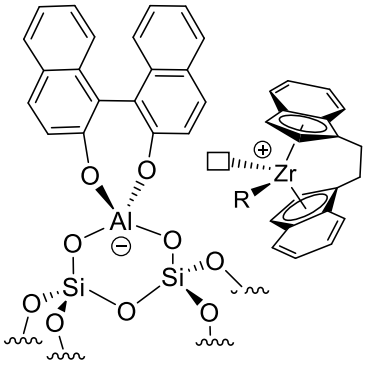

Scheme 13 – Structure of the catalyst AS3/Cat1.

The polymerizations were conducted in 300 mL of heptane, at 80°C and 4 bars of ethylene pressure for 30 minutes. The total [Zr] was 2 µM and TiBA was used as scavenger in concentration

of 1 mM. The zirconocene precursor was activated right before the start of the polymerization by contacting it with the activating support in presence of TiBA, as alkylating agent.

The polymerization results for AS3/Cat1 at different pre-contact times are reported in Table 6.

Table 6 – Polymerization results obtained with the system AS3/Cat1. General conditions: 80°C; 4 bars C_2H_4; 30 minutes; 300 mL heptane; [TiBA] 1mM.

run	Catalyst	pre-contact min	m mg	Zr µmol	$Zr/Al_{surface}$	Zr loading Wt%	C6 mol%	Yield g	Activity g g_{cat}^{-1} h^{-1}
3	AS3/*Cat1*	-	20.2	0.61	0.09	1.3	21.5	0.48	47
4	AS3/*Cat1*	45	20.5	0.67	0.10	1.4	18.8	0.42	41

The activity shown in slurry polymerization by the catalyst AS3/Cat1 was very low, with respect to all the systems previously tested, in fact for both the tests performed the obtained activity was lower than 50 g_{PE} g_{cat}^{-1} h^{-1}.

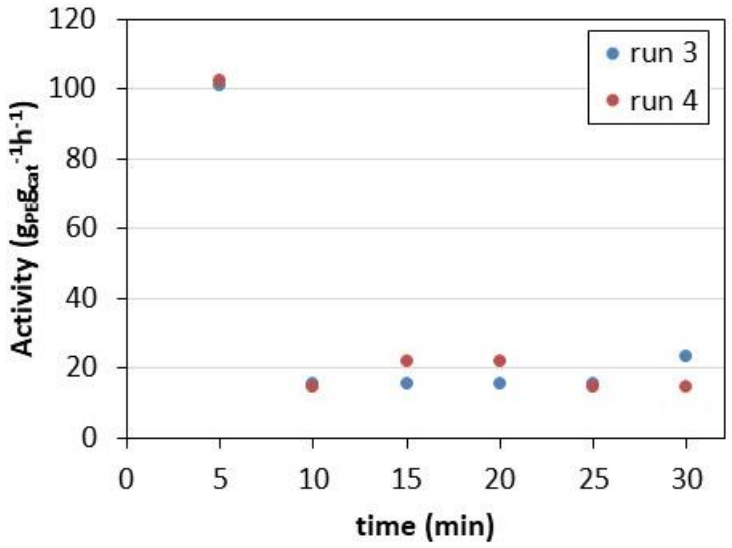

Figure 9 – Kinetic profiles for the slurry ethylene polymerization tests performed with AS3/Cat1.

Although the recorded activity is trifling confronted to the one obtained with AS1, it is interesting to notice, examining the kinetic profiles of run 3 and 4 in Figure 9, how, starting from 10 minutes of polymerization, the activity keeps stable throughout the reaction; the initial higher activity could in part be ascribed to ethylene solubilisation phenomena due to the pressurization of the reactor

at the beginning of the polymerization. A stable activity was the aim we were trying to achieve by modifying the ligand of the activating support. The loss in activity experienced with AS3 could be ascribed to a strong interaction between the new aluminate bearing binaphtol on the surface and the zirconocene so a bad dissociation of the ion pair.

Moreover, it is worth to notice that the activity and kinetic profiles for the system AS3/Cat1 remained more or less unchanged by modifying the pre-contact time between the activator and the catalyst precursor previous to the polymerization test, proving a certain stability of the, poorly, active species on the surface.

The obtained polymers in run 3 and 4 were characterized by DSC and HT-SEC. The results are reported in Table 7.

Table 7 – DSC and HT-SEC characterization results for the polymers obtained in runs 3 and 4.

run	Catalyst	Activity g g_{cat}^{-1} h^{-1}	T_{m2} °C	Crystallinity %	M_n g mol^{-1}	M_w g mol^{-1}	Đ
3	AS3/*Cat1*	47	121	51.8	27700	86800	3.1
4	AS3/*Cat1*	41	124	48.3	30600	80000	2.6

The polymers obtained are LLDPE resins, compatible with the characteristics of the products synthesized by *rac*-$EtInd_2ZrCl_2$. They have a relatively broad molecular weight distribution and Mw around 80 KDa, similar to what observed with AS1/Cat1 in the same conditions.

2.3 Synthesis of $[(\equiv SiO)_2Al(OC(CF_3)_2Ph)_2]^-[HNMe_2Et]^+$, AS4

- Synthesis and characterization

While in the case of AS3 was investigated the chelating nature of the ligand bound to the Al, in AS4 the pentafluorophenol was substituted with a fluorinated alcohol more sterically hindered around the O atom allowing to the separation of charge between the anionic activator and the cationic metallocene. P1 was reacted in toluene for two hours with 2.2 eq of $Ph(CF_3)_2COH$ (ligand

b in Scheme 11) per Al. At the end of the reaction the product was washed with toluene and pentane and dried under high vacuum (1 mPa). Scheme 14 depicts the synthesis reaction of AS4.

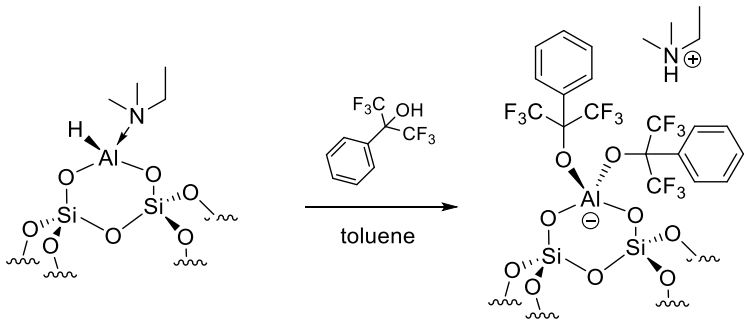

Scheme 14 – Synthesis reaction of AS4.

To prove that the ionic couple was obtained, the surface of AS4 was characterized by different techniques. In Figure 10 is reported the DRIFT spectra of AS4 in comparison with P1.

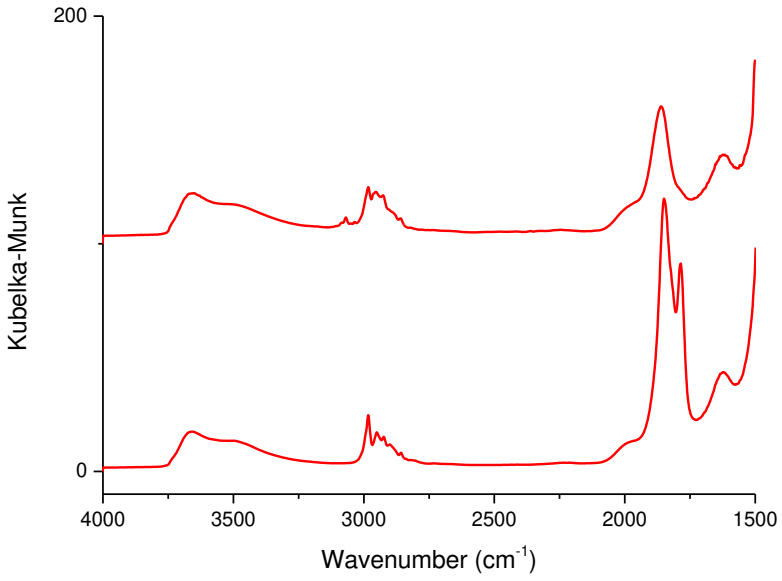

Figure 10 – DRIFT spectra for P1 (bottom) and AS4 (top).

The DRIFT spectra before and after the reaction with ligand **b** show a decrease in the intensity of the bands at 1850 and 1800 cm^{-1} and the appearance of a small peak at 3070 cm^{-1}. These two events would suggest that although some of the hydride on the surface reacted to give the desired ionic couple, and thus the presence of the peak at 3070 cm^{-1} of the N-H stretching, not all of the

species on the surface of P1 reacted with the alcohol, as indicated by the still quite intense peak at 1850 cm^{-1}, assigned to the Al-H stretching.[5] The hypothesis that the reaction didn't go to completion was further supported by the elemental analysis characterization of AS4.

Table 8 – Elemental analysis results for AS4.

wt% Al	wt% C	wt% N	wt% F	wt% H	C/N	C/Al	N/Al	F/Al	Al mmol g^{-1}
2.3	6.4	1.0	4.0	0.9	7.5 (th.23)	6.3 (th. 23)	0.8 (th. 1)	2.5 (th. 12)	0.85

Looking at the amount of C and F found by the elemental analysis on AS4, it was evident that most of the Al hadn't reacted with $Ph(CF_3)_2COH$. This low reactivity could be due to a steric impediment, which prevents two $Ph(CF_3)_2COH$ to react with $(\equiv SiO)_2AlH(NMe_2Et)$ to obtain the ionic couple.

To try to further understand the species formed on the surface of AS4, the support was characterized by ^1H MAS and ^{13}C CP MAS solid state NMR. The spectra acquired are reported in Figure 11.

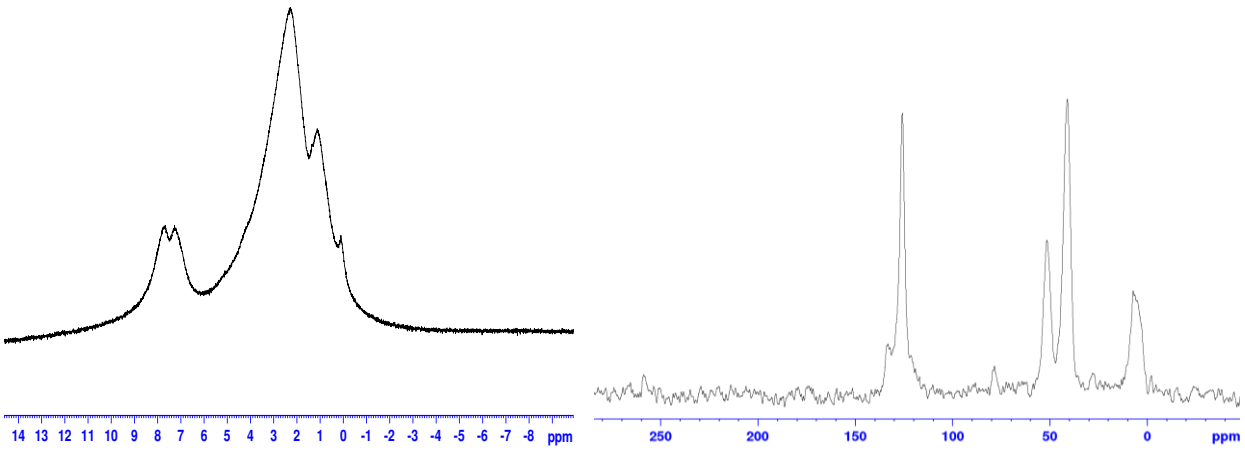

Figure 11 – ^1H MAS (right) and ^{13}C CPMAS (left) solid state NMR spectra for AS4.

The NMR spectra acquired for AS4 show that a fraction of the aluminium hydride on the surface of P1 reacted with $Ph(CF_3)_2COH$. The ^1H NMR spectrum displays a set of 4 peaks. At 7.73 and 7.58 ppm resonate the protons of the phenyl ring; at 2.23 and 1.06 ppm resonate the alkyl fragments of the amine coordinated to the Al grafted on the surface. At 2.23 ppm resonate the methylene

of the NCH_2CH_3 moiety and the methyls directly bound to the N, while at 1.06 ppm resonates the methyl of the NCH_2CH_3 fragment. The ^{13}C NMR spectrum displays six signals. At 133.1 and 125.7 ppm resonate the aromatic carbons of the phenyl ring; the small peak at 78.3 ppm was assigned to the quaternary carbon of the alkoxide ligand. The peaks at 51.5, 41.1 and 5.4 ppm are assigned to the amine coordinated to the Al. The methylene of the NCH_2CH_3 resonates at 51.5 ppm and the signal at 41.1 ppm is attributed to the methyls directly bound to the N, and the one at 5.4 ppm is assigned to the methyl of the NCH_2CH_3 fragment.

The characterization of AS4 showed clearly that, by functionalization of P1 with $Ph(CF_3)_2COH$, it was not possible to convert the totality of $(\equiv SiO)_2AlH(NMe_2Et)$ to $[(\equiv SiO)_2Al(OC(CF_3)_2Ph)_2]^-[HNMe_2Et]^+$. This clearly places $Ph(CF_3)_2COH$ as an unsuitable ligand for the synthesis of activating supports for metallocenes.

- Test in ethylene polymerization in combination with *rac*-$EtInd_2ZrCl_2$

Although it was seen that the synthesis of AS4 hadn't proceeded to completion, the activating support was tested in ethylene/1-hexene slurry copolymerization as co-catalyst for *rac*-$EtInd_2ZrCl_2$, Cat 1, to see if the small fraction of aluminates generated on the surface worked as active cocatalyst. The system AS4/Cat1 was tested in the same conditions than that used for the catalytic systems investigated previously.

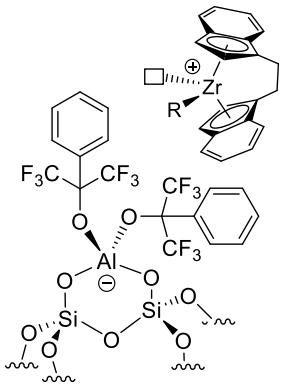

Scheme 15– Structure of the catalyst AS4/Cat1.

The polymerizations were conducted in 300 mL of heptane, at 80°C and 4 bars of ethylene pressure for 30 minutes. The total [Zr] was 2 µM and TiBA was used as scavenger in concentration

1 mM. The zirconocene precursor was activated right before the start of the polymerization by contacting it with the activating support in presence of TiBA, as alkylating agent.

The polymerization result obtained for the system AS4/Cat1 are reported in Table 9.

Table 9 – Polymerization result obtained with the systems AS4/Cat1. General conditions: 80°C; 4 bars C_2H_4; 30 minutes; 300 mL heptane; [TiBA] 1mM.

run	Catalyst	m mg	Zr µmol	$Zr/Al_{surface}$	Zr loading Wt%	C6 mol%	Yield g	Activity g g_{cat}^{-1} h^{-1}
5	AS4/*Cat1*	21.1	0.74	0.11	0.32	18.2	0.36	34.5

As expected the activity obtained was even lower than that recorded with AS3. The low activity is clearly due to the negligible amount and lack of active species on the surface, sufficient to show a certain activity to the catalyst.

Table 10 – DSC and HT-SEC characterization results for the polymer obtained in run 5.

run	Catalyst	Activity g $g_{cat}^{-1}h^{-1}$	T_{m2} °C	Crystallinity %	M_n g mol^{-1}	M_w g mol^{-1}	Đ
5	AS4/*Cat1*	34.5	125	38.2	32500	83100	2.6

The polymer obtained is a LLDPE resin, compatible with the characteristics of the products synthesized by *rac*-$EtInd_2ZrCl_2$. It has a slightly broad molecular weight distribution and Mw around 80 KDa, similar to what observed with AS1/Cat1 in the same conditions.

2.4 Synthesis of $[(\equiv SiO)_2Al(O_2C_5HF_6)_2]^-[HNMe_2Et]^+$, AS5

- Ligand characterization

For the synthesis of AS5 it was chosen to functionalize P1 with hexafluoroactylacetone, ligand **c** in Scheme 11. The choice fell on this ligand given its chelating and electro-deficient nature and the fact that it easily formed hexa-coordinated Al complexes.[9,10]

Prior to the synthesis a ^{1}H NMR spectrum in benzene-d_6 of the diketone was acquired to assess its purity. The spectrum is reported in Figure 12.

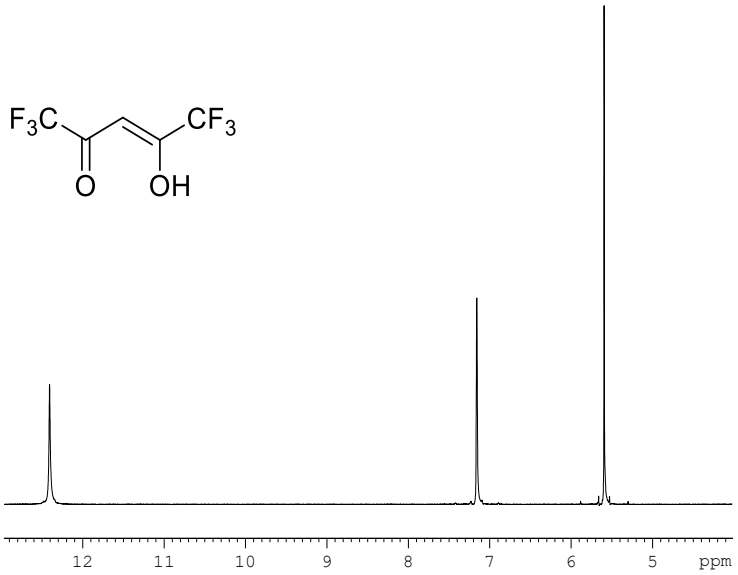

Figure 12 – ^{1}H NMR spectrum of the hexafluoroacetylacetone in benzene-d_6.

Figure 12 depicts a clean spectrum in which it is possible to see two singlets at 5.6 and 12.4 ppm, assigned respectively to the proton of the alkenyl moiety and to the proton of the hydroxyl group.

- Synthesis and characterization of the activating support

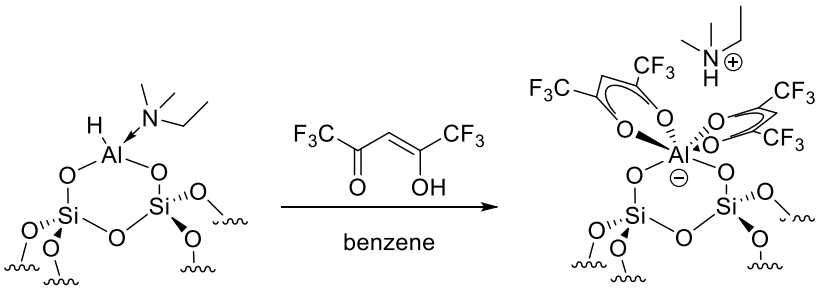

Scheme 16 – Synthesis of AS5.

2.2 eq. of hexafluoroacetylacetone were reacted in toluene with P1 for two hours. At the end of the reaction the product was washed three times with toluene and once with pentane. The powder was then dried under high vacuum. AS5 was characterized by DRIFT spectroscopy after the synthesis.

Upon functionalization of P1 the peaks relative to the Al-H stretching at 1850 and 1800 cm^{-1} were consumed completely, indicating that all the aluminium hydride on the surface had all reacted with the ligand. At 3070 cm^{-1} appears the peak relative to the N-H stretching of the ammonium, proving the presence on the surface of the desired ionic couple. After the reaction appears also a broad band around 3400 cm^{-1} due to the interaction between the surface and the ligand.

The DRIFT characterization of AS5 proved already the formation on the silica surface of the desired

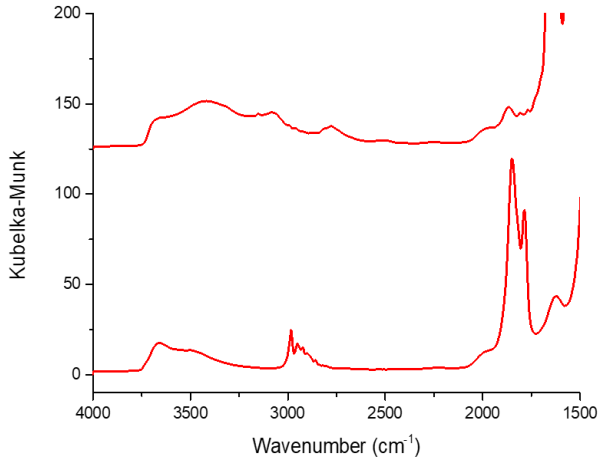

Figure 13 – DRIFT spectra of P1 (bottom) and AS5 (top).

ionic couple, $[(\equiv SiO)_2Al(O_2C_5HF_6)_2]^-[HNMe_2Et]^+$. To further confirm that the reaction went to completeness a mass balance analysis was performed on AS5.

Table 11 – Elemental analysis results for AS5.

wt% Al	wt% C	wt% N	wt% F	wt% H	C/N	C/Al	N/Al	F/Al	Al mmol·g^{-1}
0.9	6.1	0.6	8.1	0.7	11.5 (th.14)	15.3 (th. 14)	1.3 (th. 1)	12.7 (th. 12)	0.33

The mass balance characterization results highlighted the presence of 0.33 $mmolg^{-1}$ of Al on the surface of AS5. It also confirmed the formation of the ionic couple $[(\equiv SiO)_2Al(O_2C_5HF_6)_2]^-[HNMe_2Et]^+$, in fact the amount of carbon per Al and F/Al, respectively 15.3 (th. 14) and 12.7 (th. 12), show that to each grafted Al on the surface are coordinated two acetylacetonate ligands. The amount of nitrogen found, 0.6 wt%, is also in agreement with the presence of one ammonium counter ion per Al. This shows how, contrarily to $Ph(CF_3)_2COH$, the use of hexafluoroacetylacetonate as ligand allowed the synthesis of the desired aluminate on the support, and the development of well-defined species.

The surface species were furtherly characterized by ^1H MAS and ^{13}C CPMAS solid state NMR. The spectra acquired for AS5 are reported in Figure 14.

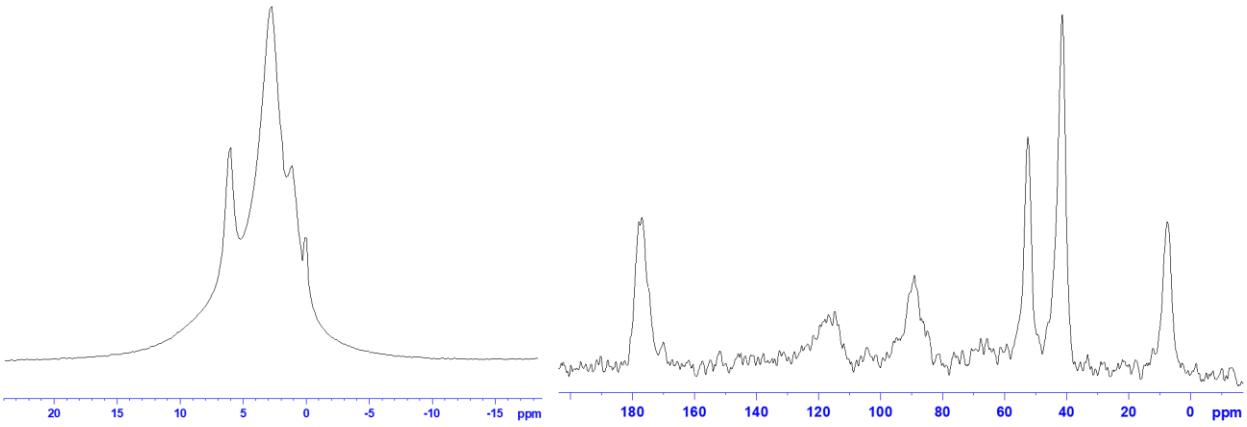

Figure 14 – ^1H MAS (left) and ^{13}C (right) CPMAS solid state NMR spectra acquired for AS5.

The NMR characterization of AS5 clearly shows the coordination of the acetylacetonate ligands to the Al. The ^1H spectrum displays three main peaks at 1.16, 2.80 and 6.05 ppm; the signal at 6.05 ppm is assigned to the olefinic proton of the acetylacetonate ligand, while the other two signals are attributed to the ammonium ion, at 1.16 ppm resonates the methyl of the ethyl moiety, while at 2.80 ppm resonate both the methyls directly bound to the N and the methylene of the NCH_2CH_3 fragment.

The ^{13}C spectrum presents six signals; at 7.5 ppm is the peak relative to the methyl of the NCH_2CH_3 moiety, at 41.4 ppm resonate the methyls directly bound to the nitrogen of the ammonium ion and at 52.5 ppm is the signal of the methylene of the NCH_2CH_3 fragment. The three remaining

signals are assigned to the acetylaceonate; the carbon of the trifluoromethyl groups resonate at 114.8 ppm, while at 89.1 ppm is the peak of the allylic CH carbon. The intense signal at 177.1 ppm is finally attributed to the carbons of the CO groups.

All the characterizations reported for AS5 prove the formation of the ionic couple $[(\equiv SiO)_2Al(O_2C_5HF_6)_2]^-[HNMe_2Et]^+$, by functionalization of P1 with two equivalents of hexafluoroacetylacetoe per Al.

The activating support was then tested in ethylene polymerization.

- Test in ethylene polymerization in combination with *rac*-EtInd$_2$ZrCl$_2$

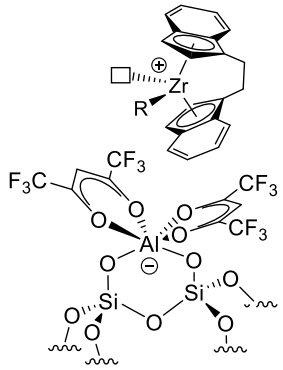

Scheme 17 – Structure of the catalyst AS5/Cat1.

AS5 was tested in ethylene/1-hexene slurry copolymerization as co-catalyst for *rac*-EtInd$_2$ZrCl$_2$, in the same conditions used for the catalytic systems investigated previously.

The polymerizations were conducted in 300 mL of heptane, at 80°C and 4 bars of ethylene pressure for 30 minutes. The total [Zr] was 2 µM and TiBA was used as scavenger in concentration 1 mM. The zirconocene precursor was activated right before the start of the polymerization by contacting it with the activating support in presence of TiBA, as alkylating agent.

The polymerization result obtained for the system AS5/Cat1 are reported in Table 12.

Table 12 – Polymerization result obtained with the system AS5/Cat1. General conditions: 80°C; 4 bars C_2H_4; 30 minutes; 300 mL heptane; [TiBA] 1mM.

run	Catalyst	m mg	Zr µmol	$Zr/Al_{surface}$	Zr loading Wt%	C6 mol%	Yield g	Activity $gg^{-1}_{cat}h^{-1}$
6	AS5/*Cat1*	20.1	0.65	0.10	0.29	19.8	0.10	10

Even though the surface of AS5 is composed of well-defined species, also in this case like for AS4 and AS3, the activating support wasn't efficient as cocatalyst of Cat1. As in the case of AS3 the possible explanation for the absence of activity could be a bad ionic couple interaction between AS5 and Cat1 and possibly the transfer of ligand giving a highly stable Zirconium acetylacetonate complex.

The little polymer obtained by run 6 was characterized by DSC. The results are reported in Table 13.

Table 13 – DSC characterization results for the polymer obtained in run 6.

run	Catalyst	Activity $gg^{-1}_{cat}h^{-1}$	Tf2 °C	Crystallinity %
6	AS5/*Cat1*	10	123	38.5

The polymer obtained is an LLDPE resin, compatible with the characteristics of the products synthesized by *rac*-$EtInd_2ZrCl_2$.

2.5 Synthesis of $[(\equiv SiO)_2Al(O_2P\text{-binaphtol})_2]^-[HNMe_2Et]^+$, AS6

- **Synthesis and characterization of the activating support**

The last activating support synthesized by functionalization of $(\equiv SiO)_2AlH(NMe_2Et)_3$ with ligands different than pentafluorophenol, was prepared by using a phosphoric acid-binaphtyl ester as ligand (the structure of the ligand is reported in Scheme 11).

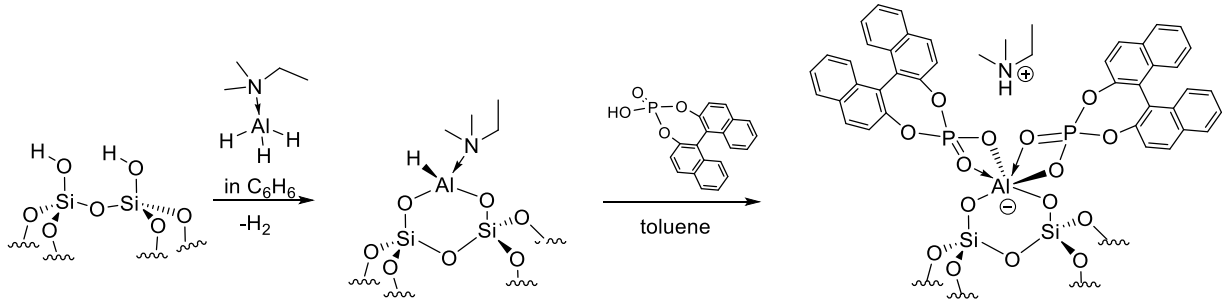

Scheme 18 – Synthesis of AS6.

P1 was reacted with 2.2 eq. of phosphoric acid-binaphtyl ester per Al in toluene overnight; the product was then washed three times with toluene and once with pentane, after removing the volatiles AS6 was dried under high vacuum.

The surface of the activating support was characterized by DRIFT spectroscopy. In Figure 15 are reported the spectra before and after the functionalization reaction of P1.

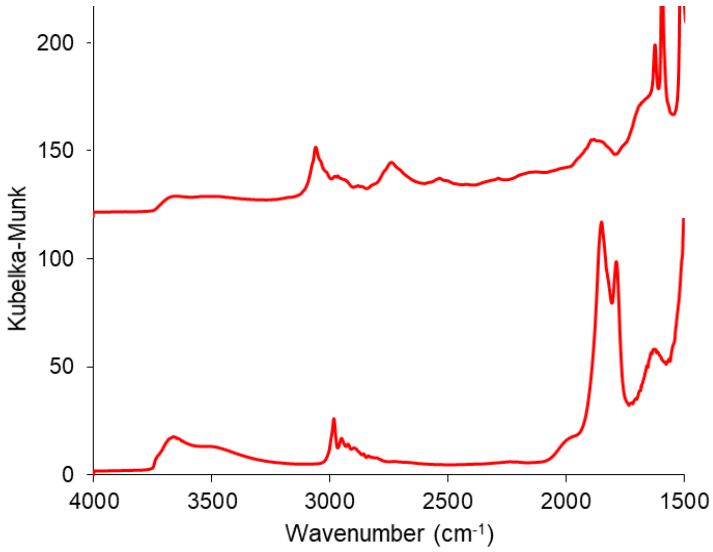

Figure 15 – DRIFT spectra for P1 (bottom) and AS6 (top).

The DRIFT spectrum of AS6 shows the complete disappearance of the peaks at 1850 and 1800 cm^{-1} of the Al-H stretching, indicating that, upon functionalization with the phosphoric acid-binaphtyl ester, all the grafted Al hydride on the surface reacted. The peak at 3060 cm^{-1} is characteristic of the N-H stretching proving the presence of the ammonium ion on the surface, and confirming the formation of the ionic couple; the sharp signals between 1500 and 1600 cm^{-1} are attributed to the C=C stretching frequencies of the aromatics.

The DRIFT spectrum of AS6 suggests that all the Al on the surface reacted with the hydrogen phosphate to obtain $[(\equiv SiO)_2Al((\kappa^2\text{-}O_2P(binaphtyl\text{-}ester)_2]^-[HNMe_2Et]^+$. To confirm the coordination of two phosphate ligands per metal centre, a mass balance analysis of the surface of AS6 was performed; the results are reported in Table 14.

Table 14 – Elemental analysis results for AS6.

wt% Al	wt% C	wt% P	wt% H	C/Al	H/Al	P/Al	Al mmol g^{-1}
1.43	29.41	1.81	2.09	46.3 (th. 44)	39.1 (th. 35)	1.1 (th. 2)	0.53

The mass balance quantification performed on AS6 confirmed the coordination of two phosphates per Al. The amount of carbon found, 29.4 wt%, in fact, gives a ratio C/Al of 46.3, very close to the theoretical value of 44 of the target species. The same can be observed for the estimated amount of H on the surface. The quantity of P recovered is lower than expected for two ligands bound to aluminium, 1.1 P/Al instead of 2. This lower estimation could be attributed to a higher difficulty of the analytical method in the quantification of heteroatoms.

The activating support thus obtained was also characterized by ^{1}H MAS and ^{13}C CPMAS solid state NMR. The spectra are reported in Figure 16.

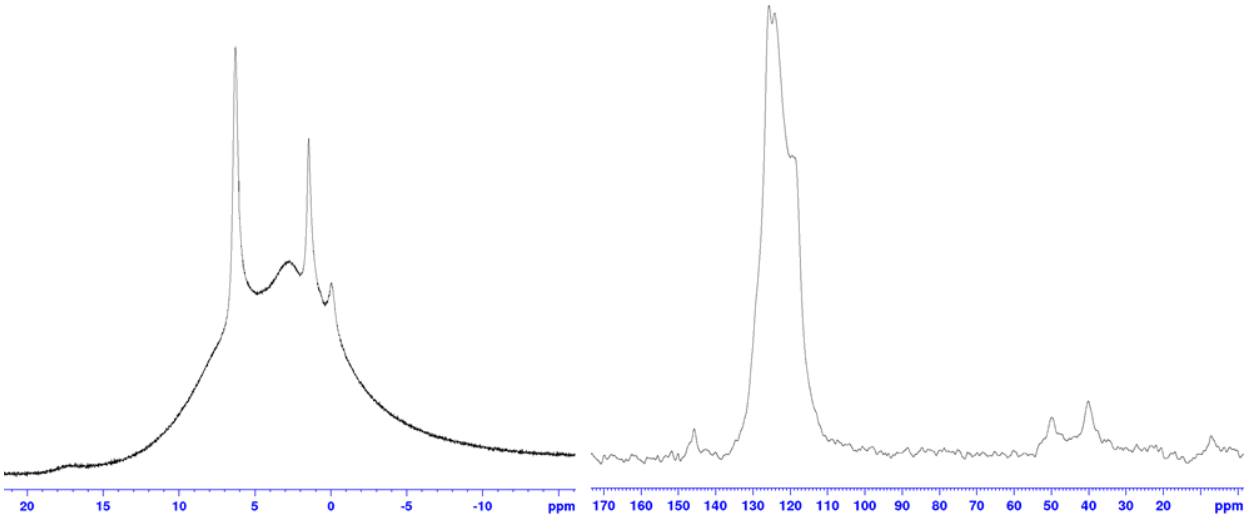

Figure 16 – ^{1}H MAS (left) and ^{13}C CPMAS (right) NMR spectra of AS6.

The solid state NMR spectra acquired for AS6 clearly show the presence of the phosphate on the aluminium. The ^{1}H spectrum is very broad but it shows the presence of one intense, sharp peak at 6.3 ppm assigned to the protons of the binaphthyl moiety, at 2.9 ppm resonate as a broad band the methylene and methyls bound to the N of the ammonium and at 1.4 ppm the methyl of the NCH_2CH_3 moiety. The last small peak visible in the spectrum is an artefact of the machine.

The ^{13}C NMR spectrum displays a huge peak at 124.2 ppm assigned to the carbons of the binaphtyl moiety of the phosphate ligands. At 145.7 ppm then resonate the C-O carbons of the same. The signal for the carbons of the ammonium are at 49.9, 40.2 and 6.8 ppm, and are respectively assigned to the methylene of the NCH_2CH_3, the NCH_3 and the methyl of the NCH_2CH_3 fragment.

From the DRIFT, solid state NMR and mass balance analysis characterization of AS6, it was possible to synthesize on the silica surface a well-defined anionic aluminium phosphate of structure $[(\equiv SiO)_2Al(O_2P\text{-binaphtol})_2]^-[HNMe_2Et]^+$, that can be applied as activating support of homogeneous catalysts in ethylene polymerization.

- Test in ethylene polymerization in combination with *rac*-EtInd$_2$ZrCl$_2$

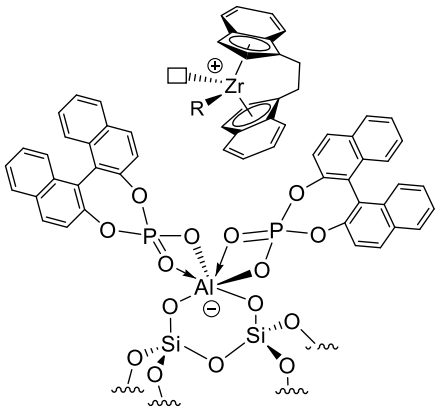

Scheme 19 – Structure of the catalyst AS6/Cat1.

AS6 was tested in ethylene/1-hexene slurry copolymerization as co-catalyst for *rac*-EtInd$_2$ZrCl$_2$, Cat 1, in the same conditions than that used for the catalytic systems investigated previously.

The polymerizations were conducted in 300 mL of heptane, at 80°C and 4 bars of ethylene pressure for 30 minutes. The total [Zr] was 2 µM and TiBA was used as scavenger in concentration 1 mM. The zirconocene precursor was activated right before the start of the polymerization by contacting it with the activating support in presence of TiBA, as alkylating agent.

The polymerization result obtained for the system AS6/Cat1 are reported in Table 15.

Table 15 – Polymerization result obtained with the system AS6/Cat1. General conditions: 80°C; 4 bars C_2H_4; 30 minutes; 300 mL heptane; [TiBA] 1mM.

run	Catalyst	m mg	Zr µmol	Zr/Al$_{surface}$	Zr loading Wt%	C6 mol%	Yield g	Activity g g_{cat}^{-1} h^{-1}
7	AS6/*Cat1*	20.3	0.67	0.06	0.3	19.3	0.32	31.5

Even though the aluminate on the surface was easily obtained, AS6 didn't reveal to be an efficient activating support for Cat1. The activity was very low, 31.5 g_{PE} g_{cat}^{-1} h^{-1}. Even in this case the ionic interaction between the aluminate on the surface and the zirconocene was not optimal for the polymerization reaction.

The little polymer obtained from run 7 was characterized by DSC and HT-SEC. the results are reported in Table 16.

Table 16 – DSC characterization results for run7.

run	Catalyst	Activity g g_{cat}^{-1} h^{-1}	T_{m2} °C	Crystallinity %
7	AS6/*Cat1*	31.5	123	37.5

The polymer obtained is an LLDPE resin, compatible with the characteristics of the products produced with *rac*-$EtInd_2ZrCl_2$.

Conclusions

In this chapter was presented the synthesis of five activating supports, AS2-AS6.

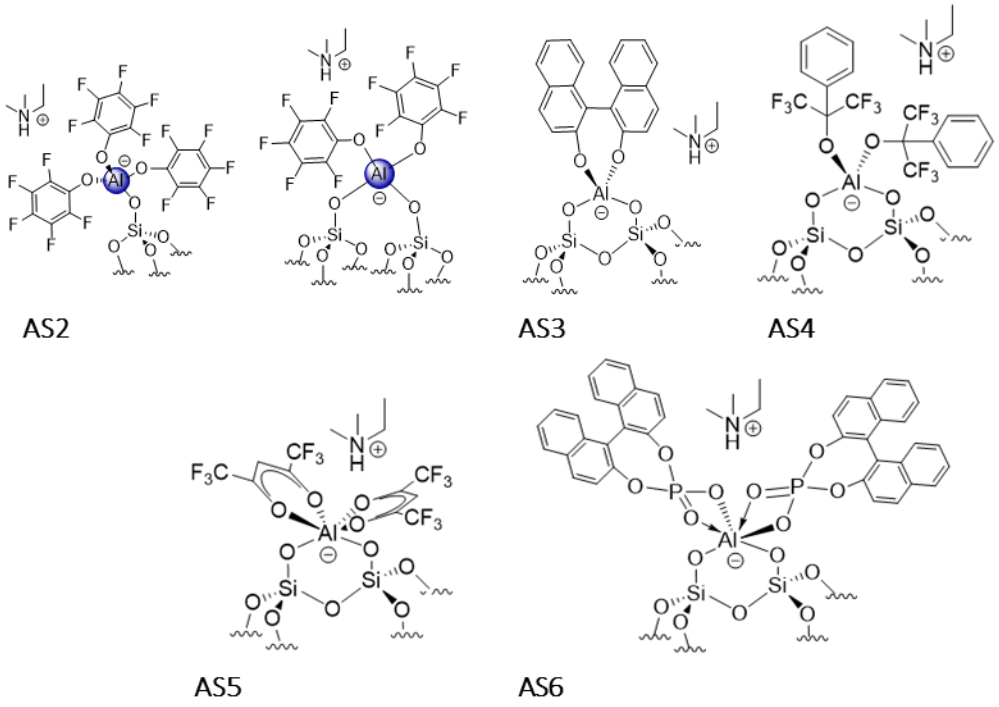

Scheme 20 – Structure of the activating supports synthesized in Chapter III.

The idea was to investigate the effect of the different nature of the ligand of the AS on the activity. With the only exception of AS4, for all the five activating supports it was possible to successfully

obtain and characterize the ionic couple aluminate/ammonium on the surface. Once all the characterizations were performed, the activating supports were tested in ethylene/1-hexene slurry copolymerization as cocatalyst of *rac*-EtInd$_2$ZrCl$_2$.

With the exception of AS2 which showed a discreet polymerization activity, 370 $g_{PE}g_{cat}^{-1}h^{-1}$, the other systems exhibited a negligible efficiency as activators for polymerization catalysts. This could be due to the fact that, changing the ligand on the activators, the ionic interaction between the aluminate on the surface and the zirconocene gets too tight to favour the polymerization process.

In the next chapter it is going to be investigated the effect on the activity of increasing the acidity of the activating support by preparing AS having an halogen bound to the Al.

Moreover, four activating supports in which the Aluminium centre was substituted with a Yttrium element are going to be studied. The aim is to avoid the transfer of ligand to Zirconium cationic complex by the increase the stability of M-O bond by changing the metal centre of the anionic activator (Al *vs* Y), as reported by Marks for similar molecular systems.[1]

References

(1) Metz, M. V.; Sun, Y.; Stern, C. L.; Marks, T. J. Weakly Coordinating Al-, Nb-, Ta-, Y-, and La-Based Perfluoroaryloxymetalate Anions as Cocatalyst Components for Single-Site Olefin Polymerization. *Organometallics* 2002, *21* (18), 3691–3702. https://doi.org/10.1021/om020087s.

(2) Howell, J. G.; Li, Y.-P.; Bell, A. T. Propene Metathesis over Supported Tungsten Oxide Catalysts: A Study of Active Site Formation. *ACS Catal.* 2016, *6* (11), 7728–7738. https://doi.org/10.1021/acscatal.6b01842.

(3) Zhuravlev, L. T. The Surface Chemistry of Amorphous Silica. Zhuravlev Model. *Colloids Surf. Physicochem. Eng. Asp.* 2000, *173* (1–3), 1–38.

(4) Sauter, D. W.; Chiari, V.; Aykac, N.; Bouaouli, S.; Perrin, L.; Delevoye, L.; Gauvin, R. M.; Szeto, K. C.; Boisson, C.; Taoufik, M. Preparation of Monopodal and Bipodal Aluminum Surface Species by Selective Protonolysis of Highly Reactive [AlH_3 (NMe_2 Et)] on Silica. *Dalton Trans.* 2017, *46* (35), 11547–11551. https://doi.org/10.1039/C7DT02575K.

(5) Humphries, T. D.; Munroe, K. T.; Decken, A.; McGrady, G. S. Lewis Base Complexes of AlH3: Prediction of Preferred Structure and Stoichiometry. *Dalton Trans.* 2013, *42* (19), 6965. https://doi.org/10.1039/c3dt00047h.

(6) Mazoyer, E.; TrØbosc, J.; Baudouin, A.; Boyron, O.; Pelletier, Jø.; Basset, J.-M.; Vitorino, M. J.; Nicholas, C. P.; Gauvin, Rø. M.; Taoufik, M.; Delevoye, L. Heteronuclear NMR Correlations To Probe the Local Structure of Catalytically Active Surface Aluminum Hydride Species on G-Alumina*. *Angew Chem Int Ed* 2010, 5.

(7) Sauter, D. W.; Popoff, N.; Bashir, M. A.; Szeto, K. C.; Gauvin, R. M.; Delevoye, L.; Taoufik, M.; Boisson, C. The Design of a Bipodal Bis(Pentafluorophenoxy)Aluminate Supported on Silica as an Activator for Ethylene Polymerization Using Surface Organometallic Chemistry. *Chem. Commun.* 2016, *52* (26), 4776–4779. https://doi.org/10.1039/C6CC00060F.

(8) Gou, S.; Wang, J.; Liu, X.; Wang, W.; Chen, F.-X. Asymmetric Cyanoethoxycarbonylation of Aldehydes Catalyzed by Heterobimetallic Aluminum Lithium Bis(Binaphthoxide) and Cinchonine. *Adv. Synth. Catal.* 2007, *349* (3), 343–349. https://doi.org/10.1002/adsc.200600336.

(9) Naruse, Y.; Esaki, T.; Yamamoto, H. Kinetic Resolution of Epoxides by Chiral Organoaluminum Catalyst Short Synthesis of (-)-C16 Juvenile Hormone. *Tetrahedron* 1988, *44* (15), 4747–4756.

(10) Kroll, W. R.; Kuntz, I.; Birnbaum, E. Investigation of Organoaluminum β-Diketonates. *J. Organomet. Chem.* 1971, *26* (3), 313–320.

CHAPTER IV:

Halogenated Al-based and post-Al Activating supports

Index

Introduction

In Chapter II and III was presented the synthesis of six activating supports that featured a bipodal aluminate on the surface of the silica treated at different temperatures. Specifically, in Chapter III, it was investigated the effect of the nature of the aluminate's ligand on the activity, using AS1 as reference to evaluate the efficiency in polymerization.

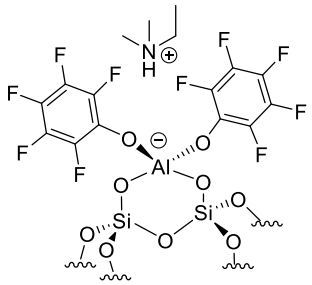

Scheme 1 – Structure of the aluminate on the surface of AS1.

All the synthesised supports were tested as cocatalysts of the zirconocene *rac*-EtInd$_2$ZrCl$_2$ in ethylene/1-hexene slurry copolymerization. Of the six presented, AS1 was the only one to exhibit high productivities (1111 $g_{PE}\, g_{cat}^{-1}\, h^{-1}$ at lab scale and over 5000 $g_{PE}\, g_{cat}^{-1}\, h^{-1}$ at pre-industrial scale), for the other supports the activities recorded were negligible (lower than 50 $g_{PE}\, g_{cat}^{-1}\, h^{-1}$). In fact, changing the nature of the ligand on the Al centre, modifies the interaction between the aluminate and the active zirconocene, resulting in very low productivities.

In this chapter is going to be presented the development of a series of well-defined activating supports in which one of the pentafluorophenoxy ligand on the Al was substituted by an electro attracting heteroatom (F, Cl).

Previous literature studies have demonstrated the central role of the supported activator's Lewis acidity in the activation of the catalyst precursor.[1–3] It is widely reported in literature the synthesis of halogenated solid activators by calcination of the support at high temperatures in presence of halogenated anions, highly efficient in the activation of metallocene precursors.[2] In 2008 McDaniels demonstrated that by reacting silica or alumina surface with different anions (fluoride, chloride, sulfate, triflate, etc.) it was possible to increase the Bronstead and Lewis acidity of the support's surface.[2]

In 2013 Boisson et al.[4] reported the development of two routes for the synthesis of fluorinated solid activators; either, the silica was treated with an alkylaluminium fluoride compound and

then calcined a high temperature, or a grafted alkylaluminium precursor was functionalized by reaction with HF produced by decomposition of $(NH_4)_2SiF_6$. Scheme 2 reports the two possible routes. This paper highlights the principal behaviour of previously patented fluorinated activating supports developed by the group in Lyon.[5–7]

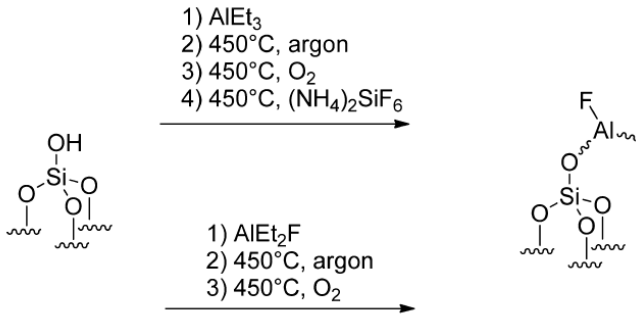

Scheme 2 – Routes for the synthesis of fluorinated solid activators reported by Boisson et al.

The obtained activities were quite good, 750 $g_{PE}\, g_{cat}^{-1}\, h^{-1}$ in combination with *rac*-$EtInd_2ZrCl_2$ at 80°C under 4 bars.

For all the halogenated supports reported in the literature, although the great polymerization activity results, nothing can be said about the exact structure of the species present on the surface of the solid activators, due to the classical preparation methods used.

The aim of this chapter is then, not only to improve the performances of AS by increasing the acidity of the aluminium centre, but also the synthesis of well-defined halogenated activating supports bearing an aluminium-halide bond. In order to achieve this goal, the preparation of a well-defined grafted halogenated precursor is fundamental. In 2014 Copéret et al.[8] studied the grafting of chlorodiethylaluminum (DEAC) on silica and investigated the structure of the species formed on the surface by means of theoretic calculations and solid state NMR experiments. The study shows that upon reaction of DEAC with the surface, a mixture of species is formed of which the majority are bipodal dinuclear species with a bridging ethyl or chloride group (Scheme 3).

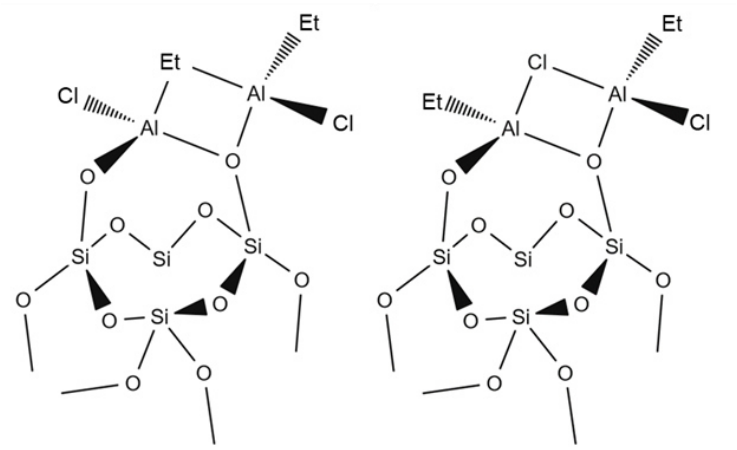

Scheme 3 – Reported structure of the majority of the species formed during the grafting of DEAC on silica.[8]

Formation of dinuclear species after the grafting of alkylaluminum complexes on silica is renown in literature. Numerous studies have been performed on the grafting of trimethyl-[9,10] and triethyl-[11] aluminium showing the formation of dinuclear species on the surface, with physisorption of the trialkylaluminium complex. This phenomenon can be limited by the use of a dative base, such as Et_2O, which interacts with the aluminium centre maintaining the Al tetracoordination.[12,13]

1. Halogenated Al-based activating supports

1.1 Synthesis of $[(\equiv SiO)_2AlCl(OC_6F_5)]^-[HNEt_2Ph]^+$, AS7

The first halide tested in the synthesis of an activating support was the chloride in the synthesis of AS7. The synthesis proceeded in three steps, as reported in Scheme 4.

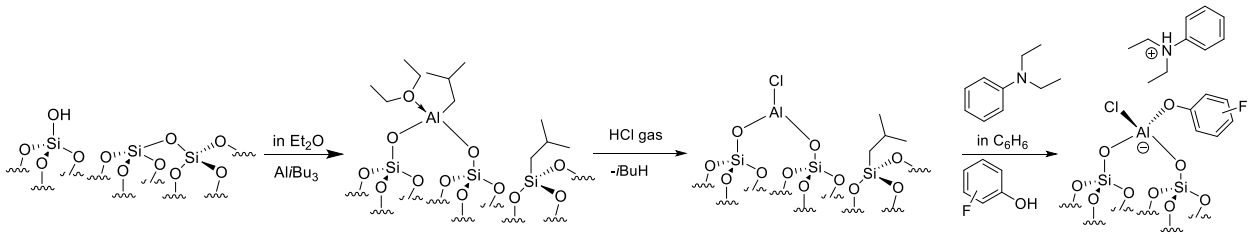

Scheme 4 – Synthetic pathway for AS7.

The first step of the synthesis is the generation of an alkyl aluminium precursor, P3, on the silica surface by reaction of Al*i*Bu$_3$ with $SiO_{2\text{-}700}$ (Grace silica Sylopol 2408 dehydroxylated at 700°C). The obtained bipodal alkylaluminium was then reacted with gaseous HCl to obtain the grafted chloride, P4. And as last step the chloride was functionalized with pentafluorophenol and Et_2NPh to obtain the ionic couple of the activating support.

1.1.1 Synthesis of $(\equiv SiO)_2Ali Bu(Et_2O)$, P3

P3 was synthesized by grafting Al*i*Bu$_3$ in ether on $SiO_{2\text{-}700}$. The silica employed in the synthesis was Grace silica Sylopol 2408, partially dehydroxylated at 700°C as described in Chapter III.

Triisobutylaluminium was reacted for two hours with the silica surface in Et_2O, the use of the coordinating solvent was found by our group to force the formation of bipodal species, of structure $(\equiv SiO)_2Ali Bu(Et_2O)$.[6,7]

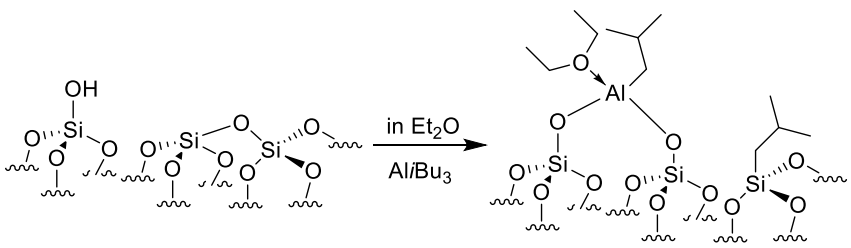

Scheme 5 – Grafting of AliBu$_3$ on $SiO_{2\text{-}700}$, P3.

At the end of the reaction the powder was dried and the surface characterized to confirm the synthesis of P3. In Figure 1 is reported the DRIFT spectra before and after the reaction.

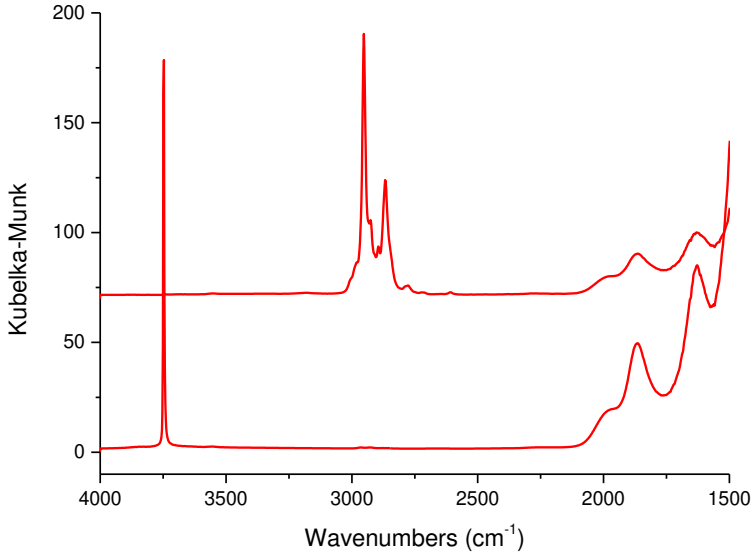

Figure 1 – DRIFT spectra of $SiO_{2\text{-}700}$ (bottom) and P3 (top).

The acquired DRIFT spectrum for P3 after the grafting of TiBA, shows a complete consumption of the of the isolated silanols which are characterized by a peak at 3743 cm^{-1} for the OH stretching, proving that all the silanols present on the surface have reacted with TiBA. The spectrum of P3 is also characterised by the presence of an intense group of peaks in 2500-3000 cm^{-1} region, for the C-H stretching of the alkyl fragments.

The DRIFT spectroscopy characterization of P3, confirms that the reaction of TiBA with the surface of $SiO_{2\text{-}700}$ consumed all the surface silanols and that alkyl species are grafted on the silica surface. In Table 1 are reported the results for the mass balance analysis of P3.

Table 1 – Elemental analysis results for P3.

wt% Al	wt% C	wt% H	C/Al	H/Al	Al mmol g^{-1}
1.25	5.87	1.15	10.5 (th. 12)	27.0 (th. 28)	0.46

From the mass balance analysis 0.46 mmol g^{-1} of Al resulted present on the surface of the support. The ratio C/Al, 10.5, and H/Al, 27.0, derived from the content in mass of the two elements, respectively 5.87 and 1.15 wt%, are in agreement with the formation of the bipodal species. The values are in fact very close to the theoretical ones, as can be seen in Table 1.

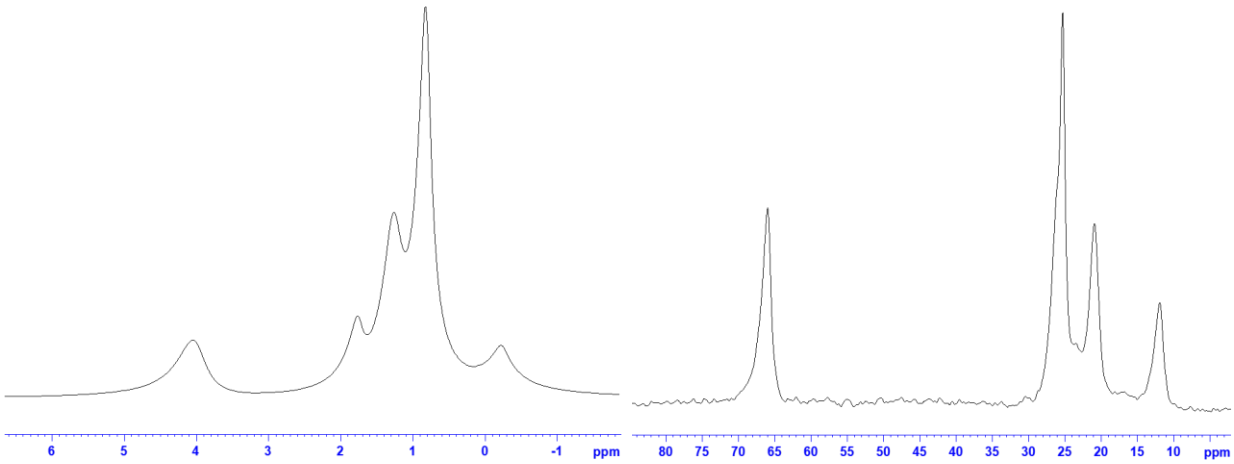

Figure 2 – ^{1}H MAS (left) and ^{13}C CPMAS (right) solid state NMR spectra for P3.

P3 was characterized by ^{1}H MAS and ^{13}C CPMAS solid state NMR. In Figure 2 are reported the spectra acquired for the support. Both spectra clearly show the signals of the isobutyl aluminium fragment and the coordinated Et_2O. The ^{1}H spectrum exhibits at 4.05 and 1.26 ppm the signals of the diethyl ether; the peaks are assigned respectively to the methylene and the methyl of the O-ethyl fragment. There are then peaks at 1.77, 0.83 and -0.22 ppm, assigned to the isobutyl bound to the Al; at 1.77 ppm resonates the methyne, at 0.83 the methyl groups and at -0.22 the methylene.

The ^{13}C spectrum displays at 66.0 and 11.9 ppm the signals of the diethyl ether molecule, respectively for the methylene and the methyl. It is then possible to see three other peaks attributed to the isobutyl moieties either bound to the Al or to the Si. At 25.3 ppm resonate both the methyne and methyl groups of the $AlCH_2CH(CH_3)_2$ moiety, at 23.4 ppm is the peak for the methylene and methyl of the $SiCH_2CH(CH_3)_2$ and at 20.9 ppm the signal of the methylene of $AlCH_2CH(CH_3)_2$ and the methyne of $SiCH_2CH(CH_3)_2$.

Once the surface of P3 was characterized, it was reacted with gaseous HCl, in order to release isobutane and to obtain an aluminium chloride on the surface.

1.1.2 Synthesis of $(\equiv SiO)_2AlCl$, P4

In order to synthesize a chlorinated aluminate as activating support, it was necessary, first, to generate an aluminium chloride on the surface; to do so, P3 was reacted for one hour with gaseous HCl in a glass reactor. Scheme 5 depicts the reaction pattern.

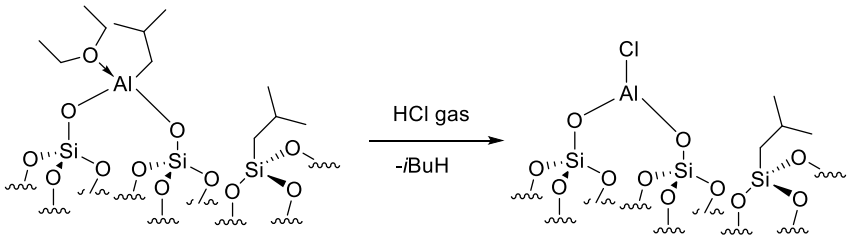

Scheme 6 – Functionalization of P3 with HCl_{gas}.

At the end of the reaction the reactor was evacuated and the powder characterized by DRIFT spectroscopy, to confirm that all the species on the surface had reacted with HCl. The spectrum acquired is reported in Figure 3.

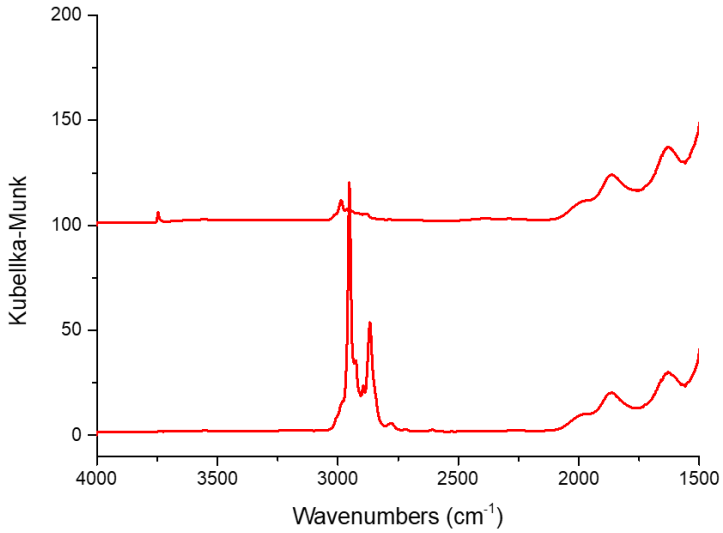

Figure 3 – DRIFT spectra of P3 (bottom) and $(\equiv SiO)_2AlCl$ (top).

Upon reaction with HCl there was a big decrease in the intensity of the signals between (2500-3000 cm^{-1}) attributed to the C-H stretching of the alkyl moieties on the surface. This indicates that all the bipodal isobutylaluminium species reacted with the hydrochloric acid. The small peaks remaining can be assigned to the stretching of the isobutyl directly bound to the silica surface. It is also possible to see the regeneration of a small fraction of silanol groups on the surface, as indicated by the small peak at 3743 cm^{-1}. This was probably caused by some water impurities present in the balloon of HCl.

The species on the surface of P4 were characterized by mass balance analysis, the results are reported in Table 2.

Table 2 – Elemental analysis results for P4.

wt% Al	wt% C	wt% Cl	wt% H	C/Al	Cl/Al	H/Al	Al mmol g^{-1}
1.18	2.21	1.78	0.46	4.2 (th. 4)	1.1 (th. 1)	10.4 (th. 9)	0.44

The amount of chloride found on the surface of P4, 1.78 wt%, confirms the presence of one chloride bound per aluminium, as targeted. The mass balance analysis also shows the presence of one isobutyl fragment per Al, it is the alkyl that got transferred to the silica surface upon grafting of the TiBA and that wasn't reacted with HCl by protonolysis . It is worth mentioning that P4 is a unique example of well-defined bipodal aluminium chloride $(\equiv SiO)_2AlCl$.

Once the surface of P4 was characterized, the support was functionalized with pentafluorophenol and diethylaniline, to generate the ionic couple of AS7.

1.1.3 Functionalization of P4 with pentafluorophenol, AS7

The synthesis of AS7 required the functionalization of P4 with both pentafluorophenol and diethylaniline. The addition of the aniline was necessary because, contrarily to the cases of P1 and P2, in P4 there isn't an amine coordinated to the aluminium that could generate the counter ion for the aluminate.

P4 was reacted in benzene with 1.2 eq. of pentafluorophenol and diethylaniline overnight. Scheme 6 reports the reaction pattern.

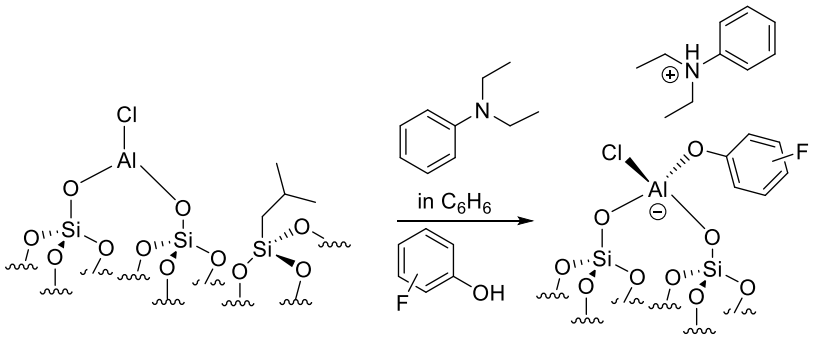

Scheme 7 – Synthesis pathway of AS7.

At the end of the reaction the product was washed with benzene and pentane and dried under vacuum. The surface was characterized to confirm the formation of the ionic couple. In Figure 4 is reported the DRIFT spectrum for the activating support.

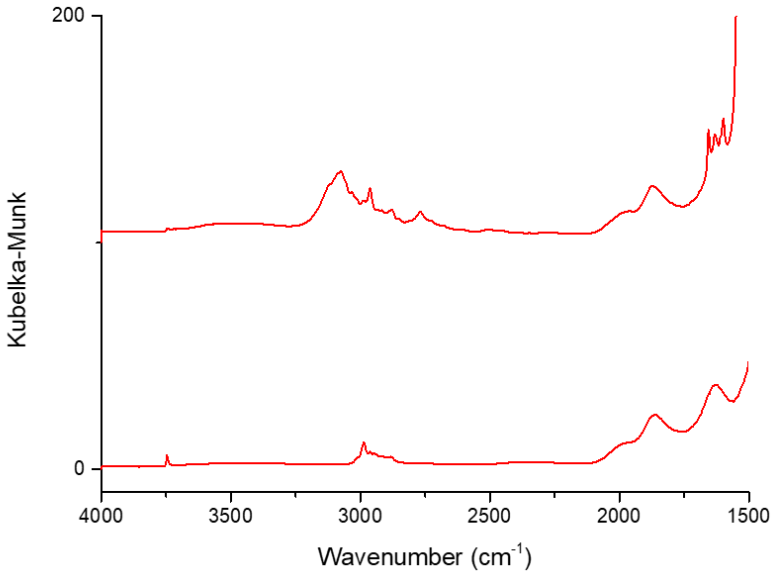

Figure 4 – DRIFT spectra for P4 (bottom) and AS7 (top).

Upon reaction of $(\equiv SiO)_2AlCl$ with pentafluorophenol and the aniline, a huge peak appears at 3070 cm^{-1} for the N-H stretching of the anilinium, proving the formation of the anionic couple on the surface. Additional sharp peaks appear also between 1500 and 1600 cm^{-1} for the C-H and C=C stretching of the aromatic moiety.

The species on the surface of AS7 were also characterized by mass balance analysis. The results are reported in Table 3.

Table 3 – Elemental analysis results for AS7.

wt% Al	wt% C	wt% N	wt% Cl	C/Al	Cl/Al	N/Al	Al mmol g^{-1}
1.14	5.25	0.57	2.60	10.4 (th. 20)	1.7 (th. 1)	1.0 (th. 1)	0.42

The amount of nitrogen found on the surface of AS7, 0.57 wt%, is compatible with one ammonium per Al. It appears, though, that there was a misevaluation of the carbon and chloride amounts on the surface. In fact, it was measured 1.7 chlorides per Al, which is not coherent, not only with the theoretical value of 1 for the desired species, but also with the

ratio Cl/Al found for P4, 1.1. In the same way the amount of carbon found on the surface is way lower than what was expected for the product. 5.25 wt% of C on the surface would correspond to 10.4 C/Al, when the theoretical value would be 18. Looking just to the results of the elemental analysis, it could be affirmed that upon functionalization of P4, only the coordination of the aniline occurred, with no reaction with the pentafluorophenol.

Although this conclusion would be very straightforward, it is in great contrast with the DRIFT spectrum reported in Figure 4, in which the peak of the N-H stretching is very intense and also from the ^{19}F MAS NMR spectrum acquired for AS7, reported in Figure 5, which clearly displays the signals of the fluorines of the pentafluorophenoxy ligand.

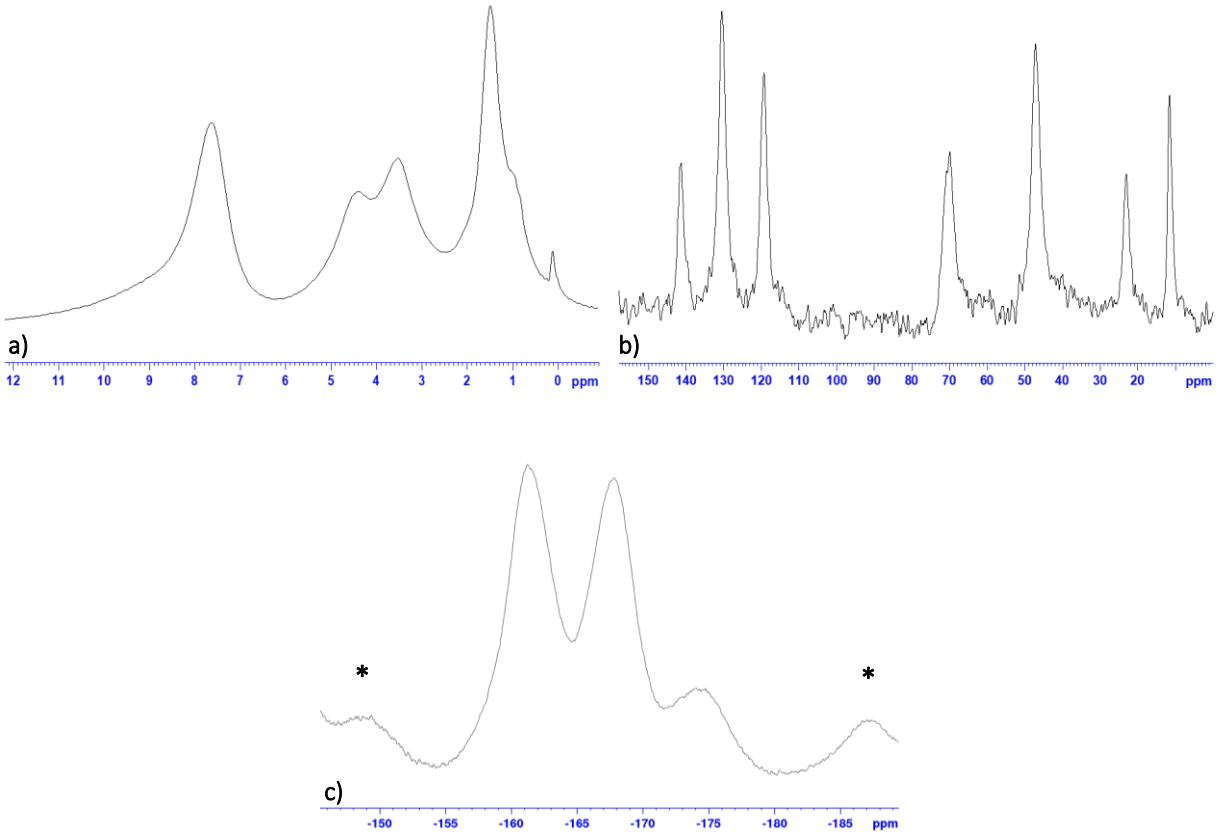

Figure 5 – a) ^{1}H MAS, b) ^{13}C CPMAS and c) ^{19}F MAS solid state NMR spectra for AS7.

AS7 was characterized by ^{1}H MAS, ^{13}C CPMAS and ^{19}F MAS NMR spectroscopy. While the ^{1}H and ^{13}C spectrum show just peaks assigned to the anilinium, the ^{19}F spectrum shows three signals at -161.2, -167.8 and -173.8 ppm assigned respectively to the fluorines in ortho meta and para of the pentafluorophenoxy ligand, proving the presence of the pentafluorophenol on the surface, and more specifically bound to the Al. The chemical shifts are in fact in agreement with those reported in literature for similar structures.[13,14]

The ^{1}H spectrum displays three peaks assigned to the anilinium ion at 7.63, 4.40 and 0.95 ppm respectively assigned to the protons of the aromatic ring, the methylene and the methyl of the ethyl fragment. At 3.52 and 1.49 ppm are present two additional peaks that were assigned to THF impurities present on the surface (from glove-box).

The ^{13}C NMR spectrum shows at 11.6 ppm and 47.2 the resonances of the methyl and methylene groups of the ethyl moiety of the anilinium and at 141.3, 130.5 and 119.3 ppm the signals of the carbons of the phenyl ring. Also at the ^{13}C spectrum it is possible to see the peaks due to the THF impurities at 69.9 and 23.1 ppm.

Although the NMR characterization of the activating support confirms the presence of a pentafluorophenol bound to the Al on the surface, and the DRIFT spectrum bears evidence of the presence of the anilinium on the surface, indicating thus the formation of the ionic couple, the low amount of carbon found by elemental analysis calls for further studies to clarify the structure on the surface.

1.2 Synthesis of $[(\equiv SiO)_2AlCl_2]^-[HNEtMe_2]^+$, AS8

After the synthesis of AS7, the possibility of generating a dichloride species on the silica surface was investigated, as well as the effect on the activity of completely substituting the pentafluorophenoxy ligands with heteroatoms.

For the synthesis of AS8 the bipodal aluminium precursor functionalized is P1. The synthesis and characterization of $(\equiv SiO)_2AlH(NEtMe_2)$ is reported in Chapter II.

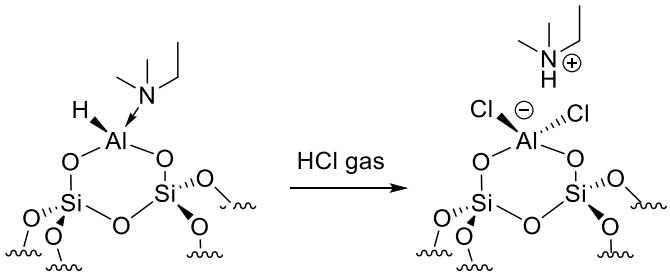

Scheme 8 – Synthesis of AS8.

P1 was reacted with gaseous HCl in great excess for an hour in a glass reactor. At the end of the reaction the surface of the product was characterized. In Figure 6 are reported the DRIFT spectra before and after the chlorination reaction.

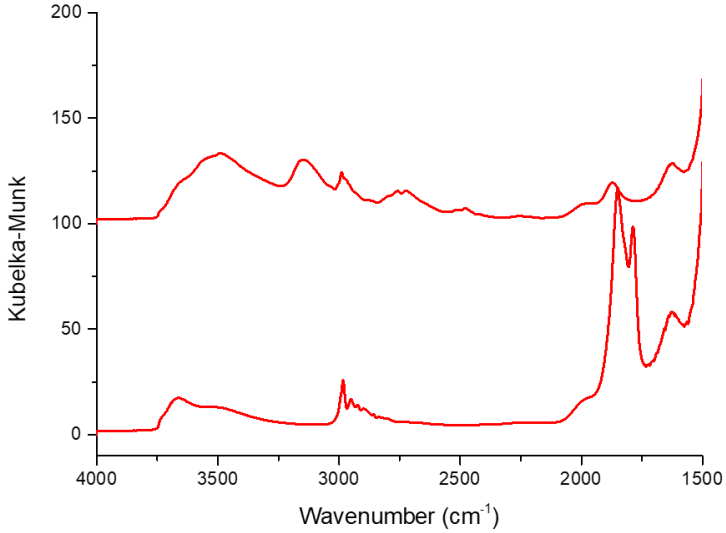

Figure 6 – DRIFT spectra of P1 (bottom) and AS8 (top).

Upon reaction with HCl the signals for the Al-H stretching at 1800 cm^{-1} and 1850 cm^{-1} were completely consumed, meaning that all the species on the surfaces reacted. The spectrum of AS8 displays also a peak at 3148 cm^{-1} that can be attributed to the N-H stretching of the ammonium of the ionic couple.

The DRIFT characterization of AS8, proved that all the species on the surface reacted with HCl to generate a bipodal dichloride aluminates. To further confirm the exact structure of AS8, the hydrogen evolved during the reaction was quantified and a mass balance analysis of the support was performed; the results are reported in Table 4.

Table 4 – Elemental analysis results and H_2 quantification for AS8.

wt% Al	wt% C	wt% N	wt% H	wt% Cl	Al mmol g^{-1}	N/Al	C/Al	C/N	Cl/Al	H_2/Al evolved
1.72	3.3	1.14	0.99	5.27	0.64	1.3 (th. 1)	4.3 (th. 4)	3.4 (th. 4)	2.3 (th. 2)	0.93 (th. 1)

As expected for the bipodal aluminium hydride, the amount of H_2 evolved per Al was 0.9, very close to the theoretical value of 1. The gas quantification analysis thus confirms that all the species on the support reacted. Moreover, the mass balance analysis reported the presence on the surface of 2.3 Cl/Al which is in line with the expected value of 2 for AS8. Finally, the amounts of carbon and nitrogen found, 3.3 and 1.14 wt% respectively, confirm the presence of one ammonium per aluminium chloride.

AS8 was then characterized by ^{1}H MAS and ^{13}C CPMAS solid state NMR. In Figure 7 are reported the spectra acquired.

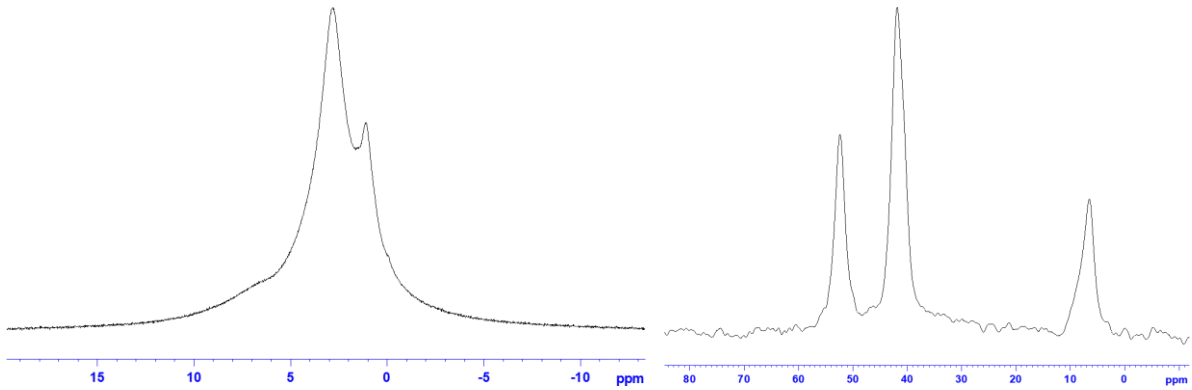

Figure 7 – ^{1}H MAS (left) and ^{13}C CPMAS (right) NMR spectra of AS8.

Both NMR spectra of AS8 displays the signals of the alkyl fragments of the ammonium ion.

The ^{1}H spectrum displays two peaks: the signal at 1.1 ppm is assigned to the methyl of the NCH_2CH_3, while the one at 2.8 ppm is attributed to the protons of the methylene of the NCH_2CH_3 and the methyls directly bound to the nitrogen atom.

The ^{13}C NMR spectrum exhibits three signals. The peak at 52.4 ppm is the resonance of the methylene of the NCH_2CH_3, at 41.8 ppm resonate the carbons of the NCH_3 groups and at 6.5 ppm there's the peak of the NCH_2CH_3 fragment.

The characterization of AS8 showed that after reaction of P1 with HCl, a dichloride aluminium was obtained on the surface, $[(\equiv SiO)_2AlCl_2]^-[HNEtMe_2]^+$. AS8 was then tested in polymerization as cocatalyst for *rac*-$EtInd_2ZrCl_2$ in presence of alkylating agent TiBA. The results are reported in comparison with those of the other activating supports presented in this Chapter.

After the synthesis of AS8, it was studied the effect of an Al-F bond on the efficiency of the activating supports.

1.3 Synthesis of $[(\equiv SiO)AlF(OC_6F_5)_2]^-[HNEtMe_2]^+$, AS9

The molecular aluminium fluoride precursor used in the synthesis of activating supports AS9-11 was Al*i*Bu_2F. It was synthesized according to the exchange reaction reported in Scheme 9.

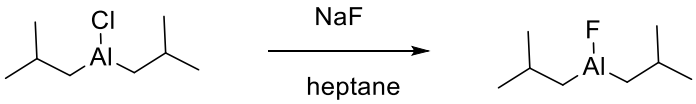

Scheme 9 – Synthesis of Al*i*Bu$_2$F.

In 1970 Krieg et. reported an IR investigation proving the trimeric form of [Al*i*Bu$_2$F]$_3$.[15] The tendency of alkylaluminum complexes to dimerize or trimerize has been known in literature for a long time.[8,16,17] The equilibrium between the two form, monomeric and polymeric, is dependent on the steric hindrance of the alkyl group.

1.3.1 Synthesis of (≡SiO)AlF(*i*Bu)(Et$_2$O), P5

The silica used as support for the first synthesis was Grace Silica Sylopol 2408 dehydroxylated at 700°. Al*i*Bu$_2$F was grafted on SiO$_{2\text{-}700}$ in Et$_2$O for two hours. Scheme 10 reports the reaction pathway.

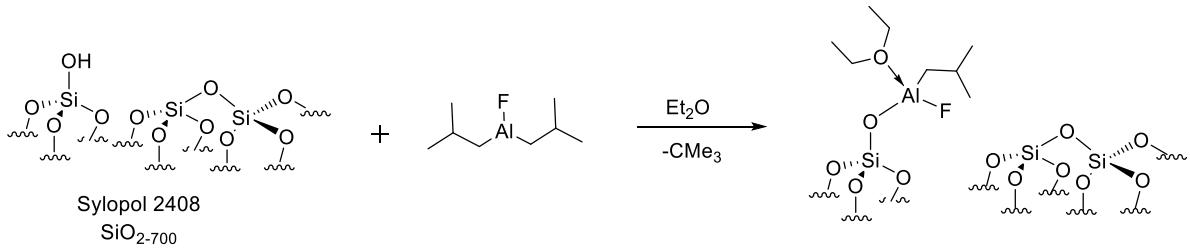

Scheme 10 – Synthesis of P5.

The product was characterized to ascertain the structure of the species on the surface. In Figure 8 is reported the DRIFT spectrum acquired for the sample.

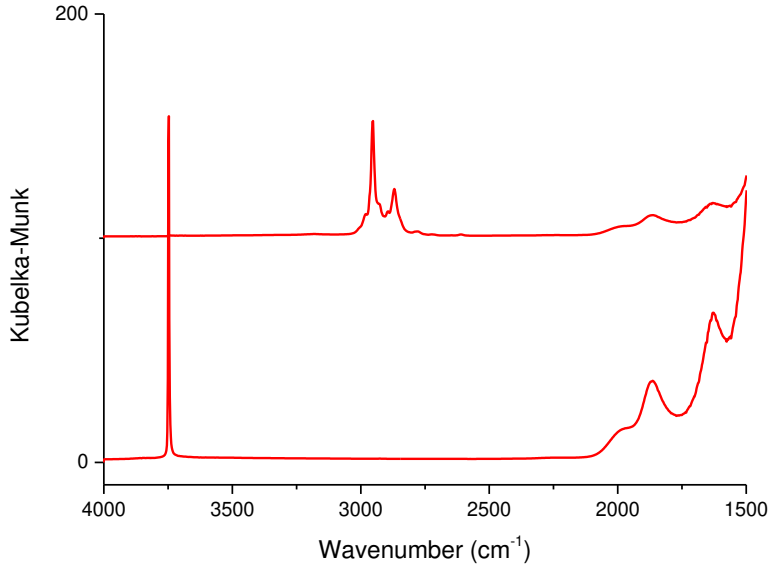

Figure 8 – DRIFT spectra for SiO$_{2\text{-}700}$ (bottom) and P5 (top).

The DRIFT characterization of the surface of the support confirms that all the silanols groups reacted with the diisobutylaluminium fluoride, in fact the sharp peak at 3743 cm^{-1} characteristic of the O-H stretching of the SiOH disappears completely after the grafting. The group of signals between 2500-3000 cm^{-1} is attributed to the C-H stretching of the isobutyl moiety of the grafted species.

The amount of the elements present on the surface was quantified together with the amount of isobutane evolved by the grafting reaction and the hydrolysis of P5. The results are reported in Table 5.

Table 5 – Elemental analysis and isobutane quantification results for P5.

wt% Al	wt% C	wt% H	wt% F	Al mmol g^{-1}	C/Al	F/Al	*i*BuH/Al	
							Grafting	Hydrolysis
1.71	5.86	1.13	0.91	0.63	7.7 (th. 8)	0.8 (th. 1)	0.55 (th. 1)	1.0 (th. 1)

The elemental analysis found 1.71 wt% of Al on the surface of P5, corresponding to 0.63 $mmolg^{-1}$ of aluminium centre on the surface. Combining then the results obtained from the quantification of the carbon and fluorine and of the isobutane evolved, it is possible to confidently affirm that the aluminium species grafted on the surface are monopodal. In fact the amounts of 5.86 wt% of C and 0.91 wt% of F, corresponding to 7.7 C/Al and 0.8 F/Al are very close to the theoretic values of 8 and 1 for monopodal species (≡SiO)Al(*i*Bu)F(Et_2O). Moreover, from the hydrolysis of P5 were released exactly one isobutane per aluminium. The quantification of the isobutane released during the grafting was highly underestimated due to a problem occurred at the moment of the collection of the volatiles after the reaction.

The surface was then characterized by ^{1}H MAS and ^{13}C CPMAS solid state NMR, the spectra are reported in Figure 9.

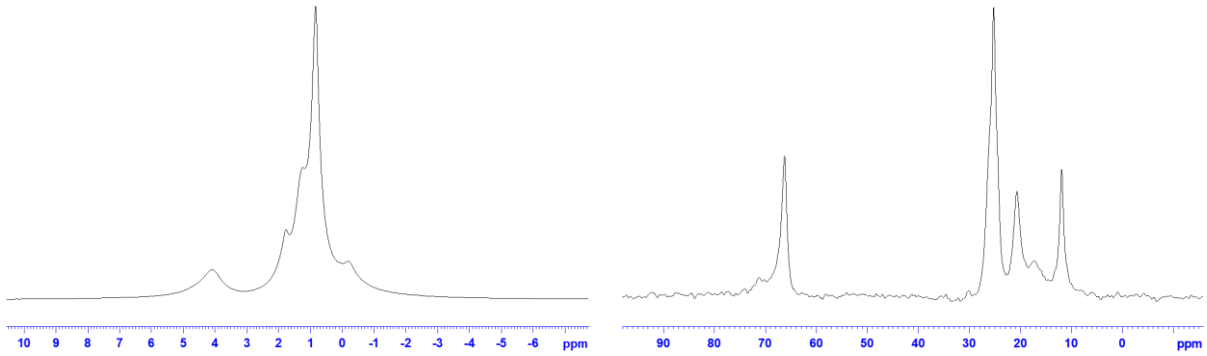

Figure 9 – ^{1}H MAS (left) and ^{13}C CPMAS (right) NMR spectra of P5.

The spectra acquired for P5 appear very similar to those of P3, it is principally possible to see the resonances of the isobutyl fragments, slightly shifted with respect to P3 due probably to the presence of the F on the Al.

The ^{1}H NMR spectrum shows at 4.10 and 1.25 ppm the peaks relative to the methylene and methyl groups of the Et_2O respectively. The signal at 1.77 ppm was assigned to the methyne of the isobutyl moiety, at 0.83 ppm resonate the methyls of the same group and -0.19 ppm is the peak of the methylene.

The ^{13}C NMR displays two signals at 66.3 and 12.0 ppm for the diethylether molecule, while at 20.8 ppm is the resonance of the methylene of the $–Al(CH_2CH(CH_3)_2)$ moiety, and at 25.4 ppm the peak of the methyne and the methyls of the $–Al(CH_2CH(CH_3)_2)$. In addition to the signals due to (≡SiO)A(l*i*Bu)F(Et_2O), are present other three peaks of low intensity at 71.3, 30.1 and 17.3 ppm, these were assigned to the oxidized $–Al(OCH_2CH(CH_3)_2)$, they are respectively assigned to the methylene, the methyne and methyl groups of the ligand. The fraction of oxidized product on the surface, although being worthy of acknowledgment, is negligible with respect to (≡SiO)Al(*i*Bu)F. The acquisition of ^{29}Si solid state NMR spectrum showed no sign of isobutyl or fluoride transfer to the surface, thus far proving the monopodal structure of P5. The presence of Al-F in this species will be proved by additional characterization such as ^{27}Al, ^{19}F solid state NMR. But due to the high stability of Al-F bond (640 Kj/mol) compared to Si-F bond (540 kj/mol) the formation of bipodal species by fluorine transfer to silicon is not favourable. This phenomenon was observed during the grafting of R_3N-AlH_3 or ether-$AliBu_3$ on

silica dehydroxylated at 700°C. This is due to the stability of Si-H (291 kj/mol) and Si-C = 435 Kj/mol) compared to Al-H (285 kj/mol) and Al-C (255 Kj/mol).[18–21]

By reacting Al*i*Bu$_2$F with SiO$_{2\text{-}700}$ in Et$_2$O it was possible to obtain the monopodal grafted species (≡SiO)Al(*i*Bu)F. A full characterization of the surface was performed.

P5 was then functionalized with pentafluorophenol and NEtMe$_2$.

1.3.2 Functionalization of P5 with pentafluorophenol, AS9

P5 was reacted with 2.2 eq. of pentafluorophenol and 1.2 eq. of tertiary-amine per Al in benzene overnight. Scheme 11 reports the reaction pattern.

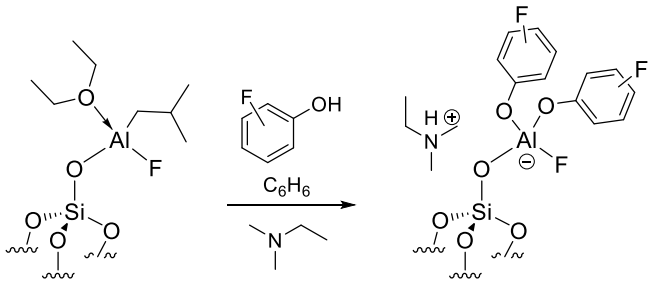

Scheme 11 – Synthesis of AS9.

The surface of the activating support was then characterized, to confirm the completion of the reaction. In Figure10 is reported the DRIFT spectra before and after the reaction.

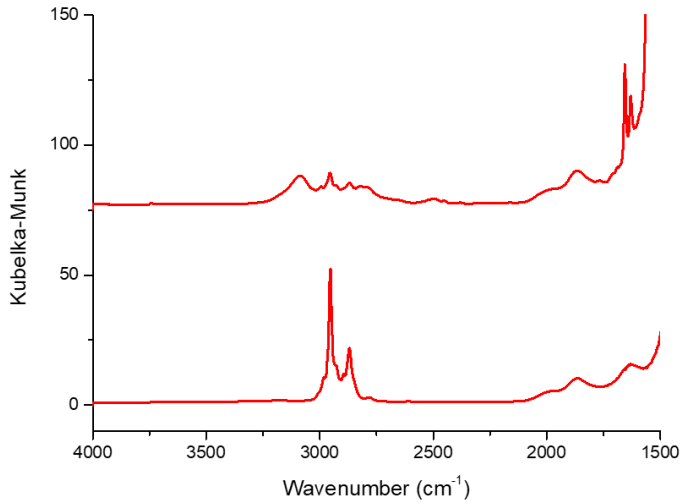

Figure 10 – DRIFT spectra of P5 (bottom) and AS9 (top).

Upon functionalization there is a big decrease in the intensities of the C-H stretching peaks between 2500-3000 cm^{-1} and the appearance of sharp peaks at lower wavelengths, between 1500 and 1600 cm^{-1}, for the C=C stretching of the aromatic rings. An additional peak appears at 3070 cm^{-1}, characteristic of the N-H stretching of an ammonium, indicates the presence on the surface of the support of the ionic couple $[(\equiv SiO)AlF(OC_6F_5)_2]^-[HNEtMe_2]^+$.

The species formed were furtherly characterized by mass balance analysis to confirm the structure. The results are reported in Table 6.

Table 6 – Elemental analysis results for AS9.

wt% Al	wt% C	wt% H	wt% F	Al mmol g^{-1}	C/Al	F/Al	H/Al
1.27	8.1	0.59	8.22	0.47	14.3 (th. 16)	9.2 (th. 11)	12.4 (th. 12)

The elemental analysis results confirm the formation of the ionic couple on the surface. The amount of carbons of 8.1 wt% found corresponds, in fact, to 14.3 C/Al very close to the theoretical value of 16 for the anionic couple. The same can be said to the number of 9.2 F/Al found. The activating support was then characterized by ^1H MAS and ^{13}C CPMAS solid state NMR.

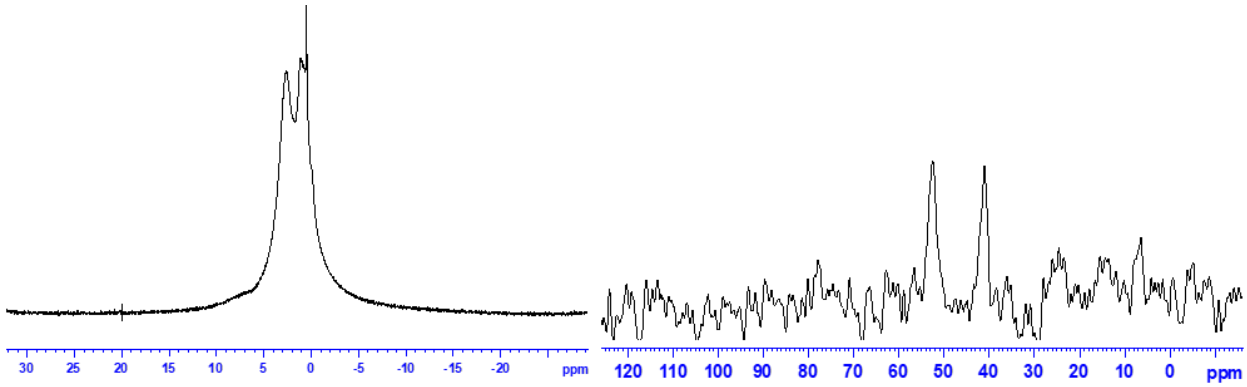

Figure 11 – ^1H MAS (left) and ^{13}C CPMAS (right) NMR spectra of AS9.

In Figure 11 are reported the spectra acquired for AS9. At the ^1H NMR spectrum displays two peaks: at 2.62 ppm resonate the carbons of methyl groups and of the methylene of the ethyl group of the ammonium and at 0.52 ppm the methyl of the ethyl bound to the N.

At the ^{13}C NMR spectrum the peak at 52.6 ppm was assigned to the $–CH_2$ of the ethyl group of $[HNMe_2Et]^+$, the one at 41.1 ppm at the $–NCH_3$ and the one at 6.6 ppm at the $–CH_3$ of the ethyl of $[HNMe_2Et]^+$.

The activating support AS9 was then tested in polymerization as cocatalyst for *rac*-EtInd$_2$ZrCl$_2$. The results are reported in comparison with those of the other activating supports presented in this Chapter.

1.4 Synthesis of [(≡SiO)AlF(OC$_6$F$_5$)$_2$]$^-$[HNEtMe$_2$]$^+$, AS10

An accurate choice of the solvent used during the grafting of a complex, is crucial for the definition of the final structure of the species bound on the support. In fact, in the specific cases of trialkylaluminium complexes, the use of a coordinating solvent, like diethyl ether or THF, can favour the monomeric form of the alkylaluminum, preventing the formation of Al-C-Al bridges in solution (or on the silica surface).[10,11] The saturation of the coordination sphere of the aluminium, moreover, not only could prevent undesired interactions of the complex with itself, but also with Si-O-Si bridges present on the support, making easier the removal of the reagent in excess.

The employment of Et$_2$O as a coordinating solvent, to favour the grafting of Al*i*Bu$_3$ was studied efficiently in our group,[6,7] and applied in the synthesis of P3.

In order to investigate the effect of using differently coordinating solvents during the grafting of Al*i*Bu$_2$F on SiO$_{2\text{-}700}$, P6 was prepared by grafting the alkylaluminium fluoride in pentane, to be compared with P5.

1.4.1 Synthesis of (≡SiO)Al*i*BuF, P6

Al*i*Bu$_2$F was reacted with SiO$_{2\text{-}700}$ (Grace Silica Sylopol 2408) for two hours in pentane. In Scheme 12 is depicted the reaction.

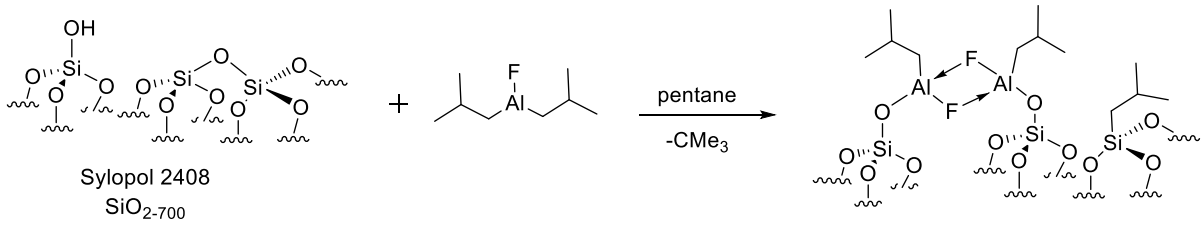

Scheme 12 – Synthesis of P6.

The use of pentane as solvent for the grafting would favour the formation of intermolecular interactions between the species on the surface with the formation of dimers, and an increase in the number of grafted aluminium centres.

To identify the species obtained the surface was characterized. In Figure 12 is reported the DRIFT spectrum of P6.

The DRIFT characterization of the surface of the support confirms that all the silanol groups reacted with the diisobutylaluminium fluoride, in fact the sharp peak at 3743 cm^{-1} characteristic of the O-H stretching of the SiOH disappears completely after the grafting. In the spectrum of P6 is visible a very intense group of signals between 2500-3000 cm^{-1}, attributed to the C-H stretching of the isobutyl moieties of the grafted species.

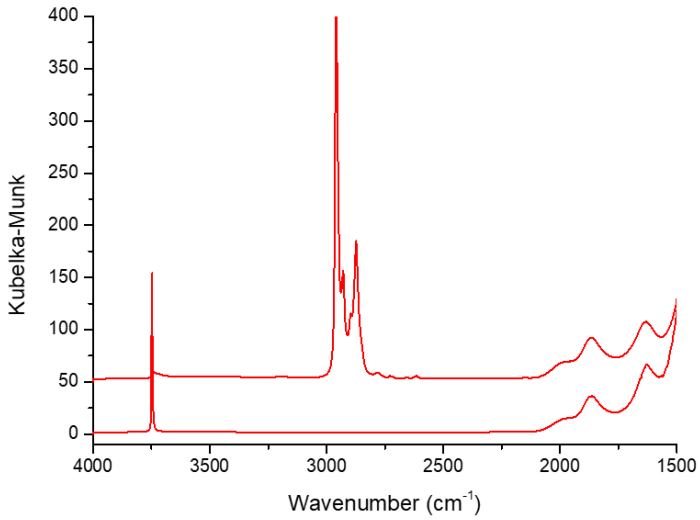

Figure 12 – DRIFT spectra of $SiO_{2\text{-}700}$ (bottom) and P6 (top).

The DRIFT characterization proved that the aluminium species reacted with all the silanols present on the surface. To have more information on the amount of Al centres present on the support, a mass balance analysis of P6 was performed, and the amount of isobutene evolved by the grafting reaction and the hydrolysis of P6 was quantified. The results are reported in Table 7.

Table 7 – Elemental analysis and isobutane quantification results for P6.

wt% Al	wt% C	wt% H	wt% F	Al mmol g^{-1}	C/Al	F/Al	*i*BuH/Al	
							Grafting	Hydrolysis
2.14	5.34	0.95	0.98	0.79	5.6 (th. 6)	0.9 (th. 1)	0.5 (th. 0.5)	1 (th. 1)

The amount of Al found on the surface of P6, 2.14 wt%, 0.79 mmol g^{-1}, was higher than the amount of silanols for $SiO_{2\text{-}700}$, 0.58 mmol g^{-1}; indicating that, as expected, the Al*i*Bu_2F reacted with both silanols and siloxane bridges on the surface. This is confirmed by the amount of isobutane evolved during the grafting, 0.5 *i*BuH/Al. In fact, just the species reacting with the SiOH groups would give isobutane evolution, and the amount of *i*BuH found for the synthesis of P6 is coherent with this hypothesis.

The monopodal and dimeric nature of the grafted species is then confirmed by carbon and fluoride quantification, and the quantitative evaluation of the gases evolved by the hydrolysis of P6. The ratios of 0.9 F/Al and 5.6 C/Al found are in fact coherent with the formation of the species shown in Scheme 11; also the evolution of one isobutane per aluminium matches the theoretical value of 1 *i*BuH/Al for monopodal species.

The formation of surface dimers is in agreement with what already observed in literature for the grafting of metal alkyls of Group 13.[8,11,24] The grafting of both $AlEt_3$[11] and Ga*i*Bu_3[24] on $SiO_{2\text{-}700}$ have been shown to result in the formation of dimeric by protonolysis reaction with reaction and transfer of an alkyl fragment to the surface. More recently Copéret et al. reported something similar for the grafting of $AlClEt_2$ on $SiO_{2\text{-}700}$[8] demonstrating the formation of a mixture of dimeric structures differently bound to the silica surface.

The surface was then analysed by ^1H MAS and ^{13}C CPMAS NMR spectroscopy. The spectra are reported in Figure 13.

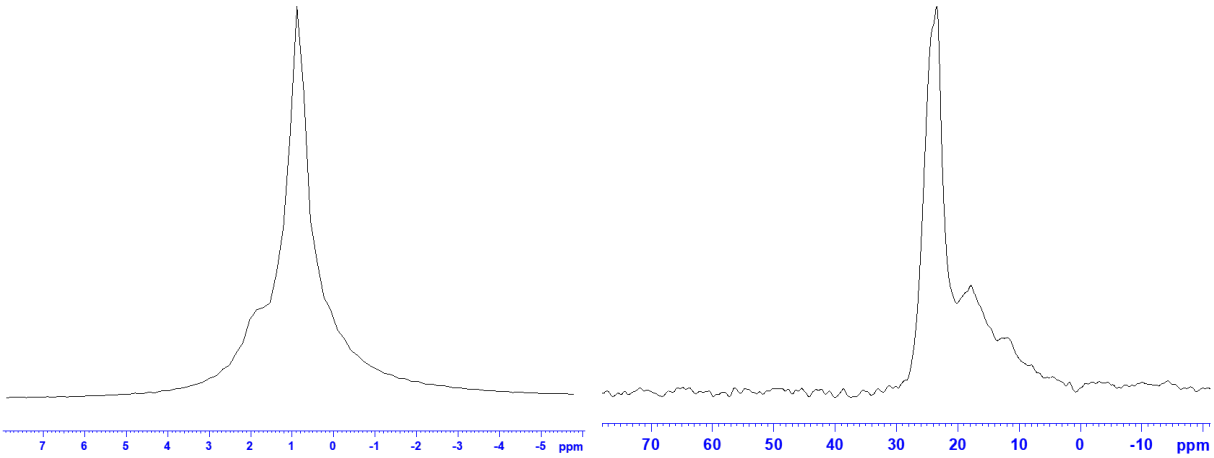

Figure 13 – ^1H MAS (left) and ^{13}C CPMAS (right) spectra for P6.

The ^{1}H spectrum shows just two signals, the peak at 0.87 ppm assigned to the methyls while the methylene and the methyne group resonate as shoulders respectively at 0.11 and 1.85 ppm. Something similar is shown in the ^{13}C spectrum; at 23.3 ppm resonate the methyne and methyl groups of the isobutyl as a sharp peak, whereas the broad shoulder at 17.9 ppm is assigned to the methylene groups.

To confirm the isobutyl transfer on the silica surface, P6 was reacted with O_2 in gas phase. This treatment occurs selectively on the $[(\equiv SiO)AlF(i\text{Bu})]_2$ fragment generating aluminium isobutoxide species along with $SiCH_2CH(CH_3)_2$ species.[12] As shown in Scheme 13.

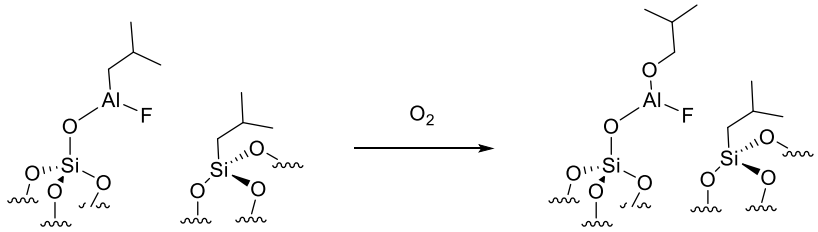

Scheme 13 – Oxidation reaction of P6.

The adduct thus obtained was characterized by ^{13}C CPMAS solid state NMR. The spectrum is reported in Figure 14.

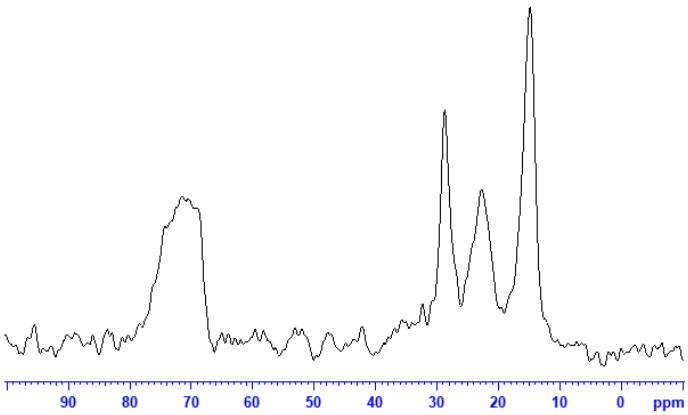

Figure 14 – ^{1}H (left) and ^{13}C (right) solid state NMR for P6 after reaction with O_2.

The spectrum shows four peaks at 14.8, 22.8, 28.7 and 71.5 ppm. The three peaks at 14.8, 28.7 and 71.5 ppm are assigned respectively to the methyls, the methyne and the methylene of the $-AlOCH_2CH(CH_3)_2$ moiety.[12] The remaining peak at 22.8 ppm is characteristic for the resonances of the carbons of the Si-*i*Bu fragment, confirming the transfer of an isobutyl to the silica surface during the synthesis of P6.

Once the structure of the species on the surface of P6 was ascertained, the precursor was functionalized with C_6F_5OH and $NEtMe_2$.

1.4.2 Functionalization of P6 with pentafluorophenol, AS10

P6 was reacted in benzene with 2 eq. of pentafluorophenol and 1 eq. of $NEtMe_2$. The reaction proceeded overnight and is depicted in Scheme 14.

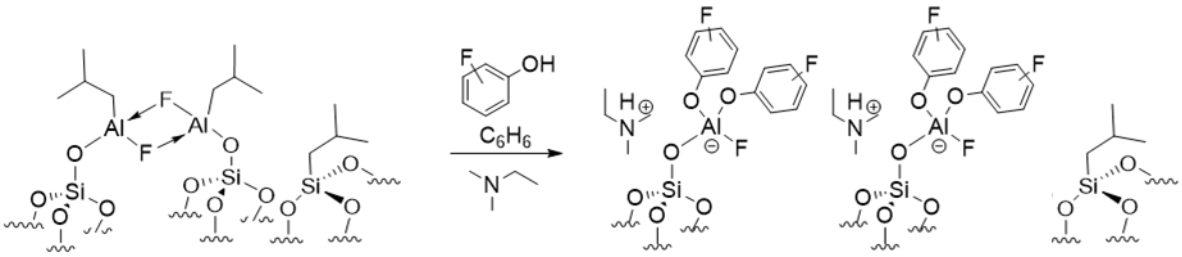

Scheme 14 – Synthesis of AS10.

The surface of the activating support was then characterized, to confirm the completion of the reaction. In Figure15 is reported the DRIFT spectra before and after the reaction.

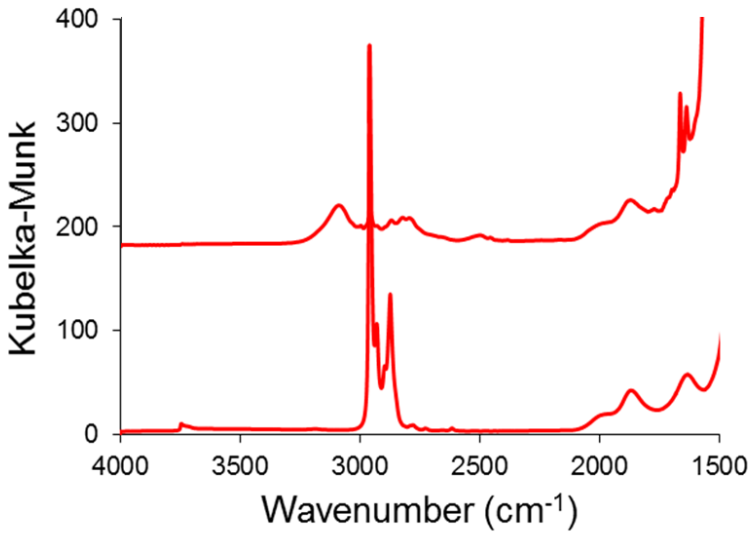

Figure 15 – DRIFT spectra of P6 (bottom) and AS10 (top).

Upon functionalization there is a big decrease in the intensities of the C-H stretching peaks between 2500-3000 cm^{-1} and the appearance of sharp peaks at lower wavelengths (1500-1600 cm^{-1}) for the C=C stretching of the aromatic rings. An additional peak appears at 3070 cm^{-1}, characteristic of the N-H stretching of an ammonium, indicates the presence on the surface of the support of the ionic couple $[(\equiv SiO)AlF(OC_6F_5)_2]^-[HNEtMe_2]^+$.

The species formed where furtherly characterized by mass balance analysis to confirm the structure. The results are reported in Table 8.

Table 8 – Elemental analysis results for AS10.

wt% Al	wt% C	wt% N	wt% H	wt% F	Al mmol g^{-1}	C/Al	F/Al	N/Al	H/Al
1.41	8.56	0.85	0.6	8.66	0.5	13.7 (th. 16)	8.7 (th. 11)	1.2 (th. 1)	11.9 (th. 12)

The elemental analysis results confirm the formation of the ionic couple on the surface. The 8.6 wt% of carbons found corresponds, in fact, to 13.7 C/Al close enough to the theoretical value of 16 for the anionic couple. The same can be said for the ratio of 9.2 F/Al found.

The presence of one ammonium ion is also confirmed by the quantification of nitrogen on the surface, 0.85 wt%, corresponding to 1.2 N per Al. The activating support was then characterized by ^{1}H MAS and ^{13}C CPMAS solid state NMR.

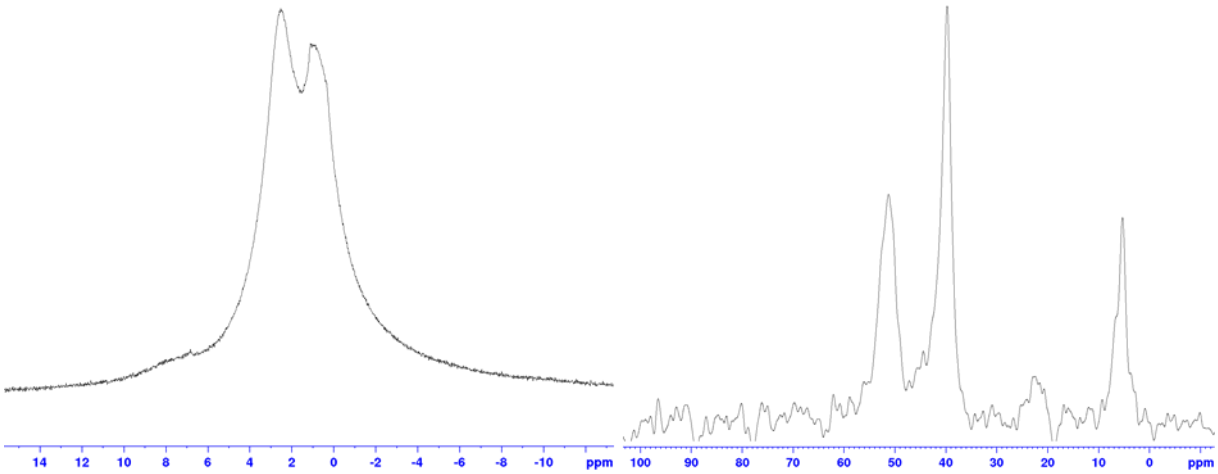

Figure 16 – ^{1}H MAS (left) and ^{13}C CPMAS (right) NMR spectra of AS10.

In Figure 16 are reported the spectra acquired for AS10. The ^{1}H NMR spectrum displays two peaks: at 2.52 ppm resonate the methyls and methylene of the ethyl group of the ammonium and at 1.0 ppm the methyl of the ethyl bound to the N.

At the ^{13}C NMR spectrum the peak at 51.3 ppm was assigned to the $–CH_2$ of the ethyl group of $[HNMe_2Et]^+$, the one at 39.7 ppm at the $–NCH_3$ and the one at 5.3 ppm at the $–CH_3$ of the ethyl

of $[HNMe_2Et]^+$. The additional peak at 22 ppm is assigned to the methylene and methyl groups of the –Si*i*Bu fragment.

The activating support AS10 was then tested in polymerization as cocatalyst for *rac*-$EtInd_2ZrCl_2$. The results are reported in comparison with those of the other activating supports presented in this Chapter.

1.5 Synthesis of $[(\equiv SiO)_2AlF(OC_6F_5)]^-[HNEtMe_2]^+$, AS11

After the effect of the solvent on the modality of grafting of Al*i*Bu_2F on $SiO_{2\text{-}700}$, the complex was grafted on $SiO_{2\text{-}200}$ to study the effect of the structure (monopodal vs bipodal) of the grafted Al centres.

1.5.1 Synthesis of $(\equiv SiO)AlF(i\text{Bu})_2$, P7

In order to increase the concentration of Al centre on the surface, one eq. of iBu_2AlF was reacted per SiOH on the surface of $SiO_{2\text{-}200}$ (Grace silica Sylopol 2408). The reaction was conducted in pentane for two hours. Scheme 15 reports the reaction pattern.

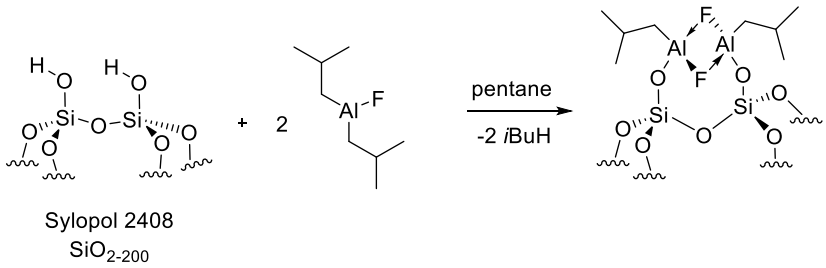

Scheme 15 – Synthesis P7.

The surface of P7 was characterized after the reaction. In Figure 17 is reported the DRIFT spectra before and after the reaction with Al*i*Bu_2F.

The DRIFT characterization of the surface of the support confirms that all the accessible silanol groups reacted with the diisobutylaluminium fluoride, in fact the sharp peak at 3743 cm^{-1} characteristic of the O-H stretching of the isolated SiOH disappears completely after the grafting. The group of signals between 2500-3000 cm^{-1} is attributed to the C-H stretching of the isobutyl moiety of the grafted species.

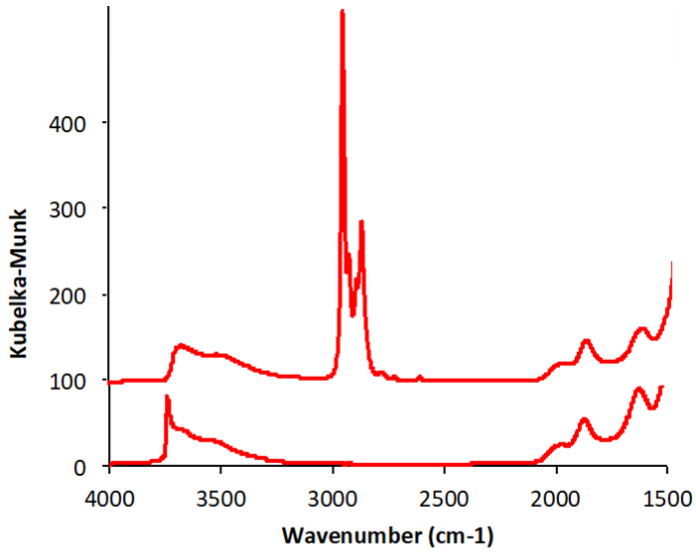

Figure 17 – DRIFT spectra of $SiO_{2\text{-}700}$ (bottom) and P7 (top).

The DRIFT characterization proved that the aluminium species grafted on all the accessible sites on the surface. To have more information the amount of the elements present on the surface was quantified by mass balance analysis. The results are reported in Table 9.

Table 9 – Elemental analysis and isobutane quantification results for P7.

wt% Al	wt% C	wt% H	wt% F	Al mmol g^{-1}	C/Al	H/Al	F/Al
3.67	6.65	1.25	2.11	1.36	4.1 (th. 4)	9.1 (th. 9)	0.8 (th. 1)

By reacting the aluminium fluoride in ratio 1:1 it was indeed possible to increase the amount of Al precursors on the silica surface, 1.36 mmol g^{-1} of Al were found for P7. Moreover, the quantification of carbon and fluoride also confirmed the monopodal nature of the species; 4.1 carbons were found per Al (th. 4), and 0.8 fluorides per metal centre (th.1).

The surface was then analysed by ^{1}H MAS and ^{13}C CPMAS NMR spectroscopy. The spectra are reported in Figure 18.

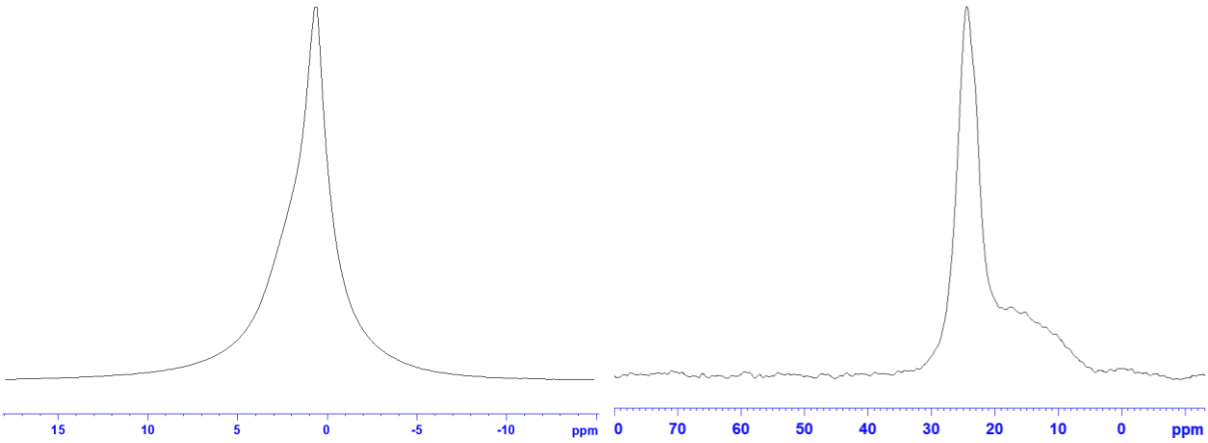

Figure 18 – ^{1}H MAS (left) and ^{13}C CPMAS (right) NMR spectra of P7.

Both spectra show just the peaks of the isobutyl groups, as expected. The ^{1}H spectrum shows broad signals, the peak at 0.70 ppm is assigned to the methyl and methylene fragments of isobutyl and the shoulder at 2.17 ppm to the methyne group. Something similar is shown in the ^{13}C spectrum; at 24.4 ppm resonate the methyne and methyl groups of the isobutyl as a sharp peak, whereas the broad shoulder at 15.3 ppm is assigned to the methylene group.

Once the structure of the species on the surface of P7 was ascertained, the precursor was functionalized with C_6F_5OH and $NEtMe_2$.

1.5.2 Functionalization of P7 with pentafluorophenol, AS11

P7 was reacted in benzene with 2 eq. of pentafluorophenol and 1 eq. of $NEtMe_2$. The reaction proceeded overnight and is depicted in Scheme 16.

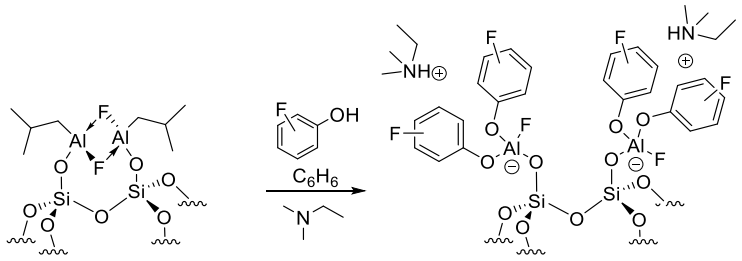

Scheme 16 – Synthesis of AS10.

The surface of the activating support was then characterized, to confirm the completion of the reaction. In Figure 19 is reported the DRIFT spectra before and after the reaction.

Upon functionalization there is a big decrease in the intensities of the C-H stretching peaks between 2500-3000 cm^{-1} and the appearance of sharp peaks between 1500 and 1600 cm^{-1} for the C=C stretching of the aromatic rings. An additional peak appears at 3070 cm^{-1}, characteristic of the N-H stretching of an ammonium, proving the formation of the ionic couple $[(\equiv SiO)AlF(OC_6F_5)_2]^-[HNEtMe_2]^+$.

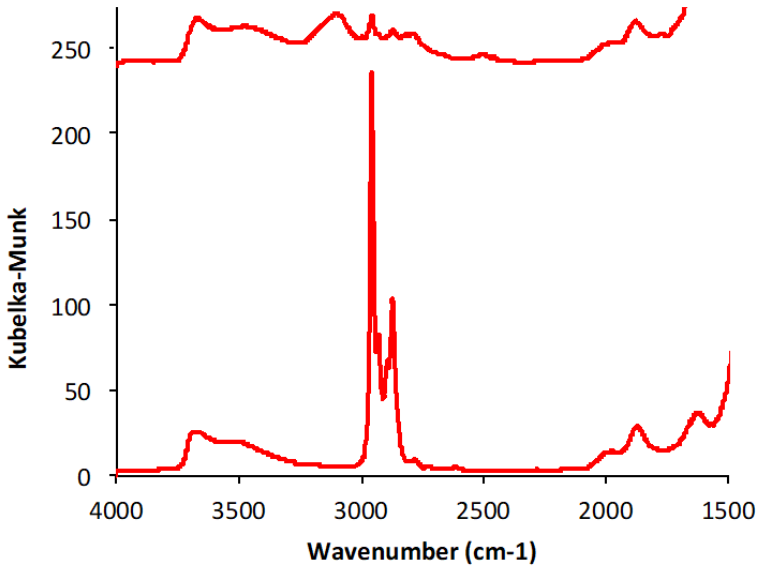

Figure 19 – DRIFT spectra of P6 (bottom) and AS10 (top).

The species formed were furtherly characterized by mass balance analysis to confirm the structure. The results are reported in Table 10.

Table 10 – Elemental analysis results for AS11.

wt% Al	wt% C	wt% N	wt% H	wt% F	Al mmol g^{-1}	C/Al	F/Al	N/Al	H/Al
2.25	8.78	0.87	0.73	9.57	0.8	8.8 (th. 16)	6 (th. 11)	0.7 (th. 1)	9.1 (th. 12)

The elemental analysis results suggest that upon functionalization with pentafluorophenol and ethyl dimethylamine, it was forced the formation of a bipodal aluminate. In fact the ratio of 8.8 C/Al on the surface is way closer what is found for bipodal $[(\equiv SiO)_2AlF(OC_6F_5)]^-[HNEtMe_2]^+$, 10 C/Al, than for the monopodal $[(\equiv SiO)AlF(OC_6F_5)_2]^-[HNEtMe_2]^+$, 16 C/Al. The same thing can be said for what concerns the ratio F/Al; 6 fluorine where found per aluminium centre, matching perfectly the expected value for a bipodal aluminate. The nitrogen quantification confirms the presence of one ammonium per Al, and the protonation of the N was confirmed by DRIFT. In addition, the Al content dropped from 1.36 mmol g^{-1} in P7 to 0.80 mmol g^{-1} in AS11 The actual structure of AS11 is the one reported in the following Scheme 17.

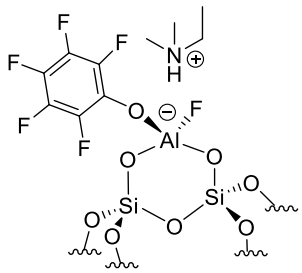

Scheme 17 – Real structure of AS11.

The activating support was then characterized by ^1H MAS and ^{13}C CPMAS solid state NMR.

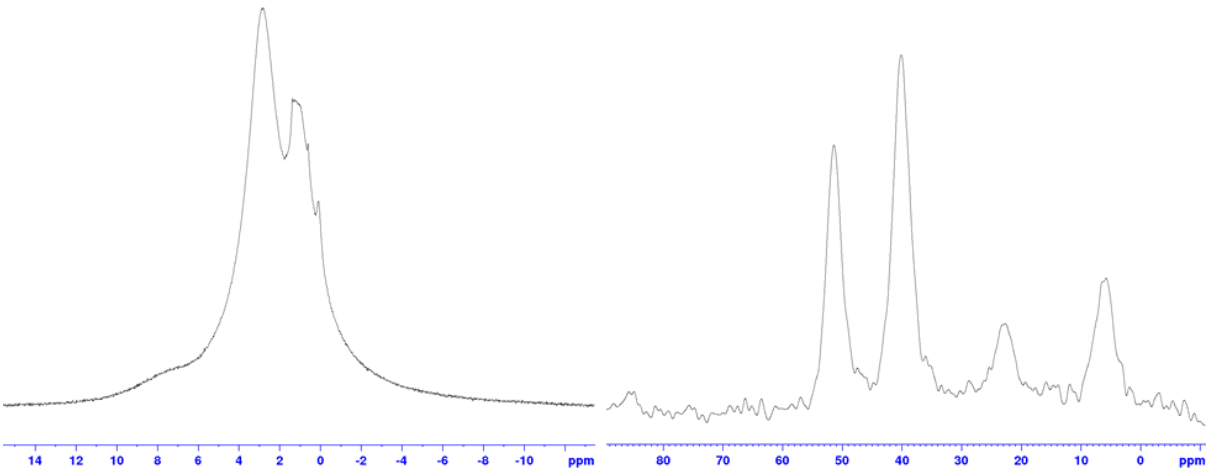

Figure 20 – ^1H MAS (left) and ^{13}C CPMAS (right) NMR spectra of AS11.

In Figure 20 are reported the acquired spectra for AS11. At the ^1H NMR spectrum displays two peaks: at 2.9 ppm resonate the methyl groups and the methylene of the ethyl group of the ammonium and at 1.14 ppm the methyl of the ethyl bound to the N.

At the ^{13}C NMR spectrum the peak at 51.4 ppm was assigned to the $–CH_2$ of the ethyl group of $[HNMe_2Et]^+$, the one at 40.1 ppm at the $–NCH_3$ and the one at 5.8 ppm at the $–CH_3$ of the ethyl of $[HNMe_2Et]^+$. An additional peak is present at 22.6 ppm, probably due to some Al*i*Bu on the surface.

The activating support AS11 was then tested in polymerization as cocatalyst for *rac*-$EtInd_2ZrCl_2$. The results are reported in comparison with those of the other activating supports presented in this Chapter.

1.6 Test in polymerization of the halogenated Al-based support activators AS with *rac*-$EtInd_2ZrCl_2$

The five activating supports presented in this chapter until now were tested as cocatalyst for *rac*-$EtInd_2ZrCl_2$ in ethylene/1-hexene slurry copolymerization. The conditions used were the same employed for AS1. The tests were conducted in 300 mL of heptane, at 80°C for 30 minutes at 4 bars of ethylene pressure. 20 mg of activating support were used during the polymerizations. TiBA in concentration 1 mM was employed as scavenger and alkylating agent. In Table 11 are reported the polymerization results for the five activating supports.

Table 11 – Polymerization results obtained with the activating supports AS7-11 in combination with *rac*-$EtInd_2ZrCl_2$. General conditions: 80°C; 4 bars C_2H_4; 30 minutes; 300 mL heptane; 20 mg AS; [TiBA] 1mM.

run	Activating support	1-hexene mol%	$Zr/M_{surface}$	Zirconocene Wt%	Zr µmol	[Zr] µM	Yield g	Activity $g\ g^{-1}_{cat}\ h^{-1}$
1	AS7	19.5	0.08	1.4	0.66	1.9	0.33	32
2	AS8	17.9	0.03	1.4	0.62	1.9	-	-
3	AS9	17.4	0.08	1.6	0.81	2.3	0.40	39
4	AS10	19.8	0.08	1.6	0.62	2.2	0.17	22
5	AS11	20.9	0.04	1.4	0.68	2.4	0.38	37

After testing the synthesized activating supports in ethylene polymerization, it resulted evident that substituting one or both pentafluorphenoxy ligand of the aluminate support had a hugely detrimental effect on the catalyst's activity. In fact, none of the tested systems showed productivities higher than 40 $g_{PE}\ g_{cat}^{-1}\ h^{-1}$.

The reason why these systems presents negligible activities as activating supports for metallocenes catalysts could be ascribed to the instauration a strong ionic interaction between happens during the formation of the active species it could be useful to make reference to a work published by Marks et al. in 2007.[25,26] In this work is presented the development of a series of halo-perfluoroarylmetalates as activators for metallocenes in stereospecific polymerization of propylene.

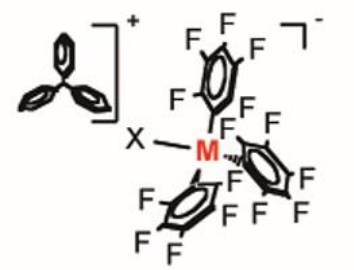

Scheme 18 – Example of the structure of some of the activators reported by Marks et al. in 2007. M = B, Al; X = F, Cl, Br.

The structure reported by Marks and collaborators could be recognizable as homologous in the homogeneous phase of the activating supports reported in the previous paragraphs. What the study shows is that, upon activation of the zirconocene in presence of a mononuclear fluoroaluminate, a kinetically inert Zr-F-Al linkage is formed, having detrimental effects on the activity of the catalyst.[25–27] At the same time, these systems could undergo to deactivation phenomena similar to those observed for AS1, by transfer of a phenoxy group from the activator to the active species.[14,28,29]

It could be supposed that an interaction of the same kind is formed in the case of activating supports AS7-11 for the cationic zirconocene complex. We can then assume that solid activators obtained by an inorganic route involving fluorination by HNR_3F of surface aluminium compounds[2,4] feature a different structure than that obtained by surface organometallic chemistry. However, it is necessary to considerate also that the Al and F loading on the surface of the AS7-11 is lower than what observed in literature for the solid acid activators.

The polymers obtained in runs 1 to 5 were characterized by DSC and HT-SEC. The results are reported in Table 12.

Table 12 – DSC and HT-SEC characterization results for the polymer obtained in run 1-5.

run	Activating support	Activity $g\ g^{-1}_{cat}\ h^{-1}$	T_f °C	ΔH $J\ g^{-1}$	Crystallinity %	M_n $g\ mol^{-1}$	M_w $g\ mol^{-1}$	Đ
1	AS7	32	125	128.4	43.8	30700	80700	2.6
2	AS8	-	-	-	-	-	-	-
3	AS9	39	120	108.0	36.8	37300	117400	3.1
4	AS10	22	123 133	93.6	31.9	-	-	-
5	AS11	37	123 133	193.3	66.0	-	-	-

The polymer obtained is an LLDPE resin, compatible with the characteristics of the products synthesized by *rac*-$EtInd_2ZrCl_2$.

The synthesis of well-defined mono-and bipodal halogenated activating supports, didn't bring to the development of a highly efficient cocatalyst for Zr metallocenes in ethylene/1-hexene co-polymerization. This is due to the formation of Zr-X-Al (X=Cl or F) bonds, upon activation of the zirconocene or transfer of halogen atom to zirconium to form a neutral species.

Having found that this approach didn't lead to the synthesis of more efficient activators than AS1, we decided to investigate the effect of changing the nature of the metal centre grafted on the silica surface.

In the remaining of this chapter it is going to be presented the synthesis of four different yttrium based activating supports.

2. Y based activating supports

In Chapter II it was discussed the synthesis and application of activating support AS1, $[(\equiv SiO)_2AlF(OC_6F_5)_2]^-[HNEtMe_2]^+$. This activating support resulted to be very efficient as cocatalyst of two zirconocene complexes, *rac*-$EtInd_2ZrCl_2$ and (*n*-$BuMeCp)_2ZrCl_2$. For both zirconocenes it was also possible to isolate the active species on the surface of the support; this led to the synthesis of active 'dry' catalysts for ethylene/1-hexene slurry polymerization.

Although the very good activity shown by these systems, it was found that over the span of a few days at ambient temperature the catalysts would deactivate due to the transfer of a phenoxy group from the aluminate to the zirconocene species, killing the catalyst.

In order to limit the occurring of this ligand transfer in Chapter III was presented the development of a series of activating support with chelating ligands. All the species synthesized, although structurally well-defined, when tested in polymerization in association with a metallocene complex exhibited negligible activities.

We remind that the phenomenon of catalyst deactivation by ligand transfer between activators and metallocenes, had already been described by Marks et al. in 2002 for molecular systems homologues to the activating supports presented in this thesis.[14] The solution proposed in the article to limit the transfer phenomenon, was to change the metal centre of the activator from Al to Y, in order to strengthen the M-O bond of the complex.

Table 13 – Dissociation energies for three different M-O bonds as reported in Lange's Handbook of Chemistry.[30]

M-O bond	Dissociation energy KJ mol^{-1}
Al-O	512
Zr-O	760
Y-O	715

In Table 13 are reported the dissociation energies for Al-O, Zr-O and Y-O bonds.[30] It results clear that the transfer of the pentafluorophenoxy group from the aluminate to the zirconocene is favoured thermodynamically. The Zr-O is highly more stable than the Al-O bond, and it doesn't surprise so that the active species quickly evolve on the surface at room temperature in the case of an Al-centred activator in presence of a zirconocene.

Different could be the case of a Y-based activating support in the presence of the same zirconocene. In fact, the dissociation energies for the M-O bonds involving Y and Zr are close, 715 and 760 KJ mol^{-1} respectively. In theory this would render the ionic couple on the surface more stable, and impede at least partly, if not completely, the ligand transfer.

With this in mind we developed four different activating supports obtained by functionalization of grafted precursors with pentafluorophenol. These precursors were prepared by reacting two different Y complexes, Y(*o*-$CH_2PhNMe_2)_3$ and Y{1,3-$C_3H_3(SiMe_3)_2\}_3$, on $SiO_{2\text{-}200}$ and $SiO_{2\text{-}700}$.

2.1 Choice of the complex Y(*o*-$CH_2PhNMe_2)_3$

Y(***o***-$CH_2PhNMe_2)_3$ was chosen because its synthesis had already been achieved in our group at the gram scale. Moreover, the amine functionality of the toluidine ligand is very useful in the successive synthesis of the grafted ionic couple. It won't be in fact necessary to add an amine to generate the cation, because it is already present on the grafted precursor.

Y(*o*-$CH_2PhNMe_2)_3$ was synthesized according to the reaction reported in Scheme 19.

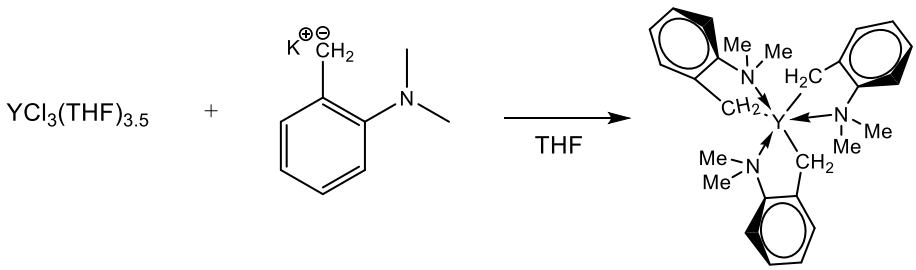

Scheme 19 – Synthesis of Y($CH_2PhNMe_2)_3$.

The complex was characterized by ^1H and ^{13}C solution NMR in THF. The spectra are reported in Figure 21.

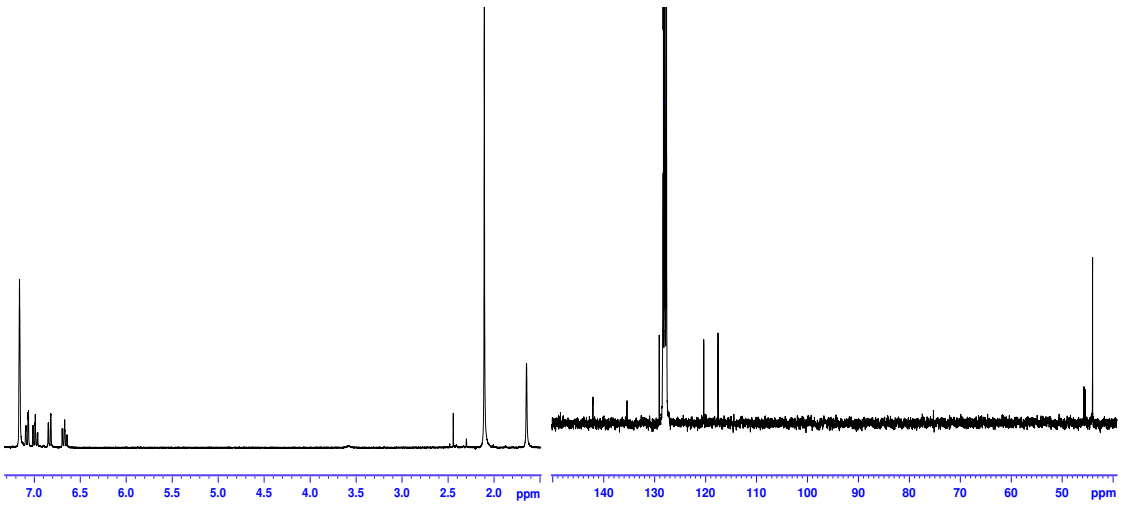

Figure 21 – ^1H and ^{13}C solution NMR of Y(*o*-$CH_2PhNMe_2)_3$ in THF.

The ^{1}H NMR spectrum shows five signals. At 1.65 ppm resonates the protons of the CH_2 bound to Y, the singlet at 2.1 ppm is relative to the methyls bound to the N atom, while the triplet at 6.67 ppm (J = 7.7 Hz), the doublet at 6.84 ppm (J = 8.4 Hz), the triplet at 6.99 ppm (J = 7.4 Hz) and the doublet at 7.08 ppm (J = 8.1 Hz) are assigned to the protons of the aryl ring.

The ^{13}C NMR spectrum shows 7 signals. At 44.03 ppm resonate the methyls bound to the N, at 45.6 ppm there's the doublet due to the coupling of the CH_2 with the Y ($^{1}J_{13C\text{-}89Y}$ = 21.3 Hz). At 117.56, 120.36, 129.12, 135.46, 142.15 ppm resonate the carbons of the aryl fragment, the sixth peak is overlapped with the signal of the deuterated solvent.

2.2 Synthesis of $[(\equiv SiO)Y(OC_6F_5)_3]^-[HNMe_2(PhMe)]^+$, AS12

The first Y-based activating support was grafted on $SiO_{2\text{-}700}$ using Y(*o*-$CH_2PhNMe_2)_3$ as molecular precursor. The synthesis of AS12 was a two-step process, and it is depicted in Scheme 20.

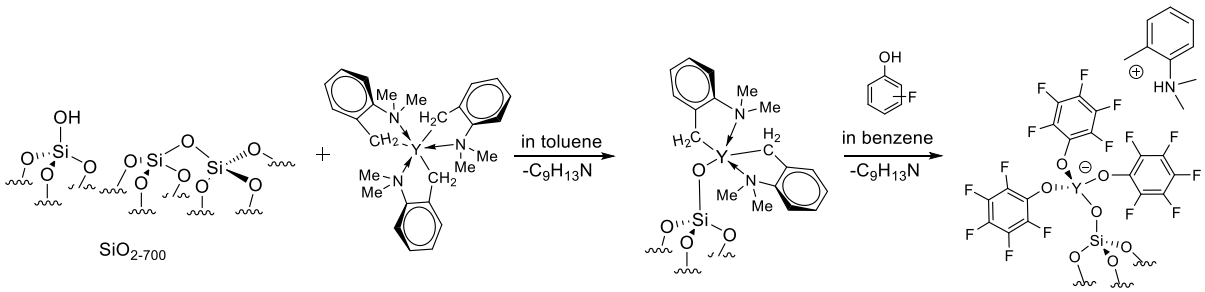

Scheme 20 – Synthetic pathway for the grafting of the trisbenzyl-yttrium with silica for preparing AS12.

2.2.1 Synthesis of $(\equiv SiO)Y(CH_2PhNMe_2)_2$, P8

The silica used for the synthesis of the yttrium precursor was Grace silica Sylopol 2408 dehydroxylated at 700°C. 1.2 eq. of Y(*o*-$CH_2PhNMe_2)_3$ were reacted per SiOH on the surface in toluene.

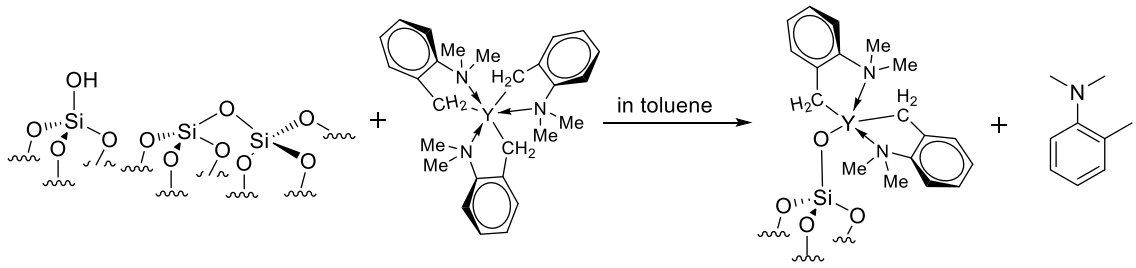

Scheme 21 – Synthesis of P8.

The reaction proceeded overnight, at the end of the grafting the lightly yellow powder obtained was dried under high vacuum. The surface of P8 was characterized to understand what species were obtained on the silica surface. In Figure 22 is reported the DRIFT spectrum of the product.

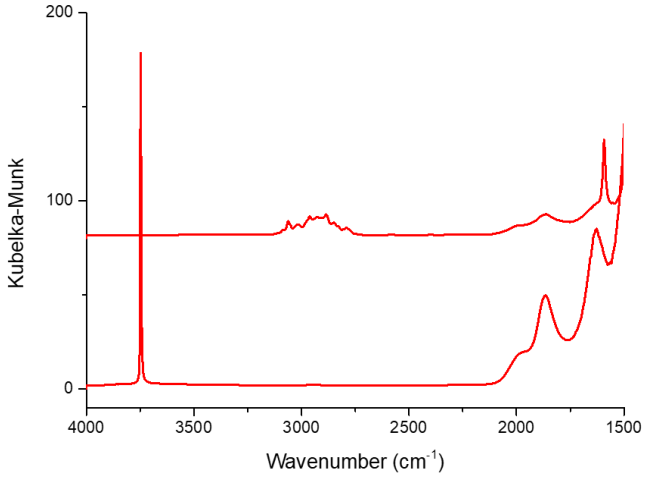

Figure 22 – DRIFT spectra of $SiO_{2\text{-}700}$ (bottom) and P8 (top).

The reaction of the Y complex on the surface consumed all the SiOH groups, in fact the DRIFT spectrum of P8 shows the complete disappearance of the sharp peak at 3743 cm^{-1}, characteristic of the O-H stretching of the isolated silanols. A broad band of signals also appear around 3000 cm^{-1} for the C-H stretching of the N,N-dimethyl-toluidine ligands bound to the Y. As usual though the DRIFT characterization gives only a qualitative indication of the degree of surface coverage the grafting has achieved (if the molecular complex reacted with all the silanols or not). However, it displays no indications on the nature of the grafted species.

To have more exhaustive information the amount of N,N-dimethyl-toluidine released by the grafting and by the hydrolysis of P8 was quantified and $(\equiv SiO)Y(o\text{-}CH_2PhNMe_2)_2$ was characterized by mass balance analysis.

Table 14 – Elemental analysis and N,N-dimethyl-toluidine quantification results for P8.

wt% Y	wt% C	wt% N	wt% H	C/N	C/Y	N/Y	Y mmol g^{-1}	NNDIMT /Y grafting	NNDIMT /Y hydrolysis
3.82	9.29	1.26	1.18	8.6 (th. 9)	18.0 (th. 18)	2.1 (th. 2)	0.43	1.1 (th. 1)	1.2 (th. 2)

From the elemental analysis it resulted that 0.43 mmol g^{-1} of yttrium were grafted on the surface. The quantification of the N,N-dimethyl-toluidine molecule (NNDIMT) released from the grafting reaction revealed 1.1 NNDIMT/Y released, almost matching the value of 1 for monopodal grafted Y species. In the same way the quantification of C and N present on the surface of P8 are in agreement with the formation of monopodal (≡SiO)Y(*o*-CH_2PhNMe_2)$_2$ as shown in Scheme 19. In fact, 9.29 and 1.26 wt% of C and N respectively were found on the surface, corresponding to 18.0 C/Y (th. 18) and to 2.1 N/Y (th.2).

The quantification of the N,N-dimethyl-toluidine released after the hydrolysis of P8, though, reported just 1.2 *o*-CH_3PhNMe_2 evolved per yttrium, instead of the 2 expected for monopodal species. This suggests the presence on the surface of a mixture of mono- and bi-podal species. The formation of bipodal Y complexes of structure (≡SiO)$_2$Y(*o*-CH_2PhNMe_2) is due to the opening of a siloxane bridge with the transfer of one of the N,N-dimethyl-toluidine ligands to the surface.

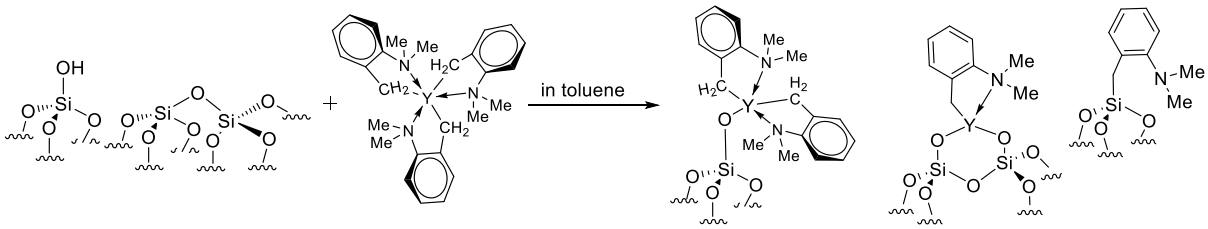

Scheme 22 – Real surface composition of P8.

Based on the GC quantification after the hydrolysis, the ratio mono-/bi-podal species on the surface is 20/80. The degree of ligand transfer to the surface obtained with Y(*o*-CH_2PhNMe_2)$_3$, is very high, but it is coherent with what is reported in literature for the grafting of benzyl-lanthanide complexes.[31]

The surface of P8 was then characterized by ^{1}H MAS and ^{13}C CPMAS solid state NMR. The spectra are reported in Figure 23.

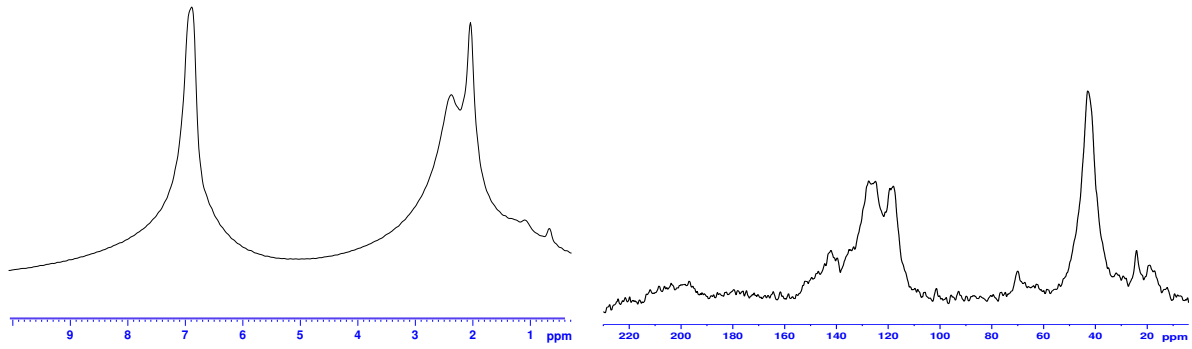

Figure 23 – ^{1}H MAS (left) and ^{13}C CPMAS (right) solid state NMR spectra of VC8.

Both spectra clearly shows the signals for the N,N-dimethyl-toluidine ligand. The ^{1}H NMR spectrum shows three peaks, the one at 6.9 ppm relative to the aromatic protons of the phenyl ring, and those at 2.4 and 2.0 ppm assigned respectively to the methyls bound to the N and to the methylene bound to Y.

At the ^{13}C NMR we can find the resonance of the methyl and methylene of the N,N-dimethyl-toluidine at 43.1 ppm and between 119 and 150 ppm resonate the peaks relative to the aromatic carbons. The last signal at 17.2 ppm is assigned to the CH_2 carbon of the Si(*o*-$CH_2C_6H_4N(CH_3)_2$), due to the transfer of the ligand to the silica surface. At 24.1 and 69.9 ppm are the peaks of THF impurities on the silica surface.

The characterization of P8 showed the presence on the surface of a mixture of mono and bipodal species of structure (≡SiO)Y(*o*-$CH_2PhNMe_2)_2$ and (≡SiO)$_2$Y(*o*-CH_2PhNMe_2) in ratio 20:80.

The grafted precursor thus obtained was used for the synthesis of the activating support AS12.

2.2.2 Functionalization of P8 with pentafluorophenol, AS12

P8 was reacted in benzene with 3.2 eq. of pentafluorophenol per yttrium. The reaction proceeded overnight. In Scheme 23 is reported the reaction pattern.

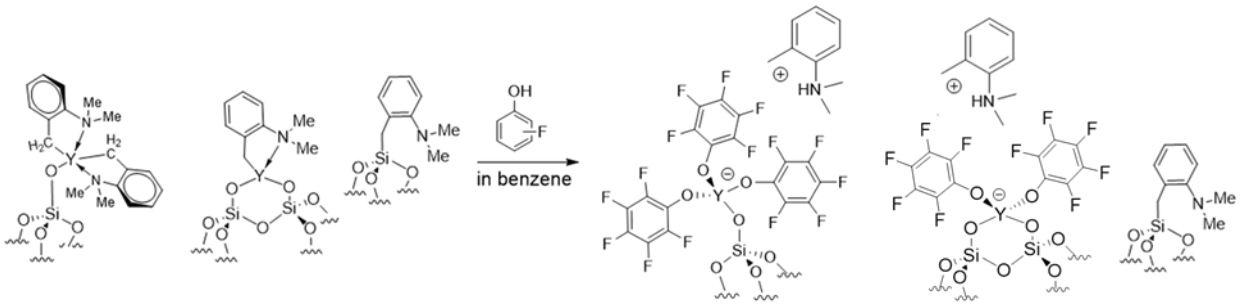

Scheme 23 – Synthesis of AS12.

At the end of the reaction the resulting material was characterized to confirm the formation of the ionic couple. In Figure 24 is reported the DRIFT spectrum for AS12.

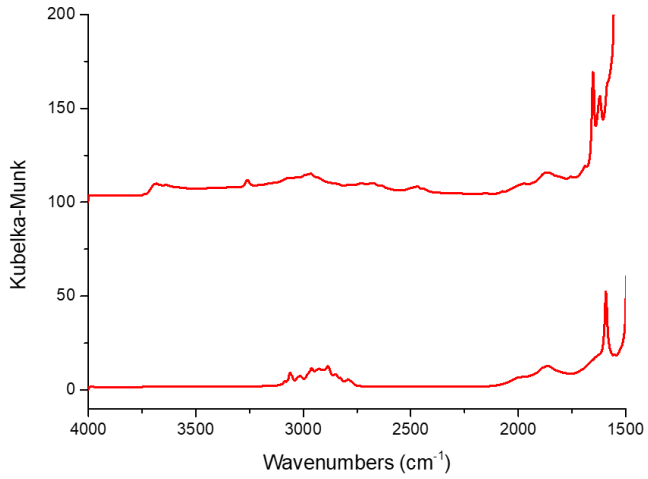

Figure 24 – DRIFT spectra of P8 (bottom) and AS12 (top).

The DRIFT characterization confirms the formation of the ionic couple on the surface of AS12, there is in fact the appearance of a peak at 3077 cm^{-1} characteristic of the N-H stretching. Between 1500 and 1600 cm^{-1} it is also possible to see the signals for the C=C stretching of the aromatics.

The amount of N,N-dimethyl-toluidine released by the grafting was quantified. The results are reported in Table 15 together with the elemental analysis results.

Table 15 – Elemental analysis and N,N-dimethyl-toluidine quantification results for AS12.

wt% Y	wt% C	wt% N	wt% H	wt% F	C/N	C/Y	N/Y	F/Y	Y mmol g^{-1}	NNDIMT/Y grafting
3.15	12.49	0.58	0.60	10.5	25.1 (th. 27)	29.3 (th. 27)	1.2 (th. 1)	15.6 (th.15)	0.31	0.9 (th. 0.2)

The elemental analysis results would suggest the presence on the surface of three pentafluorophenoxyl groups per Y (C/Y and F/Y ratio respectively of 29.3 and 15.6 for AS12) Moreover, the amount of 0.58 wt% N found would suggest the presence of one toluidine coordinated per yttrium. These quantifications are in disagreement with the presence on the surface of a majority of bipodal Y species, and would suggest the formation of an ionic couple featuring a monopodal yttrium. After the functionalization reaction the N,N-dimethyl-toluidine released by the reaction and was quantified: 0.9 NNDIMT per Y were found in the washing solution after the reaction. According to Scheme 22, 0.2 NNDIMT/Y were expected to be evolved after the reaction, the higher amount observed could be explained if we consider that the part of the protonation of the toluidine could take place at the ligand transferred to the silica surface, leading to a structure similar to that reported in Scheme 24.

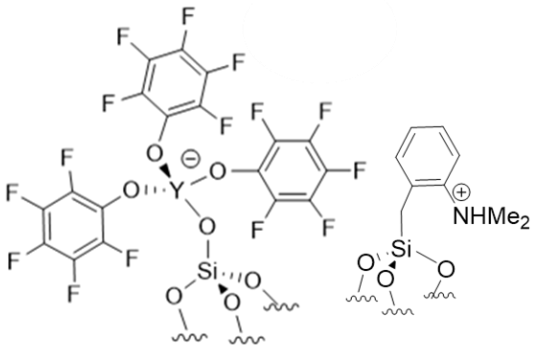

Scheme 24 – Possible structure of the ionic couple present on the surface of AS12.

In order to confirm this hypothesis further studies are necessary.

The activating support was characterized by ^{1}H MAS and ^{13}C CPMAS solid state NMR spectroscopy. The spectra acquired are reported in Figure 24.

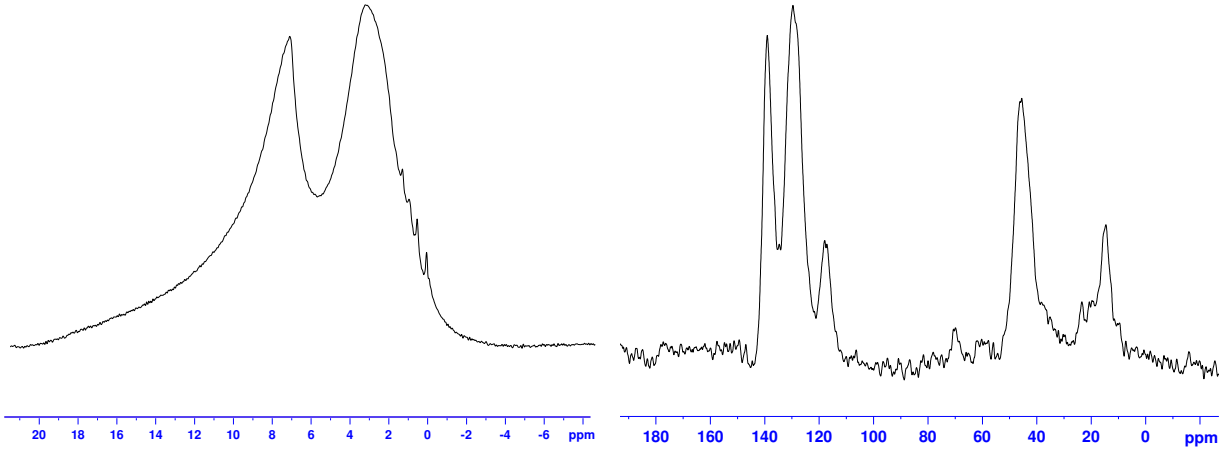

Figure 25 – ^{1}H MAS (left) and ^{13}C CPMAS (right) solid state NMR spectra for AS12.

The ^{1}H spectrum appears quite broad with respect to the one of P8, it exhibits two peaks, one broad signal centered at 3.2 ppm assigned to the methyls bound to the ammonium and to the phenyl, and one at 7.1 ppm assigned to the aromatic protons of the phenyl group.

The ^{13}C NMR shows seven peaks. At 117.9, 129.6 and 139.0 ppm resonate the aromatic carbons of the phenyl, at 45.5 ppm the carbons of the –$NH(CH_3)_2$ fragment of the ammonium, while at 14.6 ppm resonates the CH_3 bound directly to the aromatic ring of the ammonium. At 23.4 and 69.9 ppm are the signals of THF impurities on the surface.

The characterization of AS12 would suggest the formation on the surface of monopodal species of structure $[(\equiv SiO)Y(OC_6F_5)_3]^-[HNMe_2(PhMe)]^+$. This would be in contrast with the obtained results from the characterization of P8, presenting a mixture of mono and bipodal species on the surface. In order to better understand the obtained species, further studies are necessary. The activating support was then tested in ethylene/1-hexene slurry copolymerization as cocatalyst for *rac*-$EtInd_2ZrCl_2$. The results reported in comparison with the other Y-based activating support.

2.3 Synthesis of $[(\equiv SiO)_2Y(OC_6F_5)_2]^-[HNMe_2(PhMe)]^+$, AS13

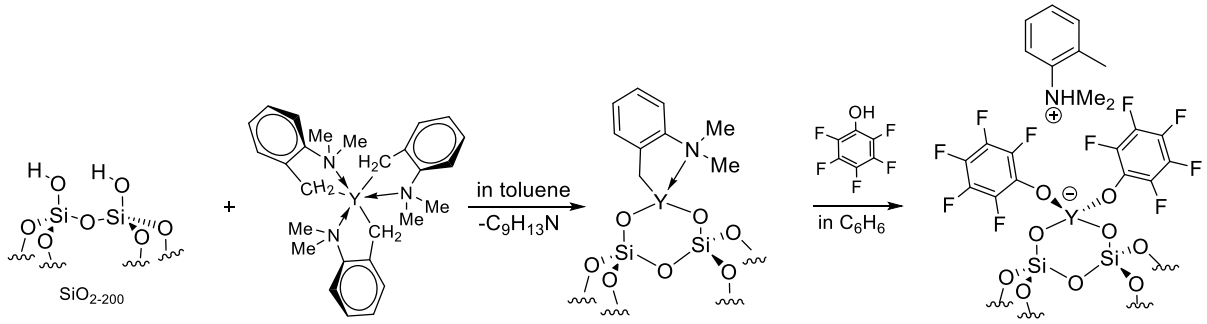

Scheme 25 – Synthesis of AS13.

The second Y-based activating support was grafted on $SiO_{2\text{-}200}$ using $Y(o\text{-}CH_2PhNMe_2)_3$ as molecular precursor. The synthesis of AS13 was a two-step process, and it is depicted in Scheme 25.

2.3.1 Synthesis of $(\equiv SiO)_2Y(o\text{-}CH_2PhNMe_2)$, P9

The silica used for the synthesis of the yttrium precursor was Grace silica Sylopol 2408 partially dehydroxylated at 200°C. 1.2 eq. of $Y(o\text{-}CH_2PhNMe_2)_3$ were reacted per 2eq. of SiOH on the surface in toluene.

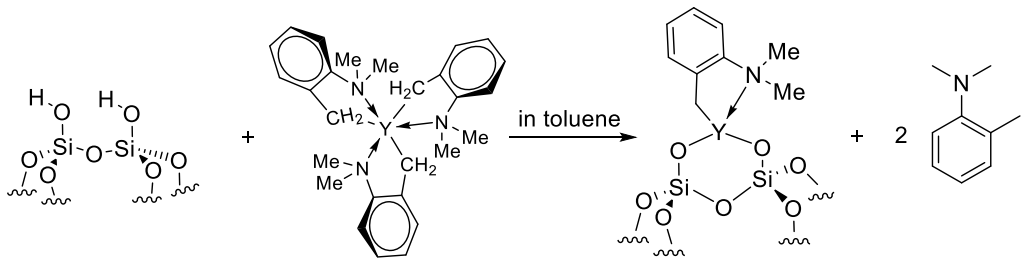

Scheme 26 – Synthesis of P9.

The reaction proceeded overnight, at the end of the grafting the lightly yellow powder obtained was dried under high vacuum.

P9 was then characterised by DRIFT spectroscopy, in Figure 26 is reported the spectra of the surface before and after the reaction.

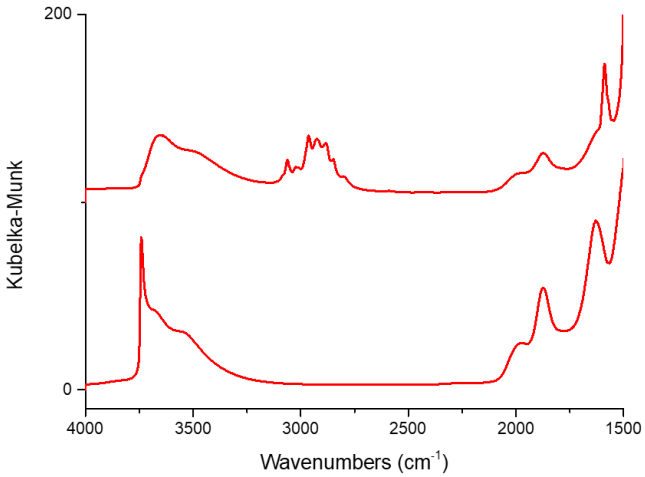

Figure 26 – DRIFT spectra of $SiO_{2\text{-}200}$ (bottom) and P9 (top).

The DRIFT characterization of the surface confirms that Y(*o*-CH_2PhNMe_2)$_3$ reacted with all the accessible silanols, the peak at 3740 cm^{-1} proper of the O-H stretching of isolated SiOH, is completely consumed in the spectrum of P9. As second consequence of the grafting a group of signals appears between 2750 and 3000 cm^{-1} for the C-H stretching of the N,N-dimethyl-toluidine ligand.

Like in the case of P8 the precursor was characterized by mass balance analysis and the released N,N-dimethyl-toluidine by the grafting and hydrolysis of P9 was quantified, to ascertain the presence of bipodal species on the support. The results are reported in Table 16.

Table 16– Elemental analysis and N,N-dimethyl-toluidine quantification results for P9.

wt% Y	wt% C	wt% N	wt% H	C/N	C/Y	N/Y	Y mmol g^{-1}	NNDIMT/Y grafting	NNDIMT/Y hydrolysis
5.43	7.84	1.10	1.01	8.3 (th. 9)	10.7 (th. 9)	1.3 (th. 1)	0.61	2.4 (th. 2)	0.93 (th. 1)

From the elemental analysis it resulted that 0.61 mmol g^{-1} of yttrium were grafted on the surface. The quantification of the released N,N-dimethyl-toluidine ligand from the grafting reaction revealed 2.4 NNDIMT/Y, close enough to the value of 2 for bipodal grafted Y species. In the same way the quantification of C and N present on the surface of P9 are in agreement with the formation of bipodal (≡SiO)$_2$Y(*o*-CH_2PhNMe_2) as shown in Scheme 25. In fact, respectively 7.84 and 1.10 wt% of C and N were found on the surface, corresponding to 8.3

C/Y (th. 9) and to 1.3 N/Y (th. 1). Also the quantification of N,N-dimethyl-toluidine released by the hydrolysis of the precursor is perfectly compatible with the formation of only bidpodal species on the silica surface, 0.9 NNMT/Y were in fact released, to be confronted with the theoretical value of 1 for $(\equiv SiO)_2Y(o\text{-}CH_2PhNMe_2)$.

P9 was then characterized by ^{1}H MAS and ^{13}C CPMAS solid state NMR. The spectra are reported in Figure 27.

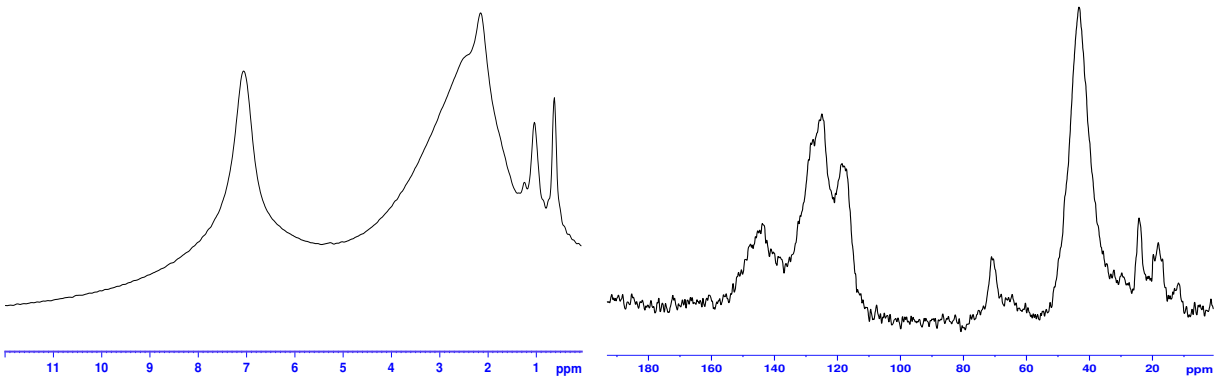

Figure 27 – ^{1}H MAS (left) and ^{13}C CPMAS (right) solid state NMR spectra for AS12.

The ^{1}H NMR spectrum displays four signals: two broad peaks at 7.1 and 2.2 ppm relative to the protons of the aromatic ring and of the methyls of the amine fragment respectively, and two sharp peaks at 1.04 and 0.63 ppm. The peak at 1.04 ppm could be assigned to the protons of the methylene directly bound to the Y, the peak at 0.63 ppm is more indicative of the presence of a –Si-CH_2- fragment, possibly indicating a transfer to the surface of the ligand. This hypothesis would have to be corroborated by additional characterization studies such as ^{29}Si solid state NMR.

At the ^{13}C NMR it is possible to identify between 118 and 145 ppm the signals due to the aromatic carbons of the phenyl ring. The broad signal at 43.3 ppm is due to the Y-CH_2 and the methyls bound to the N. The presence of a peak at 18.1 ppm would seem to be in line with what already observed at the ^{1}H NMR spectrum: a signal attributed to a –Si-CH_2- fragment, due to a possible ligand transfer to the surface. At 71.1 and 24.3 ppm resonate the CH_2(2,5) and CH_2(3,4) of THF impurities present on the surface of the adduct.

The characterization of P9 showed the presence on the surface of a single bipodal species $(\equiv SiO)_2Y(o\text{-}CH_2PhNMe_2)$. The grafted precursor thus obtained was used then for the synthesis of the activating support AS13.

2.3.2 Functionalization of P9 with pentafluorophenol, AS13

P9 was reacted in benzene with 2.2 eq. of pentafluorophenol per yttrium. The reaction proceeded overnight. In Scheme 27 is reported the reaction pattern.

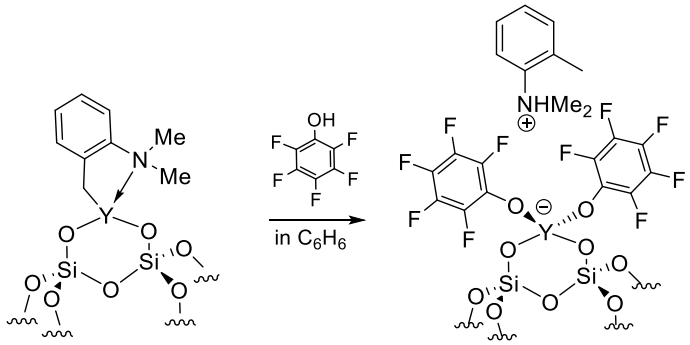

Scheme 27 – Synthesis of AS13.

At the end of the reaction the resulting material was characterized to confirm the formation of the ionic couple. In Figure 28 is reported the DRIFT spectrum for AS13.

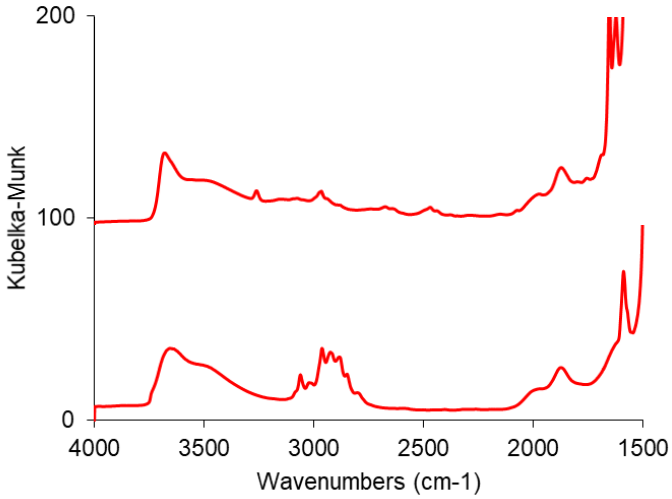

Figure 28 – DRIFT spectra of P9 (bottom) and AS13 (top).

The DRIFT characterization confirms the formation of the ionic couple, the peak at 3078 cm^{-1} is characteristic of the N-H stretching of the ammonium. Between 1500 and 1600 cm^{-1} appear also sharp peaks for the C=C stretching of the aromatic rings of the pentafluorophenol. To further confirm the structure of the species on the surface, the product was characterized by mass balance analysis, and the solution recovered after the functionalization was analysed to measure N,N-dimethyl-toluidine realised during the reaction.

Table 17 – Elemental analysis and N,N-dimethyl-toluidine quantification results for AS13.

wt% Y	wt% C	wt% N	wt% H	wt% F	C/Y	N/Y	F/Y	Y mmol g^{-1}	NNMT/Y
4.57	11.90	0.44	0.66	10.6	19.3 (th. 21)	0.6 (th. 1)	10.9 (th. 10)	0.51	0.43 (th. 0)

The elemental analysis results report 0.51 mmol g^{-1} of Y present on the surface of AS13, and the amount of C and F found on the support are compatible with the formation of the ionic couple. The 11.9 wt% of C found on the surface corresponds to 19.3 carbons per yttrium, close to the theoretical value of 21 for the ionic couple $[(\equiv SiO)_2Y(OC_6F_5)_2]^-[HNMe_2(PhMe)]^+$. The same can be said for the fluorines, 10.9 F were found per Y, almost matching the theoretical value of 10. Looking at these very good values it appears weird the very low amount of nitrogen found on the surface, only 0.6 N/Y, and the fact that there actually was a fraction of N,N-dimethyl-toluidine released during the reaction, implying that almost half of the species on the surface were not involved in an ionic couple. Taking into account the C and F quantifications obtained by the elemental analysis, the best hypothesis we could formulate is that while 60% of the Y species on the surface are involved in the ionic couple as shown in Scheme 28, the remaining 40% presents just one pentafluorophenoxy group bound, while the second pentafluorophenol is just coordinated; thus explaining the N,N-dimethyl-toluidine released during the grafting reaction.

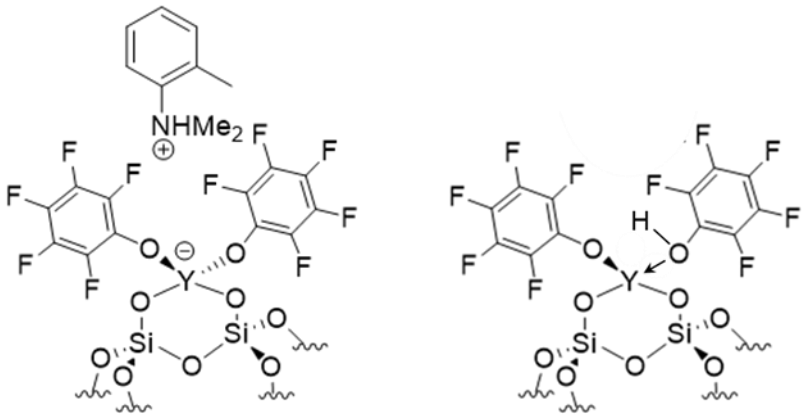

Scheme 28 – Possible surface structures on AS13.

The activating support was then characterized by ^{1}H MAS and ^{13}C CPMAS solid state NMR spectroscopy. In Figure 29 are reported the spectra.

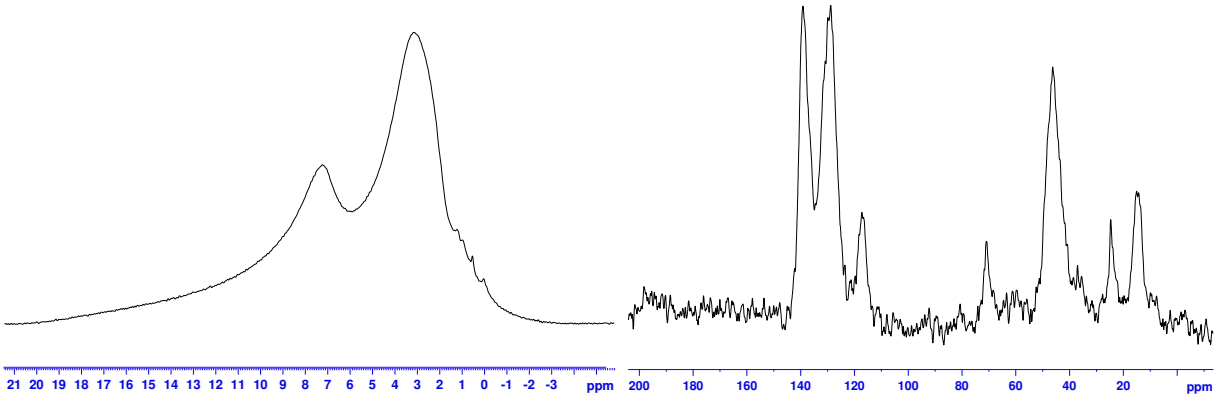

Figure 29 – ^{1}H MAS (left) and ^{13}C CPMAS (right) solid state NMR spectra for AS13.

The ^{1}H spectrum shows quite broad signals with respect to that of P9. It exhibits two peaks, one broad signal centered at 3.3 ppm assigned to the methyls bound to the ammonium and to the phenyl, and one at 7.2 ppm assigned to the aromatic protons of the phenyl group.

The ^{13}C spectrum shows seven peaks. Between 118 and 140 ppm resonate the aromatic carbons of the phenyl, at 45.6 ppm the carbons of the $–NH(CH_3)_2$ fragment of the ammonium, while at 15.5 ppm resonates the CH_3 bound directly to the aromatic ring of the ammonium. At 24.8 and 71.1ppm are the signals of the THF impurities on the surface.

The characterization of AS13 would suggest the synthesis on the surface of a bipodal species of structure $[(\equiv SiO)_2Y(OC_6F_5)_2]^-[HNMe_2(PhMe)]^+$, even though there are some incongruences in the elemental analysis quantifications. The activating support was then tested in ethylene/1-hexene slurry copolymerization as cocatalyst for *rac*-$EtInd_2ZrCl_2$. The results are reported in comparison with the other Y-based activating support.

2.4 Choice of the complex Y{1,3-$C_3H_3(SiMe_3)_2$}$_3$

The molecular precursor used for the synthesis of AS14 and AS15 was Y{1,3-$C_3H_3(SiMe_3)_2$}$_3$. Because of the high stability of the fragment Y-alllyl, the complex was chosen to avoid the opening of siloxane bridges upon grafting on $SiO_{2\text{-}700}$. The complex was synthesized at gram scale following the reaction reported in Scheme 29.

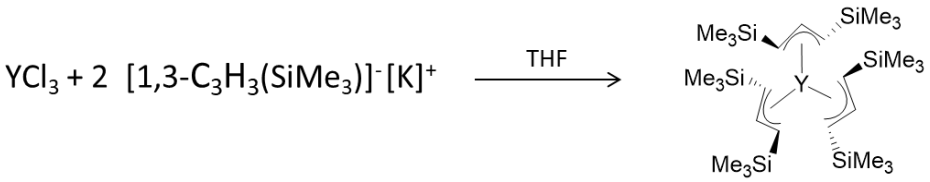

Scheme 29 – Synthesis of Y{1,3-$C_3H_3(SiMe_3)_2$}$_3$

The product was characterized by ^1H and ^{13}C solution NMR in THF. In Figure 30 are reported the spectra.

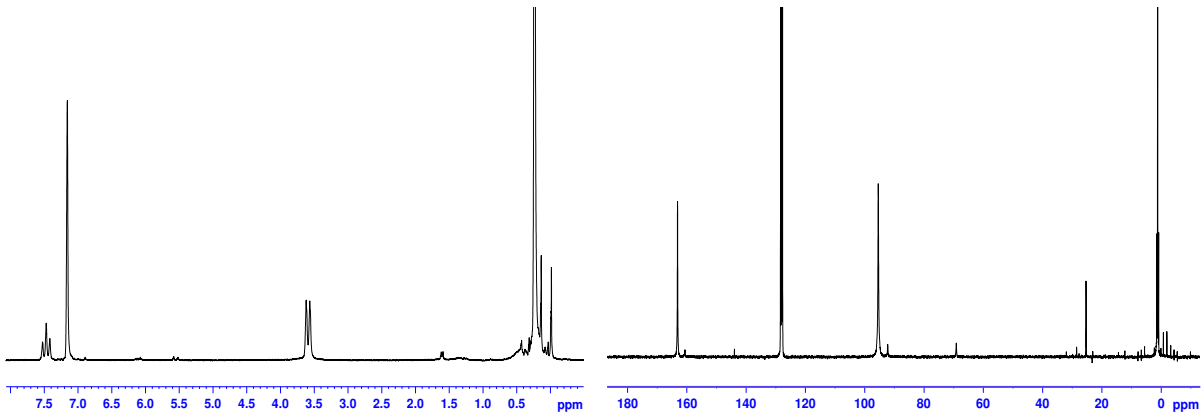

Figure 30 – ^1H (left) and ^{13}C (right) solution NMR spectra for Y{1,3-$C_3H_3(SiMe_3)_2$}$_3$.

The ^1H spectrum displays three signals: a triplet at 7.47 ppm (J = 16.0 Hz) assigned to the allylic proton $Me_3SiCHC\boldsymbol{H}CHSiMe_3$, a doublet at 3.59 ppm (J = 16.4 Hz) attributed to the equivalent protons of the methynes, $Me_3SiC\boldsymbol{H}CHC\boldsymbol{H}SiMe_3$, while the singlet at 0.23 ppm was assigned to the methyls of the trimethylsilyl groups.

The ^{13}C NMR displays also three peaks. The allylic carbon, $Me_3SiCH\boldsymbol{C}HCHSiMe_3$, resonates at 163.2 ppm, at 95.4 ppm resonate the two equivalent carbons $Me_3Si\boldsymbol{C}HCH\boldsymbol{C}HSiMe_3$, while at 1.2 ppm is possible to find the signals of the methyls of the –$SiMe_3$ groups.

The complex was then grafted on both $SiO_{2\text{-}200}$ and $SiO_{2\text{-}700}$ to generate the organometallic precursors for AS14 and AS15.

2.5 Synthesis of $[(\equiv SiO)Y(OC_6F_5)_3]^-[HNMe_2Et]^+$, AS14

The aim in the synthesis of AS14 and AS15, is to isolate well-defined structures on the surface of the support and to investigate if changing the ammonium ion has any effect on the activating support's efficiency.

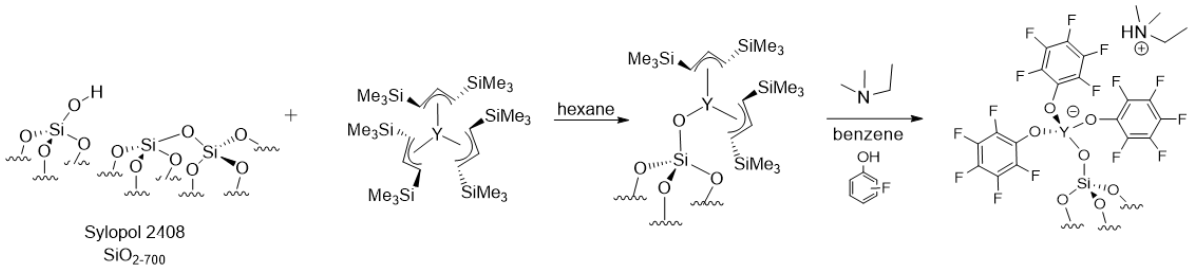

Scheme 30 – Synthesis of AS14.

Scheme 30 depicts the two step synthesis of AS14. Once generated, the grafted yttrium precursor on the surface P10 is functionalized with pentafluorophenol and $NEtMe_2$, to obtain an ionic couple.

2.5.1 Synthesis of $(\equiv SiO)Y\{1,3\text{-}C_3H_3(SiMe_3)_2\}_2$, P10

The chosen silica for the synthesis of P10 was Grace silica Sylopol 2408 dehydroxylated at 700°C. The support was reacted with 1.2 eq. of $Y\{1,3\text{-}C_3H_3(SiMe_3)_2\}_3$ per eq. of SiOH in hexane. The reaction of the complex was almost immediate, the support turned rapidly yellow upon the occurring of the reaction shown in Scheme 31.

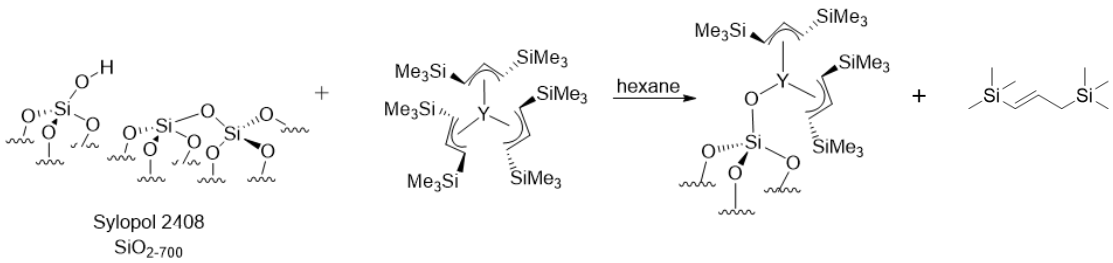

Scheme 31 – Synthesis of P10.

After two hours the reaction was interrupted and the product dried. The obtained bright yellow support was characterized to confirm the structure of the species on the surface.

In figure 31 is reported the DRIFT spectrum of P10.

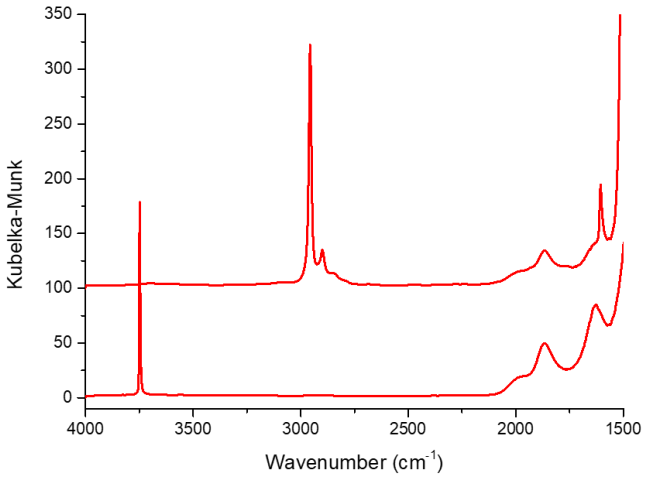

Figure 31 – DRIFT spectra of $SiO_{2\text{-}700}$ (below) and P10 (above).

The analysis of the DRIFT spectrum of P10 confirms that Y{1,3-$C_3H_3(SiMe_3)_2$}$_3$ reacted with all the silanols present on the surface. After the grafting reaction the peak at 3743 cm^{-1} characteristic of the O-H stretching is completely consumed. Between 2750 and 3000 cm^{-1} appear a series of sharp and intense peaks for the C–H stretching of the allyl ligand on the Y centre.

Once confirmed that all the active site on the surface were consumed, P10 was characterized by mass balance analysis to establish the structure of the species on the surface. The $C_3H_4(SiMe_3)_2$ released after the grafting and the hydrolysis of P10 was quantified.

Table 18 – Elemental analysis results and olefin quantification after grafting and hydrolysis of P10.

wt% Y	wt% C	wt% H	C/Y	H/Y	Y mmol g^{-1}	1,3-$C_3H_4(SiMe_3)_2$/Y	
						Grafting	Hydrolysis
3.7	8.54	1.6	17.1 (th.18)	38.1 (th.42)	0.42	0.9 (th. 1)	1.5 (th. 2)

The mass balance analysis evidenced 0.42 mmol g^{-1} of yttrium grafted on the support. It also confirms, together with the quantification of the olefin released, the formation of monopodal Y species with two allyl ligands bound per metal centre. The 8.54 wt% of carbon found on the surface corresponds to a 17.1 C/Y ratio, which is very close to the theoretical value for (≡SiO)Y{1,3-$C_3H_3(SiMe_3)_2$}$_2$, 18 C/Y. The amount of olefin $C_3H_4(SiMe_3)_2$ released during the grafting matches perfectly the generation of monopodal species on the surface, 0.9 olefin/Y

were obtained (th. 1). For what concerns the olefin quantification after hydrolysis, the value obtained is lower than the expected of 2 $C_3H_4(SiMe_3)_2$/Y due to the fact that this di-substituted olefin has a high coordinating ability and tends to remain coordinated to the species on the surface.

This theory is endorsed by the ^{1}H MAS and ^{13}C CPMAS NMR spectroscopy characterization of P10.

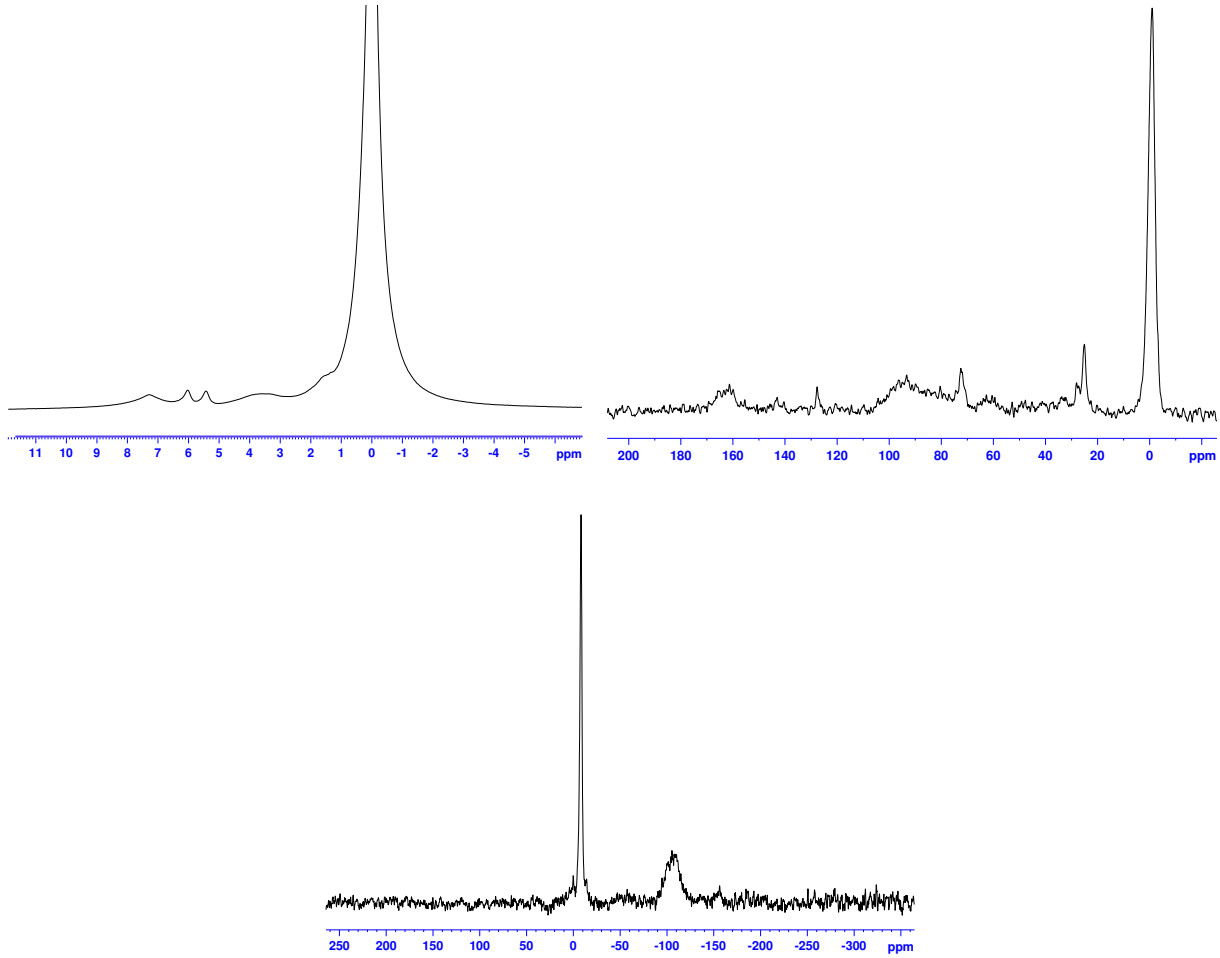

Figure 32 – ^{1}H MAS (top left), ^{13}C CPMAS (top right) and ^{29}Si CPMAS (bottom) NMR spectra acquired for P10.

P10 was characterized by ^{1}H MAS, ^{13}C CPMAS and ^{29}Si CPMAS NMR spectroscopy, acquired the spectra for the sample are reported in Figure 32. The interpretation of the ^{29}Si atom is straightforward, two signals are in fact present in the spectrum, one sharp peak at -8.20 ppm assigned to the silicons of the –$SiMe_3$ substituents of the allyl ligands and of the coordinated olefins, and one broad band centred at -105.4 ppm assigned to the tetrahedral Si of the silica bulk.

The ^{1}H and ^{13}C spectra display signals for both the allyl ligand and the coordinated olefin. The ^{1}H NMR spectrum presents six signals. The intense peak resonating at -0.03 ppm is assigned to the protons of the methyl groups of the $–SiMe_3$ fragments of both the allyl and the olefin. At 7.28 ppm resonate the allylic proton of the central methyne of the allyl ligand while the band at 3.56 ppm is assigned to the protons of the methynes bound to the Si. The remaining peaks are assigned to the protons of the coordinated $Me_3Si\text{-}CH_2\text{-}CH{=}CH_2\text{-}SiMe_3$. At 6.03 ppm resonate the olefinic proton of the allyl group ($–CH_2\text{-}CH{=}$), the peak at 5.42 ppm is assigned to the proton of the $=CHSiMe_3$ fragment, finally the shoulder at 1.45 ppm is attributed to the methylene group.

Likewise the ^{13}C spectrum displays both the signals for the olefin and the allyl ligand. The sharp and intense peak at -0.97 ppm is assigned to the methyls of the $–SiMe_3$ fragments on both species, while the bands at 93.6 and 161.4 ppm are assigned to the methynes of the $=CHSiMe_3$ groups and to the methyne of the allyl ligands respectively. The peaks at 143.2 and 127.7 ppm are assigned to the sp^2 carbons of the olefin while at 28.1 ppm resonates the methylene group of $C_3H_4(SiMe_3)_2$.
Two additional peaks are present at 72.5 and 25.1 ppm due to THF impurities on the surface (from glovebox).

P10 (3.7 wt% Y) was studied by X-ray absorption spectroscopy, EXAFS, (Table 19 and Figure 33), in order to furtherly prove the monopodal nature of the grafted species.

Table 19 – EXAFS parameters for P10[(a)] The error intervals generated by the EXAFS fitting program “RoundMidnight” are indicated between parentheses.

Type of Neighbor	Number of neighbors	Distance (Å)	σ^2 (Å^2)
Y-*O*Si≡	1.1(2)	2.15(2)	0.0056(12)
Y-*C*	5.7[(b)]	2.58(2)	0.0056[(b)]
Y---*O*(*Si*≡)$_2$	0.9(4)	2.36(2)	0.0030(27)
W--*Si*O$_4$	1.1 [(b)]	3.39(4)	0.0082(35)
W--*Si*C$_4$	3.8[(b)]	3.55(7)	0.042(16)

[(a)] Δk: [1.3 - 14 Å^{-1}] - ΔR: [0.6-3.9 Å]; $S_0^2 = 0.66$; $\Delta E_0 = 5.5 \pm 0.9$ eV (the same for all shells); Fit residue: ρ = 11.9 %; Quality factor: $(\Delta\chi)^2/\nu = 4.7$ ($\nu = 16 / 28$). [(b)] Shell constrained to a parameter above.

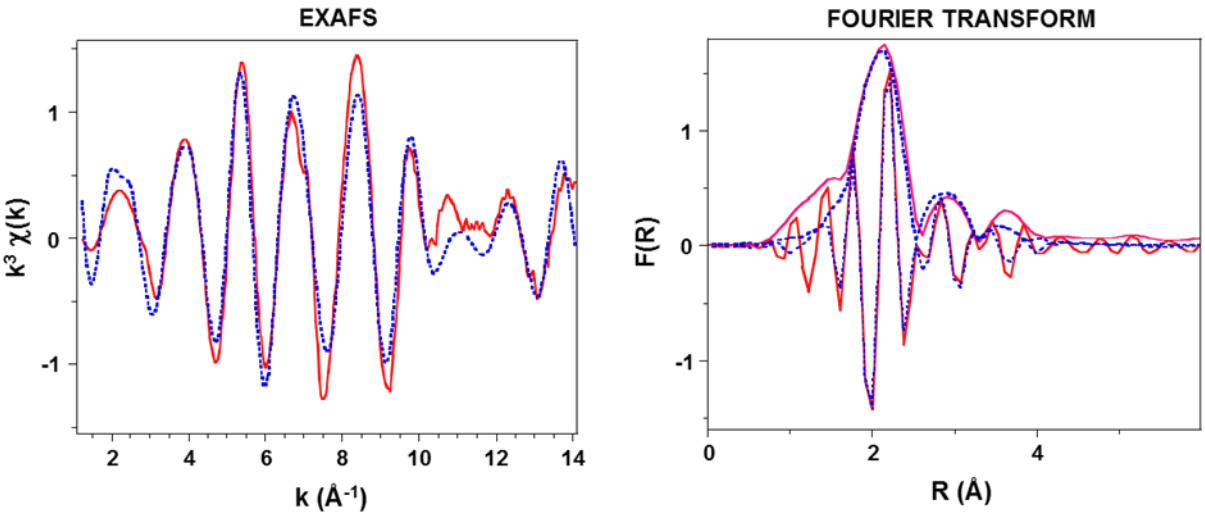

Figure 33 - Y K-edge k^3-weighted EXAFS (left) and Fourier transform (right) of solid $Y(Me_3SiCHCHCHSiMe_3)_2/SiO_{2-700}$. Solid lines: Experimental; Dashed lines: Spherical wave theory.

The parameters thus extracted from the fits of the EXAFS signals are in agreement with a $\equiv SiO\text{-}Y(\eta^3\text{-}Me_3SiCHCHCHSiMe_3)_2$ structure on SiO_{2-700}, with ca. one oxygen atoms at 2.15(2) Å and ca. six carbon atoms at 2.58(2) Å. The Y-O distance is longer but still in the range (2.07-2.14 Å) observed by DRX for the three X-type siloxy ligands in $[Y(OSi(OtBu)_3)_3(\eta^2\text{-}HOSi(OtBu)_3)]$ molecular complex[32] and the Y-C distances are close to those observed in $[Y(\eta^5{:}\eta^1\text{-}C_5Me_4SiMe_2NCMe_3)(PMe_3)(\mu\text{-}H)]_2$ (2.542(6)-2.729(7) Å)[33] or calculated by DFT for the average Y-C distance in a series of $Y(\eta^3\text{-}Me_3SiCHCHCHSiMe_3)_x$ complexes[34] (2.574-2.614 Å). Besides, a contribution of second oxygen neighbors, ca. one to two oxygen atoms at 2.35-2.36(2) Å, would be most probably due to surface siloxane bridges. Similar distances were observed for such types of second oxygen neighbors by XRD in $[Y(OSi(OtBu)_3)_3(\eta^2\text{-}HOSi(OtBu)_3)]$ (2.3538(11)-2.5158(10) Å) or by EXAFS (2.40 Å) in the surface species resulting from the grafting of this last complex onto SiO_{2-700}.[32] Moreover the fits could be also improved by adding contributions of further paths, in particular with two types of silicon back-scatters (at 3.39(4) and 3.55(7) Å for P10), which can be attributed to silicon atoms of X-type siloxy ligands for the shorter distance and to silicon atoms of the $(\eta^3\text{-}Me_3SiCHCHCHSiMe_3)$ allyl ligands for the longer distance.

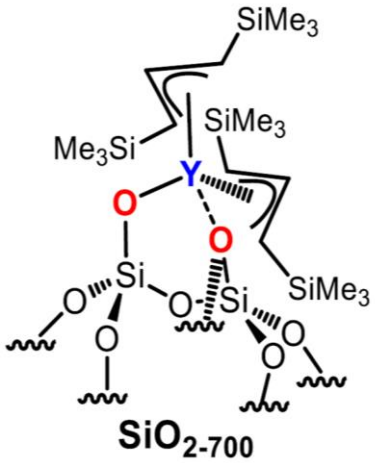

Scheme 32 – Structure of P10 as evidenced by the EXAFS results.

The characterization of P10 clearly shows the formation of monopodal grafted Y species on the surface of structure (≡SiO)Y{1,3-$C_3H_3(SiMe_3)_2$}$_2$. The grafted precursor thus obtained was used then for the synthesis of the activating support AS14.

2.5.2 Functionalization of P10 with pentafluorophenol, AS14

Once obtained the grafted precursor, P10 was functionalized with 3.2 eq. of pentafluorophenol and 1.2 eq. of $NEtMe_2$ to obtain the ionic couple $[(\equiv SiO)Y(OC_6F_5)_3]^-[HNMe_2Et]^+$. The reaction proceeded in benzene overnight.

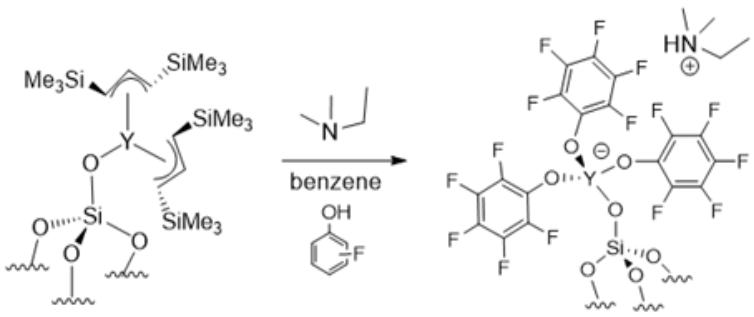

Scheme 33 – Synthesis of AS14.

At the end of the reaction a DRIFT spectrum of the product was acquired to ascertain if all the species on the surface had reacted.

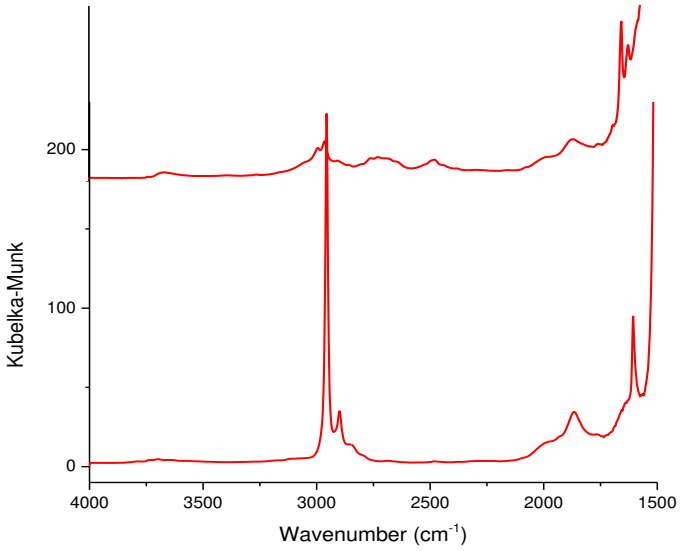

Figure 34 – DRIFT spectra of P10 (below) and AS14 (above).

The spectrum of AS14 sees a great decrease in the peaks around 3000 cm^{-1} confirming that the allyl groups on the Y reacted to be substituted by the pentafluorophenol. This is also proved by the presence of sharp peaks between 1500 and 1600 cm^{-1} of the C=C stretching of the aromatic rings. At 3045 cm^{-1} is present a shoulder for the N-H stretching of the ammonium.

The activating support was further characterized by mass balance analysis. The results are reported in Table 20.

Table 20 – Elemental analysis results for AS14.

wt% Y	wt% C	wt% N	wt% F	C/N	C/Y	N/Y	F/Y	Y mmol g^{-1}
3.66	8.38	0.62	7.66	15.8 (th. 22)	17.0 (th. 22)	1.1 (th. 1)	9.8 (th.15)	0.35

The results reported in Table 20 show clearly that only two pentafluorphenoxy ligands are present per Y on the silica surface and that the desired species wasn't obtained. The presence of 1.1 N/C implies that after the reaction the amine stayed coordinated to the neural grafted species. Scheme 34 reports the structure of AS14, as it was evinced by the characterizations of the product.

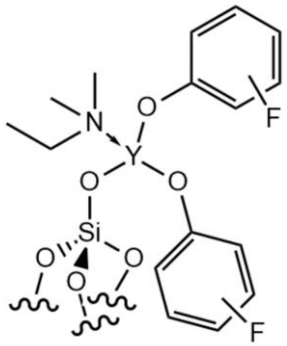

Scheme 34 – Possible structure of AS14, according to the characterization results.

AS14 was then characterized by ^{1}H MAS and ^{13}C CPMAS solid state NMR spectroscopy. In Figure 35 are reported the spectra.

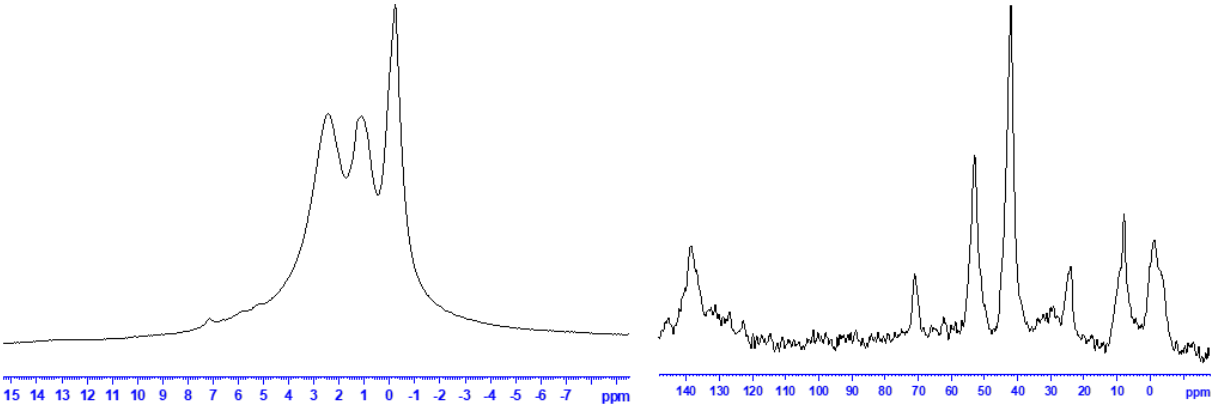

Figure 35 – ^{1}H MAS (left) and ^{13}C CPMAS (right) solid state NMR spectra for AS12.

The ^{1}H NMR spectrum shows at 2.57 ppm the peak relative to the carbons of the methyl of the $–NCH_3$ and of the methylene of the $–NCH_2CH_3$ fragment of the amine coordinated to the surface, at 1.27 ppm resonate the methyls of $–NCH_2CH_3$. The signal at -0.15 ppm is attributed to the $–SiMe_3$ of the olefin, while at 5.92 and 5.27 ppm resonate the two olefinic carbons. It is difficult to say if the olefin is just adsorbed on the silica surface (like in the case of the grafted Y precursor P10), or if it has been transferred to the surface during the functionalization reaction.

At the ^{13}C NMR, the peaks at 52.9, 42.0 and 7.8 ppm are respectively attributed to the methylene of the $–NCH_2CH_3$, the methyls of the $–NCH_3$ and the methyl of the $–NCH_2CH_3$. At 138.6 ppm there's the signal due to the olefinic carbons of the olefin on the surface. At -1.4 ppm it is possible to see the resonance of the $–SiMe_3$ fragments of the olefin on the surface. The peaks at 71.1 and 25.0 ppm are assigned to the carbons of THF impurities present on the surface.

Although the conversion in ionic couple was not achieved for the totality of the species on the surface, the activating support was then tested in ethylene/1-hexene slurry copolymerization as cocatalyst for *rac*-EtInd$_2$ZrCl$_2$. The results are going to be reported in comparison with the other Y-based activating support.

2.6 Synthesis of $[(\equiv SiO)_2Y(OC_6F_5)_2]^-[HNMe_2Et]^+$, AS15

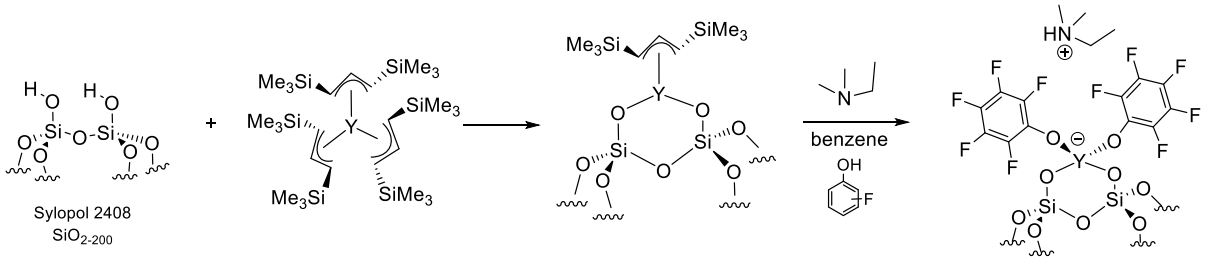

Scheme 35 – Synthesis of AS15.

Scheme 35 depicts the two step synthesis of AS15; like in the case of AS14 to obtain the ionic couple it was necessary to add an amine to create the counter-cation.

2.6.1 Synthesis of $(\equiv SiO)_2Y\{1,3\text{-}C_3H_3(SiMe_3)_2\}$, P11

The chosen silica for the synthesis of P11 was Grace silica Sylopol 2408 partially dehydroxylated at 200°C. The support was reacted with 1.2 eq. of $Y\{1,3\text{-}C_3H_3(SiMe_3)_2\}_3$ per 2 eq. of SiOH in hexane. The reaction of the complex was almost immediate, the support turned rapidly yellow upon the occurring of the reaction showed in Scheme 36.

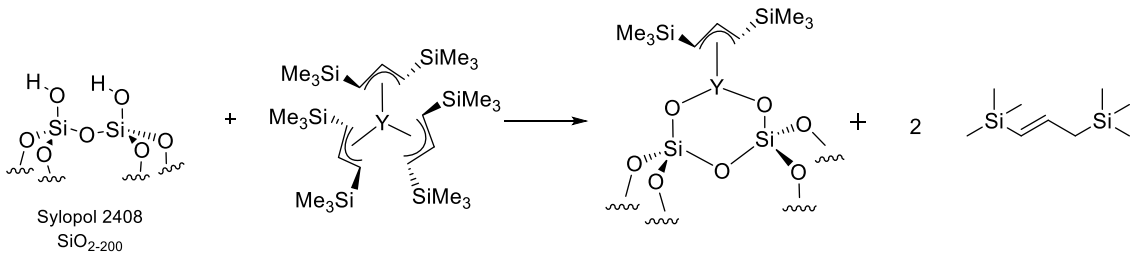

Scheme 36 – Synthesis of P11.

After two hours the reaction was interrupted and the product dried. The obtained light yellow support was characterized by DRIFT spectroscopy, in Figure 36 are reported the spectra of the surface before and after the reaction.

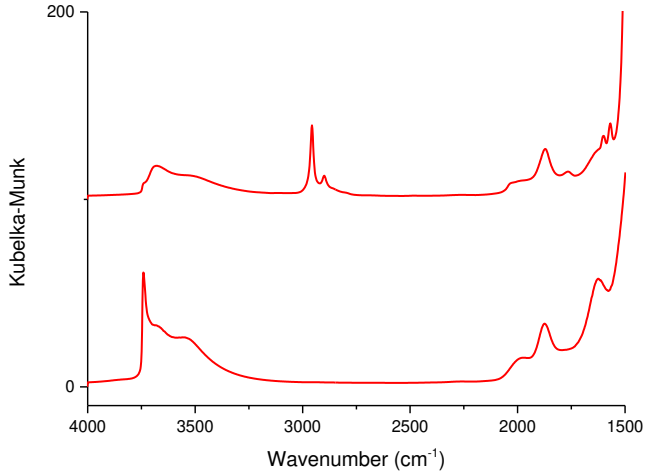

Figure 36 – DRIFT spectra for $SiO_{2\text{-}200}$ (below) and P11 (above).

The analysis of the DRIFT spectrum of P11, reported in Figure 36, confirms that Y{1,3-$C_3H_3(SiMe_3)_2$}$_3$ reacted with all the accessible silanols present on the surface. After the grafting reaction the peak at 3743 cm^{-1}, characteristic of the O-H stretching of isolated silanols, is completely consumed. Between 2750 and 3000 cm^{-1} appear two sharp peaks for the C–H stretching of the allyl ligand on the Y centre.

To confirm the bipodal nature of the grafted species, P11 was characterized by mass balance analysis and the amount of olefin released during the grafting and the hydrolysis of P11 was quantified. The results are reported in Table 21.

Table 21 – Elemental analysis and olefin quantification results for P11.

wt% Y	wt% C	wt% H	C/Y	H/Y	Y mmol g^{-1}	1,3-$C_3H_4(SiMe_3)_2$/Y	
						Grafting	Hydrolysis
4.92	5.15	1.11	7.75 (th.9)	19.9 (th.21)	0.55	1.7 (th. 2)	0.45 (th.1)

The mass balance analysis evidenced 0.55 mmol g^{-1} of yttrium grafted on the support. It also confirms, together with the quantification of the olefin released, the formation of bipodal Y species with one allyl ligand bound per metal centre. The 5.15 wt% of carbon found on the surface corresponds to a 7.75 C/Y ratio, which is very close to the theoretical value for (≡SiO)$_2$Y{1,3-$C_3H_3(SiMe_3)_2$}, 9 C/Y. The amount of olefin $C_3H_4(SiMe_3)_2$ released during the grafting matches the generation of bipodal species on the surface, 1.7 olefin/Y were obtained

(th. 2). For what concerns the olefin quantification after hydrolysis, the value obtained is below the expected of 1 $C_3H_4(SiMe_3)_2$/Y, as found for the case of P10, due to the fact that this olefin has a high coordinating ability and tends to remain coordinated to the Y species on the surface.

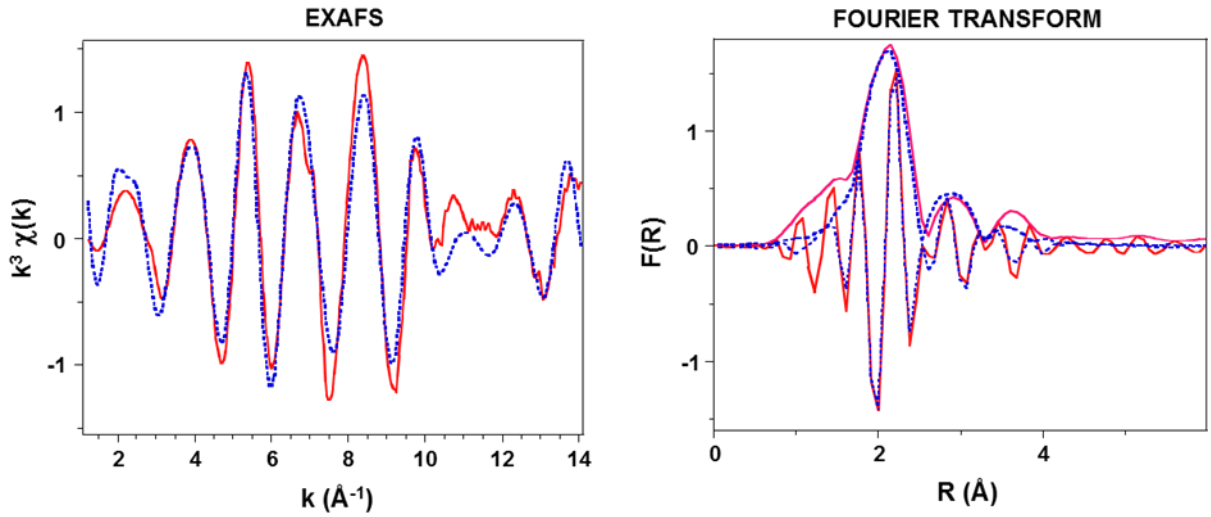

Figure 37 – Y K-edge k^3-weighted EXAFS (left) and Fourier transform (right) of solid $Y(Me_3SiCHCHCHSiMe_3)_2/SiO_{2-700}$. Solid lines: Experimental; Dashed lines: Spherical wave theory.

P11 was studied by X-ray absorption spectroscopy (Table 22 and Figure 37), in order to confirm the bipodal nature of the species.

Table 22 – EXAFS parameters for P11.[(a)] The error intervals generated by the EXAFS fitting program "RoundMidnight" are indicated between parentheses.

Type of Neighbour	Number of neighbours	Distance (Å)	σ^2 (Å^2)
*Y-O*Si≡	2.1(1)	2.15(1)	0.0044(7)
Y-C	2.8[(b)]	2.56(2)	0.0044[(b)]
Y---O(Si≡)$_2$	1.3(4)	2.35(2)	0.0029(19)
*W--Si*O$_4$	2.1 [(b)]	3.43(3)	0.0106(31)
*W--Si*C$_4$	1.9[(b)]	3.63(5)	0.0115(41)

[(a)] Δk: [1.3 - 14 Å^{-1}] - ΔR: [0.5-4.00 Å]; S_0^2 = 0.66; ΔE_0 = 5.1 ± 0.9 eV (the same for all shells); Fit residue: ρ = 10.7 %; Quality factor: $(\Delta\chi)^2/\nu$ = 3.9 (ν = 16 / 28). [(b)] Shell constrained to a parameter above.

The parameters thus extracted from the fits of the EXAFS signals are in agreement with a $(\equiv SiO)_2Y(\eta^3\text{-}Me_3SiCHCHCHSiMe_3)$ structure on SiO_{2-200}, with ca. two oxygen atoms at 2.15(1) Å and ca. three carbon atoms at 2.56(2) Å. The Y-O distance is longer but still in the range (2.07-2.14 Å) observed by DRX for the three X-type siloxy ligands in $[Y(OSi(OtBu)_3)_3(\eta^2\text{-}HOSi(OtBu)_3)]$ molecular complex[32] and the Y-C distances are close to those observed in $[Y(\eta^5{:}\eta^1\text{-}$

$C_5Me_4SiMe_2NCMe_3)(PMe_3)(\mu\text{-}H)]_2$ (2.542(6)-2.729(7) Å)[33] or calculated by DFT for the average Y-C distance in a series of $Y(\eta^3\text{-}Me_3SiCHCHCHSiMe_3)_x$ complexes[34] (2.574-2.614 Å). Besides, a contribution of second oxygen neighbors, ca. one to two oxygen atoms at 2.35-2.36(2) Å, would be most probably due to surface siloxane bridges. Similar distances were observed for such types of second oxygen neighbors by XRD in $[Y(OSi(OtBu)_3)_3(\eta^2\text{-}HOSi(OtBu)_3)]$ (2.3538(11)-2.5158(10) Å) or by EXAFS (2.40 Å) in the surface species resulting from the grafting of this last complex onto $SiO_{2\text{-}700}$.[32] Moreover the fits could be also improved by adding contributions of further paths, in particular with two types of silicon back-scatters (at 3.43(3) and 3.63(5) Å for P11, which can be attributed to silicon atoms of X-type siloxy ligands for the shorter distance and to silicon atoms of the $(\eta^3\text{-}Me_3SiCHCHCHSiMe_3)$ allyl ligands for the longer distance.

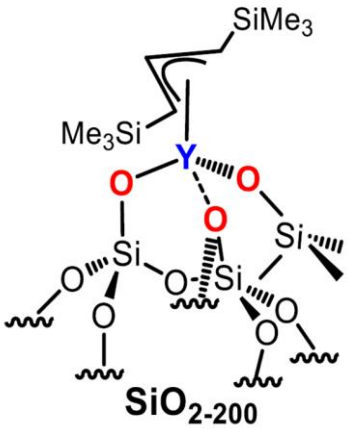

Scheme 37 – Structure of P11 as evidenced from the EXAFS results.

The product was then furtherly characterized by ^1H MAS and ^{13}C CPMAS solid state NMR.

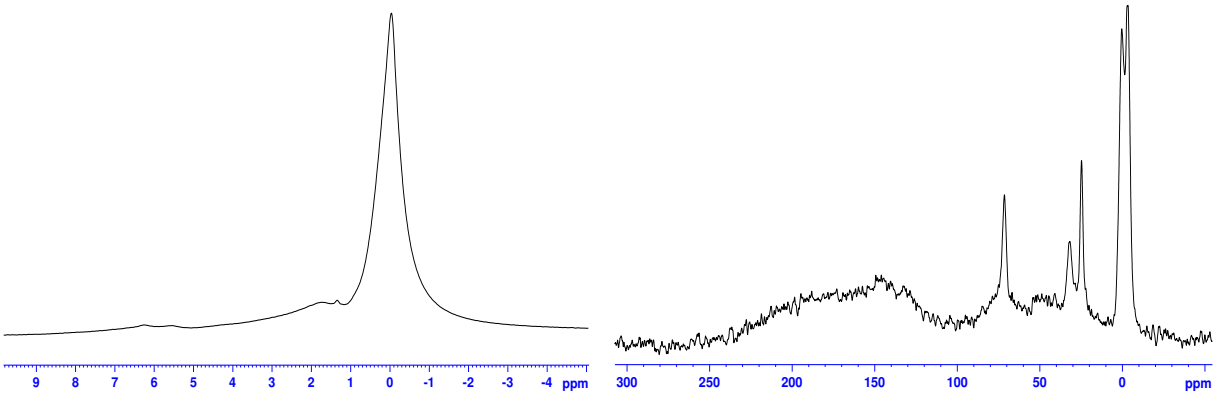

Figure 38 – ^1H MAS (left) and ^{13}C CPMAS (right) solid state NMR spectra for AS12.

Like in the case of P10, the ^1H and ^{13}C spectra display both signals for the allyl ligand and the coordinated olefin. The ^1H NMR spectrum display five signals. At -0.04 ppm resonate the

proton of the –$SiMe_3$ fragment of both allyl and olefin. At 1.74 ppm resonate the signal of the methyne of the –$CHSiMe_3$ of the allyl, the signal of the proton of the allylic methyne is not visible because of the low intensity and broadness of the signals. At 6.26 ppm resonate the olefinic proton of the –CH_2-CH= group, the peak at 5.58 ppm is assigned to the olefinic proton of the =$CHSiMe_3$ group, and resonance at 1.34 ppm is attributed to the methylene of the –CH_2SiMe_3 fragment.

The ^{13}C NMR spectrum exhibits two peaks for the –$SiMe_3$; the signal at -3.39 ppm is assigned to the trimethylsilyl groups of the allyl while the one at 0.35 ppm to those of the olefin. Centred around 133 ppm is a very broad signal under which fall the resonances of the allylic carbons of the allyl and of the sp^2 C of the olefin. Finally, the peak at 31.8 ppm is assigned to the methylene of the –CH_2SiMe_3 moiety of the coordinated olefin. The two additional peaks at 71.4 and 24.7 ppm are attributed to THF impurities on the surface.

2.6.2 Functionalization of P11 with pentafluorophenol, AS15

Once obtained the grafted precursor, P11 was functionalized with 2.2 eq. of pentafluorophenol and 1.2 eq. of $NEtMe_2$ to obtain the ionic couple $[(\equiv SiO)_2Y(OC_6F_5)_2]^-[HNMe_2Et]^+$. The reaction proceeded in benzene overnight.

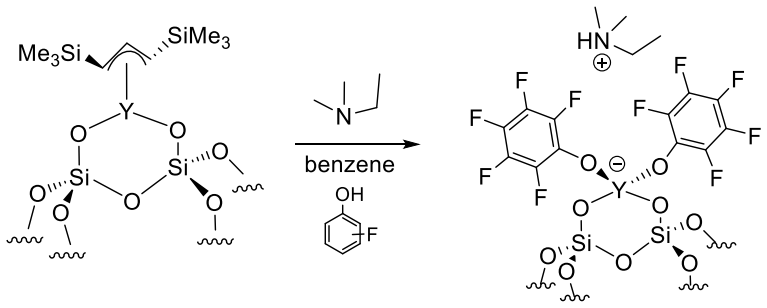

Scheme 38 – Synthesis of AS15.

At the end of the reaction a DRIFT spectrum of the product was acquired. In Figure 39 is reported the spectrum for AS15.

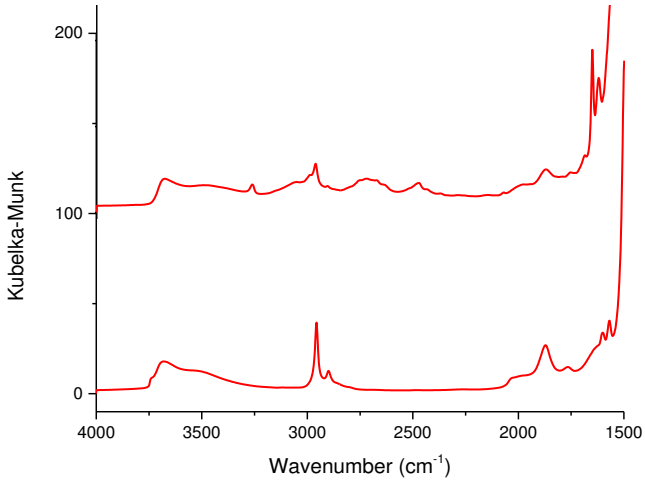

Figure 39 – DRIFT spectra for P11 (bottom) and AS15 (top).

The DRIFT spectrum acquired after the functionalization, positively confirms the formation of the ionic couple. The peak at 3077 cm^{-1} is in fact due to the N-H stretching of the ammonium. Upon functionalization with pentafluorophenol at the DRIFT spectrum also appear sharp peaks between 1500 and 1600 cm^{-1}, characteristic of the C=C stretching of the aromatic ring.

The formation of the ionic couple was further characterized by mass balance analysis of AS15. The results are reported in Table 23.

Table 23 – Elemental analysis results for AS15.

wt% Y	wt% C	wt% N	wt% F	C/Y	N/Y	F/Y	Y mmol g^{-1}
3.86	4.8	1.02	11.4	9.2 (th. 16)	1.7 (th. 1)	9.8 (th.10)	0.43

From the elemental analysis the presence of 0.43 mmol g^{-1} of Y was found on the surface. The fluorine quantification confirms the presence of two pentafluorophenoxy ligands bound per metal centre. The 11.4 wt% of fluorine found on the surface corresponds in fact to 9.8 F/Y ratio, close to the theoretical amount of 10 wanted for the pure $[(\equiv SiO)_2Y(OC_6F_5)_2]^-[HNMe_2Et]^+$.

It appears also that more than one amine per Y stays coordinated, N/Y is in fact 1.7 instead of 1. The amount of C found was also underestimated.

The surface was then characterized by ^{1}H MAS and ^{13}C CPMAS solid state NMR. The spectra are reported in Figure 40.

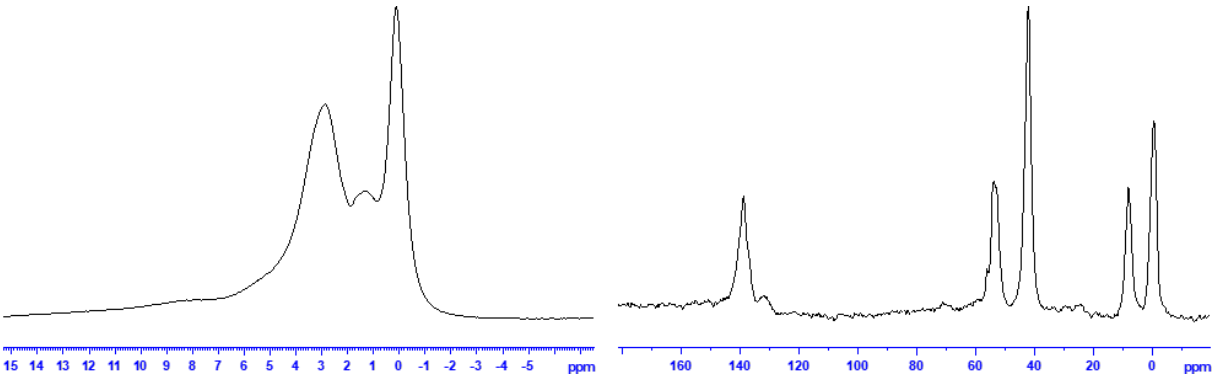

Figure 40 – ^{1}H MAS (left) and ^{13}C CPMAS (right) solid state NMR spectra for AS15.

From the spectra reported in Figure 40, it was clear that some of the ligand remained on the surface after the functionalization reaction. Like in the case of AS14 it is difficult to say if is just physisorbed on the activating support or if the allyl ligand underwent a transfer to the surface during the functionalization reaction. The peak at 0.12 ppm in the ^{1}H spectrum and the signals at -0.56 ppm and 139 ppm at the ^{13}C can be assigned in fact to the $–SiMe_3$ fragments and the olefinic carbons of the residual $Me_3Si\text{-}CH_2\text{-}CH{=}CH_2\text{-}SiMe_3$. At the ^{1}H spectrum are present other two peaks at 1.38 and 2.88 ppm assigned, the first to the methyl of the $–NCH_2CH_3$ moiety, and the second to the methyls directly bound to the N and the methylene of the $–NCH_2CH_3$. Three additional peaks are also present in the ^{13}C spectrum for the alkyl fragments bound to the N at 53.8, 42.1 and 8.1 ppm. These peaks are assigned respectively to the methylene of the $–NCH_2CH_3$, the methyl groups bound to the N and the methyl of the $–NCH_2CH_3$.

The activating support was characterized and the formation of the ionic couple on the surface was confirmed. It was also seen that some of the olefin remained coordinated on the surface after the functionalization and the washing and drying of the product. AS15 was then tested in ethylene/1-hexene slurry copolymerization as cocatalyst for *rac*-$EtInd_2ZrCl_2$. The results are reported in comparison with the other Y-based activating support.

2.7 Test in polymerization of the Y-based AS with *rac*-$EtInd_2ZrCl_2$

The activating supports AS12-15 were tested in ethylene/1-hexene slurry copolymerization in combination with *rac*-$EtInd_2ZrCl_2$. The conditions used were the same employed for AS1. The tests were conducted in 300 mL heptane, at 80°C for 30 minutes at 4 bars of ethylene pressure.

20 mg of activating support were used during the polymerizations and TiBA in concentration 1 mM was employed as scavenger. In Table 24 are reported the polymerization results for the five activating supports.

Table 24 – Polymerization results obtained with the activating supports AS12-15 in combination with *rac*-EtInd$_2$ZrCl$_2$. General conditions: 80°C; 4 bars C_2H_4; 30 minutes; 300 mL heptane; [TiBA] 1mM.

run	Catalyst	m sup mg	Zr/M$_{surface}$	Zr Wt%	Zr µmol	[Zr] µM	1-hexene mol%	Yield g	Activity g g$^{-1}_{cat}$ h^{-1}
6	AS12	20.2	0.10	0.30	0.67	2.0	18.1	0.05	4
7	AS13	20.4	0.06	0.29	0.65	2.1	19.8	0.34	33
8	AS14	20.0	0.07	0.28	0.61	2.0	19.8	0.30	30
9	AS15	20.0	0.08	0.32	0.70	2.0	18.6	0.54	54

All the yttrium based activators showed very low, in the case of AS12 negligible, activities. The higher productivity obtained was 54 g g$^{-1}_{cat}$ h^{-1} for the system AS15/*rac*-EtInd$_2$ZrCl$_2$. Furthermore, the same problem of deactivation observed for AS1 was seen also for these systems, as it is clearly depicted in the plot in Figure 41.

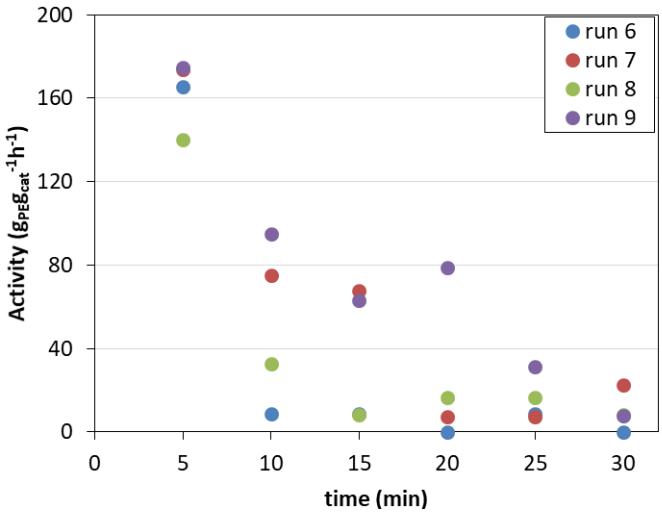

Figure 41 – Productivity profiles for the polymerization tests conducted with AS12-15.

To rationalize the low activity obtained it is worthy to notice a few points. The first is that for the four systems it was not easy to obtain a well-defined activator on the surface, while the grafting of the two Y complexes generated structurally defined precursors on both silicas, the functionalization with pentafluorophenol was not as straightforward; in addition, in the cases of AS12 and AS13, on the surface were still present traces of THF impurities, probably coming

from the starting molecular complex. This could have led to a not complete activation of the zirconocene complex.

The polymers obtained in runs 6-9 were characterized by DSC and HT-SEC. The results are reported in Table 25.

Table 25 – DSC and HT-SEC characterization results for the polymer obtained in run 6-9.

run	Catalyst	Activity g g^{-1}_{cat} h^{-1}	T_f °C	Crystallinity %	M_n g mol^{-1}	M_w g mol^{-1}	PDI
6	AS12	4	124	30.0	-	-	-
7	AS13	33	123	27.7	-	-	-
8	AS14	30	124 126	36.0	27500	66000	2.4
9	AS15	54	124	40.9	-	-	-

The polymer obtained is an LLDPE resin, compatible with the characteristics of the products synthesized by *rac*-$EtInd_2ZrCl_2$.

The mediocre results obtained with these systems didn't push us to continue the investigation on Y based activating supports.

Conclusions

In this chapter was presented the synthesis, characterization and application of nine different activating supports based on aluminium and yttrium.

AS7-11 were activating supports of general structure $[(\equiv SiO)_nAlX(OC_6F_5)_{(3-n)}]^-[HNR_3]^+$, where X = Cl, F and n=1, 2. The aim was to synthesize well-defined halogenated aluminates to increase the acidity of the activating support and study the effect on the activity. The different supported aluminium species were well-defined, highlighting a good control of the surface chemistry. These systems were then tested in ethylene/1-hexene slurry copolymerization as cocatalysts of *rac*-$EtInd_2ZrCl_2$. The activities obtained for all the catalytic systems were definitely lower than the reference AS1 (1111 $g_{PE}\, g_{cat}^{-1}\, h^{-1}$), the maximum productivity was obtained with AS9 in the order of 40 $g_{PE}\, g_{cat}^{-1}\, h^{-1}$. The reason behind the low activity could be ascribed to the formation of a too strong interaction of the kind Al-X-Zr between the activating supports and the active zirconocene. The exception in this series of activators was AS8, of structure $[(\equiv SiO)_2AlCl_{2)}]^-[HNEtMe_2]^+$ which showed no activity towards the activation of the tested metallocene.

The second set of activators presented in this Chapter is AS12-15. These activating supports are homologous to AS1 and AS2 but the metal centre grafted on the surface was yttrium instead of Al. In this case the objective was to increase the strength of the M-O bond on the surface of the support to avoid the deactivation phenomena discussed in Chapter II. Both mono- and bi-podal activating supports were synthesized starting from two different Y precursors. The four species obtained were then tested in ethylene/1-hexene slurry copolymerization as cocatalysts of *rac*-$EtInd_2ZrCl_2$. Also in this case the recorded activity for the catalytic systems were very low. The most efficient support was AS15 with 54 $g_{PE}\, g_{cat}^{-1}\, h^{-1}$ of productivity. This could be due to the fact that passing from Al to Y the ionic nature of the M-O bond increases, affecting the activation ability of AS12-15.

Although the Y-based activating supports presented in this chapter demonstrated low efficiency as activators for metallocene catalysts in slurry ethylene polymerization, in the second section of this chapters was presented the synthesis of four neutral grafted Y species, well-defined structurally: P8-11.

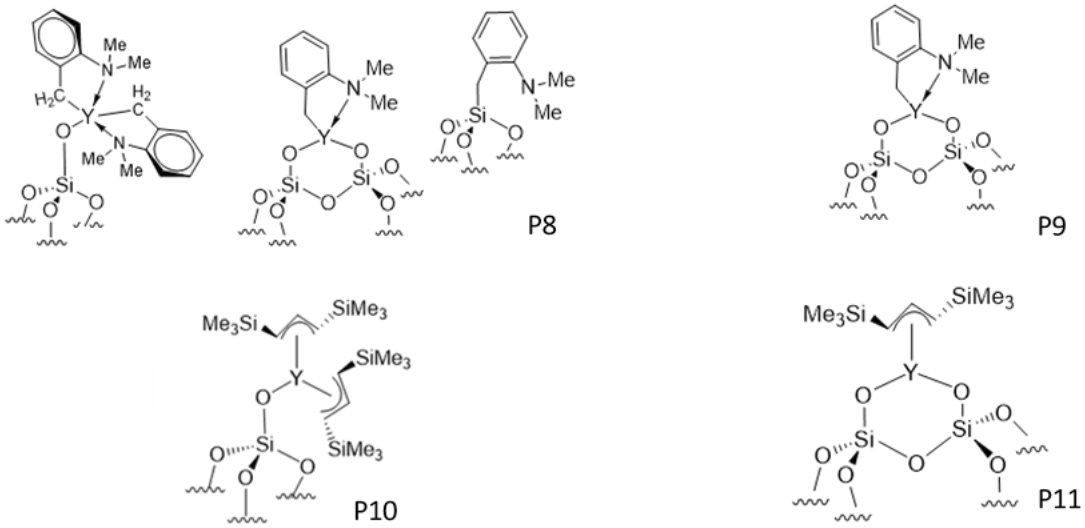

Figure 42 – Well-defined grafted Y species synthesized.

Y catalysts are widely known to be active in olefin polymerization,[35–37] in Chapter V we exploit the species shown in Figure 42 as catalysts in ethylene slurry polymerization.

Refecences

(1) Severn, J. R.; Chadwick, J. C.; Duchateau, R.; Friederichs, N. "Bound but Not Gagged"Immobilizing Single-Site α-Olefin Polymerization Catalysts. *Chem. Rev.* 2005, *105* (11), 4073–4147. https://doi.org/10.1021/cr040670d.

(2) *Tailor-Made Polymers: Via Immobilization of Alpha-Olefin Polymerization Catalyst*; Severn, J., Ed.; Wiley-VCH: Weinheim, 2008.

(3) Velthoen, M. E. Z.; Muñoz-Murillo, A.; Bouhmadi, A.; Cecius, M.; Diefenbach, S.; Weckhuysen, B. M. The Multifaceted Role of Methylaluminoxane in Metallocene-Based Olefin Polymerization Catalysis. *Macromolecules* 2018, *51* (2), 343–355. https://doi.org/10.1021/acs.macromol.7b02169.

(4) Prades, F.; Broyer, J.-P.; Belaid, I.; Boyron, O.; Miserque, O.; Spitz, R.; Boisson, C. Borate and MAO Free Activating Supports for Metallocene Complexes. *ACS Catal.* 2013, *3* (10), 2288–2293. https://doi.org/10.1021/cs400655y.

(5) Prades, F.; Boisson, C.; Spitz, R.; Razavi, A. Activating Supports for Metallocene Catalysis. WO2005075525 (A2), August 18, 2005.

(6) Prades, F.; Spitz, R.; Boisson, C.; Sirol, S.; Razavi, A. Transition Metal Complexes Supported on Activating Fluorinated Support. WO2007014889 (A1), February 8, 2007.

(7) Prades, F.; Spitz, R.; Boisson, C.; Sirol, S.; Razavi, A. Activating Fluorinated Supports with Iron-Based Non-Metallocene Complexes. WO2007014890 (A1), February 8, 2007.

(8) Kermagoret, A.; Kerber, R. N.; Conley, M. P.; Callens, E.; Florian, P.; Massiot, D.; Delbecq, F.; Rozanska, X.; Copéret, C.; Sautet, P. Chlorodiethylaluminum Supported on Silica: A Dinuclear Aluminum Surface Species with Bridging M2-Cl-Ligand as a Highly Efficient Co-Catalyst for the Ni-Catalyzed Dimerization of Ethene. *J. Catal.* 2014, *313*, 46–54. https://doi.org/10.1016/j.jcat.2014.02.006.

(9) Bartram, M. E.; Michalske, T. A.; Rogers, J. W. A Reexamination of the Chemisorption of Trimethylaluminum on Silica. *J. Phys. Chem.* 1991, *95* (11), 4453–4463. https://doi.org/10.1021/j100164a054.

(10) Anwander, R.; Palm, C.; Groeger, O.; Engelhardt, G. Formation of Lewis Acidic Support Materials via Chemisorption of Trimethylaluminum on Mesoporous Silicate MCM-41. *Organometallics* 1998, *17* (10), 2027–2036. https://doi.org/10.1021/om9710632.

(11) Kerber, R. N.; Kermagoret, A.; Callens, E.; Florian, P.; Massiot, D.; Lesage, A.; Copéret, C.; Delbecq, F.; Rozanska, X.; Sautet, P. Nature and Structure of Aluminum Surface Sites Grafted on Silica from a Combination of High-Field Aluminum-27 Solid-State NMR Spectroscopy and First-Principles Calculations. *J. Am. Chem. Soc.* 2012, *134* (15), 6767–6775. https://doi.org/10.1021/ja3008566.

(12) Pelletier, J.; Espinas, J.; Vu, N.; Norsic, S.; Baudouin, A.; Delevoye, L.; Trébosc, J.; Le Roux, E.; Santini, C.; Basset, J.-M.; Gauvin, R. M.; Taoufik, M. A Well-Defined Silica-Supported Aluminium Alkyl through an Unprecedented, Consecutive Two-Step Protonolysis–Alkyl Transfer Mechanism. *Chem. Commun.* 2011, *47* (10), 2979. https://doi.org/10.1039/c0cc04986g.

(13) Popoff, N.; Espinas, J.; Pelletier, J.; Szeto, K. C.; Thivolle-Cazat, J.; Delevoye, L.; Gauvin, R. M.; Taoufik, M. Design and Application of a Hybrid Material Featuring Well-Defined, Tuneable Grafting Sites for Supported Catalysis. *ChemCatChem* **2013**, *5* (7), 1971–1977. https://doi.org/10.1002/cctc.201200850.

(14) Metz, M. V.; Sun, Y.; Stern, C. L.; Marks, T. J. Weakly Coordinating Al-, Nb-, Ta-, Y-, and La-Based Perfluoroaryloxymetalate Anions as Cocatalyst Components for Single-Site Olefin Polymerization. *Organometallics* **2002**, *21* (18), 3691–3702. https://doi.org/10.1021/om020087s.

(15) Krieg, V.; Weidlein, J. Die schwingungsspektren von di-n-propyl- und di-isobutylaluminium-flrourid. *J. Organomet. Chem.* **1970**, *21* (2), 281–284. https://doi.org/10.1016/S0022-328X(00)83624-4.

(16) Hoffmann, E. G. Adiabatische Kryometrie Und Ihre Anwendung Auf Organoaluminium-Verbindungen. *Justus Liebigs Ann. Chem.* **1960**, *629* (1), 104–121. https://doi.org/10.1002/jlac.19606290110.

(17) Benn, R.; Janssen, E.; Lehmkuhl, H.; Rufińska, A. "Ethylaluminiumdiethoxid" - Ein Gemisch einer Vielzahl von Verbindungen. *J. Organomet. Chem.* **1987**, *333* (2), 181–185. https://doi.org/10.1016/0022-328X(87)85149-5.

(18) Cottrell, T. L. *The Strengths of Chemical Bonds*; Butterworths: London, 1958.

(19) Darwent, B. deB. *Bond Dissociation Energies in Simple Molecules,*; NSRDS-NBS-31; NATIONAL STANDARD REFERENCE DATA SYSTEM, 1970.

(20) Benson, S. W. III - Bond Energies. *J. Chem. Educ.* **1965**, *42* (9), 502. https://doi.org/10.1021/ed042p502.

(21) Kerr, J. A. Bond Dissociation Energies by Kinetic Methods. *Chem. Rev.* **1966**, *66* (5), 465–500. https://doi.org/10.1021/cr60243a001.

(22) Li, J.; DiVerdi, J. A.; Maciel, G. E. Chemistry of the Silica Surface: Liquid−Solid Reactions of Silica Gel with Trimethylaluminum. *J. Am. Chem. Soc.* **2006**, *128* (51), 17093–17101. https://doi.org/10.1021/ja065497c.

(23) Weichert, K.; Carlson, B.; Reinke, H.; Krempner, C. A Dimeric Aluminium Hydroxide Supported by a New Disiloxide Ligand. *Dalton Trans.* **2010**, *39* (48), 11513. https://doi.org/10.1039/c0dt00507j.

(24) Szeto, K. C.; Jones, Z. R.; Merle, N.; Rios, C.; Gallo, A.; Le Quemener, F.; Delevoye, L.; Gauvin, R. M.; Scott, S. L.; Taoufik, M. A Strong Support Effect in Selective Propane Dehydrogenation Catalyzed by Ga(*i* -Bu) $_3$ Grafted onto γ-Alumina and Silica. *ACS Catal.* **2018**, *8* (8), 7566–7577. https://doi.org/10.1021/acscatal.8b00936.

(25) Roberts, J. A. S.; Chen, M.-C.; Seyam, A. M.; Li, L.; Zuccaccia, C.; Stahl, N. G.; Marks, T. J. Diverse Stereocontrol Effects Induced by Weakly Coordinating Anions. Stereospecific Olefin Polymerization Pathways at Archetypal C_s - and C_1 -Symmetric Metallocenium Catalysts Using Mono- and Polynuclear Halo-Perfluoroarylmetalates as Cocatalysts. *J. Am. Chem. Soc.* **2007**, *129* (42), 12713–12733. https://doi.org/10.1021/ja0680360.

(26) Chen, M.-C.; Roberts, J. A. S.; Seyam, A. M.; Li, L.; Zuccaccia, C.; Stahl, N. G.; Marks, T. J. Diversity in Weakly Coordinating Anions. Mono- and Polynuclear

Halo(Perfluoroaryl)Metalates as Cocatalysts for Stereospecific Olefin Polymerization: Synthesis, Structure, and Reactivity. *Organometallics* **2006**, *25* (11), 2833–2850. https://doi.org/10.1021/om0508334.

(27) Arndt, P.; Spannenberg, A.; Baumann, W.; Burlakov, V. V.; Rosenthal, U.; Becke, S.; Weiss, T. Reactions of Zirconocene 2-Vinylpyridine Complexes with Diisobutylaluminum Hydride and Fluoride. *Organometallics* **2004**, *23* (20), 4792–4795. https://doi.org/10.1021/om049589r.

(28) Sun, Y.; Metz, M. V.; Stern, C. L.; Marks, T. J. Al-, Nb-, and Ta-Based Perfluoroaryloxide Anions as Cocatalysts for Metallocene-Mediated Ziegler−Natta Olefin Polymerization. *Organometallics* **2000**, *19* (9), 1625–1627. https://doi.org/10.1021/om990946l.

(29) Popoff, N.; Gauvin, R. M.; De Mallmann, A.; Taoufik, M. On the Fate of Silica-Supported Half-Metallocene Cations: Elucidating a Catalyst's Deactivation Pathways. *Organometallics* **2012**, *31* (13), 4763–4768. https://doi.org/10.1021/om3003224.

(30) *Lange's Handbook of Chemistry*, 15. ed.; Dean, J. A., Lange, N. A., Eds.; McGraw-Hill handbooks; McGraw-Hill: New York, NY, 1999.

(31) Vancompernolle, T.; Valente, A.; Chenal, T.; Zinck, P.; Del Rosal, I.; Maron, L.; Taoufik, M.; Harder, S.; Gauvin, R. M. Silica-Grafted Lanthanum Benzyl Species: Synthesis, Characterization, and Catalytic Applications. *Organometallics* **2017**, *36* (20), 3912–3920. https://doi.org/10.1021/acs.organomet.7b00538.

(32) Lapadula, G.; Bourdolle, A.; Allouche, F.; Conley, M. P.; del Rosal, I.; Maron, L.; Lukens, W. W.; Guyot, Y.; Andraud, C.; Brasselet, S.; Copéret, C.; Maury, O.; Andersen, R. A. Near-IR Two Photon Microscopy Imaging of Silica Nanoparticles Functionalized with Isolated Sensitized Yb(III) Centers. *Chem. Mater.* **2014**, *26* (2), 1062–1073. https://doi.org/10.1021/cm404140q.

(33) Arndt, S.; Voth, P.; Spaniol, T. P.; Okuda, J. Dimeric Hydrido Complexes of Rare-Earth Metals Containing a Linked Amido−Cyclopentadienyl Ligand: Synthesis, Characterization, and Monomer−Dimer Equilibrium. *Organometallics* **2000**, *19* (23), 4690–4700. https://doi.org/10.1021/om000506q.

(34) White, R. E.; Hanusa, T. P. Prediction of 89Y NMR Chemical Shifts in Organometallic Complexes with Density Functional Theory. *Organometallics* **2006**, *25* (23), 5621–5630. https://doi.org/10.1021/om060695y.

(35) Schumann, Herbert.; Meese-Marktscheffel, J. A.; Esser, Lothar. Synthesis, Structure, and Reactivity of Organometallic .Pi.-Complexes of the Rare Earths in the Oxidation State Ln3+ with Aromatic Ligands. *Chem. Rev.* **1995**, *95* (4), 865–986. https://doi.org/10.1021/cr00036a004.

(36) Zeimentz, P. M.; Arndt, S.; Elvidge, B. R.; Okuda, J. Cationic Organometallic Complexes of Scandium, Yttrium, and the Lanthanoids. *Chem. Rev.* **2006**, *106* (6), 2404–2433. https://doi.org/10.1021/cr050574s.

(37) Le Roux, E.; Anwander, R. Surface Organolanthanide and -Actinide Chemistry. In *Modern Surface Organometallic Chemistry*; Basset, J.-M., Psaro, R., Roberto, D., Ugo, R., Eds.;

Wiley-VCH Verlag GmbH & Co. KGaA: Weinheim, Germany, 2009; pp 455–512. https://doi.org/10.1002/9783527627097.ch12.

CHAPTER V :

Application in slurry ethylene polymerization of monopodal and bipodal silica supported Y catalysts

Index

Introduction

In this chapter is going to be presented the application of the grafted Y precursors, described in Chapter IV as catalysts for slurry ethylene homo- and copolymerization.

Yttrium and other rare-earth metal molecular complexes have been long known in literature to be active catalysts toward ethylene polymerization.[1] The fact that complexes of general structure $(C_5H_5)_2YR$ were isoelectronic with Ti(IV) cationic species, has rendered them particularly interesting as molecular models for Ziegler-Natta catalysts. In the 80s great interest was put in the study of this kind of complexes both as models for ZN catalysts but also for the advantage of being active in absence of cocatalysts.[2–13]

In the following years the chemistry of rare-earth metal complexes, both neutral and cationic, has flourished with the development of many post-metallocene catalysts, getting further away from mere modeling of group 4 polymerization catalysts.[6,14–17] rare-earth metal catalysts (comprising Y and Sc complexes) have been widely applied in polymerization of a great variety of monomers (eg. Ethylene, α-olefins, styrene, 1,3-dienes) as well as in other organic transformations (eg. hydroamination, hydrosilylation, hydroarylation, etc.).

Recently, then, SOMC of rare-earth metals has considerably advanced,[18] even taking into account the difficulty in accessing homoleptic Ln complexes with reactive Ln-C bonds[19] and their high reactivity to moisture.[20] This had as a consequence that the development of an SOMC chemistry of rare-earth metals was based on pseudo-organometallic complexes such as aryloxide, alkoxide (Ln-OR) or (silyl)amide complexes ($Ln-Nr_3$).[21] These complexes present (as the alkyl derivatives) hydrolysable Ln-X groups, which can easily react with the surface silanols.

The grafting of a neodymium alkoxide complex, $Nd(tritox)_3$ (tritox $=OC^tBu_3$, tris-*tert*-butylmethoxide) on mesoporous silica lead to the formation of bipodal species.[18] It was observed that upon the reaction not all the silanols on the surface were consumed, due to the weak basicity of the alkoxo ligands.[18] However, it was also proven that the bulkiness of the employed alkoxo ligand would avoid lanthanide cluster formation on the surface.[18]

Formation of monopodal species was observed during the grafting of an α,γ-diketonate yttrium complex, $Y(fod)_3$ (fod=1,1,1,2,2,3,3-heptafluoro-7,7-dimethyl-4,6-octanedionate), on MM-41, with consumption of half of the silanols surface groups.[22] The limited reactivity with the silanols,[18] together with the formation of agglomerates[23] and limited secondary ligand exchange, makes alkoxy and diketonate complexes of difficult application as precursor for the synthesis of supported rare-earth metal catalysts.[18]

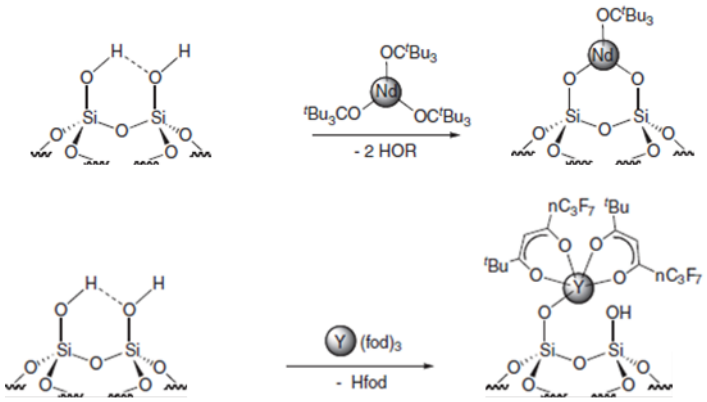

Scheme 1 – Grafting of alkoxy (top) and ketonate (bottom) rare-earth metal complexes on silica.

Of more successful employment are rare-earth silylamide derivatives,[18,21,22,22,24–34] allowing mild reaction conditions, formation of stable lanthanide siloxo bonds, complete reaction with the surface silanols, no formation of agglomerates, release of weakly coordinating silylamine, ease of silylamido secondary ligand exchange and characterization.[18]

The first to investigate silylamide rare-earth metal complexes as possible precursor were Anwander et al.[18,25] who initially investigated the reactivity of complexes $Nd(N\textit{i}Pr_2)_3(THF)$, $Nd[N(SiMe_3)_2]_3$ and $Nd[N(SiHMe_2)_2]_3(THF)_2$ on mesoporous alumosilicate Al-MCM-41, proving the formation of predominantly bipodal species. The same approach was then used for the grafting of complexes $Ln[N(SiMe_3)_2]_3$ on silica, where Ln = Sc[27], Y[27–30], La[27–30], Nd[25–30], Sm[27,29–31], Gd[27] and Dy[27]. It was shown that the nature of the grafted species was deeply affected by the thermal pretreatment of the support:[29] while at low or intermediate partial dihydroxylation temperatures there is predominantly the formation of mixtures of monopodal and bipodal species, at high dehydroxilation temperature monopodal species prevailed.[35,36]

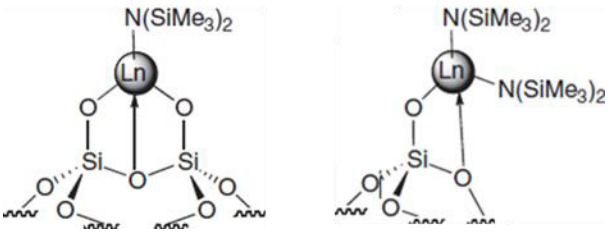

Scheme 3 – Possible structure obtained after grafting of $Ln[N(SiMe_3)_2]_3$ on silica.

It is renown that rare-earth metal silylamido bonds show a certain reactivity towards organoaluminium reagents, with the formation of tetraalkylaluminate ligands.[37] It was leveraging this reactivity that the first grafted methyl scandium species was obtained, by silylamide elimination on $[(\equiv SiO)_2Sc\{N(SiHMe_2)_2\}(THF)]$ as shown in Scheme 3.[32]

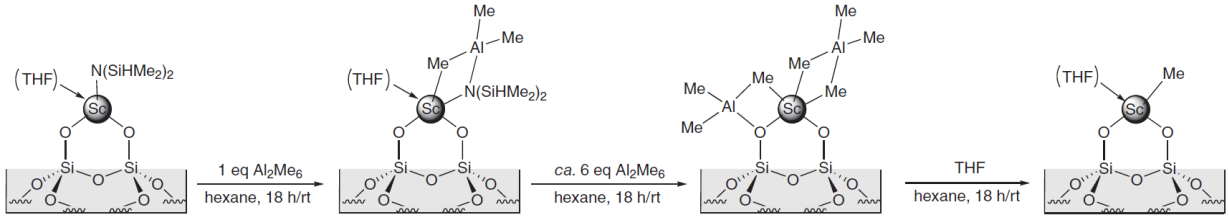

Scheme 2 – Synthesis of a bipodal grafted methyl scandium species.

Although the great amount of works reported on molecular rare-earth metal catalysts for olefin and diene polymerization, very little literature is present on supported catalysts in the same field. In 2005 Bochmann et al. reported the use in ethylene and 1,3-butadiene polymerization of seven different grafted alkyl rare-earth metals (M= Sc, Gd, Sm, Nd, La, Dy, Y),[27] obtained by modification of $(\equiv SiO)_2LnN(SiMe_2)_2$[25,33,38] with an alkylaluminium.

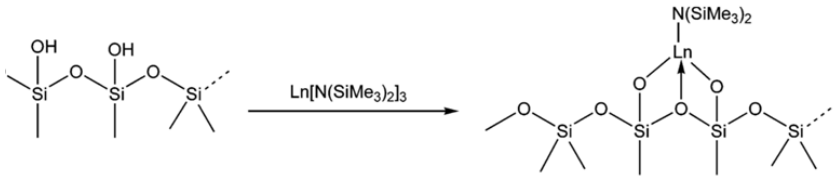

Scheme 4 – Synthesis of grafted lanthanide catalysts for ethylene polymerization reported by Bochmann in 2005.

All the resulting amide species reported were active in presence of alkylaluminium in ethylene polymerization with Sc and Y being the most actives (67.4 and 32.9 Kg_{PE} mol_M^{-1} h^{-1} bar^{-1} respectively).

Very recently Copéret et al. published a work in which SOMC was successfully employed for the synthesis of grafted lanthanide based catalyst, active in ethylene polymerization in absence of an activator.[39] In the work is presented the grafting, characterization and application in ethylene polymerization of Cp^*_2Yb and Cp^*_2Sm on $SiO_{2\text{-}700}$. The two catalysts obtained, although not presenting any M-C for the first ethylene insertion, revealed great ethylene polymerization activities, up to 12800 kg_{PE} mol_{Ln}^{-1} h^{-1} at 50°C under 20 bars of ethylene. The hypothesis advanced in the paper is that the initiation takes pace through a single electron transfer, with the mechanism shown in Scheme 5.

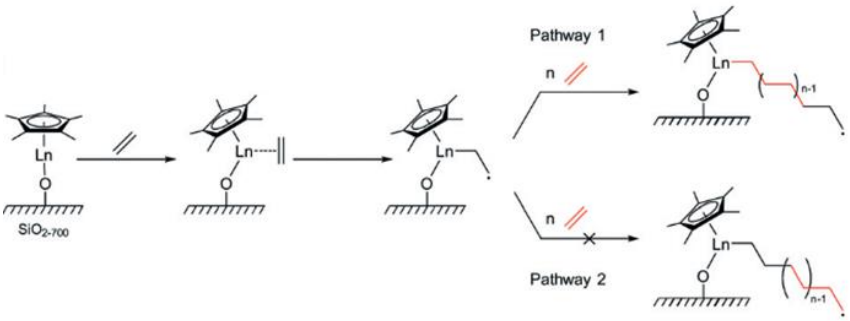

Scheme 5 – Initiation and propagation mechanism proposed by Copéret et al.

In 2017 Gauvin et al.[40] reported the grafting of a lanthanum tribenzyl derivative on $SiO_{2\text{-}700}$ which resulted with the formation of a mixture of species on the surface. It resulted in fact that upon grafting of the lanthanum complex it occurred a transfer of one of the benzyl ligands to the surface with opening of a siloxane bridge. The surface characterization showed a surface composition featuring 80% of bipodal species and 20% of monopodal ones.

Given this precedent, we decided to test the grafted Y benzyl and allyl complexes presented in Chapter IV, P8 to P11, in slurry ethylene homo- and co-polymerization with 1-hexene.

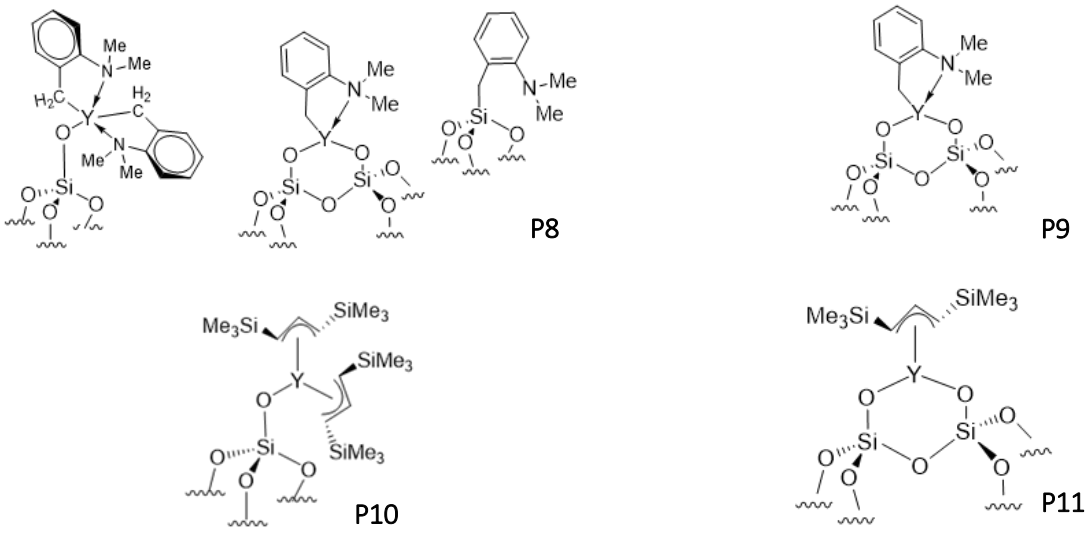

Scheme 6 – Structure of the grafted Y species P8-11.

1. Test in ethylene polymerization of P8 and P9

As seen in Chapter IV, catalysts P8 and P9 were synthesized by grafting $Y(o\text{-}CH_2PhNMe_2)_3$ respectively on $SiO_{2\text{-}700}$ and $SiO_{2\text{-}200}$. From the surface' characterization of the two catalysts, it resulted that the surface of P9 was composed solely of bipodal Y species, while P8 presented a 20:80 mixture of mono-bipodal structures. This species distribution is in agreement with what was reported by Gauvin et al. in 2017 for the grafting of $La(CH_2Ph)_3(THF)_3$ on $SiO_{2\text{-}700}$.[40] The obtained La catalyst had very low activity 1.9 kg_{PE} mol_{La}^{-1} h^{-1} in ethylene polymerization.

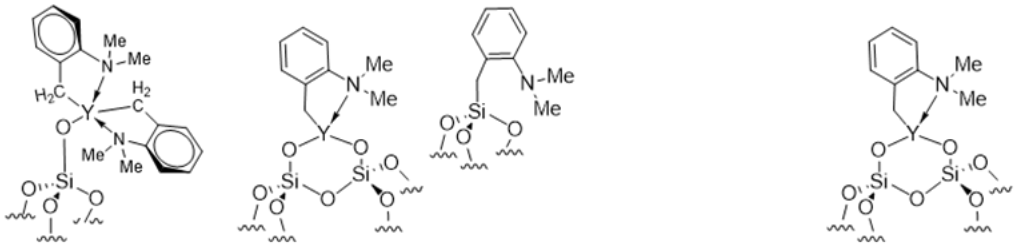

Scheme 7 – Structures of P8 and P9.

The Y catalysts were tested in ethylene polymerization in a glass reactor in 300 mL of heptane at 80°C and 4 bars of ethylene pressure for 30 min. TiBA was used as scavenger in concentration 1 mM. The polymerization results are reported in Table 1.

Table 1 – Polymerization results obtained with catalysts P8 and P9.

run	Catalyst	m cat mg	n Y µmol	1-hexene mol%	Yield g	Activity $g\ g_{cat}^{-1}\ h^{-1}$	Activity $Kg\ mol_Y^{-1}\ h^{-1}\ bar^{-1}$
1	P8	21.4	9.2	-	1.2	117	67.8
2	P8	20.4	8.8	20.9	0.77	76	44.3
3	P9	20.9	12.7	18.8	0.40	38	15.5

Both catalysts were active in ethylene polymerization. The activities recorded were in the same order of magnitude of those reported by Bochmann et al..[27] Some interesting considerations can be evinced by the analysis of the polymerization results obtained; catalyst P8 was tested in both homo- and copolymerization, run 1 and 2, and what is clear is that the presence of 1-hexene is

detrimental for the polymerization: the presence of comonomer causes a drop in activity from 117 g g_{cat}^{-1} h^{-1} to 76 g g_{cat}^{-1} h^{-1}, almost cutting it in half.

Table 1 also shows very clearly that P8 is almost three times more active than P9. This suggests that the monopodal specie is more efficient for ethylene polymerization.

The obtained polymers were characterized by DSC. The results are reported in Table 2.

Table 2 – DSC results for run 1-3.

run	Catalyst	Activity g g_{cat}^{-1} h^{-1}	Activity Kg mol_Y^{-1} h^{-1} bar^{-1}	T_f °C	ΔH_f J g^{-1}	Crystallinity %
1	P8	117	67.8	136	136.6	46.6
2	P8	76	44.3	135	130.8	44.6
3	P9	38	15.5	135	138.0	47.1

The DSC results show high melting temperatures, proper of highly linear HDPE resins, for the three obtained polymers from runs 1 to 3. While this was expected for run 1, conducted in absence of 1-hexene, it wasn't the cases of runs 2 and 3. The high T_m suggests that the catalysts tend not to incorporate the comonomer, so that also in presence of a certain amount of 1-hexene, purely HDPE resins were obtained.

Grafting of a homoleptic organometallic complex of yttrium on the silica surface activated it towards ethylene polymerization. Recent theoretical studies reported in literature, prove in fact that the functional groups on silica surface take active part in the polymerization process stabilizing its intermediate states.[41] The activities found for P8 and P9 fell in the same range of those reported in literature for grafted alkyl Y complexes as catalysts for ethylene polymerization,[25,27,33,38,39] and highlighted how the grafting fashion of the molecular complex has a huge impact on the final activity: the results of runs 1 to 3 show clearly that monopodal species are more active than bipodal ones.

After testing P8 and P9 in ethylene homo and copolymerization we tested also the allyl Y supported complexes described in Chapter IV, P10 and P11.

2. Test in ethylene polymerization of P11, (≡SiO)$_2$Y{1,3-C$_3$H$_3$(SiMe$_3$)$_2$}

P11 was obtained by grafting Y{1,3-C$_3$H$_3$(SiMe$_3$)$_2$}$_3$ on silica partially dehydroxylated at 200°C. The synthesis and characterizations of the catalyst are reported in Chapter IV, and confirmed that after the reaction the surface was composed entirely of bipodal species (≡SiO)$_2$Y{1,3-C$_3$H$_3$(SiMe$_3$)$_2$}.

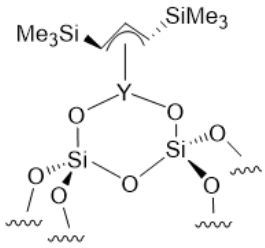

Scheme 8 – Structure of P11.

P11 was tested in a 70 mL autoclave, in 50 mL of heptane at 80°C and 10 bars of ethylene for 30 minutes. The catalyst was tested in both homopolymerization and ethylene/1-hexene copolymerization. The effect of the presence of TiBA as scavenger for the reaction was also investigated. The results of performed tests with catalyst P11 are reported in Table 3.

Table 3 – Results of the polymerization tests performed with P11. General conditions: 50 mL heptane, 80°C, 10 bars ethylene, 30 minutes.

run	$m_{support}$ mg	$Y_{surface}$ µmol	[TiBA] mM	1-hexene mol%	Yield g	Activity g g_{cat}^{-1} h^{-1}	Activity Kg mol_Y^{-1} $h^{-1}$$bar^{-1}$
4	20.7	11.4	-	-	1.89	183	33.3
5	20.0	11.0	1	-	3.32	332	60.0
6	18.7	10.3	1	21	5.91	633	115

P11 was tested in three different conditions: in ethylene homopolymerization with and without scavenger and in ethylene/1-hexene copolymerization. The activity demonstrated by this catalyst was higher than that found for P8 and P9, and, interestingly, it showed a very different behaviour with respect to the comonomer effect on the activity. In fact, while the activity of P8 dropped in presence of the comonomer, in the case of P11 1-hexene caused great boost in activity (doubled activity).

For what concerns the effect of the TiBA, it could be said that it is merely scavenging. The activity of the catalyst is higher in presence of TiBA merely because those impurities present in the solvent that could kill the catalyst are scavenged by the alkylaluminium.

The obtained polymers were characterized by DSC. The results of the 1st and 2nd isotherm are reported in Table 4 for the three resins.

Table 4 – DSC results for the polymers obtained with P11.

Run	1-hexene	Yield	Activity	T_m (1st melting)	Crystallinity (1st melting)	T_m (2nd melting)	Crystallinity (2nd melting)
	mol%	g	g g_{cat}^{-1} h^{-1}	°C	%	°C	%
4	-	1.89	183	140.5	79	135.5	75.1
5	-	3.32	332	142.5	58	135.2	50.2
6	21	5.91	633	141.0	58	134.5	51.1

The melting temperatures found for the resins of runs 4-6 in the second heating, 135°C, are proper of a highly linear HDPE-like polymer, confirming how, like in the case of P8 and P9, the yttrium catalyst shows no aptitude towards the incorporation of the α-olefin, even though the presence of the hexene gives a high boost in the catalyst activity. In this case the comonomer effect could be due to the coordination of olefin to the active site, participating to the polymerization as an ancillary ligand, favouring the ethylene insertion. A similar effect, without incorporation of the longer α-olefin in the polymer chain, is already known for Phillips catalysts.[42]

The DSC characterization of resins 4-6 also revealed very high T_m in the first heating, between 140°C-142°C for the three samples. This suggests that the polymer obtained with catalyst P11 is an Ultra High Molecular Weight PE resin.[43] The melting temperature recorded during the first heating, 141°C, is due to the melting of the disentangled nascent crystals, with a higher crystallinity order, while during the second heating is possible to see the endotherm of melt-crystallized polyethylene crystals at 135°C.[44]

The very high molar masses of the resins made it impossible to characterize them by HT-SEC: either the solubilisation process would degrade irreversibly the polymer chain, or the polymer solution would block the columns of the machine.

To conclude, P11 resulted to be fairly active in ethylene polymerization, it showed no affinity towards ethylene/α-olefin copolymerization, although the presence of the comonomer favours a boost in the catalyst's activity. The obtained resins were UHMWPE. Moreover, the morphology of the powder appears to be perfectly controlled, given the fact that the active species are chemically bound to the surface of the support.

Successively catalyst P10 was tested in the same conditions used for P11, in order to make a comparison between bipodal and monopodal species bearing the same ligand.

3. Test in ethylene polymerization of P10, (≡SiO)Y{1,3-$C_3H_3(SiMe_3)_2$}$_2$

P10 was obtained by grafting Y{1,3-$C_3H_3(SiMe_3)_2$}$_3$ on silica partially dehydroxylated at 700°C. The synthesis and characterizations of the catalyst are reported in Chapter IV, and confirmed that after the reaction the surface was composed entirely of the monopodal species (≡SiO)Y{1,3-$C_3H_3(SiMe_3)_2$}$_2$.

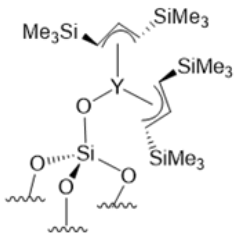

P10

Scheme 9 – Structure of P10.

- Lab-scale polymerization

P10 was tested in ethylene homo- and co-polymerization in a stainless steel autoclave, in 50 mL of heptane at 80°C under 10 bars of ethylene for 30 minutes. The catalyst was tested in both homopolymerization and copolymerization ethylene/1-hexene. The effect of the presence of TiBA as scavenger was also investigated. The results of the tests performed with catalyst P10 are reported in Table 5.

Table 5 – Results of the polymerization tests performed with P10. General conditions: 50 mL heptane, 80°C, 10 bars ethylene, 30 minutes.

Run	$m_{support}$ mg	$Y_{surface}$ µmol	[TiBA] mM	1-hexene mol%	Yield g	Activity $g\ g_{cat}^{-1}\ h^{-1}$	Activity $Kg\ mol_Y^{-1}\ h^{-1}\ bar^{-1}$
7	16.5	6.9	-	-	6.19	752	180
8	9.0	3.8	-	21	5.76	1280	305
9	11.2	4.7	1	21	4.77	855	203

P10 revealed to be the most active of the grafted Y catalysts tested. It is in fact almost four times as productive as P11. When run in homopolymerization conditions in absence of TiBA P10 gave 752 $g_{PE}\ g_{cat}^{-1}\ h^{-1}$ as opposed to the 183 $g_{PE}\ g_{cat}^{-1}\ h^{-1}$ obtained with P11 in the same running conditions.

Like in the case of P11, when the polymerization is run in presence of 1-hexene a big boost in activity is recorded, it jumps from 752 to 1280 $g_{PE}\ g_{cat}^{-1}\ h^{-1}$. Also in this case the catalyst is evidently very sensitive to the comonomer effect.

Run 9 reported in Table 5 was conducted in the same conditions of run 8, but in presence of TiBA as scavenger, interestingly enough the presence of TiBA caused the activity to drop from 1280 to 855 $g_{PE}\ g_{cat}^{-1}\ h^{-1}$. This is very interesting because it would mean that the TiBA added in the polymerization medium, not only takes on a scavenging role, but it also goes to interact with the active species on the surface of the support, reducing their affinity toward ethylene insertion.

This is even better explained from the plot of the activity profiles reported in Figure 1.

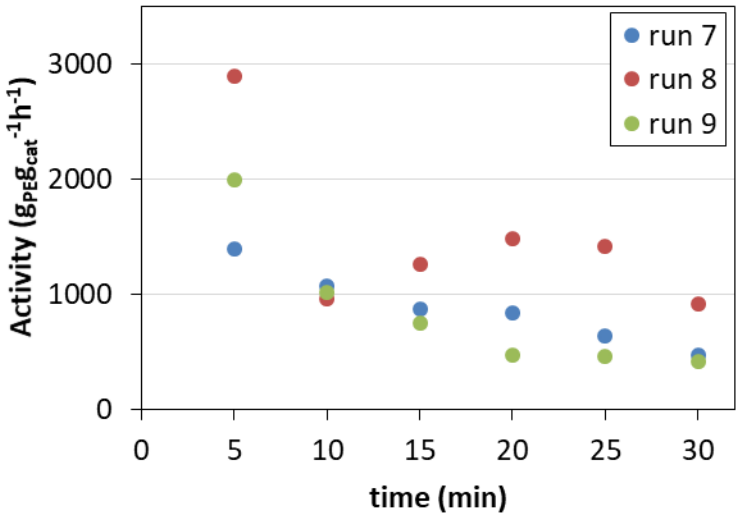

Figure 1 – Activity profiles of the polymerization tests performed with P10.

Figure 1 shows clearly how the activity profiles change in going from run 7 to run 8, suggesting, like in the case of P11, an interaction of the olefin with the active site to boost the activity. In the same way, but with the opposite effect, the activity profile changes upon addition of TiBA in the polymerization system.

It was previously seen in literature how TiBA would easily react with grafted Y species on the silica surface, to generate a catalyst for ethylene polymerization.[27] Similarly the TiBA could react with (≡SiO)Y{1,3-$C_3H_3(SiMe_3)_2$}$_2$ modifying the active species and affecting the activity.

The produced polymers in runs 7-8 were analysed by DSC and HT-SEC. The results are reported in Table 6.

Table 6 – DSC and HT-SEC characterization of the resins obtained with P10.

Run	Activity g g_{cat}^{-1} h^{-1}	T_{m1} °C	Crystallinity$_1$ %	T_{m2} °C	Crystallinity$_2$ %	M_n g mol^{-1}	M_w g mol^{-1}	Đ
7	752	143	84.4	135	67.4	224000	2.1E06	9
8	1280	141	62.4	134	54.0	56300	1.5E06	27
9	856	143	70.5	135	55.7	45200	2.1E06	46

The same considerations performed for the polymers obtained with P11 can be done for the resins produced in runs 7-9. The DSC characterization of these polymers revealed very high melting

temperatures for the first heating, 143 °C, and crystallinities over 70%. Upon second heating the melting temperatures found for the three sample were around 135°C with 55-60% of crystalline fraction. As discussed in the previous paragraph, this thermal behaviour is proper of UHMWPE resins.[43] During the first heating of the resins the melting of nascent, highly ordered, crystals formed during the polymerization process occurs, while during the second isotherm is possible to see the endotherm of melt-crystallized polyethylene crystals.

The DSC characterization also confirms to us that no comonomer was incorporated in the polymer chain during runs 8 and 9, both presenting melting temperatures of highly linear polyethylene. Like in the case of P11 it can be supposed that the role played by the comonomer during the polymerization reaction is ancillary to the active site.

Additionally, the resins were characterized by HT-SEC, confirming the UHMWPE nature of the products. All the M_w recovered for the samples were higher than 1.5 E06 g mol^{-1} with a very wide molar mass distribution (Đ comprised between 9 and 46).

In order to better study the comonomer effect on P11, an additional polymerization test was performed using cyclohexene instead of 1-hexene as comonomer. The aim was to investigate if, by using an olefin even less likely to insert than 1-hexene, the same interaction with the active site takes place, with enhancement of the activity.

The results of the polymerization performed with cyclohexene are reported in Table 7 in comparison with those of run 8.

Table 7 – Results of the polymerization tests performed with P10 with 1-hexene and cyclohexene. General conditions: 50 mL heptane, 80°C, 10 bars ethylene, 30 minutes, no TiBA.

Run	$m_{support}$ mg	Comonomer	$Y_{surface}$ µmol	1-hexene mol%	Yield g	Activity g g_{cat}^{-1} h^{-1}	Activity Kg mol_Y^{-1} h^{-1} bar^{-1}
8	9.0	1-hexene	3.8	21	5.76	1280	305
10	5.5	cyclohexene	2.3	21	5.14	1887	449

Not only a boost in activity was obtained also in presence of cyclohexene, but it was even more important than that observed with 1-hexene. For run 10 a very high activity of 1887 g g_{cat}^{-1} h^{-1} was

obtained. This phenomenon could signify that the coordination of a bulkier olefin to the active site has a better activation effect than the simple α-olefin.

The produced resin during run 10 was characterized by DSC, and presents the same characteristic already observed for runs 7-9. The results are reported in Table 8.

Table 8 – DSC and HT-SEC characterization of the resins obtained with P10.

Run	Activity g g_{cat}^{-1} h^{-1}	T_m (1st melting) °C	Crystallinity (1st melting) %	T_m (2nd melting) °C	Crystallinity (2nd melting) %
10	1887	143	70.0	135	56.6

All the fluffs obtained with P10 showed a very good particle morphology and lack of fines. This was confirmed through Scanning Electron Microscopy. The images acquired for run 7 are reported in Figure 2.

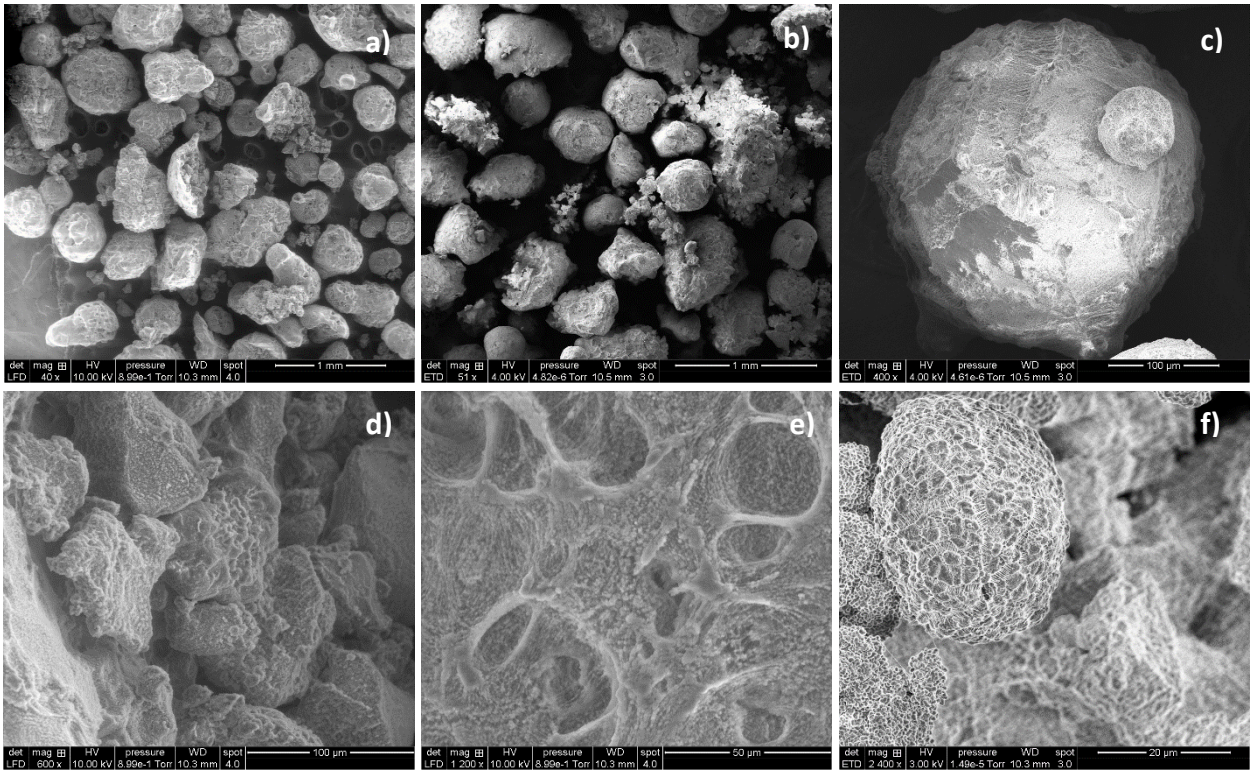

Figure 2 - SEM images acquired for the resin obtained with P10 at different magnifications: a)40x; b) 50x ; c) 400x; d) 600x; e) 1200x; f) 2400x.

In Figure 2 are depicted the SEM images acquired for the polymer obtained with P10 in run 7, in ethylene homopolymerization. From the general pictures it is possible to see the spherical particles proper of resins obtained in heterogeneous slurry polymerization processes such as the one used in this work. What is also possible to see from the pictures is the absence of undesirable fines. From the images at higher magnification is then possible to see the style of growth of the polymer.

The very good activities obtained at lab-scale, pushed towards a scale-up of the system. P10 was tested in pre-industrial polymerization conditions.

- Pre-industrial scale up

The monopodal (≡SiO)Y{1,3-$C_3H_3(SiMe_3)_2$}$_2$, after the very promising results obtained at lab-scale in Lyon, was tested at pre-industrial scale at INOES facilities in Brussels.

The tests performed at INEOS aimed at investigating the response of the catalyst to different ratios H_2/C_2H_4 and different comonomer concentrations, and the influence of the polymerization conditions on the polymer properties.

The polymerization tests were conducted in 5 L autoclaves, with 1.5 L of isobutane as solvent. The general operating temperature and ethylene pressure were 80°C and 10 bars respectively, in these conditions the total equilibrium pressure of the system was of 24.4 bars; 0.5 mmol of TiBA were used as scavenger. P10 was injected in the reactor as a 10wt% suspension in oil.

To first set a reference test and find the optimal operating conditions, the system was tested in ethylene homopolymerization in absence of hydrogen. The results of the polymerization reaction are reported in Table 9.

Table 9 – Polymerization tests with P10. Conditions: 1.5L isobutane, 80°C, 10 bars ethylene, 1 hour, 0.5 mmol TiBA.

runs	m cat	nY	H_2/C_2 (set)	1-hexene	Yield	Activity	Activity
	mg	µmol	mol%	g	g	g g_{cat}^{-1} h^{-1}	Kg mol_Y^{-1} h^{-1} bar^{-1}
11	175	73.5	0.00	0	656	3750	893

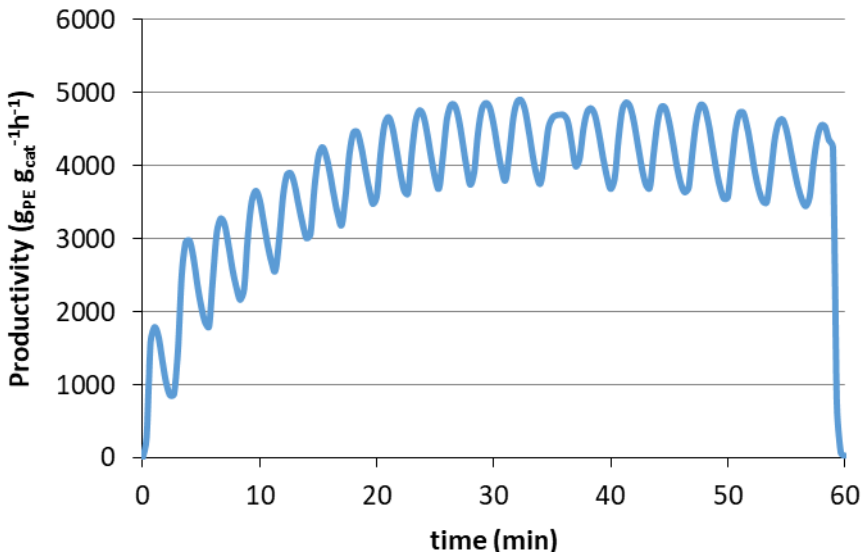

Figure 3 – Activity profile of run 11

The obtained Activity during run 11 was more than three times higher than the maximum of activity obtained previously for the catalyst. Moreover, the activity profile, reported in Figure 3, is very stable throughout the polymerization, showing an activating behaviour in the first 25 minutes of the polymerization reaction, to then stabilize around a activity of 4000 g g_{cat}^{-1} h^{-1}, and giving no sign of deactivation over the one hour of polymerization time vised for the test. This behaviour was not appreciated during the tests performed at a lower scale, most probably because of the too short polymerization times tested and operational technicalities (e.g.: the pressurization of the reactor would be done already in presence of the catalyst, affecting the first part of the kinetic plots with ethylene solubilisation phenomena).

Once a reference was set, a DOE (Design of Experiment) was put in place to study the response of the catalyst at three different levels of H_2/C_2H_4 (1.3, 2.6 and 5.2 mol%) and 1-hexene (0, 30 and 60 g). The type of DOE used is a Composite Central Plane (CCP) DOE in two variables (hydrogen and hexene). Its graphic representation is shown in Figure 4.

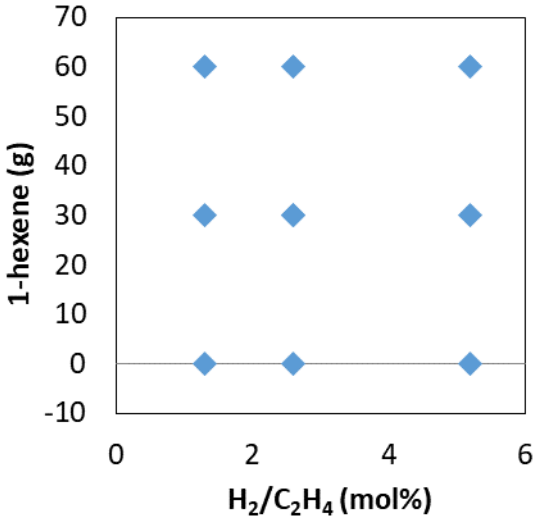

Figure 4 – Plot of the CCP DOE used to investigate the catalytic behavior of P10.

The general polymerization condition applied for the DOE were the same used during run 11: 1.5L of isobutane, 0.5 mmol of TiBA, 10 bars of ethylene, 80°C and one hour of polymerization time. The results of the different polymerization tests are reported in Table 10.

Table 10 – Results of the DOE performed with P10. Conditions: 1.5L isobutane, 80°C, 10 bars ethylene, 1 hour, 0.5mmol TiBA.

runs	m catalyst	nY	H2/C2 (set)	1-hexene	C6/C2 gas	Yield	Activity	Activity
	mg	µmol	mol%	g	%mol	g	g g_{cat}^{-1} h^{-1}	Kg mol_Y^{-1} h^{-1} bar^{-1}
12	175	73.5	1.3	0	0.0	836	4777	1140
13	100	42.0	1.3	30	1.0	242	2420	576
14	175	73.5	1.3	60	1.8	365	2086	497
15	100	42.0	2.6	0	0.0	554	5540	1320
16	100	42.0	2.6	30	1.1	241	2410	574
17	100	42.0	2.6	30	1.0	279	2790	664
18	100	42.0	2.6	60	1.9	222	2220	529
19	100	42.0	5.2	0	0.0	460	4600	1100
20	100	42.0	5.2	30	1.0	265	2650	631
21	100	42.0	5.2	60	1.8	313	3130	745

The data reported in Table 10 make the activating effect of H_2 on P10 clear, and at the same time how this phenomenon is highly diminished whenever 1-hexene is present in the reaction system,

independently of its amount. But real interesting considerations can be evinced by the representation of the kinetic profiles reported in Figure 5.

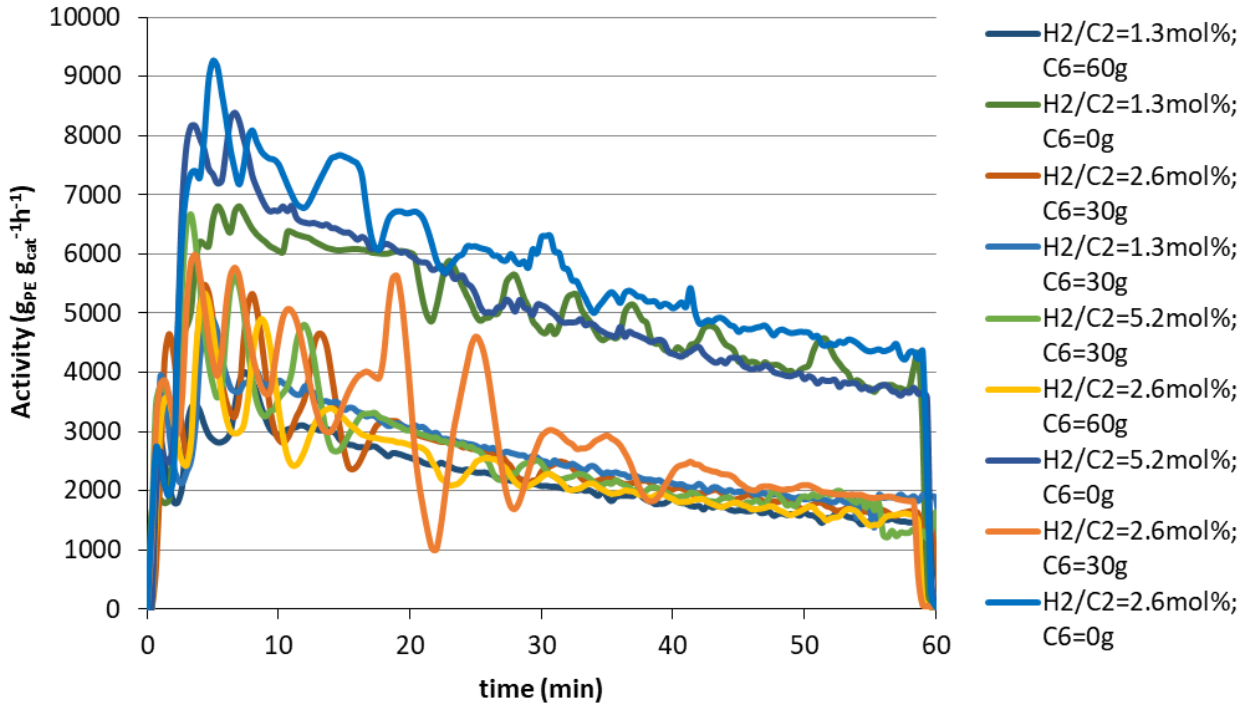

Figure 5 – Activity profiles for the polymerization tests performed according to the DOE for P10.

From Figure 5 it is possible to see that the profiles acquired for the tests performed in presence of hydrogen and 1-hexene have a very different shape with respect to the one of run 11, in all the tests of the DOE in fact a maximum in activity is reached in the first five minutes of the polymerization, followed by a gradual deactivation. Additionally, from the plot of the kinetics of the polymerizations is very clear how the presence of hexene almost nullifies the activating effect of the hydrogen, independently of the amounts of both in the reactor. Figure 5 shows clearly how the three profiles for runs 12, 15 and 19 (no 1-hexene in the reactor) are almost superimposable, as well as the profiles for the remaining tests, performed in presence of both H_2 and the olefin.

All these outcomes suggest that the hydrogen introduced in the reactor reacts with the surface, modifying the active species, probably generating an yttrium hydride, and that this new species is more active than the monopodal allyl yttrium; but, differently from the latter, the new adduct

responds negatively to the presence of 1-hexene as comonomer. This latter issue will be discussed further in the following pages.

The resins obtained in runs 12-21 were characterized by DSC, GPC, IR and MVS. The results are reported in Table 11.

Table 11 – Characterization results of the resins produced during the DOE testing with P10.

runs	H2/C2	BD	T_{m2}	Crystallinity	M_n	M_w	M_w/M_n	SCB	Comonomer	MVS
	mol%	kg/m³	°C	%	g mol^{-1}	g mol^{-1}		n/1000 C	mol%	kg/m³
12	1.3	332	135.4	62.8	88600	616800	7.0	-	-	946
13	1.3	345	133.3	66.2	51600	400300	7.8	2.2	0.4	948
14	1.3	348	133.3	65.3	47600	401100	8.4	2.6	0.5	947
15	2.6	330	135.1	67.5	69700	407300	5.8	-	-	951
16	2.6	348	133.6	68.3	36100	338700	9.4	2.9	0.6	951
17	2.6	335	133.5	69.4	43000	368500	8.6	2.3	0.5	951
18	2.6	347	133.0	68.0	34600	302000	8.7	1.7	0.3	951
19	5.2	343	134.3	70.2	32500	339100	10.4	-	-	954
20	5.2	341	133.6	69.2	27500	253000	9.2	2.4	0.5	955
21	5.2	336	132.3	71.5	20900	219300	10.5	<1	-	956

The characterization results reported in Table 11 give numerous information on the behaviour of the catalyst. The values of density and the melting temperature of the resins produced are proper of a highly linear, HDPE like, polyethylene resin. Like what we observed at lab scale, almost no comonomer was incorporated in the polymer chain, for all the comonomer feed ratios tested. On the other hand, the hydrogen had an evident effect on the resins' molar masses. In Figure 6 are reported the GPC traces for runs 12-21.

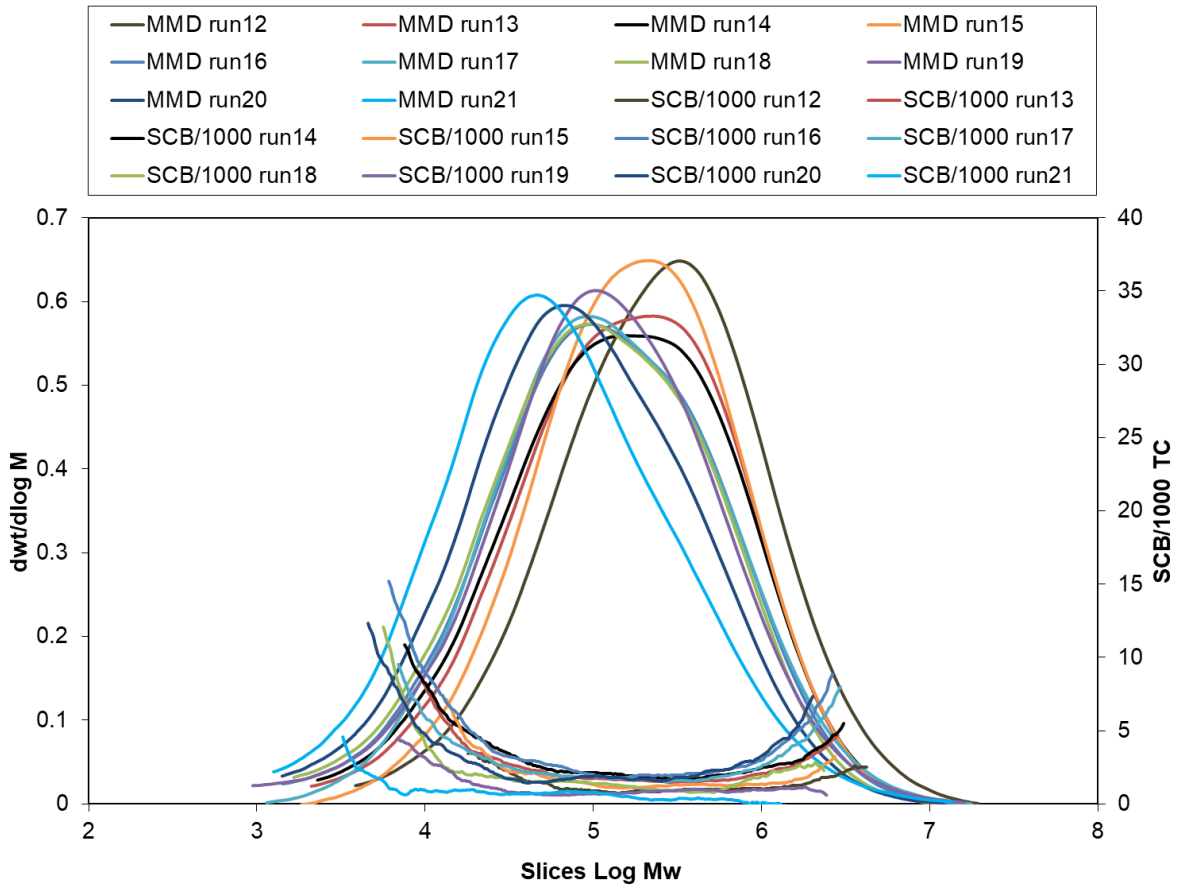

Figure 6 – GPC traces of the resins produced in runs 12-21.

The presence of hydrogen had an important effect on the molar masses of the polymers produced by P10. In fact, the highest M_w obtained for these resins is 617000 g mol^{-1}, way lower than the 2.1E06 g mol^{-1} previously recorded in Lyon. It is also worth noting that also the presence of the hexene has an impact on the final molar masses.

As can be seen in Figure 7, there's a linear relationship between the logarithm of the weight average molar mass and the logarithm of the ratio H_2/C_2 during the polymerization, both with and without hydrogen. Moreover, what the plot in Figure 7 clearly shows is that in presence of 1-hexene the molar masses accessible to P10 are lower than in homopolymerization.

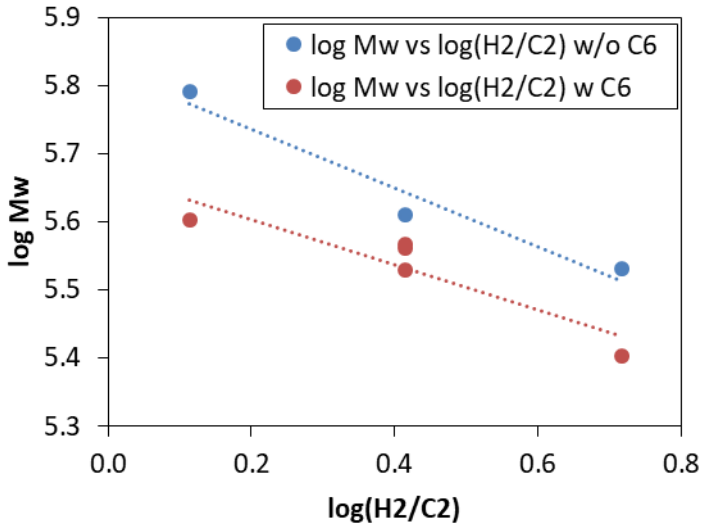

Figure 7 – Plot logM_w vs log(H_2/C_2) with and without 1-hexene.

It is here worth to notice also that the detrimental effect of the 1-hexene on the activity is in contradiction with what was discussed in the previous paragraph, on the polymerizations performed at lab-scale. In order to check if, also in pre-industrial scale, was possible to see the activating effect of the comonomer in absence of H_2, an additional test was performed and confronted with the results obtained in run 11, 15 and 16.

Table 12 – Polymerization results with P10 at different loading of C6 and H2. Conditions: 1.5L isobutane, 80°C, 10 bars ethylene, 1 hour, 0.5mmol TiBA.

runs	m catalyst	nY	H_2/C_2 (set)	1-hexene	C_6/C_2 real	Yield	Activity	Activity
	mg	µmol	mol%	g	%mol	g	g g_{cat}^{-1} h^{-1}	Kg mol_Y^{-1} h^{-1} bar^{-1}
11	175	73.5	0.0	0	0.0	656	3749	839
15	100	42.0	2.6	0	0.0	554	5540	1320
16	100	42.0	2.6	30	1.1	241	2410	574
22	100	42.0	0.0	30	1.0	460	4600	1100

Table 12 reports four tests performed NOH, homopolymerizations with and without hydrogen (run 15 and 11 respectively) and ethylene/1-hexene copolymerizations with and without hydrogen (run 16 and 22 respectively). From Table 12 and Figure 7, displaying the kinetic profiles for the four tests, it is clear that the presence of H_2 changes drastically the catalyst' activation pathway and its response to the comonomer during the polymerization reaction.

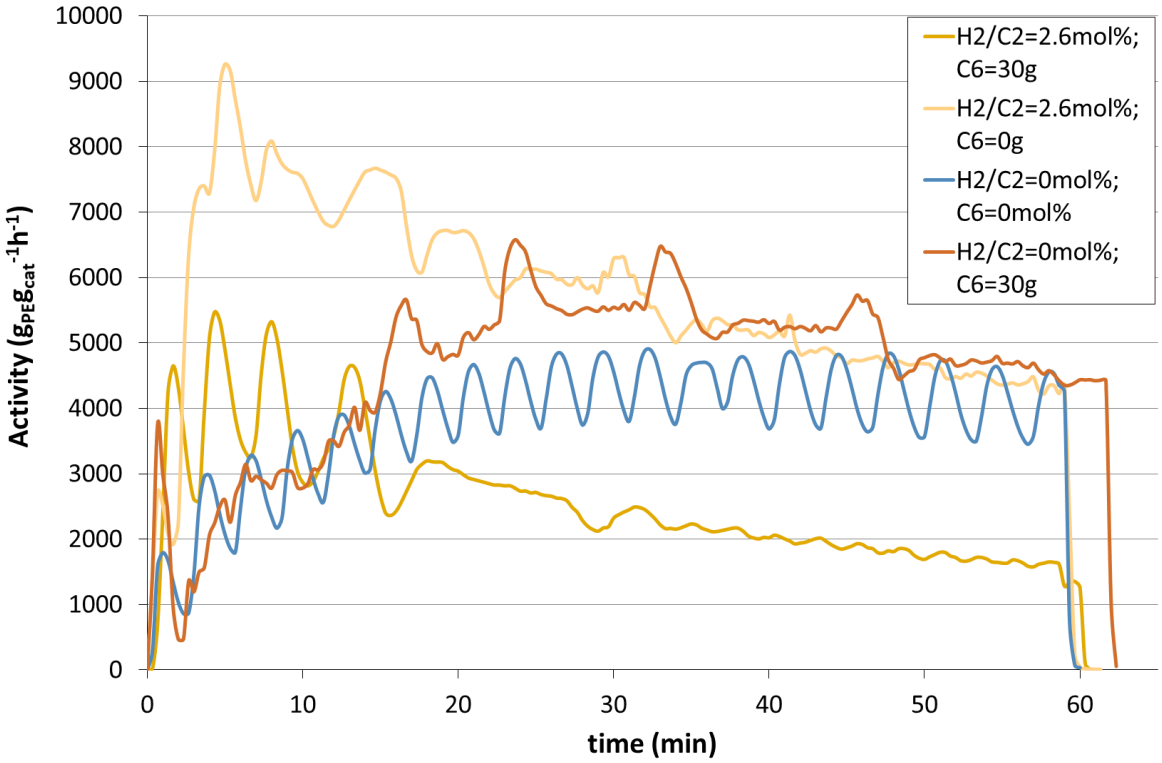

Figure 8 – Activity profiles for runs 11, 15, 16 and 22 performed with P10.

Figure 8 shows clearly how in absence of hydrogen the kinetic profiles for both run 11 and 22 passes through an activation phase in the first 15 minutes of the polymerization to reach than a more or less stable activity until the end of the polymerization. In addition, in no hydrogen conditions, the comonomer has an activating effect, even though not as pronounced as what had been previously observed at laboratory scale.

On the other side, upon introduction of H_2, the activity reaches quickly a maximum in the very first minutes of the polymerization to then gradually decrease. Moreover, as already stated, the addition of a comonomer causes a sharp drop in activity, erasing the activating effect of the hydrogen.

The great difference in the shape of the activity profiles between run 11, 22 and run 15, 16 would suggest that the H_2 introduced in the reactor interacts with P10 favouring the first insertion. We could in fact attribute the initial activation period in run 11 and 22 to the time for a first ethylene molecule to insert in all the Y-allyl bonds, to reach a plateau once all the species on the surface

have reacted. When hydrogen is added to the reactor it can react with the grafted yttrium species probably generating an yttrium hydride on the surface. The insertion of the ethylene in an Y-H bond is faster, thus explaining the maximum of activity at the beginning of the reaction.

Molecular Y hydride complexes, such as Cp_2YH, are known to be fairly active in ethylene polymerization, but show no activity in propene polymerization.[45,46] It was proved that in propene polymerization the chain termination reaction proceeds via hydrogen abstraction on the allylic methyl C-H from the propene, generating an allyl-Y which doesn't react with a second propene unit. Something similar could occur in ethylene/1-hexene polymerization: in presence of hydrogen the 1-hexene might react with the active site to generate an allyl-Y, slowing the successive ethylene insertion (scheme 10).[47] Further studies are though necessary to prove this hypothesis.

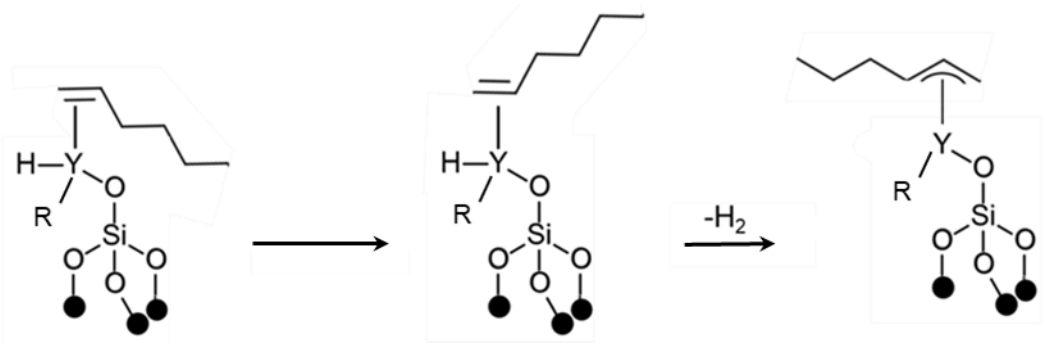

Scheme 10 – Possible allyl formation after the coordination of the 1-hexene to the yttrium hydride, according to the mechanism proposed by Busico et al.

The polymers obtained in run 11 and 22 were then characterized by DSC, GPC, IR and MVS. The results are reported in Table 13.

Table 13 – Characterization results of the resins produced in runs 11, 15, 16 and 22.

run	H2/C2 (set)	BD	T_{m2}	Crystallinity	M_n	M_w	M_w/M_n	SCB	Comonomer	MVS
	mol%	kg/m³	°C	%	g mol^{-1}	g mol^{-1}		n/1000 C	mol%	kg/m³
11	0.0	326	134	56.3	-	-	-	-	-	935
15	2.6	330	135.1	67.5	69700	407300	5.8	1.6	0.3	951
16	2.6	348	133.6	68.3	36100	338700	9.4	2.9	0.6	951
22	0.0	326	133	61.8	76500	1393000	18.2		-	941

Given the ultra-high molecular weight nature of the polymers obtained with P10 in absence of hydrogen it was not possible to measure the molar masses of resin obtained in run 11 by SEC. In both runs the polymer was highly linear and for what concerns run 22 the M_w obtained was close to 1400 Kg mol^{-1}. The molar mass distribution for run 22 was very broad, 18.2, wider than that of the resins synthesized in presence of hydrogen, as shown in Figure 9.

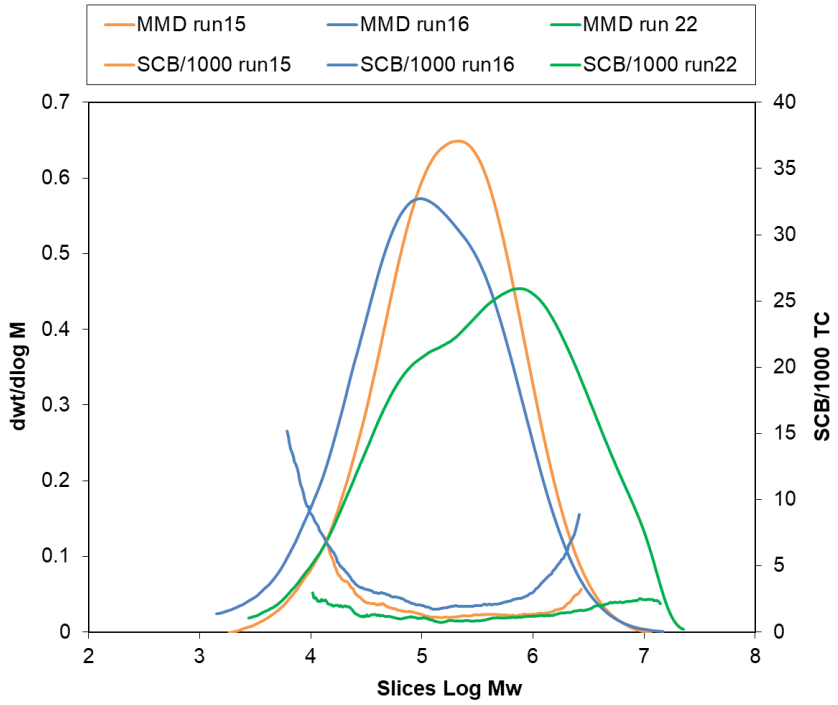

Figure 9 – GPC-FTIR plot of the resin obtained in run 22.

Another remarkable aspect that was evidenced during the tests performed at lab-scale, was the detrimental influence of TiBA on the catalyst activity (comparison between run 8 and 9 in Table 5 and Figure 1). In order to further investigate this aspect, additional tests were performed at INEOS facilities at different scavenger loadings. The other conditions applied to the reaction were those already employed during run 16: 1.5 L isobutane, 80°C, 10 bars of ethylene, 2.6 mol% H2/C2, 30g 1-hexene,100 mg of catalysts in 10 wt% oil suspension. The polymerization lasted 1 hour. The TiBA amounts tested were 0.5, 0.25 and 0.05 mmol. The results of the polymerizations are reported in Table 14 while Figure 10 depicts the kinetic profiles for the three tests.

Table 14 – Polymerization results for the tests performed at different TiBA loading with P10. Conditions: 1.5 L isobutane, 80°C, 10 bars of ethylene, 2.6 mol% H2/C2(set), 30g 1-hexene,100 mg catalyst, 1hour.

runs	m catalyst	nY	H2/C2 (real)	C6/C2 real	TiBA	Yield	Activity	Activity
	mg	mmol	mol%	%mol	µmol	g	g g_{cat}^{-1} h^{-1}	Kg mol_Y^{-1} h^{-1} bar^{-1}
16	100	42	2.9	1.1	0.50	241	2410	574
23	100	42	2.7	1.0	0.25	353	3530	840
24	100	42	2.5	0.9	0.05	740	7400	1760

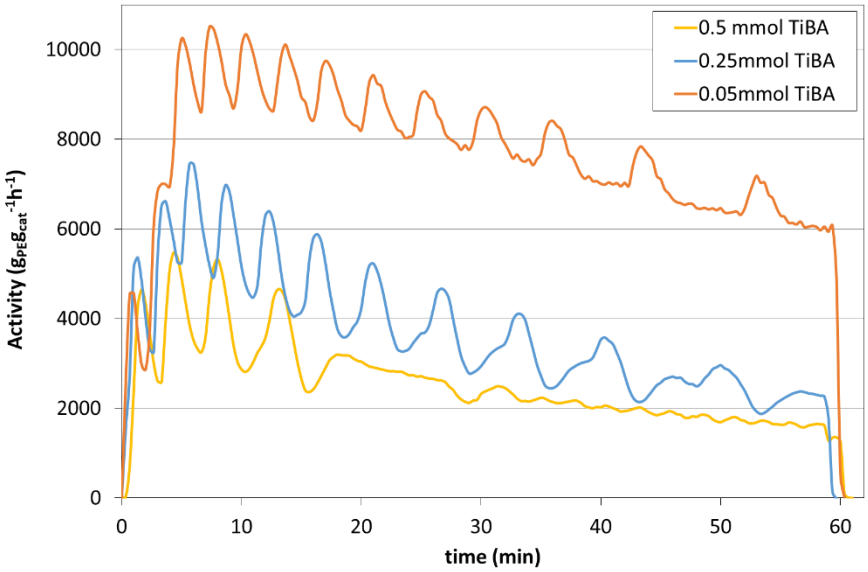

Figure 10 – Kinetic profiles of the polymerization tests performed with P10 at different TiBA loadings.

The tests performed in Brussels confirm and even exceed what had already been observed in Lyon. Decreasing the amount of TiBA in the polymerization medium causes an enormous boost in activity; lowering the amount of TiBA from 0.5 to 0.05 mmol in the reactor causes the activity to shoot from 2410 to 7400 g_{PE} g_{cat}^{-1} h^{-1}.

As shown in Figure 11 the activity of P10 decreases linearly with the increasing of the moles of TiBA in the reactor. This could be due to the fact that TiBA reacts in part with the active species on the surface of the support decreasing their efficiency towards ethylene polymerization.

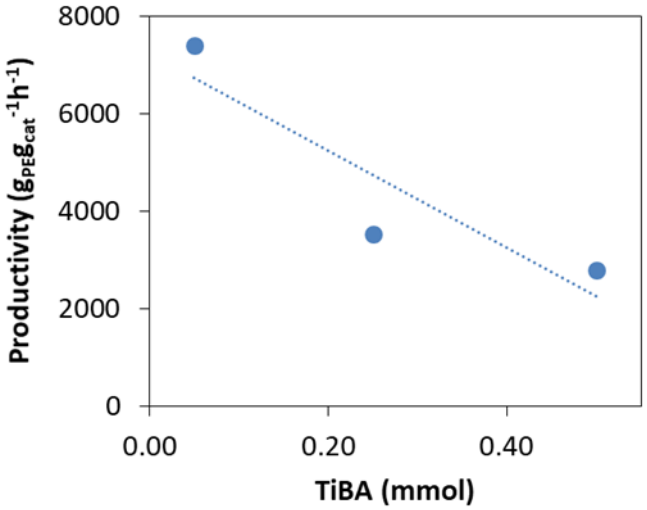

Figure 11– Plot of the activity of P10 in function of the amount of TiBA at 80°C, 10 bars of ethylene, 2.6 mol% H2/C2 and 30 g 1-hexene.

Also in this case the obtained polymers were characterized by DSC, GPC, IR and MVS. The results are reported in Table 15.

Table 15 – Characterization results of the resins produced in runs 11 and 22.

runs	TiBA mmol	BD kg/m³	Tf2 °C	Crystallinity %	M_n g mol^{-1}	M_w g mol^{-1}	M_w/M_n	SCB n/1000 C	Comonomer mol%	MVS kg/m³
16	0.50	348	133.6	68.3	36100	338700	9.4	2.9	0.6	951.2
23	0.25	337	133.1	67.1	37300	364300	9.8	<1	-	952.2
24	0.05	346	133.0	69.0	31600	262200	8.3	<1	-	953.1

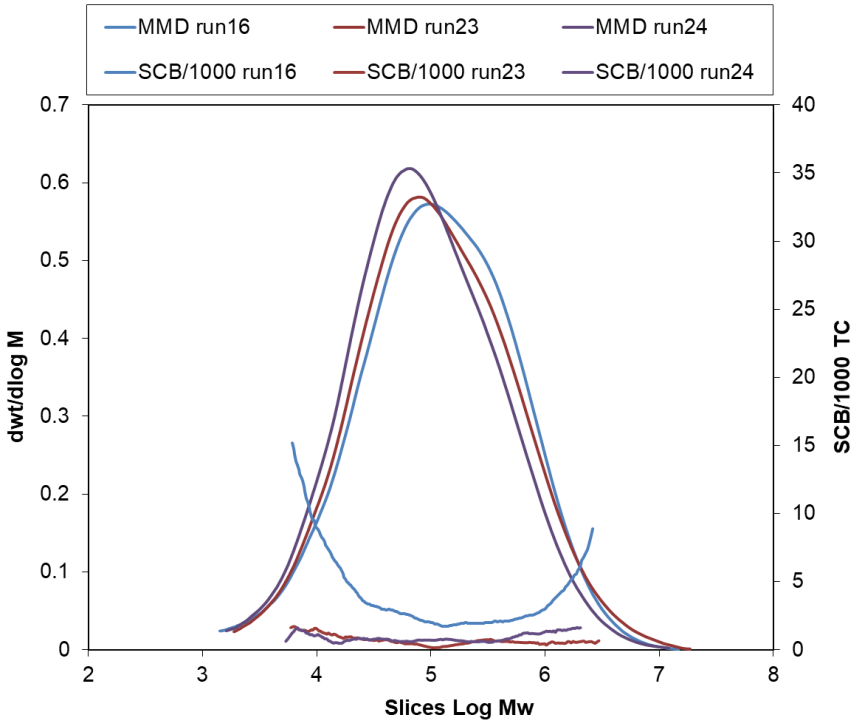

Figure 12 – GPC-FTIR traces of the resins produced in runs 16, 23 and 24 with P10.

The polymers produced in runs 16, 23 and 24 have very high crystallinities, over 67 %, and melting temperatures, 133 °C; coupled with the high densities, above 951 kg/m^3, it is possible to confirm the HDPE nature of these resins, like for the other products obtained with the supported-Y catalysts. This products, like the others obtained with P10 in presence of hydrogen present M_w below 400 Kg mol^{-1} and broad molar mass distributions. In Figure 11 are reported the SEC traces for the three samples.

As a consequence of P10's intrinsic nature (the Y species are chemically bound to the surface of the silica support), all the fluffs produced in runs 11-24 are well-behaved from a morphology point of view. And in order to confirm the absence of undesirable fines a particle size distribution analysis was performed on some of the samples. The results are reported in Table 16.

Table 16 – Particle size distribution results for the resins obtained with P10.

runs	span	d10 µm	d50 µm	d90 µm
11	0.94	415	679	1054
12	0.90	448	737	1138
13	0.97	354	586	921
21	0.93	400	656	1008
22	0.91	459	753	1142
23	0.97	397	658	1032
24	0.92	483	803	1220

As a title of example in Figure 12 is also reported the plot of the particle size distribution of the fluff produced in run 21.

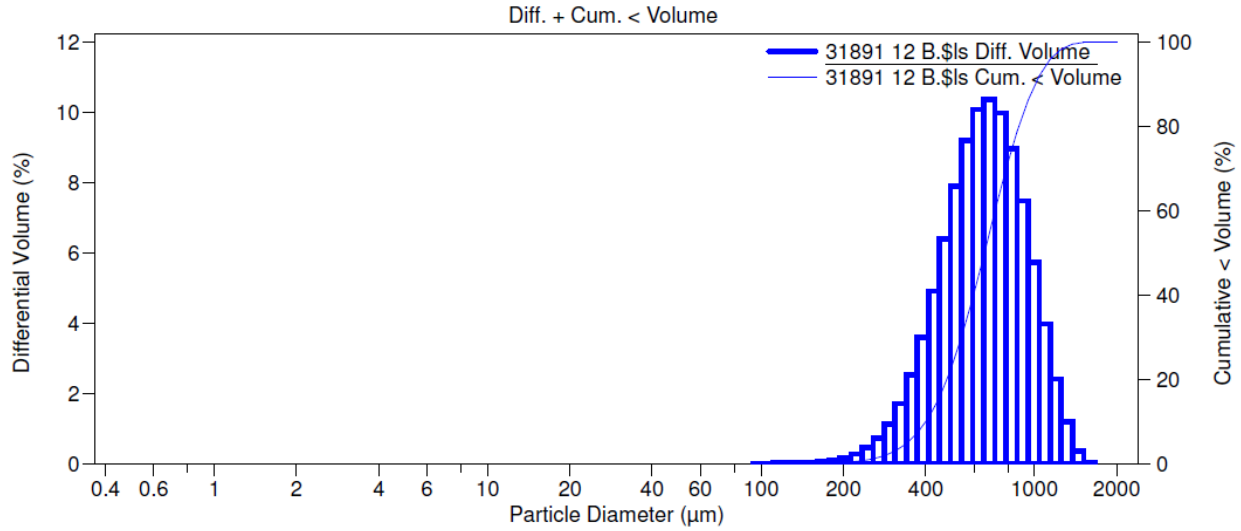

Figure 13 – plot of the particle size distribution of the fluff produced in run 21.

Both Table 16 and Figure 13 show that the obtained resins have a homogeneous particle size distribution and there are no undesired fines. All the characterization and polymerization results reported in this paragraph clearly show how the technology upgrade from laboratory to pre-industrial scale was successful. In addition, the new catalyst displays unprecedented activity in ethylene polymerization for a supported rare-earth system. The HDPE features a broad molar mass distribution which could be of interest for applications.

- Conclusions

The application of catalyst P10 in ethylene homo and copolymerization showed that the well-defined (≡SiO)Y{1,3-$C_3H_3(SiMe_3)_2$}$_2$ prepared by SOMC of Y{1,3-$C_3H_3(SiMe_3)_2$}$_3$ on silica dehydroxylated at 700°C shows one order of magnitude more active than other supported Y catalysts present in literature.[27] P10 was tested at both lab and pre-industrial scale, given the initial good results obtained in slurry polymerization.

P10 revealed to be active in both ethylene homopolymerization and ethylene/1-hexene copolymerization, though the catalyst showed no aptitude towards the incorporation of the comonomer. In fact, all the obtained resins were highly linear polyethylenes with melting temperatures above 133°C, crystallinity higher than 55% (depending on the molar masses of the resins) and densities above 950 Kg/m^3.

On the other side the presence of hydrogen during the polymerization highly affected the catalysts behaviour from both an activity and final molar masses point of view. When polymerizing ethylene in absence of H_2, the catalyst P10 shows an activating kinetic profile which reaches a stable activity after 15 minutes of polymerization, until the end of the reaction, with final productivities of 4000 g g_{cat}^{-1} h^{-1}. In presence of hydrogen the activity quickly reaches a maximum in the very first minutes of the reaction to then slowly decreases during the rest of the polymerization, reaching an average activity of 5500 g g_{cat}^{-1} h^{-1}.

The catalyst responds very well to the hydrogen; in fact, in no hydrogen conditions, P10 produces UHMWPE resins, while when H_2 is added to the reactor M_w can decrease down to 300 Kg mol^{-1}.

An additional factor that highly affects the productivity of P10 is the amount of TiBA present in the reactor, decreasing the alkylaluminium compound from 0.5 to 0.05 mmol causes the average activity of the catalyst to rocket from 2410 to 7400 g_{PE} g_{cat}^{-1} h^{-1} at parity of all other conditions.

The results obtained confirmed that the upgrade of the system was achieved with success, and that we developed a catalyst highly superior in activity to what previously reported in literature for supported Y catalysts.

4. Synthesis and polymerization tests of cationic Y species on silica surface

After testing the performances of the neutral supported yttrium catalysts P10 and P11, it was investigated the possibility of generating stable cationic Y species on the silica surface, active towards ethylene polymerization.

4.1 Synthesis of $[(\equiv SiO)Y\{1,3\text{-}C_3H_3(SiMe_3)_2\}]^+[B(C_6F_5)_4]^-$, P12

P10, $(\equiv SiO)Y\{1,3\text{-}C_3H_3(SiMe_3)_2\}_2$, was reacted with 1.2 eq. of trityl tetrakis-pentafluorophenyl borate, $[C(C_6H_5)_3]^+[B(C_6F_5)_4]^-$, in benzene overnight in order to obtain the catalyst $[(\equiv SiO)Y\{1,3\text{-}C_3H_3(SiMe_3)_2\}]^+[B(C_6F_5)_4]^-$, P12 on the surface of the support.

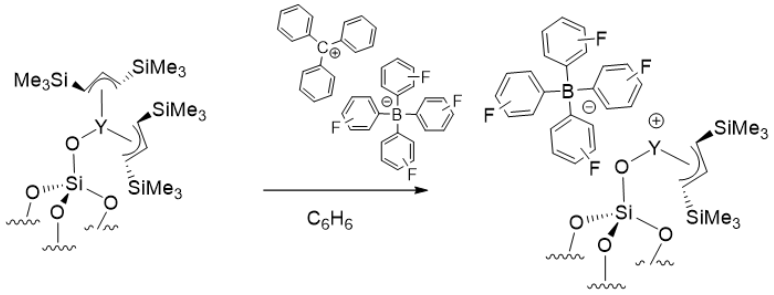

Scheme 11 – Synthesis of $[(\equiv SiO)Y\{1,3\text{-}C_3H_3(SiMe_3)_2\}]^+[B(C_6F_5)_4]^-$, P12.

As soon as the borate solution entered in contact with P10, the suspension turned dark red, indicating the two complexes reacted. After 16h the product was bottle green; the surface was characterized by DRIFT spectroscopy to investigate the outcome of the reaction.

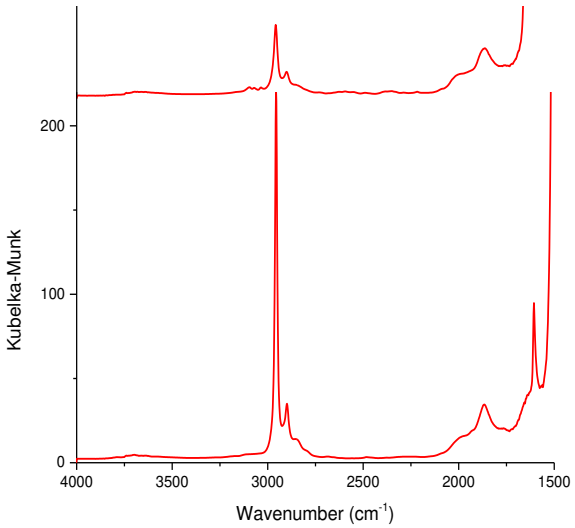

Figure 14 – DRIFT spectra of P10 (bottom), and P12 (top).

The DRIFT spectrum of P12 shows a decrease in the intensity of the group of peaks between 2750 and 3000 cm^{-1} assigned to the C-H stretching of the allyl and the appearance of new peaks above 3000 cm^{-1} and between 1500-1600 cm^{-1} for the stretching of the aromatic rings.

To confirm that the reaction proceeded as expected and that $Ph_3C(C_3H_3(SiMe_3)_2)$ was obtained as side product, a GC-MAS analysis of the washing solution was performed. The presence of a peak at 428 uma confirmed the formation of the expected side product.

After the reaction the cationic Y resulted to be unstable on the surface. After a few days, the green powder recovered at the end of the reaction (stored in a storage tube in the glove box, H_2O<0.1ppm, O_2<0.1ppm at 20°C) turned deep blue, indicating a modification in the nature of the species present on the silica surface. Although this change in P12 was observed, the surface was characterized by mass balance analysis and solid state NMR.

Table 17 reports the results of the quantification of the species present on the surface of P12.

Table 17 – Elemental analysis results for P12.

wt% Y	wt% C	wt% B	wt% F	Y mmol g^{-1}	C/Y	F/B	B/Y
3.4	11.4	0.27	9.1	0.42	24.8 (th. 30)	19.6 (th. 20)	0.7 (th. 1)

The theoretical values reported in Table 17 are calculated on the base of the coordination of 1 borate per Y, from the amount of boron found on the surface, 0.27 wt%, it was clear that only 70% of the yttrium on the surface reacted to give the cationic species. Assuming the coordination of only 0.7 B/Y, it is possible to say that the ratio of 24.8 C/Y found on the support is in agreement with the theoretical value of 28.5 for a surfaces of the composition showed in Scheme 12.

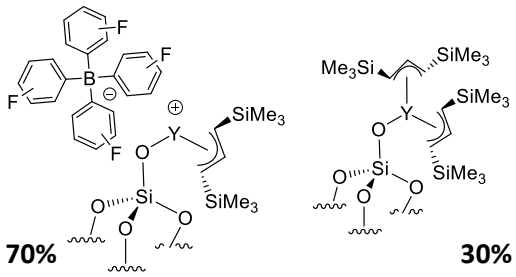

Scheme 12 – Surface composition of P12.

The solid state NMR spectra reported in Figure 15 were acquired after the color change of P12, but can anyway help to understand the surface composition.

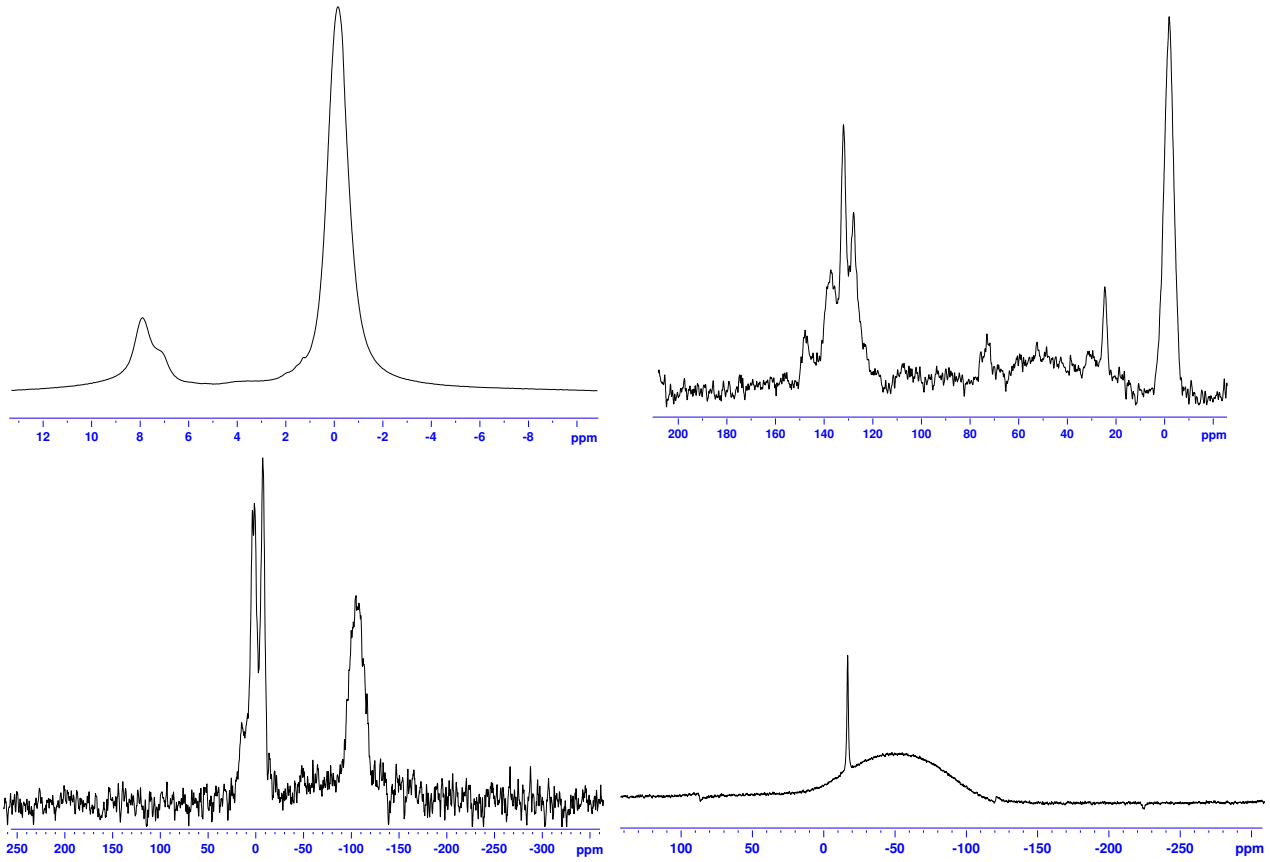

Figure 15 – ^{1}H MAS (top left), ^{13}C CPMAS (top right), ^{29}Si CPMAS (bottom left), ^{11}B MAS (bottom right) solid state NMR spectra for P12.

The ^{1}H NMR spectrum shows three main peaks at 7.91, 7.17 and -0.16 ppm and a shoulder at 3.77 ppm. The peak at 7.17, -0.16 and the shoulder at 3.77 ppm were assigned to the allyl bound to the Y while the peak at 7.91 ppm was attributed to benzene molecules which could have remained coordinated to the Y adduct.

The ^{13}C NMR spectrum shows multiple peaks in the aromatic region, 148.0, 137.6, 132.2, 128.2 ppm which can be attributed to the benzene coordinated to Y and to the carbon of the allyl fragment –CH=***C***HCH-. At -1.98 ppm resonate the methyls of the –$SiMe_3$ fragments. It is still possible to see the peaks relative to the THF impurities on the surface at 73.2 and 24.7 ppm.

The ^{11}B NMR spectrum shows one sharp peak at -15.5 ppm which is attributed to the boron of the borate ion.

The ^{29}Si NMR spectrum shows the peak proper of the silica of the support at -105.3 ppm. The two peaks at -7 and 2 ppm were attributed to the –$SiMe_3$ respectively of the neutral and cationic species on the surface, by comparison with the ^{29}Si CP MAS solid state NMR spectrum acquired for P10. The comparison of the tw spectra is reported in Figure 16.

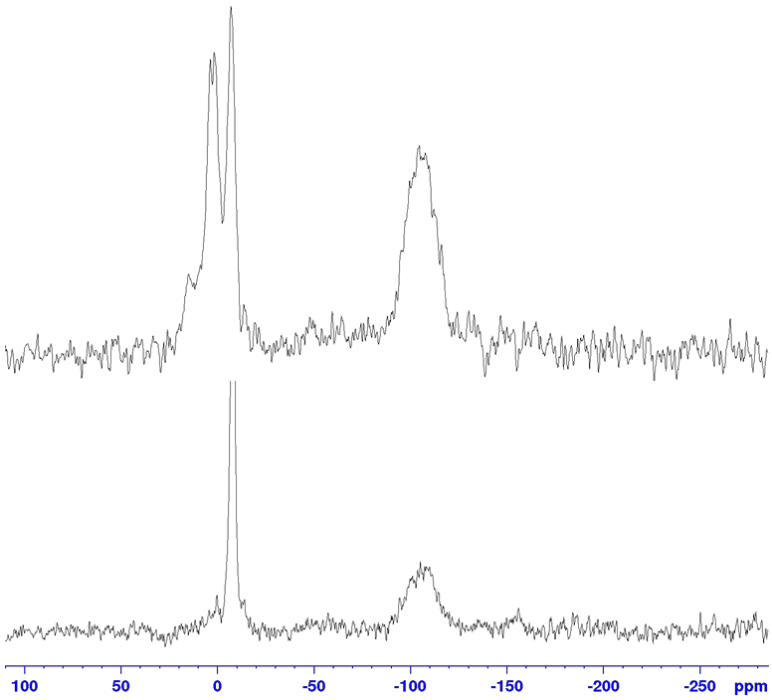

Figure 16 – ^{29}Si CPMAS spectra for P10 (bottom) and P12 (top).

The characterizations performed on P12, revealed that after the reaction, indeed the ionic couple $[(\equiv SiO)Y\{1,3\text{-}C_3H_3(SiMe_3)_2\}]^+[B(C_6F_5)_4]^-$ was formed, but that the species isn't stable on the surface. To be able to test the catalyst in polymerization was thus decided to generate the Y cation in situ in the autoclave, by pre-contacting P11 and P10 with 1 eq. of $[C(C_6H_5)_3]^+[B(C_6F_5)_4]^-$, BARF.

4.2 Test in ethylene polymerization of P10/BARF and P11/BARF

In this paragraph is presented the application in ethylene slurry polymerization of two grafted Y cationic species, generated *in situ* in the reactor prior to the polymerization. It was decided to use this approach given the instability of the cationic yttrium on the silica surface.

Both catalysts P10 and P11 were modified with $[C(C_6H_5)_3]^+[B(C_6F_5)_4]^-$ to generate respectively $[(\equiv SiO)Y\{1,3\text{-}C_3H_3(SiMe_3)_2\}]^+[B(C_6F_5)_4]^-$ and $[(\equiv SiO)_2Y]^+[B(C_6F_5)_4]^-$. The polymerization reaction was conducted in a stainless steel autoclave in 50 mL of heptane, at 80°C and 10 bars of ethylene for 30 minutes. The catalysts were tested in both ethylene homopolymerization and ethylene/1-hexene copolymerization. The results obtained are reported in Table 18.

Table 18 – Results of the slurry polymerization tests performed with P10/BARF and P11/BARF. General conditions: 50 mL heptane, 80°C, 10 bars ethylene, 30 minutes, B/Y = 1.

Runs	Catalyst	$m_{support}$ mg	$Y_{surface}$ µmol	[TiBA] mM	1-hexene mol%	Yield g	Activity $g\ g_{cat}^{-1}\ h^{-1}$	Activity $Kg\ mol_Y^{-1}\ h^{-1}\ bar^{-1}$
4	P11	20.7	11.4	-	-	1.89	183	33.3
7	P10	16.5	6.9	-	-	6.19	752	180
25	P10/BARF	20.4	8.5	-	-	8.76	860	206
26	P10/BARF	20.2	8.5	-	21	6.98	690	164
27	P10/BARF	13.5	5.7	1	-	2.09	310	74
28	P11/BARF	20.8	11.5	-	-	2.88	280	50
29	P11/BARF	20.1	11.1	-	21	0.19	20	3.3

Both catalyst showed activities in ethylene polymerization, and, like for their neutral homologues, the bipodal species was less active than the monopodal one, 280 and 860 $g_{PE}\ g_{cat}^{-1}\ h^{-1}$ respectively. Runs 25 and 27 show that also for P10/BARF, like for P10, the presence of TiBA is detrimental for the activity of the catalyst, cutting its activity almost in half, 860 to 310 $g_{PE}\ g_{cat}^{-1}\ h^{-1}$. Finally, interestingly, Table 18 shows that both cationic catalyst suffer in presence of comonomer an important drop in activity: when 1-hexene is added to the system the activity of P10/BARF goes from 860 to 690 $g_{PE}\ g_{cat}^{-1}\ h^{-1}$, while for P11/BARF it dramatically plummets from 280 to 20 $g_{PE}\ g_{cat}^{-1}\ h^{-1}$. The obtained resins were characterized by DSC, also in this case the HT-SEC analysis was

made difficult by the high molar masses of the produced polymers. The results are reported in Table 19.

Table 19 – DSC characterization of the resins obtained with the cationic Y catalysts P10/BARF and P11/BARF.

Run	Catalyst	Activity g g_{cat}^{-1} h^{-1}	T_m (1st melting) °C	Crystallinity (1st melting) %	T_m (2nd melting) °C	Crystallinity (2nd melting) %
25	**P10/BARF**	860	143	76	135	58.6
26	**P10/BARF**	690	141	58	134	48.4
27	**P10/BARF**	310	143	69	136	56.9
28	**P11/BARF**	280	140	66	135	63.2
29	**P11/BARF**	20	134	52	131	55.8

The DSC results reported in Table 19 show that the resins produced with the two cationic yttrium catalysts are highly linear and crystalline PEs, with ultra-high molar masses.

To better understand the exact nature of the cations formed on the surface and the reason behind their instability on the surface, further studies would be necessary.

Conclusions

In this chapter was showed the application of grafted yttrium complexes as catalysts for ethylene slurry polymerization. Four neutral catalysts (P8, P9, P10 and P11) and two cationic species (P10/BARF and P11/BARF) were tested and the activities obtained were confronted with literature references.[27] The most active catalyst amongst those listed above was P10, of structure (≡SiO)Y{1,3-$C_3H_3(SiMe_3)_2$}$_2$; when tested at laboratory scale in slurry copolymerization ethylene/1-hexene, it showed an activity higher than 1100 $g_{PE}\ g_{cat}^{-1}\ h^{-1}$, exhibiting an important comonomer effect, even though the polymer produced was highly linear, with 135°C T_m. As other grafted rare-earth metal catalysts the obtained resins had molar masses higher than 1500 Kg mol^{-1}, which made it most of the time impossible to characterize by HT-SEC.

Considering the results obtained at laboratory scale encouraging, P10 was scaled up to pre-industrial scale in INEOS facilities in Brussels. During this tests was investigated the hydrogen effect on the polymer molar masses and the influence of TiBA on the activity. From this study it was evidenced that by introducing up to 5.6 mol% H2/C2 it was possible to reduce the molar masses of the resins to 300 Kg mol^{-1} and positively affect the activity of the catalysts. The TiBA, on the other side, had a highly detrimental effect on activity, in fact by decreasing the amount of TiBA present in the reactor from 0.5 to 0.05 mmol the activity of P10 increased linearly up to 7000 $g_{PE}\ g_{cat}^{-1}\ h^{-1}$. The obtained resins where highly linear PE with melting temperatures of 135 °C and crystallinities of 55-60%.

Although the very good results obtained in polymerization further characterization studies must be performed on P10 to better understand what kind of interactions are formed in presence of hydrogen, 1-hexene and TiBA during the reaction, so to explain the effects observed during our studies.

References

(1) Ballard, D. G.; Courtis, A.; Holton, J.; McMeeking, J.; Pearce, R. Alkyl Bridged Complexes of the Group 3 A and Lanthanoid Metals as Homogeneous Ethylene Polymerisation Catalysts. *J. Chem. Soc. Chem. Commun.* 1978, No. 22, 994–995.

(2) Long, D. P.; Bianconi, P. A. A Catalytic System for Ethylene Polymerization Based on Group III and Lanthanide Complexes of Tris (Pyrazolyl) Borate Ligands. *J. Am. Chem. Soc.* 1996, *118* (49), 12453–12454.

(3) Jeske, G.; Lauke, H.; Mauermann, H.; Swepston, P. N.; Schumann, H.; Marks, T. J. Highly Reactive Organolanthanides. Systematic Routes to and Olefin Chemistry of Early and Late Bis (Pentamethylcyclopentadienyl) 4f Hydrocarbyl and Hydride Complexes. *J. Am. Chem. Soc.* 1985, *107* (26), 8091–8103.

(4) Jeske, G.; Lauke, H.; Mauermann, H.; Schumann, H.; Marks, T. J. Highly Reactive Organolanthanides. A Mechanistic Study of Catalytic Olefin Hydrogenation by Bis (Pentamethylcyclopentadienyl) and Related 4f Complexes. *J. Am. Chem. Soc.* 1985, *107* (26), 8111–8118.

(5) Jeske, G.; Schock, L. E.; Swepston, P. N.; Schumann, H.; Marks, T. J. Highly Reactive Organolanthanides. Synthesis, Chemistry, and Structures of 4f Hydrocarbyls and Hydrides with Chelating Bis(Polymethylcyclopentadienyl) Ligands. *J. Am. Chem. Soc.* 1985, *107* (26), 8103–8110. https://doi.org/10.1021/ja00312a051.

(6) Schaverien, C. J. Alkoxides as Ancillary Ligands in Organolanthanide Chemistry: Synthesis of, Reactivity of, and Olefin Polymerization by the .Mu.-Hydride-.Mu.-Alkyl Compounds [Y(C5Me5)(OC6H3tBu2)]2(.Mu.-H)(.Mu.-Alkyl). *Organometallics* 1994, *13* (1), 69–82. https://doi.org/10.1021/om00013a017.

(7) Ihara, E.; Yoshioka, S.; Furo, M.; Katsura, K.; Yasuda, H.; Mohri, S.; Kanehisa, N.; Kai, Y. Synthesis and Olefin Polymerization Catalysis of New Trivalent Samarium and Yttrium Complexes with Bridging Bis(Cyclopentadienyl) Ligands. *Organometallics* 2001, *20* (9), 1752–1761. https://doi.org/10.1021/om000226a.

(8) Gilchrist, J. H.; Bercaw, J. E. New NMR Spectroscopic Probe of the Absolute Stereoselectivity for Metal-Hydride and Metal-Alkyl Additions to the Carbon−Carbon Double Bond. Demonstration with a Single-Component, Isospecific Ziegler−Natta α-Olefin Polymerization Catalyst. *J. Am. Chem. Soc.* 1996, *118* (48), 12021–12028. https://doi.org/10.1021/ja962869g.

(9) Evans, W. J.; DeCoster, D. M.; Greaves, J. Metalation as a Termination Step in Polymerization Reactions Involving α-Olefins and Ethylene As Detected by Field Desorption Mass Spectrometry [1]. *Organometallics* 1996, *15* (14), 3210–3221. https://doi.org/10.1021/om960298v.

(10) Evans, W. J.; DeCoster, D. M.; Greaves, J. Field Desorption Mass Spectrometry Studies of the Samarium-Catalyzed Polymerization of Ethylene under Hydrogen. *Macromolecules* 1995, *28* (23), 7929–7936. https://doi.org/10.1021/ma00127a046.

(11) Shapiro, P. J.; Schaefer, W. P.; Labinger, J. A.; Bercaw, J. E.; Cotter, W. D. Model Ziegler-Natta .Alpha.-Olefin Polymerization Catalysts Derived from[{(.Eta.5-C5Me4)SiMe2(.Eta.1-NCMe3)}(PMe3)Sc(.Mu.2-H)]2 and[{(.Eta.5-C5Me4)SiMe2(.Eta.1-NCMe3)}Sc(.Mu.2-CH2CH2CH3)]2. Synthesis, Structures, and Kinetic and Equilibrium Investigations of the Catalytically Active Species in Solution. *J. Am. Chem. Soc.* 1994, *116* (11), 4623–4640. https://doi.org/10.1021/ja00090a011.

(12) Burger, B. J.; Thompson, M. E.; Cotter, W. D.; Bercaw, J. E. Ethylene Insertion and .Beta.-Hydrogen Elimination for Permethylscandocene Alkyl Complexes. A Study of the Chain Propagation and Termination Steps in Ziegler-Natta Polymerization of Ethylene. *J. Am. Chem. Soc.* 1990, *112* (4), 1566–1577. https://doi.org/10.1021/ja00160a041.

(13) Shapiro, P. J.; Bunel, E.; Schaefer, W. P.; Bercaw, J. E. Scandium Complex [{(.Eta.5-C5Me4)Me2Si(.Eta.1-NCMe3)}(PMe3)ScH]2: A Unique Example of a Single-Component .Alpha.-Olefin Polymerization Catalyst. *Organometallics* 1990, *9* (3), 867–869. https://doi.org/10.1021/om00117a055.

(14) Piers, W. Non-Cyclopentadienyl Ancillaries in Organogroup 3 Metal Chemistry: A Fine Balance in Ligand Design. *Coord. Chem. Rev.* 2002, *233–234*, 131–155. https://doi.org/10.1016/S0010-8545(02)00016-4.

(15) Edelmann, F. T.; Freckmann, D. M. M.; Schumann, H. Synthesis and Structural Chemistry of Non-Cyclopentadienyl Organolanthanide Complexes. *Chem. Rev.* 2002, *102* (6), 1851–1896. https://doi.org/10.1021/cr010315c.

(16) Schumann, Herbert.; Meese-Marktscheffel, J. A.; Esser, Lothar. Synthesis, Structure, and Reactivity of Organometallic .Pi.-Complexes of the Rare Earths in the Oxidation State Ln3+ with Aromatic Ligands. *Chem. Rev.* 1995, *95* (4), 865–986. https://doi.org/10.1021/cr00036a004.

(17) Zeimentz, P. M.; Arndt, S.; Elvidge, B. R.; Okuda, J. Cationic Organometallic Complexes of Scandium, Yttrium, and the Lanthanoids. *Chem. Rev.* 2006, *106* (6), 2404–2433. https://doi.org/10.1021/cr050574s.

(18) Le Roux, E.; Anwander, R. Surface Organolanthanide and -Actinide Chemistry. In *Modern Surface Organometallic Chemistry*; Basset, J.-M., Psaro, R., Roberto, D., Ugo, R., Eds.; Wiley-VCH Verlag GmbH & Co. KGaA: Weinheim, Germany, 2009; pp 455–512. https://doi.org/10.1002/9783527627097.ch12.

(19) Dietrich, H. M.; Raudaschl-Sieber, G.; Anwander, R. Trimethylyttrium and Trimethyllutetium. *Angew. Chem. Int. Ed.* 2005, *44* (33), 5303–5306. https://doi.org/10.1002/anie.200463109.

(20) Anwander, R. Principles in Organolanthanide Chemistry. In *Lanthanides: Chemistry and Use in Organic Synthesis*; Kobayashi, S., Ed.; Topics in Organometallic Chemistry; Springer: Berlin, Heidelberg, 1999; pp 1–61. https://doi.org/10.1007/3-540-69801-9_1.

(21) Anwander, R. SOMC@PMS. Surface Organometallic Chemistry at Periodic Mesoporous Silica. *Chem. Mater.* 2001, *13* (12), 4419–4438. https://doi.org/10.1021/cm0111534.

(22) Gerstberger, G.; Palm, C.; Anwander, R. The Danishefsky Hetero Diels–Alder Reaction Mediated by Organolanthanide-Modified Mesoporous Silicate MCM-41. *Chem. – Eur. J.* 1999, *5* (3), 997–1005. https://doi.org/10.1002/(SICI)1521-3765(19990301)5:3<997::AID-CHEM997>3.0.CO;2-D.

(23) Bouh, A. O.; Rice, G. L.; Scott, S. L. Mono- and Dinuclear Silica-Supported Titanium(IV) Complexes and the Effect of TiOTi Connectivity on Reactivity. *J. Am. Chem. Soc.* 1999, *121* (31), 7201–7210. https://doi.org/10.1021/ja9829160.

(24) Nagl, I.; Widenmeyer, M.; Grasser, S.; Köhler, K.; Anwander, R. Surface Confined Ketyl Radicals via Samarium(II)-Grafted Mesoporous Silicas. *J. Am. Chem. Soc.* 2000, *122* (7), 1544–1545. https://doi.org/10.1021/ja9932535.

(25) Anwander, R.; Roesky, R. Grafting of Versatile Lanthanide Silylamide Precursors onto MesoporousMCM-41. *J. Chem. Soc. Dalton Trans.* 1997, No. 2, 137–138.

(26) Tortosa, K.; Hamaide, T.; Boisson, C.; Spitz, R. Homogeneous and Heterogeneous Polymerization of ε-Caprolactone by Neodymium Alkoxides Prepared In Situ. *Macromol. Chem. Phys.* 2001, *202* (7), 1156–1160. https://doi.org/10.1002/1521-3935(20010401)202:7<1156::AID-MACP1156>3.0.CO;2-9.

(27) Woodman, T. J.; Sarazin, Y.; Fink, G.; Hauschild, K.; Bochmann, M. Heterogenized "Ligand-Free" Lanthanide Catalysts for the Homo- and Copolymerization of Ethylene and 1,3-Butadiene. *Macromolecules* 2005, *38* (8), 3060–3067. https://doi.org/10.1021/ma047454r.

(28) Gauvin, R. M.; Mortreux, A. Silica-Supported Lanthanide Silylamides for Methyl Methacrylate Polymerisation: Controlled Grafting Induces Controlled Reactivity. *Chem. Commun.* 2005, No. 9, 1146. https://doi.org/10.1039/b416533k.

(29) Gauvin, R. M.; Chenal, T.; Hassan, R. A.; Addad, A.; Mortreux, A. Grafted Lanthanide Amides: Versatile Catalysts for Various Transformations. *J. Mol. Catal. Chem.* 2006, *257* (1–2), 31–40. https://doi.org/10.1016/j.molcata.2006.04.022.

(30) Gauvin, R. M.; Delevoye, L.; Hassan, R. A.; Keldenich, J.; Mortreux, A. Well-Defined Silica-Supported Rare-Earth Silylamides. *Inorg. Chem.* 2007, *46* (4), 1062–1070. https://doi.org/10.1021/ic0610334.

(31) Chen, Y.; Zhu, Z.; Zhang, J.; Shen, J.; Zhou, X. Modification of Mesoporous Silicate SBA-15 with Tris[Bis(Trimethylsilyl)Amido]Samarium and Its Utility in Tishchenko Reaction. *J. Organomet. Chem.* 2005, *690* (16), 3783–3789. https://doi.org/10.1016/j.jorganchem.2005.05.013.

(32) Nagl, I.; Widenmeyer, M.; Herdtweck, E.; Raudaschl-Sieber, G.; Anwander, R. Scandium Methyl Surface Species via SOMC on MCM-41 Silica. *Microporous Mesoporous Mater.* 2001, *44*, 311–319.

(33) Anwander, R.; Runte, O.; Eppinger, J.; Gerstberger, G.; Herdtweck, E.; Spiegler, M. Synthesis and Structural Characterisation of Rare-Earth Bis (Dimethylsilyl) Amides and Their Surface Organometallic Chemistry on Mesoporous MCM-41. *J. Chem. Soc. Dalton Trans.* 1998, No. 5, 847–858.

(34) Anwander, R.; Nagl, I.; Zapilko, C.; Widenmeyer, M. Methyl Methacrylate Polymerization at Samarium(II)-Grafted MCM-41. *Tetrahedron* 2003, *59* (52), 10567–10574. https://doi.org/10.1016/j.tet.2003.07.018.

(35) Lefort, L.; Chabanas, M.; Maury, O.; Meunier, D.; Copéret, C.; Thivolle-Cazat, J.; Basset, J.-M. Versatility of Silica Used as a Ligand: Effect of Thermal Treatments of Silica on the Nature of Silica-Supported Alkyl Tantalum Species. *J. Organomet. Chem.* 2000, *593–594*, 96–100. https://doi.org/10.1016/S0022-328X(99)00396-4.

(36) Le Roux, E.; Taoufik, M.; Chabanas, M.; Alcor, D.; Baudouin, A.; Copéret, C.; Thivolle-Cazat, J.; Basset, J.-M.; Lesage, A.; Hediger, S.; Emsley, L. Well-Defined Surface Tungstenocarbyne Complexes through the Reaction of [W(:CtBu)(CH2tBu)3] with Silica. *Organometallics* 2005, *24* (17), 4274–4279. https://doi.org/10.1021/om050086a.

(37) Evans, W. J.; Anwander, R.; Ziller, J. W. Inclusion of Al2Me6 in the Crystalline Lattice of the Organometallic Complexes LnAl3Me12. *Organometallics* 1995, *14* (3), 1107–1109. https://doi.org/10.1021/om00003a011.

(38) Anwander, R.; Görlitzer, H. W.; Gerstberger, G.; Palm, C.; Runte, O.; Spiegler, M. Grafting of Bulky Rare Earth Metal Complexes onto Mesoporous Silica MCM-41†. *J. Chem. Soc. Dalton Trans.* 1999, *0* (20), 3611–3615. https://doi.org/10.1039/A903096D.

(39) Allouche, F.; Chan, K. W.; Fedorov, A.; Andersen, R. A.; Copéret, C. Silica-Supported Pentamethylcyclopentadienyl Ytterbium(II) and Samarium(II) Sites: Ultrahigh Molecular Weight Polyethylene without Co-Catalyst. *Angew. Chem. Int. Ed.* 2018, *57* (13), 3431–3434. https://doi.org/10.1002/anie.201800542.

(40) Vancompernolle, T.; Valente, A.; Chenal, T.; Zinck, P.; Del Rosal, I.; Maron, L.; Taoufik, M.; Harder, S.; Gauvin, R. M. Silica-Grafted Lanthanum Benzyl Species: Synthesis, Characterization, and Catalytic Applications. *Organometallics* 2017, *36* (20), 3912–3920. https://doi.org/10.1021/acs.organomet.7b00538.

(41) Del Rosal, I.; Yahia, A.; Maron, L. Effects of the Grafting of Lanthanum Complexes on a Silica Surface on the Reactivity: Influence on Ethylene, Propylene, and 1,3-Butadiene Homopolymerization. *Inorg. Chem.* 2016, *55* (20), 10024–10033. https://doi.org/10.1021/acs.inorgchem.6b01238.

(42) Barzan, C.; Bordiga, S.; Groppo, E. Toward the Understanding of the Comonomer Effect on Cr^{II}/SiO_2 Phillips Catalyst. *ACS Catal.* 2016, *6* (5), 2918–2922. https://doi.org/10.1021/acscatal.6b00147.

(43) Wang, X.-Y.; Salovey, R. Melting of Ultrahigh Molecular Weight Polyethylene. *J. Appl. Polym. Sci.* 1987, *34* (2), 593–599. https://doi.org/10.1002/app.1987.070340214.

(44) Liu, K.; de Boer, E. L.; Yao, Y.; Romano, D.; Ronca, S.; Rastogi, S. Heterogeneous Distribution of Entanglements in a Nonequilibrium Polymer Melt of UHMWPE: Influence on Crystallization without and with Graphene Oxide. *Macromolecules* 2016, *49* (19), 7497–7509. https://doi.org/10.1021/acs.macromol.6b01173.

(45) Sändig, N.; Koch, W. Why Does Cp_2YH Catalyze the Polymerization of Ethene but Not of Propene? *Organometallics* 2002, *21* (9), 1861–1869. https://doi.org/10.1021/om0104417.

(46) Casey, C. P.; Tunge, J. A.; Fagan, M. A. Why Propene Is Not Polymerized by (Cp*2YH)2: Reactions of Yttrium Alkyl Complexes with Alkenes Produce Allyl and Vinyl Yttrium Complexes. *J. Organomet. Chem.* 2002, *663* (1–2), 91–97. https://doi.org/10.1016/S0022-328X(02)01771-0.

(47) Busico, V.; Cipullo, R.; Friederichs, Nic.; Linssen, H.; Segre, A.; Van Axel Castelli, V.; van der Velden, G. ^{1}H NMR Analysis of Chain Unsaturations in Ethene/1-Octene Copolymers Prepared with Metallocene Catalysts at High Temperature. *Macromolecules* 2005, *38* (16), 6988–6996. https://doi.org/10.1021/ma050620q.

General conclusions and perspectives

As discussed at the very beginning of this manuscript, my thesis's work is framed in the polyolefin background and, more specifically, in the field of ethylene polymerization promoted by single-site catalysts. Our efforts were focused on the development and application of structurally well-defined activating supports prepared by surface organometallic chemistry for the immobilization of metallocene complexes.

The current state of the art and developments in the heterogenization of molecular catalysts and their application in industrial processes were briefly presented in Chapter I, in order to frame the research work discussed in the following Chapters in the present scientific progresses in the field, and to clearly show its relevance for industrial application.

Chapter II focuses on the development and application in different processes of activating support AS1. The surface of AS1 was composed by bipodal aluminate species of structure $[(\equiv SiO)_2Al(OC_6F_5)_2]^-[HNMe_2Et]^+$. The synthesis procedure and surface characterization of the support was exposed at the beginning of the chapter confirming the successful synthesis of the ionic couple on the surface.

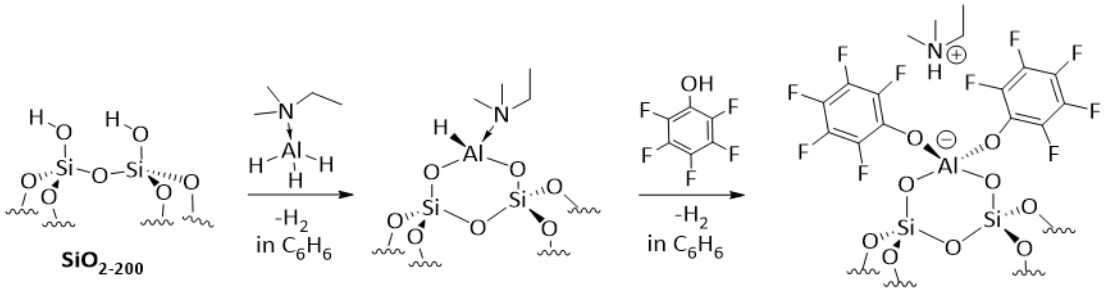

Scheme 1 - Preparation of supported activating support based on Aluminum hydrides

Once the surface composition was ascertained the efficiency of AS1 as activating support for two zirconocenes *rac*-$EtInd_2ZrCl_2$ and (n-$BuCpMe)_2ZrCl_2$ was evaluated in presence of an alkylating agent. The prepared systems were tested both at laboratory and pre-industrial scale. The obtained results were excellent both in terms of catalyst performances and controlled of polyethylene particle morphology. The observed productivities at lab-scale were for both catalysts above 900 $gg_{cat}^{-1}h^{-1}$ in ethylene/1-hexene slurry polymerization, which would become 4000 $gg_{cat}^{-1}h^{-1}$ in the scale-up to pre-industrial application.

The obtained polymers were typical mLLDPE resins, which generally presented between 1 and 3 mol% of comonomer incorporation in the polymer chain and a melting temperature between 115 and 125 °C (strictly depending on the degree of branching of the sample). Furthermore, the obtained fluffs presented very good morphology and particle size distribution, direct consequence of the fact that the activator is chemically bound to the surface of the support, reducing the risks of leaching.

Once these preliminary studies on the efficiency of the activating support were conducted, the isolation of formulated catalysts on AS1 with both complexes *rac*-EtInd$_2$ZrCl$_2$ and (*n*-BuCpMe)$_2$ZrCl$_2$ was presented. It resulted that, to be able to obtain an efficient formation of the active species and highly productive catalysts, it was necessary to methylate the zirconocene complexes prior to their immobilization. From this study two highly active catalysts, IsoCatM1 and IsoCatM2, were obtained with the two zirconocenes. The two catalysts were tested at laboratory scale in ethylene/1-hexene slurry copolymerization and IsoCatM1 also in ethylene gas phase homopolymerization. The obtained initial results were highly encouraging, in fact both catalysts were highly active and produced polymers with the same properties of those obtained previously with the zirconocene complexes. What though was quickly found out was that the active species were unstable at room temperature: in the span of 20 days the catalyst activity would drop from 1888 to 255 g g_{cat}^{-1} h^{-1}at ambient temperature.

To understand this phenomenon, the evolution of the ionic couple on the surface was studied and the occurrence of a transfer of ligand from the aluminate to the zirconocene was shown. This phenomenon was already reported by Marks for homogeneous systems. In the following chapters we focused then to find a solution to avoid the ligand transfer.

In Chapter III, in order to avoid the deactivation process it was presented the synthesis of bipodal aluminates activating supports in which the pentafluorophenol was substituted by either chelating or more sterically hindered ligands. Although most of the synthesized species were structurally well-defined, they all showed very poor efficiency in ethylene slurry polymerization, if confronted with the results observed in Chapter II. The main reason could be attributed to a variation of the dissociation of the formed ion couple, which is vital for a good activity in polymerization.

In Chapter IV we studied two different approaches to the synthesis of new activating supports. The first group of presented ASs were well-defined halogenated aluminates, either chlorides or fluorides, obtained from different alkylaluminium precursors. In literature were in fact known very efficient fluorinated solid activators for metallocene catalysts, but nothing was known on the structure of actual species that take part in the activation. All the synthesized activating supports were tested in ethylene polymerization, but also in this case the obtained activity was very low with respect to AS1. This is attributed to a too strong interaction between the Zr cation and the Al-X moiety.

The second set of activating supports presented in Chapter IV were homologous of AS1 but the aluminium centre was substituted by an yttrium centre, in order to get a stronger M-O bond for the activator which would slow the ligand transfer process reported in Chapter II. Four yttrium based activating supports were synthesized and tested in ethylene slurry polymerization, with very little success. The recorded activity was very low and nowhere comparable to that of AS1. The same comments exposed previously for all the other activating supports can be easily applied also in this case.

The development of grafted yttrium precursors for the synthesis of the activating supports, led though to the discovering of an incredibly performing catalyst for ethylene polymerization. In Chapter V of this thesis was in fact shown the application in slurry polymerization of the four grafted benzyl and allyl yttrium species used as synthesis precursors in Chapter IV. Although all of them demonstrated good activities in ethylene polymerization, one in particular highly exceeded in productivity what is currently reported in literature for this kind of catalysts: (≡SiO)Y{1,3-$C_3H_3(SiMe_3)_2\}_2$, P10. This well-defined supported complex was successfully prepared by Surface Organometallic Chemistry and characterized by elemental analysis, reactivity with water, DRIFT, Solid state NMR and EXAFS.

P10 was tested both at laboratory and pre-industrial scale in ethylene homopolymerization and copolymerization with 1-hexene, with or without hydrogen. The obtained maximum of activity was of 7000 g g_{cat}^{-1} h^{-1}. The polymerization results were of high interest for the field of PEHD. It resulted evident that the catalyst's behaviour would change dramatically depending on the amount of TiBA

and the presence of hydrogen in the reactor. TiBA is in fact a true poison for P10, decreasing its amount in the reactor, more than doubled the catalyst's productivity. Hydrogen on the other side changes completely the P10's response to the comonomer. While without H_2 the 1-hexene has a positive effect on productivity, although not being incorporated in the chain, when hydrogen is present the longer olefin causes a dramatic chute in the productivity. This could be explained by a modification, by work of H2, of the nature of the active species on the surface. To have, though, real insight on the interactions that take place during the process, a deeper characterization study is needed.

The obtained results during this work with both AS1 and P10 are very encouraging and worth pursuing. On the side of AS1 by working on the catalysts' isolation methods, that could help stabilize the active species on the surface. On the side of yttrium, a further characterization of the active species formed in presence of hydrogen, 1-hexene and TiBA is necessary, to understand what side reaction could take place during the polymerization reaction and optimize the use of the catalyst.

Another and important consideration can be evinced from all unsuccessful but interesting results reported in Chapters III and IV. We clearly saw first-hand how delicate is the balance of the ionic couple, protagonist of olefin polymerization. All the changes that we produced on the activator, not only resulted in a slightly lower efficiency of the catalyst, but in an almost complete inactivity of the system, making us understand how little we still know about the deep nature of the main actors involved in olefin polymerization.

Experimental section

Experimental section

1. General

All experiments were performed under a controlled atmosphere by using Schlenk and glove-box techniques for organometallic syntheses. For the synthesis and treatments of the surface species, reactions were performed by using high-vacuum lines (1 mPa) and glove boxes.

- Solvent purification at C2P2

All the solvents used during the synthesis of the grafted species were purified over NaK and freshly distilled prior to use. Concerning the solvents used during the polymerization tests, the heptane was collected from a MBRAUN Solvent Purification System, the toluene was distilled over NaK and then stored in the glove box on molecular sieves overnight.

- Purification of the reagents used in polymerizations at C2P2

1-hexene was dried over CaH_2 and then further purified over NaK. Ethylene (purity 99.95%) was purchased from Air Liquide. The gas was passed through three different purification columns before use: a first one filled with reduced BASF R3-16 catalyst (CuO on alumina), a second one filled with molecular sieves (13X, 3A, Sigma–Aldrich) and a final one filled with Selexsorb COS (Alcoa).

2. Characterization techniques

- Characterizations performed at C2P2

Elemental analyses of the supported products were performed at the Mikroanalytisches Labor Pascher, Remagen (Germany).

Gas-phase analyses were performed on a Hewlett–Packard 5890 series II gas chromatograph equipped with a flame ionization detector and an Al_2O_3/KCl on fused silica column (50 m x 0.32 mm).

NMR Spectroscopy Solid-state ^{1}H MAS and ^{13}C CPMAS NMR spectra were recorded on a Bruker Avance 500 spectrometer with a conventional double-resonance 4 mm CPMAS probe. Solid state ^{27}Al MAS NMR spectra were recorded on a Bruker Avance III 800 spectrometer with a conventional double-resonance 3.2 mm MAS probe. Chemical shifts were given with respect to TMS as the

external reference for ^{1}H and ^{13}C NMR spectroscopy, to $CFCl_3$ for ^{19}F NMR spectroscopy and to $Al(H_2O)_6^{3+}$ for ^{27}Al.

EXAFS spectra were acquired at ESRF, using BM23 beam-line, at room temperature at the yttrium K-edge (17.04 keV). A pair of Si(111) crystals was used as monochromator and a system based on a total reflection through a double X-ray mirror with an incidence angle variable from 2 to 5 mrad allowed harmonic rejection to better than the 10^{-5} level.[1] The spectra were recorded in the transmission mode between 16.8 and 18.15 keV. Four scans were collected for each sample. Each data set was collected simultaneously with a Y metal foil reference (17038.4 eV), and was later aligned according to that reference (maximum of the first derivative of the first peak of the Y foil). The Y supported samples were packaged within an argon filled glovebox in a double air-tight sample holder equipped with kapton windows. The data analyses were carried out using the program "Athena" and the EXAFS fitting program "RoundMidnight", from the "MAX" package, using spherical waves. The program FEFF8 was used to calculate theoretical files for phases and amplitudes based on model clusters of atoms. The refinements were carried out by fitting the structural parameters N_i, R_i, σ_i and the energy shift, ΔE_0 (the same for all shells).

Thermal characterizations were performed with a differential scanning calorimetry, Mettler Toledo DSC 1, equipped with an auto-sampler and a 120 thermocouple sensor. The temperature and the heat flow of the equipment were calibrated with an indium standard. All samples were accurately weighed (between 5 to 10 mg) and sealed in aluminum pans. They were heated from -20 °C to 180 °C at 10 °C min^{-1} with an empty aluminum pan as reference. Two successive heating and cooling were performed and only the second run was considered. Dry nitrogen with a flow rate set at 50 mL min^{-1} was used as the purge gas. The melting temperature (T_m) was measured at the top of the endothermic peak. The STARe thermal analysis software is used to calculate the melting temperature and the crystallinity of the copolymers: $X = \Delta H_f / \Delta H_{f0}$ where ΔH_f (J g^{-1}) is the melting heat of the sample and ΔH_{f0} (= 293 J g^{-1}) the melting heat of a 100 % crystalline polyethylene.

SEM images have been observed on a FEI Quanta 250 FEG microscope, after metallization of the samples by a copper film evaporation on a Baltec MED020 apparatus.

HT-SEC High temperature Size Exclusion Chromatography analyses were performed using a Viscotek system (from Malvern Instruments) equipped with three columns (Polefin 300 mm x 8 mm I. D. from Polymer Standards Service, porosity of 1000 Å, 100000 Å and 1000000 Å). 200 µL of sample solutions with concentration of 3 mg mL^{-1} were eluted in 1,2,4-trichlorobenzene using a flow rate of 1 mL min^{-1} at 150°C. The mobile phase was stabilized with 2,6-di(tert-butyl)-4-methylphenol (200 mg L^{-1}). The OmniSEC 5.12 software was used for data acquisition and data analysis. Online detection was performed with a differential refractive index detector and a dual light scattering detector (LALS and RALS) for absolute molar mass measurement.

Bulk density. The fluff was dropped with the aid of a funnel in a cylinder of known volume. As much polymer was put in the cylinder as to fill it without any compression of the powder. Once the cylinder was full the polymer was levelled to the brim of the container, without any compression, and weighed. The density of the resin was obtained by dividing the weight of the polymer per its volume.

Particle size distribution. For the analysis if the particle size distribution of the polymers was used a laser Granulometer Coulter LS 13320 coupled with a Dry powder system module (Tornado). The determination of the particle size is determined by the deviation of the laser in passing through the powder. 20 g of samples are used for the mesure.

FTIR. For the IR characterization of the polymers was used a Perkin Elmer spectrum One. The samples are pressed in a film prior to the analysis.

GPC. The polymers were analysed with a PL-GPC220 High temperature GPC system coupled with a PL-SP260 sample preparation system. 8-9 mg of sample are dissolved I 10 mL of TCM at 160°C for two hours under a light N_2 flux. The calibration of the machine is done based on polystyrene samples.

MVS. For the determination of the polymers' densities the resin was weighed a METTLER TOLEDO balance RS-232 C with a precision of 0.01 mg. The volume of the sample was determined by the unit PRISMA, constituted by a graduated becker containing undecane conditioned at 23°C and an engine to move the samples. The volume of the polymer, previously pressed in a disc, is measured by difference between the levels of undecane before and after the immersion of the disc.

DSC. For the DSC measurements was employed a DSC Perkin Elmer diamond DAL 1222. Between 1.75 and 2.25 mg of the sample (previously pressed in a film) were weighed in a 10 µL Al capsule which was then sealed. They were heated from -10 °C to 180 °C at 20 °C min^{-1} with an empty aluminum pan as reference. Two successive heating and cooling were performed and only the second run was considered.

Melt Index. The melt index measurements were done on Goettfert MI4. For the measure 5 g of polymer were weighed and put inside the cylinder with the help of a funnel. The sample was compacted inside the cylinder and the piston was position over the sample with the desired weight. After a preheating test, the measure starts once the piston descends below 50 mm. The time of the measure varies depending on the fluidity of the sample, but it can't exceed the 25 minutes.

3. Treatment of the silica support

- Partial dehydroxylation at 200°C ($SiO_{2\text{-}200}$)

The silica used was Grace Sylopol 2408. 3.00 g of the silica were put inside a 500 ml glass reactor. High vacuum (1 Pa) was pulled over the silica sample, and the temperature was brought to 200°C with a ramp of 4°C min^{-1}. The dehydroxylation reaction proceeded for 16 h, the sample was collected and stored in the glove box. The amount of silanol groups present on the surface after the partial dehydroxylation is of 1.62 mmol g^{-1}. DRIFT: 3743 cm^{-1} SiO-H(isolated) stretching; 3680-3570 cm^{-1} SiO-H(vicinal) stretching.

- Partial dehydroxylation at 700°C ($SiO_{2\text{-}700}$)

3.18 g of silica Sylopol 2408 was put inside a 500 ml quartz reactor with the top extremity open. The reactor was put in an oven and the sample was calcinated at 500°C for 2 h. High vacuum (1 Pa) was then pulled inside the reactor and the temperature brought at 700°C. The sample was left under these conditions for 16 h. Then it was collected and stored in the glove box. The amount of isolated silanol groups present on the silica surface after the partial dehydroxylation is of 0.58 mmol g^{-1}. DRIFT: 3743 cm^{-1} SiO-H(isolated) stretching.

Table 1 – Physical properties of the silica Sylopol 2408.

Silica	Silica Specific area ($m^2.g^{-1}$)	Pore volume ($g.mL^{-1}$)	Particle size (µm)	$mmol_{OH}\ g^{-1}$	OH nm^{-2}
SY2408	300	1.6	54	1.62[(a)] 0.58[(b)]	3.3[(a)] 1.14[(b)]

(a) 200°C; (b) 700°C

4. Polymerization procedures

- Polymerization procedure at C2P2, glass reactor

In a small round bottomed flask were introduced the activating support, 10 mL of a solution 1mM of TiBA in heptane and the required amount of a 2mM solution of the metallocene precursor in toluene. The suspension was then transferred in a 1L flask in which had already been put 300-350 mL of heptane, 2 mL of 1-hexene, and the right amount of a 0.5 M TiBA solution in heptane to obtain a 1 mM final solution in TiBA. This solution was then transferred rapidly in the glass reactor which was already at 80°C. All these operations were conducted under Ar flux. The Ar in excess was removed and the system was slowly pressurized with 4 bars of ethylene to start the polymerization reaction. During the polymerization the ethylene consumption was monitored. After 30 minutes the ethylene feed was interrupted and the reactor cooled to room temperature. The polymer suspension was then poured in 400 mL of a mixture 50/50 of methanol/acetone and the polymer was filtered under vacuum and washed 3 times with acetone. The polymer was left to dry overnight.

- Polymerization procedure at C2P2, autoclave

The 70 mL stainless steel autoclave was filled in the glovebox with the heptane, the eventual scavenger and comonomer and the catalyst. It was then closed inside the glovebox and furtherly sealed outside. The system was then put to heat to 80°C for 15 minutes and in the meantime the ethylene line was purged twice with 10 bar pressure of C_2H_4. Once the temperature was reached the autoclave was pressurized with 10 bars of ethylene and the reaction left running for 30 minutes. At the end of the polymerization the autoclave was cooled down and degassed. The polymer was filtered under vacuum and washed with acetone three times and left to dry.

- Polymerization procedure at NOH

A five L autoclave was filled with the desired amount of TiBA and 1.5 L of isobutane, the system was brought to 80°C and then pressurised with 10 bars of ethylene and H_2 at the ratio H2/C2 of 0.15 mol%. The desired amount of 1-hexene was added manually through a graduated column, right before the start of the polymerization.

2 mL of a 0.5 mM solution of the zirconocene precursor in toluene were pre-contacted with 0.5 mL of a solution 0.1 M of TiBA in hexane. This solution was then taken in a syringe in which had previously been weighed the activating support.

The suspension was injected in the cannon of the autoclave and flushed in the autoclave with aliquots of isobutane. The temperature inside the reactor, the ethylene consumption and the ratio C6/C2 and H2/C2 were monitored throughout the reaction. After one hour the system was degassed and cooled to room temperature. The polymer was collected and left to dry furtherly.

5. Synthesis of the grafted species

- Grafting of $AlH_3(NEtMe_2)$ on $SiO_{2\text{-}200}$, P1

2.20 g of $SiO_{2\text{-}200}$ (3.7 mmol SiOH) was put inside a double Schlenk together with 4.00 ml of 0.5 M solution of $AlH_3(NMe_2Et)$ (2.0 mmol) in toluene. A high vacuum condition was created inside the double Schlenk and 10 mL of benzene were distilled onto the alane solution. Once a homogeneous solution was obtained, this was transferred onto the silica to start the grafting reaction. The reaction lasted 2 h. The volatiles were removed and collected in a 10 L balloon. The sample was washed three times with fresh benzene and once with pentane, and then dried under high vacuum. It was collected and stored in the glove box. DRIFT: 3680-3750 cm^{-1} SiO-H(vicinal) stretching; 2700-2900 cm^{-1} C-H stretching; 1800-1850 cm^{-1} Al-H stretching; Elemental analysis: 2.69 wt% Al; 4.71 wt% C; 1.45 wt% N; 1.12 wt% H; ^{1}H MAS NMR: δ(ppm): 1.3 $N(CH_3)2(CH_2\underline{CH_3})$; δ(ppm): 2.7 $N(\underline{CH_3})_2(\underline{CH_2}CH_3)$ ^{13}C CPMAS NMR: δ(ppm): 6 $N(CH_3)_2(CH_2\underline{CH_3})$; δ(ppm): 42.3 $N(\underline{CH_3})2(CH_2CH_3)$; δ(ppm): 52.2 $N(CH_3)2(\underline{CH_2}CH_3)$.

- Synthesis of $[(\equiv SiO)_2Al(OC_6F_5)_2]^-[HNMe_2Et]^+$, AS1

1.00 g of $(\equiv SiO)_2AlH(NEtMe_2)$ (1.0 mmol SiOH) was put inside a double Schlenk with 461.8 mg (2.5 mmol) of pentafluorophenol. After having pulled high vacuum inside the double Schlenk, 10 ml of benzene were distilled on the pentafluonophenol in order to obtain a homogeneous solution. This was then transferred on the grafted Al hydride to start the reaction. After 2 h the volatiles were removed and collected in a 6 L balloon. The product was washed three times with benzene and once with pentane, then it was dried under high vacuum. It was collected and stored in the glove box. DRIFT: 3680-3750 cm^{-1} SiO-H(vicinal) stretching; 2700-2900 cm^{-1} C-H stretching; 3070 cm^{-1} N-H stretching; Elemental analysis: 1.4 wt% Al; 11.4 wt% C; 0.9 wt% N; ^{1}H MAS NMR: δ(ppm): 1.3 $N(CH_3)_2(CH_2\underline{CH_3})$; δ(ppm): 2.9 $N(\underline{CH_3})_2(\underline{CH_2}CH_3)$ ^{13}C CPMAS NMR: δ(ppm): 7.4 $N(CH_3)_2(CH_2\underline{CH_3})$; δ(ppm): 41.9 $N(\underline{CH_3})_2(CH_2CH_3)$; δ(ppm): 53.2 $N(CH_3)_2(\underline{CH_2}CH_3)$; ^{19}F MAS NMR: δ(ppm): -161 ortho-F; δ(ppm): -166 meta-F; δ(ppm): -173 para-F; ^{27}Al MAS NMR: δ(ppm): 47.5 ppm.

- Grafting of $AlH_3(NEtMe_2)$ on $SiO_{2\text{-}700}$, P2

2.90 g of $SiO_{2\text{-}700}$ (1.7 mmol SiOH) were put inside a double Schlenk together with 4.90 mL of 0.5 M solution of $AlH_3(NMe_2Et)$ (2.5mmol) in toluene. A high vacuum condition was then created inside the double Schlenk and 10 ml of benzene were distilled onto the alane solution. Once a homogeneous solution was obtained, this has been transferred onto the silica to start the grafting reaction. The reaction lasted 2 h. The volatiles were removed and collected in a 6 L balloon. The sample was washed three times with fresh benzene and once with pentane, and was then dried under high vacuum. It was then collected and stored in the glove box. DRIFT: 2700-2900 cm^{-1} C-H stretching; 1805-1865 cm^{-1} Al-H stretching; 2234 cm^{-1} Si-H stretching; Elemental analysis: 1.89 wt% Al; 3.03 wt% C; 1.19 wt% N; 0.83 wt% H; ^{1}H MAS NMR: δ(ppm): 0.9 $N(CH_3)2(CH_2\underline{CH_3})$; δ(ppm): 2.1 $N(\underline{CH_3})_2(\underline{CH_2}CH_3)$; δ(ppm): 4.9 SiH; ^{13}C CPMAS NMR: δ(ppm): 6.2 $N(CH_3)_2(CH_2\underline{CH_3})$; δ(ppm): 41.1 $N(\underline{CH_3})2(CH_2CH_3)$; δ(ppm): 51.9 $N(CH_3)2(\underline{CH_2}CH_3)$.

- Synthesis of $[(\equiv SiO)Al(OC_6F_5)_3]^-[HNMe_2Et]^+$, AS2

1.01 g of $(\equiv SiO)AlH_2(NEtMe_2)$ (0.5 mmol) was put inside a double Schlenk with 387.5 mg (2.1 mmol) of pentafluorophenol. After having pulled high vacuum inside the double Schlenk, 10 ml of

benzene were distilled on the pentafluonophenol in order to obtain a homogeneous solution. This was transferred on the grafted Al hydride to start the reaction. After 2 h the volatiles were removed and collected in a 6 L balloon. The product was washed three times with benzene and once with pentane, and then dried under high vacuum. It was collected and stored in the glove box. DRIFT: 2700-2900 cm^{-1} C-H stretching; 3070 cm^{-1} N-H stretching; Elemental analysis: 1.25 wt% Al; 9.32 wt% C; 0.74 wt% N; 0.55 wt% H; ^{1}H MAS NMR: δ(ppm): 1.3 $N(CH_3)_2(CH_2\underline{CH_3})$; δ(ppm): 2.9 $N(\underline{CH_3})_2(\underline{CH_2}CH_3)$; δ(ppm): 4.2 SiH; ^{13}C CPMAS NMR: δ(ppm): 7.1 $N(CH_3)_2(CH_2\underline{CH_3})$; δ(ppm): 42.5 $N(\underline{CH_3})_2(CH_2CH_3)$; δ(ppm): 53.7 $N(CH_3)_2(\underline{CH_2}CH_3)$; ^{19}F MAS NMR: δ(ppm): -162 ortho-F; δ(ppm): -168 meta-F; δ(ppm): -174 para-F.

- **Synthesis of $[(\equiv SiO)_2Al(O_2C_{20}H_{12})]^-[HNMe_2Et]^+$, AS3**

503.2 mg (0.5 mmol) of $(\equiv SiO)_2AlH(NEtMe_2)$ were put in a 20 mL vial with 10 mL of toluene. 174 mg (0.6 mmol) of binaphtol were added to the suspension to start the reaction. After 2 hours the reaction was stopped and the product washed 3 times with fresh toluene and once with pentane. The powder was dried under high vacuum. DRIFT: 3680-3750 cm^{-1} SiO-H(vicinal) stretching; 2700-2900 cm^{-1} C-H stretching; 3070 cm^{-1} N-H stretching; 1500-1600 cm^{-1} C=C stretching; Elemental analysis: 0.88 wt% Al; 11.0 wt% C; 0.67 wt% N; 1.11wt% H; ^{1}H MAS NMR: δ(ppm): 0.98 $N(CH_3)_2(CH_2\underline{CH_3})$; δ(ppm): 2.38 $N(\underline{CH_3})_2(\underline{CH_2}CH_3)$; 7.38 Ar; ^{13}C CPMAS NMR: δ(ppm): 9.1 $N(CH_3)_2(CH_2\underline{CH_3})$; δ(ppm): 41.6 $N(\underline{CH_3})_2(CH_2CH_3)$; δ(ppm): 51.7 $N(CH_3)_2(\underline{CH_2}CH_3)$; 130-155 Ar; 153.2 $\underline{C}$-O.

- **Synthesis of $[(\equiv SiO)_2Al(OC(CF_3)_2Ph)_2]^-[HNMe_2Et]^+$, AS4**

537.6 mg of $(\equiv SiO)_2AlH(NEtMe_2)$ (0.54 mmol) were put in a 20 mL vial with 10 mL of toluene. 0.21 mL of $(C_6H_5)(CF_3)_2COH$ (0.74 mmol) were added to the suspension to start the reaction. After 3 hours the reaction was stopped and the product washed 3 times with fresh toluene and once with pentane. The powder was dried under high vacuum. DRIFT: 3680-3750 cm^{-1} SiO-H(vicinal) stretching; 2700-2900 cm^{-1} C-H stretching; 3070 cm^{-1} N-H stretching; 1850 cm^{-1} Al-H stretching; Elemental analysis: 2.3 wt% Al; 6.4 wt% C; 1.0 wt% N; 0.9 wt% H; 4.0 wt% F; ^{1}H MAS NMR: δ(ppm): 1.06 $N(CH_3)_2(CH_2\underline{CH_3})$; δ(ppm): 2.23 $N(\underline{CH_3})_2(\underline{CH_2}CH_3)$; 7.58 Ar; 7.73 Ar; ^{13}C CPMAS NMR: δ(ppm): 5.4 $N(CH_3)_2(CH_2\underline{CH_3})$; δ(ppm): 41.1 $N(\underline{CH_3})_2(CH_2CH_3)$; δ(ppm): 51.5 $N(CH_3)_2(\underline{CH_2}CH_3)$; 125-135 Ar.

- Synthesis of $[(\equiv SiO)_2Al(O_2C_5HF_6)_2]^-[HNMe_2Et]^+$, AS5

998.7 mg of $(\equiv SiO)_2AlH(NEtMe_2)$ (1.0 mmol) were put in a double Schlenk with 0.31 mL (2.4 mmol) of $C_5H_2F_6O_2$. 20 mL of benzene were distilled over the acetylacetonate and the solution was transferred on the silica. The reaction was left going overnight. The product was then washed 3 times with benzene and once with pentane. The volatiles were removed and the product dried under high vacuum. DRIFT: 3680-3750 cm^{-1} SiO-H(vicinal) stretching; 2700-2900 cm^{-1} C-H stretching; 3070 cm^{-1} N-H stretching; Elemental analysis: 0.9 wt% Al; 6.1 wt% C; 0.6 wt% N; 0.7 wt% H; 8.1 wt% F; ^{1}H MAS NMR: δ(ppm): 1.16 $N(CH_3)_2(CH_2\underline{CH_3})$; δ(ppm): 2.80 $N(\underline{CH_3})_2(\underline{CH_2}CH_3)$; 6.05 $-O_2C_5\underline{H}F_6$; ^{13}C CPMAS NMR: δ(ppm): 7.5 $N(CH_3)_2(CH_2\underline{CH_3})$; δ(ppm): 41.4 $N(\underline{CH_3})_2(CH_2CH_3)$; δ(ppm): 52.5 $N(CH_3)_2(\underline{CH_2}CH_3)$; 89.1 –$\underline{CH}$–; 114.8 –$\underline{CF_3}$; 177.1 –$\underline{C}$-O.

- Synthesis of $[(\equiv SiO)_2Al(O_2P\text{-binaphtol})_2]^-[HNMe_2Et]^+$, AS6

997 mg of $(\equiv SiO)_2AlH(NEtMe_2)$ (1.0 mmol) were put in a vial with 10 mL of toluene and 777 mg (2.2 mmol) of hydrogenphosphate. The reaction proceeded overnight. The product was washed 3 times with toluene and once with pentane and then dried under high vacuum. DRIFT: 3680-3750 cm^{-1} SiO-H(vicinal) stretching; 2700-2900 cm^{-1} C-H stretching; 3060 cm^{-1} N-H stretching; 1500-1600 cm^{-1} C=C stretching; Elemental analysis: 1.43 wt% Al; 29.41 wt% C; 1.81 wt% P; 2.009 wt% H; ^{1}H MAS NMR: δ(ppm): 1.4 $N(CH_3)_2(CH_2\underline{CH_3})$; δ(ppm): 2.9 $N(\underline{CH_3})_2(\underline{CH_2}CH_3)$; 6.3 Ar; ^{13}C CPMAS NMR: δ(ppm): 6.2 $N(CH_3)_2(CH_2\underline{CH_3})$; δ(ppm): 40.2 $N(\underline{CH_3})_2(CH_2CH_3)$; δ(ppm): 49.9 $N(CH_3)_2(\underline{CH_2}CH_3)$; 110-140 Ar; 145.7 $\underline{C}$-O.

- Synthesis of $(\equiv SiO)_2Al\textit{i}Bu(Et_2O)$, P3

1.50 g of $SiO_{2\text{-}700}$ (0.87 mmol SiOH) were put inside a double Schlenk with 0.37 ml (1.4 mmol) of $AliBu_3$. After a high vacuum condition was created inside the double Schlenk, 10 ml of Et_2O were distilled over the triisobutyl aluminium, and a solution was obtained. The solution was then transferred on the silica to start the grafting reaction. After 2 h the volatiles were put in a 6 L balloon and the sample washed three times with fresh Et_2O. The sample was dried under high vacuum and collected and stored in the glove box. DRIFT: 2700-2900 cm^{-1} C-H stretching; Elemental analysis: 1.25 wt% Al; 5.87 wt% C; 1.15 wt% H; ^{1}H MAS NMR: δ(ppm): 4.05 Et_2O; δ(ppm):

1.77 $AlCH_2\underline{CH}(CH_3)_2$; δ(ppm): 1.26 Et_2O; δ(ppm): 0.83 $AlCH_2CH(\underline{CH_3})_2$; δ(ppm): -0.22 $Al\underline{CH_2}CH(CH_3)_2$; ^{13}C CPMAS NMR: δ(ppm): 11.9 Et_2O; δ(ppm): 20.9 $Al\underline{CH_2}CH(CH_3)_2$, $SiCH_2\underline{CH}(CH_3)_2$; δ(ppm): 23.4 $SiCH_2\underline{CH}(\underline{CH_3})_2$; δ(ppm): 25.3 $AlCH_2\underline{CH}(\underline{CH_3})_2$; δ(ppm): 66.0 Et_2O.

- **Synthesis of $(\equiv SiO)_2AlCl$, P4**

504.0 mg of $(\equiv SiO)_2AliBu(Et_2O)$ (0.23 mmol) were put in a 500 ml glass reactor, high vacuum was pulled over the sample and HCl gas at its vapour pressure was transferred inside the reactor. After 1 h the gasses were removed and the sample collected and stored in the glove box. DRIFT: 2500-2900 cm^{-1} C-H stretching; Elemental analysis: 1.18 wt% Al; 2.21 wt% C; 1.78 wt% Cl; 0.46 wt% H.

- **Synthesis of $[(\equiv SiO)_2AlCl(OC_6F_5)]^-[HNEt_2Ph]^+$, AS7**

590.3 mg of $(\equiv SiO)_2AlCl$ (0.26 mmol) were put inside a double Schlenk with 0.31 mL of a 1 M solution of diethylaniline (0.31 mmol) in benzene and 10 mL of benzene. The aniline solution was then transferred on the supported Al chloride to start the coordination reaction. After one hour the volatiles were removed and 60.2 mg (0.33mmol) of pentafluorophenol were added to the Schlenk. The pentafluorophenol was dissolved in other 10 mL of benzene and then transferred on the powder. The reaction proceeded overnight. The product was washed 3 times with benzene, the volatiles were removed and the sample dried under high vacuum. DRIFT: 2700-2900 cm^{-1} C-H stretching; 3070 cm^{-1} N-H stretching; 1500-1600 cm^{-1} C=C stretching; Elemental analysis: 1.14 wt% Al; 5.25 wt% C; 0.57 wt% N; 2.60 wt% Cl; ^1H MAS NMR: δ(ppm): 0.95 $N(CH_2\underline{CH_3})Ph$; δ(ppm): 1.49 THF; δ(ppm): 3.52 THF; δ(ppm): 4.40 $N(\underline{CH_2}CH_3)Ph$; δ(ppm): 7.63 $N(CH_2CH_3)\underline{Ph}$; ^{13}C CPMAS NMR: δ(ppm): 11.6 $N(CH_2\underline{CH_3})Ph$; δ(ppm): 23.1 THF; δ(ppm): 47.2 $N(\underline{CH_2}CH_3)Ph$; δ(ppm): 69.9 THF; δ(ppm): 118-142 $N(CH_2\underline{CH_3})Ph$; ^{19}F MAS NMR: δ(ppm): -161.2 ortho-F; δ(ppm): -167.8 meta-F; δ(ppm): -173.8 para-F.

- **Synthesis of $[(\equiv SiO)_2AlCl_2]^-[HNEtMe_2]^+$, AS8**

506.11 mg of $(\equiv SiO)_2AlH(NMe_2Et)$ (0.51 mmol) were put in a 500 ml glass reactor, the high vacuum was pulled over the sample and HCl gas at its vapour pressure was transferred inside the reactor. After 1 h the gasses were removed and the sample collected and stored in the glove box. DRIFT: 3680-3750 cm^{-1} SiO-H(vicinal) stretching; 2700-2900 cm^{-1} C-H stretching; 3148 cm^{-1} N-H

stretching; Elemental analysis: 1.72 wt% Al; 3.3 wt% C; 1.14 wt% N; 0.99 wt% H; 5.27 wt% Cl; ^{1}H MAS NMR: δ(ppm): 1.1 N(CH_3)$_2$($CH_2\underline{CH_3}$); δ(ppm): 2.8 N($\underline{CH_3}$)$_2$($\underline{CH_2}CH_3$) ^{13}C CPMAS NMR: δ(ppm): 6.5 N(CH_3)$_2$($CH_2\underline{CH_3}$); δ(ppm): 41.8 N($\underline{CH_3}$)$_2$(CH_2CH_3); δ(ppm): 52.4 N(CH_3)$_2$($\underline{CH_2}CH_3$).

- **Synthesis of (≡SiO)AlF(*i*Bu)(Et$_2$O), P5**

2.07 g of $SiO_{2\text{-}700}$ (1.2 mmol SiOH) were put in a double Schlenk with 0.23 g of AliBu_2F (1.5 mmol). 10 mL of Et_2O were then distilled on the Al(*iBu$_2$*)F and the solution was transferred on the silica to start the grafting reaction. After two hours all the volatiles were transferred in a 6 L balloon. The product was then washed four times with fresh Et_2O. All the volatiles were removed by an intermediate trap and the product was dried under high vacuum. DRIFT: 2700-2900 cm^{-1} C-H stretching; Elemental analysis: 1.71 wt% Al; 5.86 wt% C; 1.13 wt% H; 0.91 wt% F; ^{1}H MAS NMR: δ(ppm): 4.10 Et_2O; δ(ppm): 1.77 Al$CH_2\underline{CH}(CH_3)_2$; δ(ppm): 1.25 Et_2O; δ(ppm): 0.83 Al$CH_2CH(\underline{CH_3})_2$; δ(ppm): -0.19 Al$\underline{CH_2}CH(CH_3)_2$; ^{13}C CPMAS NMR: δ(ppm): 12.0 Et_2O; δ(ppm): 17.3 Al$OCH_2CH(\underline{CH_3})_2$; δ(ppm): 20.8 Al$\underline{CH_2}CH(CH_3)_2$; δ(ppm): 25.4 Al$CH_2\underline{CH}(\underline{CH_3})_2$; δ(ppm): 30.1 Al$OCH_2\underline{CH}(CH_3)_2$; δ(ppm): 66.3 Et_2O; δ(ppm): 71.3 Al$O\underline{CH_2}CH(CH_3)_2$;.

- **Synthesis of [(≡SiO)AlF(OC$_6$F$_5$)$_2$]$^-$[HNEtMe$_2$]$^+$, AS9**

753.6 mg of (≡SiO)Al*i*BuF(Et_2O) (0.45 mmol) were put in a double Schlenk with 180.6 mg (1.0 mmol) of pentafluorophenol. 10 mL of benzene were distilled over the phenol and the obtained solution was transferred on the supported adduct. Then 0.7 mL of dimethylethylamine were distilled trap to trap in the double Schlenk. The reaction proceeded overnight. The product was then washed with benzene three times and with pentane once. The volatiles were removed by an intermediate trap and the product was dried under high vacuum. DRIFT: 2700-2900 cm^{-1} C-H stretching; 3070 cm^{-1} N-H stretching; 1500-1600 cm^{-1} C=C stretching; Elemental analysis: 1.27 wt% Al; 8.1 wt% C; 08.22 wt% F; 0.59 wt% H; ^{1}H MAS NMR: δ(ppm): 0.52 N(CH_3)$_2$($CH_2\underline{CH_3}$); δ(ppm): 2.62 N($\underline{CH_3}$)$_2$($\underline{CH_2}CH_3$); ^{13}C CPMAS NMR: δ(ppm): 6.6 N(CH_3)$_2$($CH_2\underline{CH_3}$); δ(ppm): 41.1 N($\underline{CH_3}$)$_2$(CH_2CH_3); δ(ppm): 52.6 N(CH_3)$_2$($\underline{CH_2}CH_3$).

- **Synthesis of (≡SiO)AlF(*i*Bu), P6**

1.50 g of $SiO_{2\text{-}700}$ (0.87 mmol) were put in a double Schlenk with 0.24 g (1.5 mmol) of $AliBu_2F$. 10 mL of pentane were then distilled on the $Al(iBu_2)F$ and the solution was transferred on the silica to start the grafting reaction. After one hour and a half all the volatiles were transferred in a 6 L balloon. The product was then washed 3 times with fresh pentane. All the volatiles were removed by an intermediate trap and the product was dried under high vacuum. DRIFT: 2700-2900 cm^{-1} C-H stretching; Elemental analysis: 2.14 wt% Al; 5.34 wt% C; 0.95 wt% H; 0.98 wt% F; ^{1}H MAS NMR: δ(ppm): 1.85 $AlCH_2\underline{CH}(CH_3)_2$; δ(ppm): 0.87 $AlCH_2CH(\underline{CH_3})_2$; δ(ppm): 0.11 $Al\underline{CH_2}CH(CH_3)_2$; ^{13}C CPMAS NMR: δ(ppm): 17.9 $Al\underline{CH_2}CH(CH_3)_2$; δ(ppm): 23.3 $AlCH_2\underline{CH}(\underline{CH_3})_2$.

- **Synthesis of $[(\equiv SiO)AlF(OC_6F_5)_2]^-[HNEtMe_2]^+$, AS10**

1.03 g of (≡SiO)AlF*i*Bu (1.0 mmol) were put in a double Schlenk with 300.5 mg (1.6 mmol) of pentafluorophenol. 10 mL of benzene were distilled on the pentafluorophenol and the solution was transferred on the silica. 0.15 mL (1.2 mmol) of $NEtMe_2$ were then distilled in the double Schlenk. The reaction was left to proceed overnight. The product was washed 3 times with benzene and once with pentane. The volatiles were then removed and the product dried under high vacuum. DRIFT: 2700-2900 cm^{-1} C-H stretching; 3070 cm^{-1} N-H stretching; 1500-1600 cm^{-1} C=C stretching; Elemental analysis: 1.41 wt% Al; 8.56 wt% C; 0.85 wt% N; 8.66 wt% F; ^{1}H MAS NMR: δ(ppm): 1.0 $N(CH_3)_2(CH_2\underline{CH_3})$; δ(ppm): 2.52 $N(\underline{CH_3})_2(\underline{CH_2}CH_3)$; ^{13}C CPMAS NMR: δ(ppm): 5.3 $N(CH_3)_2(CH_2\underline{CH_3})$; δ(ppm): 39.7 $N(\underline{CH_3})_2(CH_2CH_3)$; δ(ppm): 51.3 $N(CH_3)_2(\underline{CH_2}CH_3)$.

- **Synthesis of (≡SiO)AlF*i*Bu$_2$, P7**

2.02 g of $SiO_{2\text{-}200}$ (2.0 mmol SiOH) were put in a double Schlenk with 0.45 mL (2.0 mmol) of $AliBu_2F$. 10 mL of pentane were then distilled on the $AliBu_2F$ and the solution was transferred on the silica to start the grafting reaction. After 2 hours all the volatiles were transferred in a 6 L balloon. The product was then washed 3 times with fresh pentane. All the volatiles were removed by an intermediate trap and the product was dried under high vacuum. DRIFT: 3560-3680 cm^{-1} SiO-H(vicinal) stretching; 2700-2900 cm^{-1} C-H stretching; Elemental analysis: 3.67 wt% Al; 6.65 wt% C;

1.25 wt% H; 2.11 wt% F; ^{1}H MAS NMR: δ(ppm): 2.17 $AlCH_2\underline{CH}(CH_3)_2$; δ(ppm): 0.70 $Al\underline{CH_2}CH(\underline{CH_3})_2$; ^{13}C CPMAS NMR: δ(ppm): 15.3 $Al\underline{CH_2}CH(CH_3)_2$; δ(ppm): 24.4 $AlCH_2\underline{CH}(\underline{CH_3})_2$.

- **Synthesis of $[(\equiv SiO)_2AlF(OC_6F_5)]^-[HNEtMe_2]^+$, AS11**

1.03 g of $(\equiv SiO)AlFiBu_2$ (1.4 mmol) were put in a double Schlenk with 491 mg (2.7 mmol) of pentafluorophenol. 10 mL of benzene were distilled on the pentafluorophenol and the solution was transferred on the silica. 0.15 mL (1.2 mmol) of $NEtMe_2$ were then distilled in the double Schlenk. The reaction was left to proceed for three hours. The product was washed 3 times with benzene and once with pentane. The volatiles were then removed and the product dried under high vacuum. DRIFT: 3560-3680 cm^{-1} SiO-H(vicinal) stretching; 2700-2900 cm^{-1} C-H stretching; 3070 cm^{-1} N-H stretching; 1500-1600 cm^{-1} C=C stretching; Elemental analysis: 2.25 wt% Al; 8.78 wt% C; 0.87 wt% N; 9.57 wt% F; 0.73 wt% H; ^{1}H MAS NMR: δ(ppm): 1.14 $N(CH_3)_2(CH_2\underline{CH_3})$; δ(ppm): 2.9 $N(\underline{CH_3})_2(\underline{CH_2}CH_3)$; ^{13}C CPMAS NMR: δ(ppm): 5.8 $N(CH_3)_2(CH_2\underline{CH_3})$; δ(ppm): 40.1 $N(\underline{CH_3})_2(CH_2CH_3)$; δ(ppm): 51.4 $N(CH_3)_2(\underline{CH_2}CH_3)$.

- **Synthesis of $(\equiv SiO)Y(CH_2PhNMe_2)_2$, P8**

854.7 mg of $SiO_{2\text{-}700}$ (0.5 mmol SiOH) were put inside a double Schlenk with 295.5 mg (0.6 mmol) of $Y(o\text{-}NMe_2\text{-benzyl})_3$. After having pulled high vacuum in the double Schlenk, 10 ml of toluene were distilled over the Y complex to solubilize it. The solution was then transferred over the silica to start the grafting reaction. The reaction proceeded overnight, the product was washed three times with toluene, the solution thus obtained was removed, and the sample washed once more with pentane. The product was dried under high vacuum and then collected and stored in the glove box. DRIFT: 2700-2900 cm^{-1} C-H stretching; Elemental analysis: 3.82 wt% Y; 9.29 wt% C; 1.18 wt% H; 1.26 wt% N; ^{1}H MAS NMR: δ(ppm): 6.9 *o*-$CH_2\underline{Ph}NMe_2$; δ(ppm): 2.4 *o*-$CH_2PhN\underline{Me_2}$; δ(ppm): 2.0 *o*-$\underline{CH_2}PhNMe_2$; ^{13}C CPMAS NMR: δ(ppm): 17.2 Si(*o*-$\underline{CH_2}PhN\underline{Me_2}$); δ(ppm): 24.1 THF; δ(ppm): 43.1 *o*-$\underline{CH_2}PhN\underline{Me_2}$; δ(ppm): 69.9 THF; δ(ppm): 119-150 *o*-$CH_2\underline{Ph}NMe_2$.

- **Synthesis of $[(\equiv SiO)Y(OC_6F_5)_3]^-[HNMe_2(PhMe)]^+$, AS12**

504.9 mg of $(\equiv SiO)Y(o\text{-}NMe_2\text{-benzyl})_2$ (0.21 mmol) were put inside a double Schlenk with 194.1 mg (1.05 mmol) of pentafluorophenol. After having pulled high vacuum in the double Schlenk 10 ml

of benzene were distilled over the pentafluorophenol to solubilize it. The solution was transferred on the (≡SiO)Y(o-NMe_2-benzyl)$_2$ to start the reaction. The reaction proceeded overnight. The product was washed three times with benzene, the solution was removed, and then the sample washed once more with pentane. The product was dried under high vacuum. It was collected and stored in the glove box. DRIFT: 2700-2900 cm^{-1} C-H stretching; 3077 cm^{-1} N-H stretching; Elemental analysis: 3.15 wt% Y; 12.49 wt% C; 0.60 wt% H; 0.58 wt% N;10.5 wt% F; ^{1}H MAS NMR: δ(ppm): 7.1 [*o*-CH_3Ph$NHMe_2$]$^+$; δ(ppm): 3.2 [*o*-CH_3PhNHMe_2]$^+$; ^{13}C CPMAS NMR: δ(ppm): 14.6 [*o*-CH_3PhNHMe_2]$^+$; δ(ppm): 23.4 THF; δ(ppm): 45.5 [*o*-CH_3PhNHMe_2]$^+$; δ(ppm): 69.9 THF; δ(ppm): 117-150 [*o*-CH_3Ph$NHMe_2$]$^+$.

- **Synthesis of (≡SiO)$_2$Y(CH_2PhNMe_2), P9**

603.0 mg of $SiO_{2\text{-}200}$ (1.0 mmol) were put inside a double Schlenk with 288.0 mg (0.6 mmol) of Y(o-NMe_2-benzyl)$_3$. After having pulled high vacuum in the double Schlenk, 10 ml of toluene were distilled over the Y complex to solubilize it. The solution was transferred over the silica to start the grafting reaction. The reaction proceeded overnight, the product was washed three times with toluene, the solution thus obtained was removed, and the sample washed once more with pentane. The product was dried under high vacuum. It was collected and stored in the glove box. DRIFT: 3560-3680 cm^{-1} SiO-H(vicinal) stretching; 2700-2900 cm^{-1} C-H stretching; Elemental analysis: 5.43 wt% Y; 7.84 wt% C; 1.01 wt% H; 1.10 wt% N; ^{1}H MAS NMR: δ(ppm): 7.1 *o*-CH_2PhNMe_2; δ(ppm): 2.2 *o*-CH_2PhNMe_2; δ(ppm): 1.04 *o*-CH_2PhNMe_2; δ(ppm): 0.63 *o*-CH_2PhNMe_2; ^{13}C CPMAS NMR: δ(ppm): δ(ppm): 24.3 THF; δ(ppm): 43.3 *o*-CH_2PhNMe_2; δ(ppm): 71.1 THF; δ(ppm): 118-150 *o*-CH_2PhNMe_2.

- **Synthesis of [(≡SiO)$_2$Y(OC_6F_5)$_2$]$^-$[$HNMe_2$(PhMe)]$^+$, AS13**

394.80 mg of (≡SiO)$_2$Y(o-NMe_2-benzyl) (0.24 mmol) were put inside a double Schlenk with 122.0 mg (0.66 mmol) of pentafluorophenol. After having pulled high vacuum in the double Schlenk 10 ml of benzene were distilled over the pentafluorophenol to solubilize it. The solution was transferred on the (≡SiO)$_2$Y(o-NMe_2-benzyl) to start the reaction. The reaction proceeded overnight. The product was washed three times with benzene, the solution was removed, and then the sample washed once more with pentane. The product was dried under high vacuum. It

was collected and stored in the glove box. DRIFT: 3560-3680 cm^{-1} SiO-H(vicinal) stretching; 2700-2900 cm^{-1} C-H stretching; 3077 cm^{-1} N-H stretching; Elemental analysis: 4.57 wt% Y; 11.90 wt% C; 0.66 wt% H; 0.44 wt% N; 10.6 wt% F; ^{1}H MAS NMR: δ(ppm): 7.3 [*o*-CH_3Ph$NHMe_2$]$^+$; δ(ppm): 3.3 [*o*-$CH_3PhNHMe_2$]$^+$; ^{13}C CPMAS NMR: δ(ppm): 15.5 [*o*-$\underline{CH_3}PhNHMe_2$]$^+$; δ(ppm): 24.8 THF; δ(ppm): 45.6 [*o*-$CH_3PhNH\underline{Me_2}$]$^+$; δ(ppm): 71.1 THF; δ(ppm): 117-150 [*o*-CH_3Ph$NHMe_2$]$^+$.

- **Synthesis of (≡SiO)Y{1,3-$C_3H_3(SiMe_3)_2$}$_2$, P10**

2.00 g of SiO_{2-700} (1.16 mmol) were put in a double Schlenk with 897.2 mg (1.4 mmol) of Y{1,3-$C_3H_3(SiMe_3)_2$}$_3$. 10 mL of hexane were distilled on the Y complex and the yellow solution obtained was transferred on the silica to start the reaction. After two hours the product obtained was washed with hexane three times. The volatiles were removed and the product was dried under high vacuum. DRIFT: 2700-2900 cm^{-1} C-H stretching; Elemental analysis: 3.7 wt% Y; 8.54 wt% C; 1.6 wt% H; ^{1}H MAS NMR: δ(ppm): -0.03 –$SiMe_3$; δ(ppm): 1.45 Me_3Si-$\underline{CH_2}$-CH=CH_2-$SiMe_3$; δ(ppm): 3.56 –$\underline{CH}SiMe_3$; δ(ppm): 5.42 Me_3Si-CH_2-CH=$\underline{CH_2}$-$SiMe_3$; δ(ppm): 6.03 Me_3Si-CH_2-$\underline{CH}$=CH_2-$SiMe_3$; δ(ppm): 7.28 –CH-$\underline{CH}$-CH–; ^{13}C CPMAS NMR: δ(ppm): -0.97 –$SiMe_3$; δ(ppm): 28.1 Me_3Si-$\underline{CH_2}$-CH=CH_2-$SiMe_3$; δ(ppm): 93.6 –$\underline{CH}SiMe_3$; δ(ppm): 161.4 –CH-$\underline{CH}$-CH–; δ(ppm): 143.0 Me_3Si-CH_2-$\underline{CH}$=CH_2-$SiMe_3$; δ(ppm): 127.0 Me_3Si-CH_2-CH=$\underline{CH_2}$-$SiMe_3$.

- **Synthesis of [(≡SiO)Y$(OC_6F_5)_3$]$^-$[$HNMe_2Et$]$^+$, AS14**

857.3 mg of P10 (0.4 mmol) were put in a double Schlenk with 149.3 mg (0.8 mmol) of pentafluorophenol. 10 mL of benzene were then distilled on the pentafluorophenol. 0.8 mL of dimethylethylamine were distilled in the double schlenk and the solution obtained was transferred on the powder to start the reaction. The reaction proceeded overnight, the product was washed with benzene five times. The volatiles were removed by an intermediate trap and the product was washed once more with pentane. The volatiles were once more removed and the product dried under high vacuum. DRIFT: 2700-2900 cm^{-1} C-H stretching; 3045 cm^{-1} N-H stretching; 1500-1600 cm^{-1} C=C stretching; Elemental analysis: 3.66 wt% Y; 8.38 wt% C; 0.62 wt% N; 7.66 wt% F; ^{1}H MAS NMR: δ(ppm): δ(ppm): -0.15 –$SiMe_3$; 1.27 $N(CH_3)_2(CH_2\underline{CH_3})$; δ(ppm): 2.57 $N(\underline{CH_3})_2(\underline{CH_2}CH_3)$; δ(ppm): 5.27 Me_3Si-CH_2-CH=$\underline{CH_2}$-$SiMe_3$; δ(ppm): 5.92 Me_3Si-CH_2-$\underline{CH}$=CH_2-$SiMe_3$;^{13}C CPMAS NMR:

δ(ppm): -1.4 –$SiMe_3$; δ(ppm): 7.8 $N(CH_3)_2(CH_2\underline{CH_3})$; δ(ppm): 42.0 $N(\underline{CH_3})_2(CH_2CH_3)$; δ(ppm): 52.9 $N(CH_3)_2(\underline{CH_2}CH_3)$; δ(ppm): 25 THF; δ(ppm): 71.1 THF; δ(ppm): 138.6 $Me_3Si\text{-}CH_2\text{-}\underline{CH}=\underline{CH_2}\text{-}SiMe_3$.

- **Synthesis of $(\equiv SiO)_2Y\{1,3\text{-}C_3H_3(SiMe_3)_2\}$, P11**

425.8 mg (0.66 mmol) of $Y\{1,3\text{-}C_3H_3(SiMe_3)_2\}_3$ were put in a double Schlenk with 1.17 g of $SiO_{2\text{-}200}$ (2.0 mmol SiOH). 10 mL of hexane were distilled on the Y complex and the solution obtained was transferred on the silica. After two hours the grafting reaction was stopped and the product was washed three times with hexane. The volatiles were removed with an intermediate trap and the yellowish powder was dried under high vacuum. To the washing solution collected were added 136.9 mg of C14 as internal standard for the GC analysis. DRIFT: 3560-3680 cm^{-1} SiO-H(vicinal) stretching; 2700-2900 cm^{-1} C-H stretching; Elemental analysis: 4.92 wt% Y; 5.15 wt% C; 1.11 wt% H; ^{1}H MAS NMR: δ(ppm): -0.04 –$SiMe_3$; δ(ppm): 1.34 $Me_3Si\text{-}\underline{CH_2}\text{-}CH=CH_2\text{-}SiMe_3$; δ(ppm): 1.74 –$\underline{CH}SiMe_3$; δ(ppm): 5.58 $Me_3Si\text{-}CH_2\text{-}CH=\underline{CH_2}\text{-}SiMe_3$; δ(ppm): 6.26 $Me_3Si\text{-}CH_2\text{-}\underline{CH}=CH_2\text{-}SiMe_3$; ^{13}C CPMAS NMR: δ(ppm): -3.39 –$SiMe_3$; δ(ppm): 0.35 –$SiMe_3$; δ(ppm): 31.8 $Me_3Si\text{-}\underline{CH_2}\text{-}CH=CH_2\text{-}SiMe_3$; δ(ppm): 24.7 THF; δ(ppm): 71.4 THF; δ(ppm): 20-200 remaining peaks.

- **Synthesis of $[(\equiv SiO)_2Y(OC_6F_5)_2]^-[HNMe_2Et]^+$, AS15**

195.1 mg (1.1 mmol) of pentafluorophenol were put in a double Schlenk with 550.5 mg (0.30 mmol) of P11. 10 mL of benzene were distilled on the pentafluorophenol and the solution was transferred on P11. 0.1 mL of dimethylethylamine was distilled trap to trap on the suspension. The reaction proceeded overnight. The product was then washed three times with benzene. The volatiles were removed with an intermediate trap and the sample was washed once more with pentane. The volatiles were removed once more and the product dried under high vacuum. DRIFT: 3560-3680 cm^{-1} SiO-H(vicinal) stretching; 2700-2900 cm^{-1} C-H stretching; 3045 cm^{-1} N-H stretching; 1500-1600 cm^{-1} C=C stretching; Elemental analysis: 3.86 wt% Y; 4.8 wt% C; 1.02 wt% N; 11.4 wt% F; ^{1}H MAS NMR: δ(ppm): δ(ppm): 0.12 –$SiMe_3$; 1.38 $N(CH_3)_2(CH_2\underline{CH_3})$; δ(ppm): 2.88 $N(\underline{CH_3})_2(\underline{CH_2}CH_3)$; ^{13}C CPMAS NMR: δ(ppm): -0.56–$SiMe_3$; δ(ppm): 8.1 $N(CH_3)_2(CH_2\underline{CH_3})$; δ(ppm): 42.1 $N(\underline{CH_3})_2(CH_2CH_3)$; δ(ppm): 53.8 $N(CH_3)_2(\underline{CH_2}CH_3)$; δ(ppm): 25 THF; δ(ppm): 71.1 THF; δ(ppm): 139 $Me_3Si\text{-}CH_2\text{-}\underline{CH}=\underline{CH_2}\text{-}SiMe_3$.

- **Synthesis of $[(\equiv SiO)Y\{1,3\text{-}C_3H_3(SiMe_3)_2\}]^+[B(C_6F_5)_4]^-$, P12**

247.1 mg (0.27 mmol) of $[C(C_6H_5)_3]^+[B(C_6F_5)_4]^-$ were put in a double Schlenk with 532.6 mg (0.21 mmol) of P10. 20 mL of benzene were distilled on the borate complex. Once an homogeneous yellow/orange solution was obtained, this was transferred on the P10. The suspension assumed immediately a deep red colour. The reaction proceeded overnight. At the end of the reaction the colour of the suspension was dark green. The product was washed with benzene five times. The solution obtained after he washings was collected and the volatiles remaining removed by intermediate trap. The product was washed once more with pentane and the volatiles removed by an intermediate trap. The dark green powder obtained was dried under high vacuum. DRIFT: 2700-2900 cm^{-1} C-H stretching; Elemental analysis: 3.4 wt% Y; 11.4 wt% C; 0.27 wt% B; 9.1 wt% F; ^1H MAS NMR: δ(ppm): -0.16 –$SiMe_3$; δ(ppm): δ(ppm): 3.77 –$\underline{CH}SiMe_3$; δ(ppm): 7.17 –CH-$\underline{CH}$-CH–; δ(ppm): 7.91 benzene; ^{13}C CPMAS NMR: δ(ppm): -1.98 –$SiMe_3$; δ(ppm): 28.1 $Me_3Si\text{-}\underline{CH_2}\text{-}CH{=}CH_2\text{-}SiMe_3$; δ(ppm): 93.6 –$\underline{CH}SiMe_3$; δ(ppm): 125-150 –CH-$\underline{CH}$-CH–, benzene; ^{11}B MAS NMR: δ(ppm): -15.5; ^{29}Si CPMAS NMR: δ(ppm): -105.3 SiO_4; δ(ppm): -7 –$SiMe_3$; δ(ppm): 2 –$SiMe_3$.

6. Synthesis of the methylated zirconocenes

- **Synthesis of $(n\text{-BuMeCp})_2ZrMe_2$**

705 mg of $(n\text{-BuMeCp})_2ZrCl_2$ (1.63 mmol) were put in a Schlenk with 10 mL of Et_2O. 2.1 mL of a solution 1.6 M of MeLi (3.36 mmol) in Et_2O were added dropwise to the suspension at -25°C. The suspension was left to react overnight at room temperature. The solvent was removed and a brown oil was obtained. The product was extracted in hexane and filtered in the glovebox over celite. The hexane was evaporated and a yellow oil was obtained. ^1H and ^{13}C solution NMR spectra in benzene-d_6 were acquired. ^1H NMR C_6D_6: δ(ppm): -0.13 Zr-CH_3 (s, 6H); 0.89 (t; J = 7.25 Hz, 6H) $CpC_3H_6\text{-}\underline{Me}$; 1.3 (m, 4H) $CpC_2H_4\text{-}\underline{CH_2}\text{-}Me$; 1.5 (m, 4H) $CpCH_2\text{-}\underline{CH_2}\text{-}C_2H_5$; 1.95 (s, 6H) Cp-$\underline{Me}$; 2.29 (m, 4H) Cp-$\underline{CH_2}\text{-}C_3H_7$; 5.40 (m, 4H) Cp; 5.66 (t, 2H, J = 2.35 Hz) Cp.

- **Synthesis of $^{13}CH_3Li$**

9.5 mL of a solution of a 2.5 M solution of *n*-BuLi (23.7 mmol) in hexane were put in a Schlenk, to which 20 mL of a iodomethane solution in hexane (obtained by solubilizing 1.55 g of CH_3I (11

mmol) and 2.28 g of $^{13}CH_3I$ (16 mmol)). The addition was performed in 15 minutes. The solution was then brought to room temperature and left to react for one hour. The white suspension was left to decant and the surnatant was removed. The product was dried. ^{1}H NMR THF-d_8: δ(ppm): -2.04 (s, 3H) $^{12}\underline{CH_3}Li$; -2.04 (d, 3H, J = 97 Hz) $^{13}\underline{CH_3}Li$; ^{13}C NMR C_6D_6: δ(ppm): -16.4 (s) $^{13}CH_3Li$.

- Synthesis of $EtInd_2ZrMe_2$

696 mg (1.66 mmol) of *rac*-$EtInd_2ZrCl_2$ were put in a Schlenk with 10 mL of Et_2O. 2.1 ml of a 1.6 M solution of LiMe (3.36 mmol) were added dropwise to the suspension in 10 minutes. The reaction proceeded overnight. The solvent was removed and the product extracted with toluene and the solution was recovered. After drying the toluene a yellow solid was obtained. ^{1}H NMR C_6D_6: δ(ppm): -2.19 (*s*) meso-$EtInd_2Zr\underline{Me_2}$; 0.14 (*s*) meso-$EtInd_2Zr\underline{Me_2}$; -0.95 (*s*) rac-$EtInd_2Zr\underline{Me_2}$; 2.5-3.2 *m* meso/rac-$\underline{Et}Ind_2ZrMe_2$; 5.66 (*d*; J = 3.30 Hz) rac-Cp; 6.43 (*d*; J = 3.30 Hz) rac-Cp; 5.71 (*d*; J = 3.30 Hz) meso-Cp; 6.46 (*d*; J = 3.30 Hz) meso-Cp; 6.8-7.4 (m) meso/rac-Ar.

7. Synthesis of the isolated catalysts

- Procedure with TiBA

The desired amount of chlorinated complex was solubilized in a 20 mL vial in 2-5 mL of toluene. To the suspension a sufficient amount of TiBA was added in order to reach a ratio 50 Al/Zr. Once a solution was obtained AS1 was added and the immobilization reaction was left to proceed for one hour. The powder was washed with 5 mL of toluene and dried under vacuum.

- Procedure without TiBA

The desired amount of methylated complex was solubilized in a 20 mL vial in 2 mL of toluene for $EtInd_2ZrMe_2$ and hexane for (n-BuMeCp)$_2ZrMe_2$. Once a solution was obtained AS1 was added and the immobilization reaction was left to proceed for one hour. The powder was washed with 5 mL of toluene for $EtInd_2ZrMe_2$ and hexane for (n-BuMeCp)$_2ZrMe_2$ and dried under vacuum.

Reference

(1) Mathon, O.; Beteva, A.; Borrel, J.; Bugnazet, D.; Gatla, S.; Hino, R.; Kantor, I.; Mairs, T.; Munoz, M.; Pasternak, S.; et al. The Time-Resolved and Extreme Conditions XAS (TEXAS) Facility at the European Synchrotron Radiation Facility: The General-Purpose EXAFS Bending-Magnet

Beamline BM23. *J. Synchrotron Radiat.* 2015, *22* (6), 1548–1554. https://doi.org/10.1107/S1600577515017786.

Abstract

In this manuscript is presented the synthesis and application of Al- and Y-based activating support for metallocene catalysts for olefin polymerization. The approach used for the synthesis of the supported species is the Surface Organometallic Chemistry which allows a certain control on the structure of the grafted species.

The activators synthesized were then tested, in presence of *rac*-$EtInd_2ZrCl_2$, in ethylene/1-hexene slurry copolymerization. Of all the species produced (differing either in the nature of the metal core, the nature of the functionalizing ligand or the acidity of the organometallic precursor) only one demonstrated a productivity sufficient to justify further studies: $[(\equiv SiO)_2Al(OC_6F_5)_2]^-[HNEtMe_2]^+$, AS1. The system AS1/*rac*-$EtInd_2ZrCl_2$ shows activities around 1100 $g_{PE}\ g_{cat}^{-1}\ h^{-1}$ at lab-scale and around 4000 $g_{PE}\ g_{cat}^{-1}\ h^{-1}$ at pre-industrial scale. AS1 was also used for the isolation of formulated 'dry' catalysts, by reaction with $EtInd_2ZrMe_2$. The catalysts thus obtained showed high initial activities followed by a rapid decomposition of the active species at room temperature.

In this thesis work, was also developed an innovative catalyst based on a silica-supported Y organometallic complex, which produces UHMWPE with activities up to 7500 $g_{PE}\ g_{cat}^{-1}\ h^{-1}$.

Résumé

Ce manuscrit décrit la synthèse et l'application de supports activateurs, basés sur Al et Y, pour des catalyseurs métallocènes pour la polymérisation des oléfines. La méthode utilisée pour la synthèse des espèces supportées est la Chimie Organométallique de surface, qui permet un contrôle certain sur la structure des produits greffés.

Les activateurs synthétisés ont été testés, en présence de *rac*-$EtInd_2ZrCl_2$, en copolymérization slurry éthylène/1-héxène. Entre toutes les espèces testées (qui différaient pour soit par la nature du centre métallique, soit par la nature du ligand fonctionnel, soit par l'acidité du précurseur organométallique), seulement un a été considéré suffisamment actif pour justifier des études ultérieures : $[(\equiv SiO)_2Al(OC_6F_5)_2]^-[HNEtMe_2]^+$, AS1. Le système AS1/*rac*-$EtInd_2ZrCl_2$ démontra des activités aux alentours de 1100 $g_{PE}\ g_{cat}^{-1}\ h^{-1}$ à échelle laboratoire et de 4000 $g_{PE}\ g_{cat}^{-1}\ h^{-1}$ à échelle préindustrielle. AS1 a aussi été utilisé pour la formulation des catalyseurs dits 'secs', par réaction avec $EtInd_2ZrMe_2$. Ces catalyseurs ont montré des activités initiales élevées, suivies d'une rapide décomposition des espèces actives à température ambiante.

Dans ce travail de thèse, on a aussi développé un catalyseur novateur basé sur un complexe organométallique d'yttrium greffé sur silice, qui produit l'UHMWPE avec des activités supérieures à 7000 $g_{PE}\ g_{cat}^{-1}\ h^{-1}$.

Key words : Polyolefin; Polyethylene; Slurry Polymerization; Activating Support; Silica; SOMC; metallocene; zirconocene; Aluminium; Yttrium.